INFORMATION TO USERS

This reproduction was made from a copy of a document sent to us for microfilming. While the most advanced technology has been used to photograph and reproduce this document, the quality of the reproduction is heavily dependent upon the quality of the material submitted.

The following explanation of techniques is provided to help clarify markings or notations which may appear on this reproduction.

1. The sign or "target" for pages apparently lacking from the document photographed is "Missing Page(s)". If it was possible to obtain the missing page(s) or section, they are spliced into the film along with adjacent pages. This may have necessitated cutting through an image and duplicating adjacent pages to assure complete continuity.

2. When an image on the film is obliterated with a round black mark, it is an indication of either blurred copy because of movement during exposure, duplicate copy, or copyrighted materials that should not have been filmed. For blurred pages, a good image of the page can be found in the adjacent frame. If copyrighted materials were deleted, a target note will appear listing the pages in the adjacent frame.

3. When a map, drawing or chart, etc., is part of the material being photographed, a definite method of "sectioning" the material has been followed. It is customary to begin filming at the upper left hand corner of a large sheet and to continue from left to right in equal sections with small overlaps. If necessary, sectioning is continued again–beginning below the first row and continuing on until complete.

4. For illustrations that cannot be satisfactorily reproduced by xerographic means, photographic prints can be purchased at additional cost and inserted into your xerographic copy. These prints are available upon request from the Dissertations Customer Services Department.

5. Some pages in any document may have indistinct print. In all cases the best available copy has been filmed.

University Microfilms International
300 N. Zeeb Road
Ann Arbor, MI 48106

Golan, David Eric

DYNAMIC INTERACTIONS IN THE HUMAN ERYTHROCYTE MEMBRANE: STUDIES ON THE LATERAL MOBILITY OF BAND 3, PHOSPHOLIPID, AND CHOLESTEROL

Yale University

PH.D. 1982

PLEASE NOTE:

In all cases this material has been filmed in the best possible way from the available copy. Problems encountered with this document have been identified here with a check mark __✓__.

1. Glossy photographs or pages _____
2. Colored illustrations, paper or print _____
3. Photographs with dark background _____
4. Illustrations are poor copy _____
5. Pages with black marks, not original copy __✓__
6. Print shows through as there is text on both sides of page _____
7. Indistinct, broken or small print on several pages __✓__
8. Print exceeds margin requirements _____
9. Tightly bound copy with print lost in spine _____
10. Computer printout pages with indistinct print _____
11. Page(s) _____ lacking when material received, and not available from school or author.
12. Page(s) _____ seem to be missing in numbering only as text follows.
13. Two pages numbered _____. Text follows.
14. Curling and wrinkled pages _____
15. Other _____

DYNAMIC INTERACTIONS IN THE HUMAN ERYTHROCYTE MEMBRANE: STUDIES ON THE LATERAL MOBILITY OF BAND 3, PHOSPHOLIPID, AND CHOLESTEROL

A Dissertation

Presented to the Faculty of the Graduate School

of

Yale University

in Candidacy for the Degree of

Doctor of Philosophy

by

David Eric Golan

December, 1982

ABSTRACT

DYNAMIC INTERACTIONS IN THE HUMAN ERYTHROCYTE MEMBRANE: STUDIES ON THE LATERAL MOBILITY OF BAND 3, PHOSPHOLIPID, AND CHOLESTEROL

David Eric Golan

Yale University

1982

The human erythrocyte membrane has served for many years as the prototypical eukaryotic cell membrane. It is composed of approximately 50% lipid, which is evenly divided between phospholipid and cholesterol, and 50% protein. Band 3, the major intrinsic protein, accounts for approximately 25% of the total membrane protein; extrinsic cytoskeletal proteins comprise most of the remaining membrane protein. Spectrin is the major cytoskeletal protein; it is attached to at least some of the band 3 by the linking protein ankyrin. Low ionic strength treatment of erythrocyte ghost membranes destabilizes many interactions within the cytoskeleton, while hypertonic ionic strength treatment leads to specific dissociation of the ankyrin-cytoskeleton linkages. This dissertation examines the lateral mobility of fluorescently labeled band 3, phospholipid, and cholesterol in the plane of the human erythrocyte membrane, using the fluorescence photobleaching recovery technique. The major conclusions reached in this study are as follows:

(1) Under physiological conditions of ionic strength and temperature, band 3 mobility is severely restricted by the proteins of the erythrocyte cytoskeleton. This restriction is mediated at least in

part by ankyrin. Thus, destabilization of the cytoskeleton by low ionic strength treatment, hypertonic ionic strength treatment, or addition of a proteolytic fragment of ankyrin leads to greatly increased lateral mobility of band 3. Loss of restriction of band 3 mobility is not associated with dissociation of spectrin from the membrane; rather, complete loss of restriction is associated with the specific proteolysis of ankyrin alone.

(2) Band 3 mobility is unrestricted under certain conditions of ionic strength and temperature. Under these conditions the ratio between the lateral diffusion coefficient of band 3 and that of phospholipid or cholesterol is approximately that expected assuming the same effective membrane viscosity for both protein and lipid components.

(3) Phospholipid and cholesterol mobilities in the erythrocyte membrane are identical under all conditions of ionic strength and temperature.

(4) Both phospholipid and cholesterol mobilities are partially restricted by membrane proteins, as shown in experiments comparing lipid mobility in erythrocyte ghost membranes with that in liposomes prepared from extracted erythrocyte membrane lipids.

DYNAMIC INTERACTIONS IN THE HUMAN ERYTHROCYTE MEMBRANE:
STUDIES ON THE LATERAL MOBILITY OF BAND 3, PHOSPHOLIPID, AND CHOLESTEROL

Preface

The human erythrocyte membrane has served for many years as the prototypical eukaryotic cell membrane. It is composed of approximately 50% lipid, which is evenly divided between phospholipid and cholesterol, and 50% protein. Band 3, the major intrinsic protein, accounts for approximately 25% of the total membrane protein; extrinsic cytoskeletal proteins comprise most of the remaining membrane protein. Spectrin is the major cytoskeletal protein; it is attached to at least some of the band 3 by the linking protein ankyrin. Low ionic strength treatment of erythrocyte ghost membranes destabilizes many interactions within the cytoskeleton, while hypertonic ionic strength treatment leads to specific dissociation of the ankyrin-cytoskeleton linkages. This dissertation examines the lateral mobility of fluorescently labeled band 3, phospholipid, and cholesterol in the plane of the human erythrocyte membrane, using the fluorescence photobleaching recovery technique. The major conclusions reached in this study are as follows:

(1) Under physiological conditions of ionic strength and temperature, band 3 mobility is severely restricted by the proteins of the erythrocyte cytoskeleton. This restriction is mediated at least in part by ankyrin. Thus, destabilization of the cytoskeleton by low

ionic strength treatment, hypertonic ionic strength treatment, or addition of a proteolytic fragment of ankyrin leads to greatly increased lateral mobility of band 3. Loss of restriction of band 3 mobility is not associated with dissociation of spectrin from the membrane; rather, complete loss of restriction is associated with the specific proteolysis of ankyrin alone.

(2) Band 3 mobility is unrestricted under certain conditions of ionic strength and temperature. Under these conditions the ratio between the lateral diffusion coefficient of band 3 and that of phospholipid or cholesterol is approximately that expected assuming the same effective membrane viscosity for both protein and lipid components.

(3) Phospholipid and cholesterol mobilities in the erythrocyte membrane are identical under all conditions of ionic strength and temperature.

(4) Both phospholipid and cholesterol mobilities are partially restricted by membrane proteins, as shown in experiments comparing lipid mobility in erythrocyte ghost membranes with that in liposomes prepared from extracted erythrocyte membrane lipids.

Band 3 was specifically labeled with the covalent fluorescent probe eosin-5-isothiocyanate. In an initial study, low temperature (21°C) and high ionic strength (46 mM sodium phosphate) favored immobilization of band 3 (10% mobile) as well as slow diffusion of the mobile fraction (diffusion coefficient (D) = 4×10^{-11} $cm^2 sec^{-1}$). Increasing temperature (37°C) and decreasing ionic strength (13 mM

sodium phosphate) led to an increase in both the fraction of mobile band 3 (90% mobile) and the diffusion rate of the mobile fraction ($D = 190 \times 10^{-11}$ cm^2sec^{-1}). The increase in the fraction of mobile band 3 was markedly dissociated, however, from the increase in the diffusion rate of the mobile fraction. Thus, the fraction of mobile band 3 always increased at higher ionic strength and lower temperature than the ionic strength and temperature at which the diffusion rate increased. This dissociation was manifested kinetically on prolonged incubation of ghosts at constant ionic strength and temperature: the diffusion rate of the mobile fraction increased very slowly at first and much more rapidly after the initial lag period, whereas the fraction of mobile band 3 increased almost immediately to 90% and remained maximal for the duration of the experiment. These experiments were repeated, using an improved and recalibrated fluorescence photobleaching appartus, in the presence of the protease inhibitors ethylenediaminetetraacetic acid (EDTA), phenylmethylsulfonyl fluoride (PMSF), and pepstatin A. The same relative dependencies of the diffusion coefficient and fraction mobility on ionic strength and temperature were found, although all diffusion coefficients were two- to four-fold lower than previously seen (i.e., extreme values of 1×10^{-11} and 50×10^{-11} cm^2sec^{-1}). These effects were shown not to be due to complete dissociation of spectrin from the membrane. Further, all increases in fractional mobility and moderate (approximately ten-fold) increases in diffusion coefficient were not associated with specific proteolysis of any major membrane component. Extreme (fifty-fold)

increases in diffusion coefficient were, however, associated with the specific and substantial ($\sim$ 70%) proteolysis of ankyrin alone.

Experiments testing the effects of hypertonic ionic strength and proteolytic fragments of cytoskeletal proteins on the lateral mobility of band 3 confirmed the central role of ankyrin in the mediation of band 3 mobility restriction. Addition of hypertonic KCl (320 mM) to 40 mM sodium phosphate in the presence of EDTA, PMSF, and pepstatin A led to increases in both the fraction of mobile band 3 (90% mobile) and the diffusion rate of the mobile fraction (50×10^{-11} $cm^2 sec^{-1}$). As seen in the low ionic strength experiments, the increase in the fraction of mobile band 3 was markedly dissociated from the increase in the diffusion rate of the mobile fraction. This dissociation was again manifested kinetically on prolonged incubation of ghosts at constant ionic strength and temperature, under which conditions there was an immediate, maximal increase in fractional mobility followed by a more gradual increase in diffusion coefficient. In a separate experiment, incubation of erythrocyte ghosts at 37°C in the presence of a 72,000 dalton proteolytic fragment of ankyrin which serves as the attachment site for spectrin on the inner membrane surface led to a three-fold increase in the diffusion coefficient and a two-and-one-half-fold increase in the fractional mobility of band 3, compared with control values at the same ionic strength and temperature. This finding implicates the ankyrin-spectrin linkage as one controlling element in band 3 lateral mobility. Incubation of ghosts in the presence of an 80,000 dalton proteolytic fragment of spectrin involved in the polymerization of dimer to tetramer spectrin did not lead to

any significant change in either the fractional mobility or the diffusion coefficient of band 3, under all conditions of ionic strength and temperature examined. It is possible, however, that this lack of effect was due to an inability to concentrate the spectrin fragment sufficiently for it to manifest a change in the spectrin dimer-tetramer equilibrium, since this fragment has much lower affinity for its spectrin binding site than does the ankyrin fragment for its spectrin attachment site.

It is striking that the diffusion coefficient of band 3 reached the same maximum value at 37°C under extreme conditions of both hypertonic and low ionic strength. This "rapid diffusion limit" for band 3 in the erythrocyte ghost membrane was compared with the diffusion of specifically labeled lipid in the same membrane under the same conditions. Lipid probes employed in fluorescence photobleaching recovery studies included the fluorescent phospholipid and cholesterol analogs N-4-nitrobenzo-2-oxa-1, 3-diazole (NBD) phosphatidylethanolamine (NBD-PE) and NBD-cholesterol (NBD-chol), respectively. In the model liposome systems dimyristoylphosphatidylcholine (DMPC), DMPC + 5-40 mole% cholesterol, egg phosphatidylcholine (egg PC), and egg PC + 10-50 mole% cholesterol, no significant differences were found between the lateral mobility parameters of the two probes, except at temperatures below the phase transition in DMPC liposomes to which 5-20 mole% cholesterol had been added. Under these conditions the cholesterol analog consistently diffused 60-80% faster than the phospholipid analog, showing that cholesterol in at least some membrane

systems may be in a different environment from the bulk phospholipid. In the erythrocyte ghost membrane, NBD-PE and NBD-chol had identical lateral mobilities under all conditions of ionic strength and temperature. The diffusion coefficient of the lipid probes showed a small temperature dependence (less than two-fold increase from 15°C to 37°C) and no ionic strength dependence; the fractional mobility was 80-85% in all cases. At 37°C the diffusion coefficient of the lipid probes was 210 x 10^{-11} cm^2sec^{-1}, or approximately four-fold greater than the "rapid diffusion limit" for band 3. This ratio of diffusion coefficients agrees with that expected for two objects of relative sizes corresponding to band 3 and phospholipid which experience the same effective membrane viscosity; i.e., in the "rapid diffusion limit" the lateral mobility of band 3 appears to be restricted only by the intrinsic viscosity of the lipid bilayer.

Comparing the lateral diffusion coefficient of lipid in the erythrocyte ghost membrane with that in the various model membranes, it was found that both NPD-PE and NBD-chol diffuse four-fold faster in liposomes prepared from chloroform/methanol extracts of ghost membranes (D = 800 x 10^{-11} cm^2sec^{-1} at 37°C) than in the ghost membranes themselves. This difference was not due to changes in the lipid composition of the membrane, as the mole fraction of cholesterol in the extracted lipid liposomes (43%) differed only slightly from that in the ghosts (53%). Rather, it appears that the membrane proteins partially restrict the lateral mobility of both phospholipid and cholesterol in the erythrocyte ghost membrane. The diffusion coefficient

of both lipid probes in extracted erythrocyte lipid liposomes at 37°C was within a factor of two of that in the model liposome system egg PC + 50 mole% cholesterol ($D = 1500 \times 10^{-11}$ $cm^2 sec^{-1}$); this difference can probably be ascribed to the unusual lipid composition of the erythrocyte membrane.

to the memory of

William R. Veatch

ACKNOWLEDGEMENTS

Dr. Will Veatch was one of those rare individuals who combine brilliance of mind with generosity of spirit and gentleness of manner. He taught me in word and deed what it means to be an inquisitive and hard-working investigator while maintaining and strengthening one's personal ties to home and family. I thank him for his example, and I shall cherish his memory always. I am grateful to other members of the Veatch laboratory for their technical assistance and good humor, especially Jane Gharibian, John Durkin, Alan Stolpen, and Peter Singer. I thank Drs. Jon Morrow and Vincent Marchesi for discussions which led to the initial hypotheses upon which this thesis is based. I am indebted to the Department of Molecular Biophysics and Biochemistry and the Medical Scientist Training Program at Yale University for their understanding and support, and especially to Drs. Frederic Richards and James Jamieson for their help and guidance. I thank the members of the Department of Pharmacology at Harvard Medical School for allowing me to pursue my research interests in their midst. I am also grateful to the Department of Medicine at Brigham and Women's Hospital, and especially to Drs. Eugene Braunwald and Marshall Wolf, for their continuing support and encouragement. Most of all I thank Laura, my constant source of strength and love.

I am pleased to acknowledge a National Institutes of Health-Medical Scientist Training Program traineeship.

CONTENTS

		Page
Introduction		1
Chapter 1.	Literature Review	7
A.	The Erythrocyte Membrane	7
1.	General Review of Structure	7
a.	The Lipid Bilayer	7
b.	The Proteins	9
2.	Band 3	13
a.	Physical and Chemical Properties	13
b.	Conformation in the Membrane	15
c.	Associations with Other Membrane Proteins.	22
d.	Functions	23
3.	Cytoskeleton	27
a.	Definition and Components	27
b.	Spectrin: Structure in Solution	29
c.	Spectrin: Polymerization with Actin and Band 4.1	31
d.	Spectrin: Binding to the Membrane	34
4.	Band 3 - Cytoskeleton Interactions	37
a.	Band 3 - Ankyrin	37
b.	Band 3 - Spectrin	39
B.	Measurements of Lateral Diffusion	44
1.	Protein Diffusion: Biological Membranes	44
a.	Cell Fusion	45
b.	Photobleaching Recovery	46
2.	Lipid Diffusion: Biological Membranes	48
3.	Protein and Lipid Diffusion: Artificial Membranes	56
Chapter 2.	Fluorescence Photobleaching Recovery	58
A.	Theory	58
1.	Design of the Experiment	58
2.	Photobleaching	60
3.	Fluorescence Recovery Curves	61
B.	Methods	67
1.	Optics and Electronics	67
2.	Experimental Data Analysis	77
3.	Calibration of Beam Size and Profile	80
C.	Results: Beam Calibration	81
D.	Discussion	82
Chapter 3.	Sample Preparations	85
A.	Eosin-isothiocyanate Labeling of Band 3	85
1.	Methods	85

Page

a. Labeling of Human Erythrocytes with Eosin-isothiocyanate..... 85
b. Identification of Labeled Membrane Components..... 87
1. SDS-Polyacrylamide Gel Electrophoresis..... 87
2. Selective Extraction Procedures..... 88
a. Low Ionic Strength Extraction.... 88
b. Triton Extraction..... 89
c. Chloroform/Methanol Extraction... 89
2. Results and Discussion..... 90
a. Eosin Labeling..... 90
b. SDS-Polyacrylamide Gel Electrophoresis... 90
c. Selective Extraction Procedures..... 92
d. Discussion..... 94
B. 72,000 Dalton Ankyrin Fragment..... 95
1. Methods..... 95
2. Results and Discussion..... 97
C. 80,000 Dalton Spectrin Fragment..... 102
1. Methods..... 102
2. Results and Discussion..... 103
D. NBD-PE and NBD-Chol Labeling of Artificial and Erythrocyte Membranes..... 103
1. Materials and Methods..... 106
a. Labeling of DMPC-Cholesterol and Egg PC-Cholesterol Multilamellar Lipsosomes.. 106
b. Preparation and Labeling of Multilamellar Liposomes from Extracted Erythrocyte Membrane Lipids..... 107
c. Labeling of Erythrocyte Ghosts..... 108
1. NBD-PE Labeling..... 108
2. NBD-Chol Labeling..... 109
2. Results and Discussion: Composition of Samples..... 109

Chapter 4. Lateral Mobility of Band 3: Effect of Low Ionic Strength..... 112
A. Methods..... 113
1. Fluorescence Photobleaching Recovery System.. 113
2. Preparation of the Sample..... 114
3. Fluorescence Photobleaching Recovery Experiment..... 118
B. Results: Initial Studies..... 121
1. Effect of Ionic Strength..... 124
2. Effect of Temperature..... 126
3. Effect of Time..... 129
4. Rebleaching Experiments..... 131

		Page
C.	Results: Addition of Protease Inhibitors	133
	1. Effect of PMSF Alone	134
	2. Effect of Ionic Strength and Temperature	137
	3. Effect of Time	140
D.	Discussion	142
Chapter 5.	Membrane Protein Dissociation and Proteolysis: Effect of Low Ionic Strength	148
A.	Ionic Strength-Dependent Dissociation of Spectrin	149
	1. Methods	149
	2. Results and Discussion	151
B.	Time-Dependent Dissociation of Spectrin	156
	1. Methods	156
	2. Results and Discussion	157
C.	Ionic Strength- and Time-Dependent Proteolysis of Membrane Proteins	159
	1. Methods	159
	2. Results and Discussion	160
Chapter 6.	Lateral Mobility of Band 3: Effect of Specific Cytoskeletal Perturbations	166
A.	Methods	168
	1. Hypertonic KCl Incubation	168
	2. 72,000 Dalton Ankyrin Fragment Incubation	168
	3. 80,000 Dalton Spectrin Fragment Incubation	169
B.	Results	170
	1. Hypertonic Ionic Strength	170
	2. 72,000 Dalton Ankyrin Fragment	176
	3. 80,000 Dalton Spectrin Fragment	177
C.	Discussion	179
Chapter 7.	Lateral Mobility of Phospholipid and Cholesterol: Model Systems	182
A.	Methods	183
B.	Results	184
	1. Lateral Mobility of NBD-PE and NBD-Chol in DMPC Liposomes: Temperature Dependence	184
	2. Lateral Mobility of NBD-PE and NBD-Chol in Binary Mixtures of DMPC and Cholesterol: Composition Dependence	184
	3. Lateral Mobility of NBD-PE and NBD-Chol in Egg PC Liposomes: Temperature Dependence	190
	4. Lateral Mobility of NBD-PE and NBD-Chol in Mixtures of Egg PC and Cholesterol: Composition Dependence	193
C.	Discussion	193

Page

Chapter 8. Lateral Mobility of Phospholipid and Cholesterol: Erythrocyte Membrane..... 200
A. Methods..... 200
B. Results..... 202
C. Discussion..... 206

Chapter 9. Discussion..... 211
A. Comparisons with Measurements of Translational and Rotational Diffusion..... 212
B. Models of Erythrocyte Membrane Structure..... 222
C. Concluding Remarks..... 238

References 240

Appendix A. Machine Language Program for KIM-1 Microprocessor 272

Appendix B. Schematic of Shutter Interface for KIM-1 Microprocessor..... 281

TABLES

		Page
1.	Erythrocyte membrane lipids	8
2.	The major erythrocyte membrane proteins and glycoproteins	11
3.	Lateral mobility of selected membrane proteins	49
4.	Lateral mobility of selected membrane lipid analogues	53
5.	Lateral mobility of selected proteins and lipids in artificial membranes	57
6.	Selective extraction experiments on eosin-labeled ghost membranes	93
7.	Effect of low ionic strength on lateral mobility of band 3: initial studies	122
8.	Rebleaching experiments on eosin-labeled ghost membranes.	132
9.	Effect of PMSF on lateral mobility of band 3	135
10.	Effect of low ionic strength on lateral mobility of band 3: addition of protease inhibitors	138
11.	Proteolysis of membrane proteins	161
12.	Effect of hypertonic KCl on lateral mobility of band 3	171
13.	Effect of 80K spectrin fragment on lateral mobility of band 3	178
14.	Lateral mobility of NBD-PE and NBD-Chol in DMPC multilamellar liposomes: direct comparisons	186
15.	Lateral mobility of NBD-PE and NBD-Chol in DMPC/cholesterol multilamellar liposomes	188
16.	Lateral mobility of NBD-PE and NBD-Chol in egg PC multilamellar liposomes	192
17.	Lateral mobility of NBD-PE and NBD-Chol in egg PC/cholesterol multilamellar liposomes	195

Page

18. Lateral mobility of NBD-PE and NBD-Chol in extracted erythrocyte lipid multilamellar liposomes..... 203

19. Lateral mobility of NBD-PE and NBD-Chol in erythrocyte ghost membranes..... 205

20. Effect of ionic strength on lateral mobility of NBD-PE in erythrocyte ghost membranes..... 207

21. Estimates of membrane viscosity..... 218

FIGURES

		Page
1.	Models for membrane structure	2
2.	SDS-polyacrylamide gel electrophorogram of erythrocyte membrane proteins.....	10
3.	Structure of band 3.....	19
4.	Structure of the erythrocyte cytoskeleton.....	28
5.	Parameters involved in a typical fluorescence photobleaching recovery experiment.....	59
6.	Fluorophore concentration profiles immediately after bleaching with a Gaussian laser beam.....	62
7.	Ratio of fluorescence immediately after bleaching to fluorescence before bleaching vs. bleaching parameter....	63
8.	Fluorescence recovery F(t) vs. t/τ_D for diffusion.....	65
9.	Fractional fluorescence recovery f(t) vs. t/τ_D for diffusion.....	65
10.	Fractional recovery f(t) vs. t/τ_F for flow.....	65
11.	Optical and electronic system for fluorescence photobleaching recovery.....	68
12.	Scheme for rapid removal and replacement of neutral density filter.....	73
13.	Factor γ vs. K for a Gaussian beam.....	79
14.	Flow recovery curve on immobile fluorophore used for beam calibration.....	83
15.	SDS-polyacrylamide gel electrophoresis of eosin-labeled ghost membranes.....	91
16.	Elution profile from DEAE-cellulose column used to purify 72,000 dalton ankyrin fragment.....	98
17.	SDS-polyacrylamide gel analysis of purification of 72,000 dalton ankyrin fragment.....	100

Page

18. SDS-polyacrylamide gel electrophoresis of purified 80,000 dalton spectrin fragment..... 104

19. Aluminum sample holder outfitted for precise temperature regulation..... 115

20. Experimental FPR curves on eosin-labeled erythocyte ghosts at the extremes of ionic strength and temperature. 123

21. Diffusion coefficients and fractional recoveries of fluorescence obtained from FPR experiments on eosin-labeled erythrocyte ghosts as functions of ionic strength, at various temperatures..... 125

22. Reversibility of diffusion coefficients and fractional recoveries of fluorescence..... 127

23. Diffusion coefficients and fractional recoveries of fluorescence as functions of incubation time at 37°C in 13 mM $NaPO_4$ buffer..... 130

24. Diffusion coefficients and fractional recoveries of fluorescence obtained from FPR experiments on eosin-labeled erythrocyte ghosts in 16.2 mM $NaPO_4$ buffer, as functions of the concentration of PMSF, at various temperatures..... 136

25. Diffusion coefficients and fractional recoveries of fluorescence obtained from FPR experiments on eosin-labeled erythrocyte ghosts, in the presence of the protease inhibitors PMSF (60 μM), EDTA (1 mM), and pepstatin A (1 μg/ml), as functions of ionic strength, at various temperatures..... 139

26. Diffusion coefficients and fractional recoveries of fluorescence obtained from two independent FPR experiments on eosin-labeled erythrocyte ghosts, in the presence of the protease inhibitors PMSF (60 μM), EDTA (1 mM), and pepstatin A (1 μg/ml), as functions of incubation time at 37°C, in 13.9 mM $NaPO_4$ buffer..... 141

27. Dissociation of spectrin from eosin-labeled erythrocyte ghosts with decreasing phosphate concentrations..... 152

28. Dissociation of spectrin from eosin-labeled erythrocyte ghosts with decreasing phosphate concentrations in the presence and absence of 100 μg/ml saponin..... 154

Page

29. Dissociation of spectrin from eosin-labeled erythrocyte ghosts with increasing time of incubation under low and high ionic strength conditions..... 158

30. Integrity of erythrocyte membrane proteins as a function of incubation time at 37°C under low and high ionic strength conditions..... 162

31. Diffusion coefficients and fractional recoveries of fluorescence obtained from FPR experiments on eosin-labeled erythrocyte ghosts, as functions of ionic strength, at various temperatures..... 172

32. Effect of specific cytoskeletal perturbation on diffusion coefficients and fractional recoveries of fluorescence obtained from FPR experiments on eosin-labeled erythrocyte ghosts..... 174

33. Diffusion coefficients and fractional recoveries of fluorescence obtained from FPR experiments on eosin-labeled erythrocyte ghosts as functions of incubation time at 37°C..... 175

34. Lateral diffusion coefficient of NBD-phosphatidylethanolamine and NBD-cholesterol in dimystoylphosphatidylcholine multilamellar liposomes..... 185

35. Lateral diffusion coefficient of NBD-phosphatidylethanolamine and NBD-cholesterol in binary mixtures of dimyristoylphosphatidylcholine and cholesterol..... 187

36. Lateral diffusion coefficient of NBD-phosphatidylethanolamine and NBD-cholesterol in egg phosphatidylcholine multilamellar liposomes..... 191

37. Lateral diffusion coefficient of NBD-phosphatidylethanolamine and NBD-cholesterol in mixtures of egg phosphatidylcholine and cholesterol..... 194

38. Lateral diffusion coefficient of NBD-phosphatidylethanolamine and NBD-cholesterol in egg phosphatidylcholine multilamellar liposomes, egg phosphatidylcholine: cholesterol multilamellar liposomes, multilamellar liposomes prepared from total lipid extracts of erythrocyte ghost membranes, and erythrocyte ghost membranes..... 204

INTRODUCTION

Cell membranes exist in a dynamic state. The observed lateral mobility of various membrane components has been instrumental in the formulation of a series of models for membrane structure and function introduced over the past decade. The fluid-mosaic model of Singer and Nicolson (ref. 1, fig. 1a) proposes that the major structural feature of cell membranes is a fluid lipid bilayer in which a population of proteins heterogeneous in size, shape, orientation, and function is embedded. Such a mosaic has no long range order, and integral proteins are free to undergo translational diffusion within the membrane at rates determined both by lipid viscosity and by specific interactions (unspecified) with other intramembranous or extramembranous components. Functional roles for unrestricted translational diffusion are hypothesized in the enhancement of reaction rates on the membrane and in the rapid communication of signals across the plane of the membrane (1,2). Evidence in support of the fluid-mosaic model has been reviewed (1-3); much of the evidence will be presented in this thesis as part of the literature review.

The concept of controls or restrictions on the lateral mobility of membrane elements has proven to be an even more interesting avenue of investigation than the notion of lateral mobility itself. The fact that ligand binding by a cell surface receptor protein, for example, can lead to restriction of the lateral mobility of

Figure 1. Models for Membrane Structure

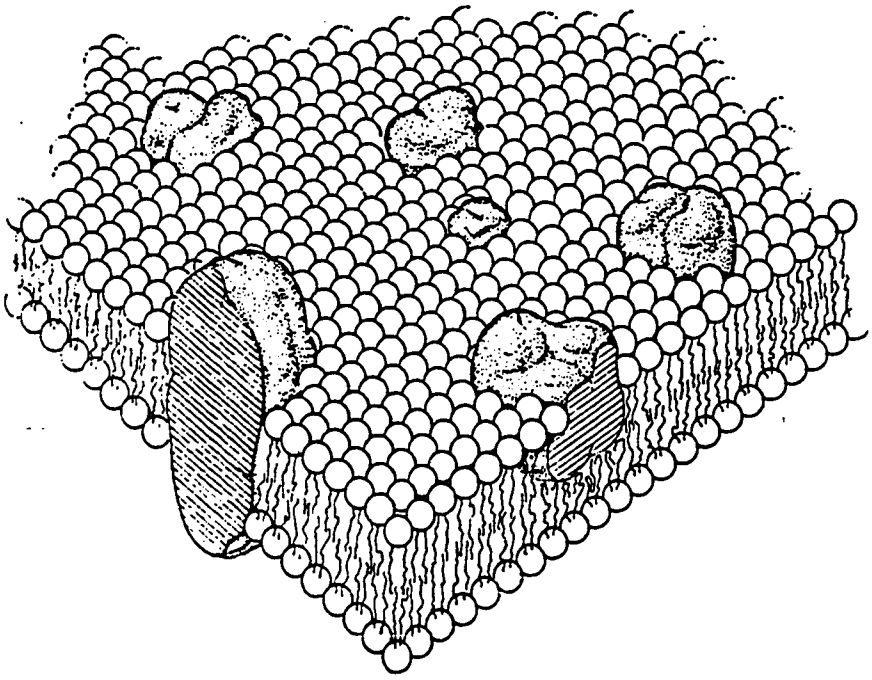

a. Fluid-Mosaic Model (ref. 1)

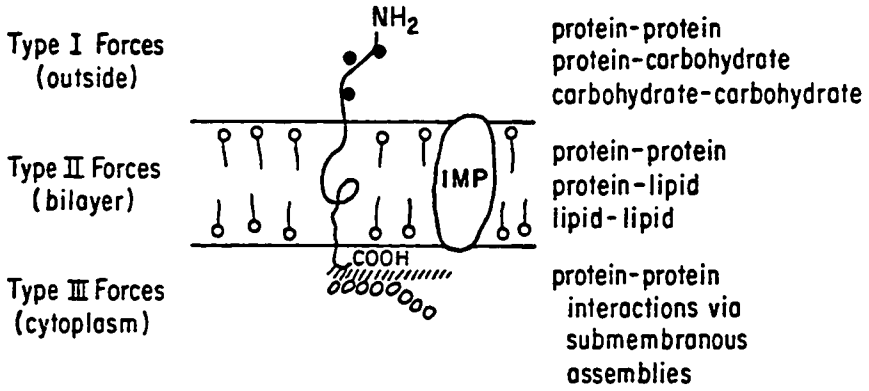

b. Forces Acting on Transmembrane Glycoproteins (ref. 5)

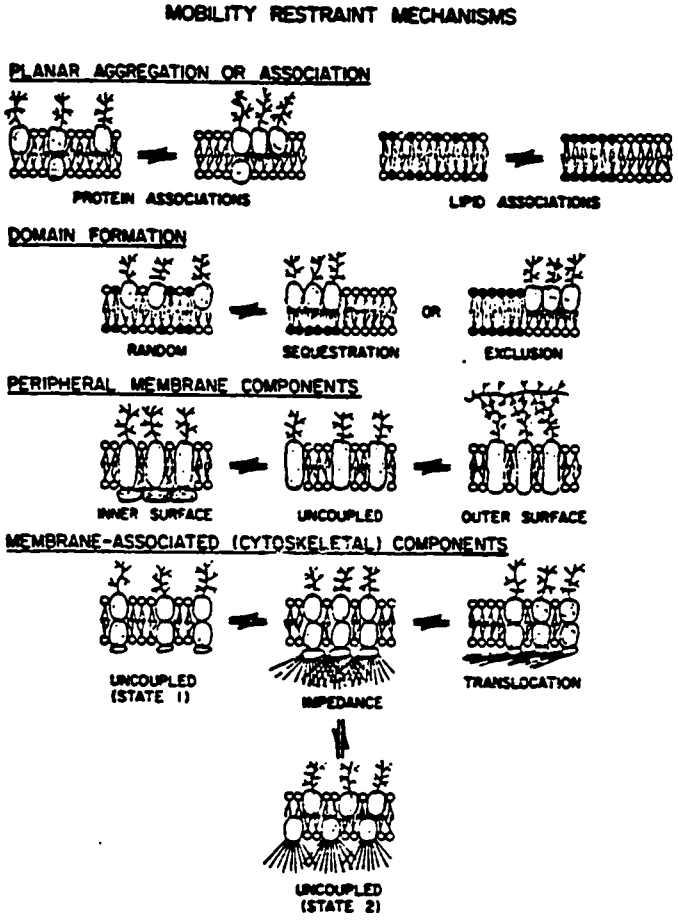

c. Restraint Mechanisms on Lateral Mobility of Membrane Glycoproteins (ref. 4)

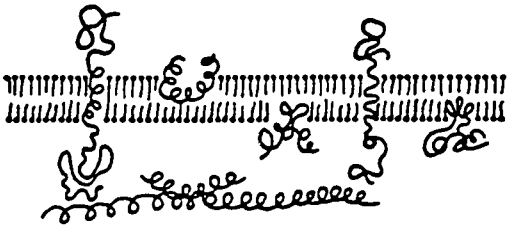

FLUID-MOSAIC

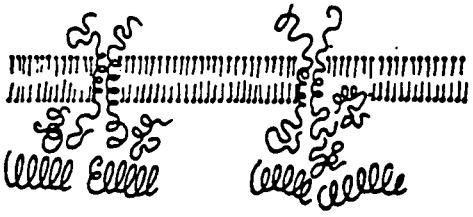

FIXED-MATRIX

d. Fixed Protein Matrix Model (ref.8)

membrane components and thereby influence cell behavior has been shown in several systems (reviewed in 2,4,5). In order to account for such observations, Edelman (ref. 5, fig. 1b) and Nicolson (ref. 4, fig. 1c) have stressed the importance of intramembranous (and especially transmembranous) forces in the modulation of lateral mobility. Unlike the earlier fluid-mosaic model, in which the dominant factor affecting protein mobility is assumed to be the fluidity of the lipids, the later models consider protein-protein interactions both within the lipid bilayer and at the inner surface of the membrane to be the controlling features of many systems. Evidence for the importance of such interactions has come mainly from studies of antibody-induced patching and capping on lymphoid cells, cross-linking of surface glycoproteins by lectins leading to inhibition of patching and capping on lymphoid cells (anchorage modulation), and ligand-induced redistribution and capping on fibroblast cells (reviewed in 4,5; see also 6,7).

With specific reference to the erythrocyte membrane, Marchesi (8) has proposed a fixed protein matrix model as an alternative to the fluid mosaic model (fig. 1d). In this formulation, protein-protein interactions are clearly of primary importance. The major peripheral protein, spectrin, is visualized as being along the inner membrane surface in a shell or matrix of closely-packed units, which may interact with integral, transmembrane proteins. This matrix could then support the overlying lipid bilayer. Translational dif-

fusion of membrane elements is not precluded by such a model, though one would expect mobility to be much more restricted in a membrane organized on a framework of fixed protein than in one governed by a fluid lipid bilayer. For example, in order for an integral transmembrane protein which is complexed to the fixed (inner surface) protein matrix to undergo lateral diffusion, either the transmembrane protein-peripheral protein complex would have to be dissociated, or the peripheral protein matrix itself would have to be disrupted.

This thesis addresses the question of restrictions on the lateral mobility of a well-characterized transmembrane protein, band 3, in a well-characterized mammalian cell membrane, that of the human erythrocyte. Although the erythrocyte does not possess the microtubule and microfilament systems important in control of lateral mobility in other mammalian cells, similar interactions between transmembrane proteins and peripheral (cytoskeletal) proteins might be expected to apply. The advantage of studying the lateral mobility of the major protein of the erythrocyte membrane is that, if mobility is restricted by membrane-associated forces, it should be possible to dissect out those forces in detail since all the major protein and lipid components of this membrane are known and fairly well characterized. Furthermore, there already exists indirect evidence for restricted lateral mobility of band 3 (ref. 9, 10). In this thesis, then, I present a systematic and direct study of the restriction on lateral mobility of band 3 in the human ery-

throcyte membrane. I demonstrate conditions under which the restrictions on mobility are progressively lifted, and correlate the changes in lateral mobility with specific biochemical perturbations of the erythrocyte cytoskeleton. Finally, I compare the lateral mobility of band 3 with that of phospholipid and cholesterol in the erythrocyte membrane, and propose a model involving at least two separate processes capable of restricting the lateral mobility of band 3. It is hoped that this research will lead to even more specific correlations between changes in lateral mobility of transmembrane proteins and both membrane structure and membrane function.

This thesis begins with a critical summary of the published literature on the erythrocyte membrane, with particular reference to band 3 and evidence for its associations with other membrane components. Various techniques for the measurement of lateral diffusion of proteins and lipids on membranes are also described, concentrating on the technique of fluorescence photobleaching recovery. Chapters 2-8 comprise the experimental sections of this report. Finally, chapter 9 includes a discussion of my data in the light of previous work in this field as well as several models for the interactions of band 3 with the erythrocyte membrane which could account for my observations.

CHAPTER 1. LITERATURE REVIEW

A. THE ERYTHROCYTE MEMBRANE

1. General Review of Structure

a. The Lipid Bilayer. The lipid composition of the erythrocyte membrane is shown in table 1. These lipids are believed to be organized as a fluid bilayer extending completely around the surface of the cell (reviewed in 2,11). The first clear demonstration of the characteristic trilaminar pattern on electron microscopic observation of the erythrocyte membrane has recently appeared (12), suggesting the presence of a continuous lipid bilayer at the erythrocyte surface. Within the membrane, various phospholipid classes are asymmetrically distributed in specific halves of the bilayer (reviewed in 3,11,13,14). Through comparison of phospholipid degradation due to the action of purified phospholipases (A_2,C, and sphingomyelinase) on intact erythrocytes *versus* that on permeable ghost membranes, it was shown that approximately 70% of the membrane phosphatidylcholine and 80-90% of the total sphingomyelin (both choline-containing phospholipids) are located in the outer half of the bilayer. Study of phospholipid labeling on intact erythrocytes by permeable *versus* impermeable amino group reagents further revealed that 80-90% of the membrane phosphatidylethanolamine and all of the phosphatidylserine (both amino-containing phospholipids) are located in the inner half of the membrane. Although erythrocyte

TABLE 1. ERYTHROCYTE MEMBRANE LIPIDS.

Component	Mole % Total Lipid	Reference
cholesterol	44.4	19
PE[a]	13.1	20
PS	7.3	20
PI	3.1	20
PC	19.0	20
SM	13.1	20

a abbreviations: PE, phosphatidylethanolamine
PS, phosphatidylserine
PI, phosphatidylinositol
PC, phosphatidylcholine
SM, sphingomyelin

membranes have a high cholesterol content (approximately equimolar with phospholipid), the distribution of this neutral lipid between the two halves of the bilayer has not been determined precisely. It is, however, present in abundance in both bilayer leaflets (15-17), and its transmembrane movement or "flip-flop" appears to be quite rapid (half-time of 3 sec at 37°C; see 18).

b. The Proteins. The literature concerning the polypeptides of the erythrocyte membrane has been extensively reviewed in the past decade (3,8,11,21-24). Denaturation and separation of the various polypeptides from the membrane lipid and from each other can be achieved by dissolution of erythrocyte membranes in sodium dodecyl sulfate (SDS). Polyacrylamide gel electrophoresis of SDS-treated membranes reveals eight major protein bands when stained with Coomassie blue and four additional glycoprotein bands when stained with PAS-Schiff reagent (25); these bands are named according to their relative mobilities on the gel (fig. 2; table 2). Singer and Nicolson (1) have categorized the polypeptides according to the ease with which they can be extracted from the membrane. Those proteins extractable by simple manipulation of the ionic strength or pH of the medium (bands 1,2,4,5,6) are considered peripheral or extrinsic to the membrane, and are presumably membrane-bound through electrostatic interactions alone. Those polypeptides extractable only with detergents or other chaotropic agents (bands

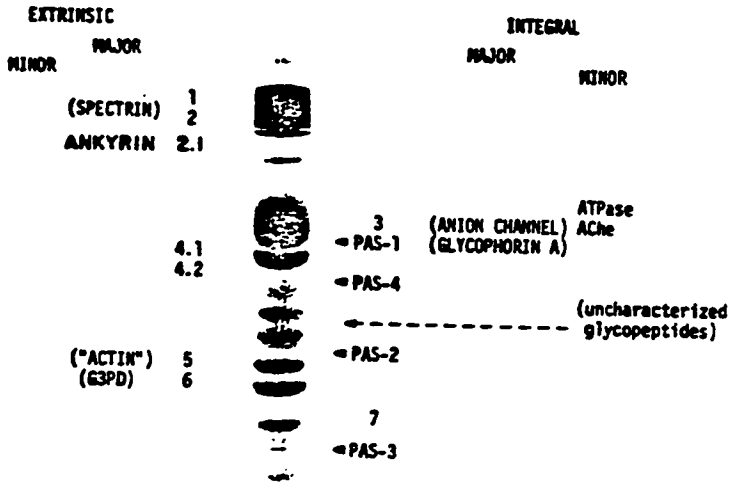

Figure 2. SDS-polyacrylamide gel electrophorogram of erythrocyte membrane proteins stained with Coomassie blue. See text for details. (taken from ref. 11)

TABLE 2. THE MAJOR ERYTHROCYTE MEMBRANE PROTEINS AND GLYCOPROTEINS[a]

Component	molecular wt. (daltons)	% of total protein	copies/cell	% carbohydrate
1	240,000	15	216,000	
2	215,000	15	235,000	
2.1[b]	200,000	6	100,000	
3	88,000	24	940,000	4-9
4.1	78,000	4.2	180,000	
4.2	72,000	5.0	238,000	
5	43,000	4.5	359,000	
6	35,000	5.5	540,000	
7	29,000	3.4	403,000	
PAS-1[c]	62,000	6.7(2.8)[d]	500,000	60
PAS-2	31,000			60

[a]All values from ref. 24 unless otherwise indicated.
[b]Values from ref. 26
[c]Values from refs. 24,27
[d]6.7% by total weight: 2.8% by weight of protein portion.

3,7,PAS-1,2,3,4) are considered integral or intrinsic membrane proteins; they are presumably anchored in the membrane through hydrophobic interactions with membrane lipid.

More recently, Marchesi (8) has classified the various membrane proteins according to function. Those polypeptides exposed to the extracellular environment are termed contact or receptor proteins; they include glycophorins A and B and band 3 as well as several minor, poorly characterized components. All of these proteins are glycoproteins oriented such that their carbohydrate is accessible at the outer membrane surface. It is interesting that the major contact proteins are also exposed to the intracellular surface (3,11); as we shall see, this may be important in their mode of attachment to various membrane elements. Transmembrane proteins involved in the transport of ions or metabolites, as well as various glycolytic enzymes which are located on the inner membrane surface, are grouped together as catalytic proteins. Bands 3 (anion permeation site) and 4.5 (glucose permeation site) are examples of transport proteins; band 6 (glyceraldehyde-3-phosphate dehydrogenase) and aldolase are two membrane-bound enzymes involved in glycolysis. The third major class of polypeptides consists of peripheral membrane proteins which are found exclusively at the inner membrane surface and are involved in stabilizing the membrane structure. These proteins are named support proteins, and include spectrin (bands 1,2), ankyrin (band 2.1),

actin (band 5), and bands 4.1 and 4.2 (refs. 11,26,28). The remainder of this review of the erythrocyte membrane will focus on band 3 and its possible interactions with other membrane proteins, including glycophorin and the various cytoskeletal or support proteins.

2. Band 3

a. Physical and Chemical Properties. Band 3 is defined as a heavily stained, diffuse band of protein of about 90,000 daltons on SDS-polyacrylamide gel electrophoresis of human erythrocyte membranes (25; reviewed in 1,11,21-24,29-31). It is the major protein component of the erythrocyte membrane, comprising approximately 25% of the total membrane protein and approximately 80% of the intrinsic membrane protein (24,25,32). An approximate calculation (24,25) estimates the number of band 3 monomers per cell at about 1×10^6. The apparent molecular weight of band 3 covers the range 85,000 - 110,000 daltons; this band spread is usually attributed to extreme heterogeneity of carbohydrate (24, 33-35), although polypeptide heterogeneity cannot be absolutely ruled out without primary sequence data. Heterogeneity of carbohydrate has also been demonstrated by the binding of lectins to band 3, in that concanavalin A binds fairly specifically to band 3 (ref. 37) but only a fraction of band 3 interacts (38,39).

Band 3 has been isolated and purified in a number of laboratories (37,39-45). Its carbohydrate content is estimated at 4-9%

(refs. 24,37,40,46), with mannose, galactose, and N-acetylglucosamine present in approximately 1:2:2 molar ratio, but with little sialic acid (34,37). This composition suggests the presence on band 3 of complex-type oligosaccharides attached to asparagine residues by N-glycosidic bonds (11). Indeed, it has been shown (34) that there is a single primary site of glycosylation in the COOH-terminal part of the molecule, in a region with composition Asx_1Ser_2. The amino acid composition of band 3 is marked by its high proportion (about 40%) of nonpolar residues (21,37,41,46). This observation is consistent with the solubility characteristics of band 3. It is a highly hydrophobic protein that is soluble only in ionic or nonionic detergents (23-25,40,47). Solubilization by Triton X-100 is accompanied by the binding of 0.77 grams of detergent per gram of protein (48).

Several functions have been ascribed to polypeptides in the band 3 region. These include anion transport (46,49-56), NaK ATPase activity (57,58), water permeation (59), acetylcholinesterase activity (60), and amino acid transport (61), and each is presumably mediated by a different protein. It is likely that some of these functions involve very small amounts of protein relative to the total amount in band 3. For example, the total content of NaK ATPase per cell is estimated at three hundred copies (62). It is also possible that some of these functions may not be present in band 3 at all, residing instead in minor proteins which do not

comigrate with band 3 on polyacrylamide gel electrophoresis but which are contaminated with band 3 protein in various other purification procedures. It is pertinent in this regard that reconstitution experiments have demonstrated that glucose transport across the membrane, originally thought to be mediated by band 3 (refs. 63-66), is in actuality probably performed by band 4.5 protein (67-69; reviewed in 70).

Chemical heterogeneity of protein in the band 3 region has been shown in several ways. Treatment of intact erythrocytes with pronase results in cleavage of most of the protein in the band 3 region, but at least three pronase-resistant polypeptides always remain at the location of native band 3 in SDS-polyacrylamide gels (30). Two-dimensional electrophoresis (71,72) and isoelectric focusing (30) separate band 3 into one major and four or five minor components. It is likely, however, that an overwhelming proportion of band 3 polypeptide is homogeneous, since well over 90% of the protein behaves uniformly in various labeling and cleavage studies (73), and peptide maps of protein taken from all parts of the band 3 region on SDS gels appear identical (35). In addition, only a single COOH-terminal amino acid is found (73), as well as a uniformly blocked NH_2-terminus (37,40,41,46,74) and a unique NH_2-terminal tetrapeptide sequence for one proteolytic fragment of band 3 (35).

b. Conformation in the Membrane. The disposition of band 3 in the

membrane has been extensively studied and recently reviewed (29-31). Portions of band 3 are exposed to both the extracellular and intracellular surfaces of the membrane, proving its transmembrane orientation. This conclusion is based on a series of experiments using membrane-impermeable reagents to label either the extracellular surface of intact erythrocytes, the intracellular surface of either resealed ghost membranes or inside-out vesicles (75), or both surfaces of leaky ghost membranes. These probes include: 1) chemical agents such as FMMP[1] (3,76,77), TNBS (78), IBSA (46), DIDS (49-51,56), NAP-taurine (79), and others (32,80-83); 2) proteolytic enzymes (22,24,51,55,75-77,84-88); and 3) iodination catalyzed by the enzyme lactoperoxidase (89-95). For example, one study demonstrated that the same band 3 fragment produced by proteolytic cleavage from the outside was iodinated from the inside (90), while another study showed that band 3 fragments labeled from the inside were different from those labeled from the outside (91). The latter experiment, as well as many others cited above, further implies that the arrangement of band 3

---

[1]Abbreviations used in this section include: formylmethionylmethylphosphate, FMMP; 2,4,6-trinitrobenzenesulfonic acid, TNBS; 1-isothiocyano-4-benzenesulfonic acid, IBSA; 4,4'-diisothiocyano-2,2'-stilbenedisulfonic acid, DIDS; N-(4-azido-2-nitrophenyl)-2-aminoethylsulfonic acid, NAP-taurine.

in the membrane is both asymmetric with respect to the two membrane surfaces and permanent on the time scale of the labeling. It has also been demonstrated that the linear band 3 sequence must cross the membrane at least twice, as the membrane-impermeable (96) sulfhydral reagent N-ethylmaleimide is found to label intracellular cysteine residues on both sides of an extracellular proteolytic cleavage point (97).

Studies completed over the past several years have greatly advanced knowledge concerning the detailed folding of band 3 in the membrane. Chymotrypsin treatment of intact cells generates a pair of membrane-bound fragments of approximate molecular weights 55,000 and 35,000 from band 3, while extracellular trypsin has no effect on band 3 at physiological ionic strength (73,85,87,98). At low ionic strength, however, cleavage by trypsin from the outside can occur (98), implying changes in band 3 conformation with ionic strength. The blocked NH_2-terminus of the protein is located in the 55,000 dalton fragment, while the COOH-terminus is associated with the 35,000 dalton piece (34,35,73,98). Intracellular trypsin treatment produces a membrane-bound fragment of molecular weight 50,000 daltons which stains with a diffuse pattern on SDS gels (55,74,85,87,98); this fragment contains the COOH-terminus. In addition, water-soluble fragments of approximate molecular weights 40,000, 18,000, and 22,000 are produced by intracellular trypsin treatment, where the latter two peptides are fragments generated

from the former by proteolysis at a second cleavage site (87, 99,100). Fukuda et al. (101) used S-cyanylation of the 55,000 dalton chymotryptic fragment of band 3 combined with lactoperoxidase-catalyzed iodination and antibodies directed against the cytoplasmic region of band 3 to show that the 40,000 dalton tryptic fragment bearing the NH_2-terminus is in an intracellular location. Finally, when cells are treated with chymotrypsin on the outer surface followed by trypsin on the inner surface, an approximately 17,000 dalton membrane-bound segment is obtained (87,102); this peptide is labeled by various anion transport inhibitors (73,87,102-105). The binding site for one specific, potent, irreversible anion transport inhibitor has been identified as a particular lysine residue on band 3 (105) located 9000 daltons from the extracellular chymotryptic cleavage site and 6000 daltons from the intracellular proteolytic cleavage site (104). Since the binding site for this inhibitor appears to be near the outer membrane surface (50,51, 106,107), the 15,000 dalton membrane-bound segment may be folded within the lipid bilayer itself. These and other features of band 3 structure have been incorporated into a linear map of various cleavage sites, together with the minimum model for folding of band 3 in the membrane consistent with experimental evidence (fig. 3a,b).

Several lines of experimentation suggest that band 3 exists as a dimer in the membrane. Solubilization of erythrocyte membranes

Figure 3. Structure of Band 3.

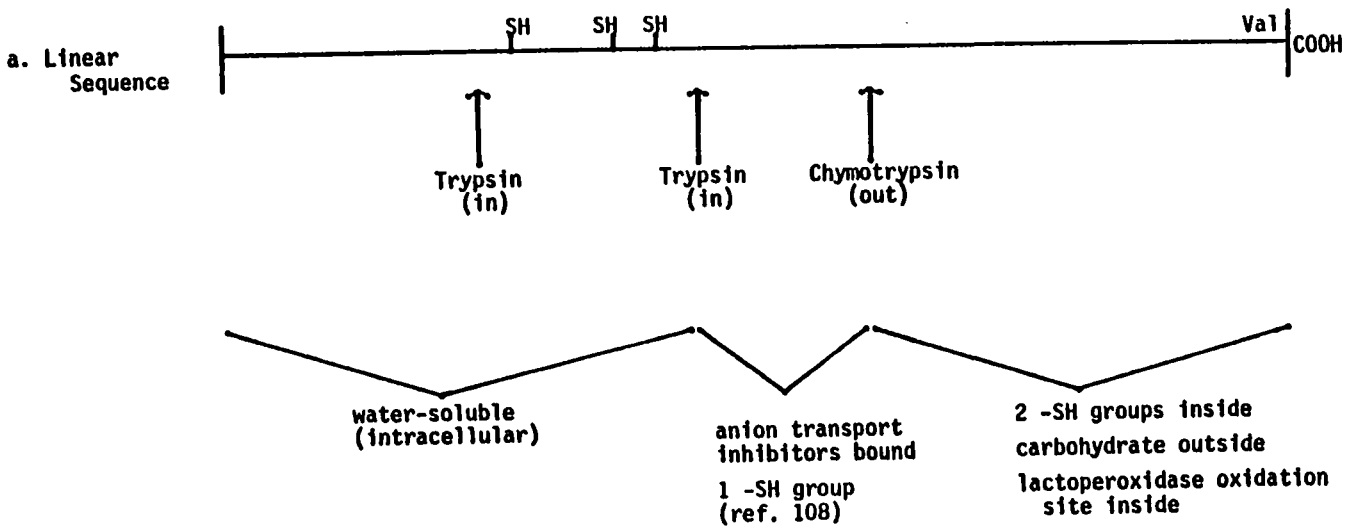

b. Folding in the Membrane.

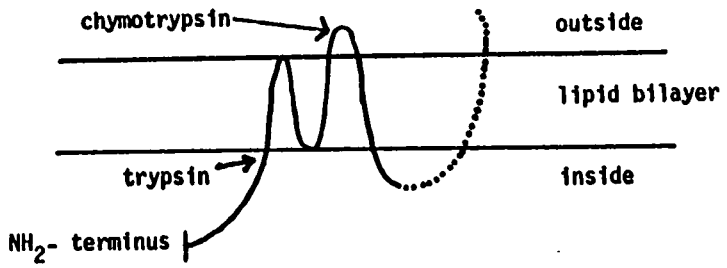

in Triton X-100 results in 180,000 dalton protein which can be quantitatively converted to 90,000 dalton band 3 monomer in denaturing detergents (43,48,109,110). Treatment of intact erythrocytes with noncleavable disulfide cross-linking reagent (111, 112), cleavable bifunctional cross-linking reagent (112,113), cleavable bifunctional photoactivatable cross-linking reagent (114), or membrane-impermeant cleavable bifunctional cross-linking reagent (115) all lead to production of dimer as the major (111-113) or only (114,115) cross-linked band 3 species. Native and cross-linked band 3 in the intact ghost membrane have been reported to have identical rotational correlation times, implying similar cross-sectional areas in the plane of the membrane before and after cross-linking and hence similar states of aggregation in the membrane (116). Negative cooperativity in the binding of aromatic disulfonates to band 3, coupled with the estimation of a relatively short distance between adjacent anion transport sites (28-52A) in the ghost membrane, suggest that adjacent band 3 monomers are very close together and may even possess overlapping transport sites (see below; ref. 117). The site of cross-linking between band 3 monomers appears to reside in the NH_2-terminal, intracellular portion of the molecule (87), specifically in the cysteine-rich 16-20,000 dalton fragment produced by intracellular trypsin cleavage at both of its major sites of proteolysis (99,118) (see fig. 3a).

Freeze-fracture electron microscopy (119-121) of erythrocyte membranes reveals the presence of 80-85A intramembranous particles (IMP) in the cleavage plane, which are presumed to be protein embedded in the center of the lipid bilayer (122). Early studies of the particles, including experiments correlating the distribution of ferritin-conjugated lectins with the distribution of the particles, suggested their connection with glycophorin (120, 122-125). Arguments were soon advanced against glycophorin being the sole constituent of the particles, however, because of its small hydrophobic (intramembrane) portion relative to the large mass of the intramembranous particle (3,21,24). More recent evidence, including correlation between the distribution of ferritin-conjugated DIDS and the particles, has implicated band 3 protein as the major component of the particles in the intact membrane (37,54,126). Eighty Angstrom particles have been seen both in Triton-extracted vesicles containing predominantly (90%) band 3 along with erythrocyte membrane lipids (127) and in membranes reconstituted from purified band 3 and egg phosphatidylcholine (128), as well as in membranes prepared from En(a-) erythrocytes which lack glycophorin A (129). The total number of particles in the intact cell is about 5×10^5 (ref. 125), which is the same as the number of band 3 dimers (24). As the number of glycophorin monomers is also about 5×10^5, some have suggested that the contents of one intramembranous particle might be one band 3

dimer combined with one glycophorin monomer (4,126). It has yet to be demonstrated, however, that there is one particle which contains both molecules. Whereas band 3 alone appears to yield particles of similar size in reconstituted membranes to those in intact cells (128), reconstituted glycophorin particles are smaller and more aggregated than those in intact cells (130). This suggests that glycophorin does not form particles of its own in intact cells, while band 3 may. Rather, glycophorin may either be included in band 3 particles as postulated above or exist free of band 3 in the membrane, becoming artificially included between the particles when they are aggregated (see below).

c. Associations with Other Membrane Proteins. As noted in the previous section, association between glycophorin monomer and band 3 dimer in the intramembranous particles has been postulated. This suggestion has been strengthened by the demonstration of rotational immobilization of band 3 with bivalent (but not univalent) antibodies directed against glycophorin (131). The observations that trypsin degradation of glycophorin in intact cells exposes additional sites on band 3 for interaction with DIDS (51) and lactoperoxidase (132) further imply that at least part of band 3 may be shielded from the outside by glycophorin. On the other hand, extraction of erythrocyte membranes by Triton X-100 readily separates glycophorin from band 3 (refs. 41,109), and cross-linking between glycophorin and band 3 has never been demonstrated chemically (133).

The latter piece of negative evidence must be tempered, however, by the knowledge that glycophorin itself is very resistant to the action of cross-linking reagents, perhaps because of its lack of -SH groups or its extensive glycosylation. Unlike glycophorin, bands 4.2 and 6 remain associated with band 3 after extraction with nonionic detergent. Dissociating agents such as p-chloromercuribenzoate must be introduced in order to separate band 4.2 from band 3, while high ionic strength is sufficient to dissociate the band 3 - band 6 complex (41, 109). The stoichiometry of band 6 binding is one-to-one with band 3, and the site is located in the cytoplasmic NH_2-terminal portion of band 3 which is susceptible to trypsin cleavage (109,134). Specific binding of the enzyme aldolase to the cytoplasmic domain of band 3 has also been demonstrated, in the ratio of one aldolase tetramer per band 3 monomer (135,136). Associations such as these have led some to suggest that the cytoplasmic region of band 3 may be the site of organization of a number of glycolytic enzymes into functional enzyme complexes (137).

Evidence implicating band 3 in direct interactions with various cytoskeletal elements has been accumulating. These data will be presented in a separate section of this literature review, after the organization of the cytoskeleton has been discussed.

d. Functions. Proteins in the band 3 region have been implicated in anion transport, NaK transport, water permeation, amino acid transport, and acetylcholinesterase activity (see above). The

amount of protein involved in the latter four activities is likely to be very small compared to the quantity concerned with anion transport (30). This summary, therefore, will focus on evidence identifying band 3 as the anion transport protein, in the expectation that the various structural properties attributed to the bulk of band 3 will also apply to this functional system.

The importance of anion transport in erythrocytes has long been recognized. Rapid exchange of chloride for bicarbonate across the erythrocyte membrane greatly increases the CO_2 carrying capacity of the blood (62,138). The evidence that band 3 is involved in anion permeation is of three kinds: 1) covalent labeling of band 3 by irreversible inhibitors of anion transport; 2) retention of the anion transport system in erythrocyte membrane-derived vesicles containing band 3 as their major component; and 3) reconstitution of anion transport activity in phospholipid vesicles using partially purified band 3 preparations (reviewed in 29,54, 139).

The most potent and site-specific covalent binding inhibitors of anion transport are the isothiocyano derivatives of stilbene-disulfonic acid such as [^{3}H]-DIDS, [^{3}H]-H_2-DIDS, and [^{125}I]-I_2-DIDS. These compounds irreversibly inhibit anion exchange upon binding, complete inhibition corresponding to 0.9-1.1 x 10^6 molecules bound per cell (49-51,56,140,141). This is also the number of band 3 monomers per cell, providing circumstantial evidence at least for

the role of band 3 in anion permeation. There is further a linear relationship between the inhibition of transport activity and the binding of inhibitor. At maximal inhibitory concentrations, more than 90% of the label is found in the band 3 region on SDS-polyacrylamide gels. The remaining 7-10% is associated mainly with glycophorin. Since anion exchange across the membrane is so rapid, it is argued that the major protein labeled by covalent anion transport inhibitors must, in fact, be the protein involved in anion permeation. Unreasonably high turnover numbers would probably have to be invoked for the exchange process if a minor labeled component, rather than band 3, were responsible for this activity (50,51).

Eosin derivatives (isothiocyanate, iodoacetamide, maleimide) inhibit anion exchange by 50% when approximately 5×10^5 molecules are bound per cell (142). These compounds are irreversibly bound and occupy common binding sites with H_2-DIDS, although other sites on band 3 are labeled as well (142). It is curious that a maleimide derivative, which should react specifically with -SH groups, is reported to be an irreversible ligand for band 3, which has no external -SH groups (97). This question is not addressed by the authors, although the recent suggestion that one band 3-associated -SH group lies within the intramembranous portion of the protein (108) may provide the explanation for this specificity.

There exist substrates of the anion transport system which are also capable of covalent reactions. Thus reduction of pyridoxal-

5-phosphate with $NaBH_4$ (ref. 83) or photoactivation of NAP-taurine (143) leads to inactivation of anion exchange and preferential (DIDS-inhibitable) labeling of band 3. When inhibitor-treated (DIDS, pyridoxal phosphate, or NAP-taurine) intact cells are reacted with proteolytic enzymes under conditions which do not affect anion transport in native erythrocytes (51), nearly all of the nonspecific membrane label, as well as the glycophorin-associated label, is removed from the membrane without affecting band 3-associated label (51,83,143). Taken together, covalent labeling studies provide very strong evidence that inhibition of anion transport is associated with modification of band 3.

Anion permeability is retained in erythrocyte membranes from which almost all the major proteins have been removed except band 3. Changes in ionic strength and pH can be used to remove extrinsic membrane proteins and low concentrations of Triton X-100 to extract the sialoglycoproteins. The remaining vesicles contain essentially all the original lipid of the erythrocyte plus bands 3 and 7. They retain nearly all the permeability parameters of the anion transport system, although some kinetic features cannot be entirely reproduced (127). DIDS-inhibitable anion fluxes can be reconstituted into artificial lipid vesicles using crude Triton X-100 extracts of erythrocyte ghosts (containing band 3 and glycophorin) (52). Purified band 3 protein reconstituted in vesicles containing lecithin, erythrocyte lipids, and exogenous glycophorin mediates

anion exchange which is 60% inhibited by pyridoxal phosphate - $NaBH_4$ (42), although it is not at all certain whether this preparation could transport ions in the absence of glycophorin. More recently, highly purified band 3 (43-45) has been reconstituted into egg lecithin/cholesterol (144) and egg lecithin/phosphatidic acid (43) liposomes; these systems both exhibit sulfate fluxes which are inhibitable by stilbene disulfonates. Reconstitution studies are clearly the only direct and definitive method for proving the relationship between band 3 and anion transport in the erythrocyte membrane, and the reconstitution results to date are not definitive. Nonetheless, an overwhelming body of indirect data implicates more than 90% of band 3 protein in the activity of anion transport.

3. Cytoskeleton

a. Definition and Components. The erythrocyte membrane cytoskeleton can be operationally defined as the insoluble material remaining after extraction of intact erythrocytes or ghosts with the nonionic detergent Triton X-100 (47,145; see 8,146-149 for review). This material contains approximately 60% of the original membrane protein, including all the spectrin (bands 1 and 2), actin (band 5), ankyrin (bands 2.1,2.2,2.3,2.6) and band 4.1 as well as portions of bands 3, 4.2,4.9, and 7 (refs. 47,145,150; fig. 4a). The core of the cytoskeleton apparently comprises bands 1,2,5,4.1, and 4.9, since the shape and structure of the skeleton are retained when

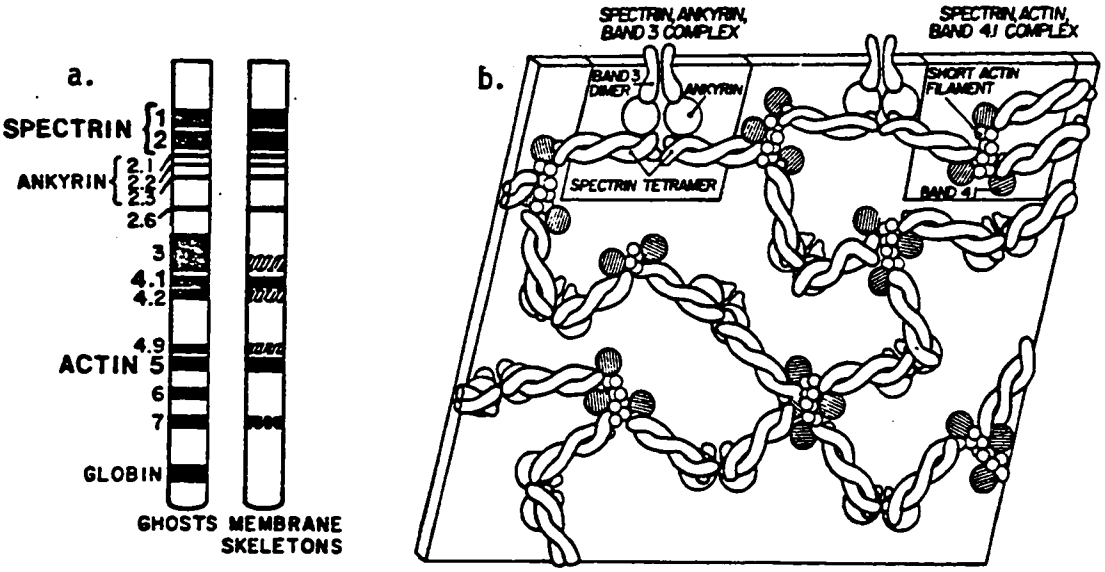

Figure 4. Structure of the Erythrocyte Cytoskeleton

a. Schematized SDS-polyacrylamide gel electrophorogram of erythrocyte ghost proteins and cytoskeletal proteins, as revealed on staining with Coomassie blue.

b. Postulated organization of the cytoskeleton (not to scale).

(taken from ref. 147)

the other elements are eluted with hypertonic KCl (151) but destroyed if either spectrin or actin is removed (152). Spectrin can be localized to the inner membrane surface through the use of ferritin-conjugated antibodies (153); this is the orientation of the cytoskeleton as well.

Early electron micrographs of the cytoskeleton revealed a continuous web-like reticulum consisting of twisted, randomly orientated microfilaments (5-40 nm diameter) irregularly coated with nodular protrusions (30-100 nm diameter) (154). The network appeared to cover approximately 30-35% of the inner membrane surface (146). More recently, thin-section electron microscopy was used to visualize two distinct layers in the cytoskeleton: the first, a granular layer of vertical components which are in direct contact with the overlying lipid bilayer; the second, an anastomosing meshwork of horizontal filamentous components which are attached to the vertical components (155). This bipartite character of the cytoskeleton is reflected in various biochemical studies as well (see below). In combination with the cholesterol-rich lipid bilayer, the cytoskeletal assembly provides support and stability for the erythrocyte membrane, endowing the erythrocyte with both its characteristic shape and its unusual flexibility (see 149, 156 for review; see also 150,157-165).

b. Spectrin: Structure in Solution. The major protein of the cytoskeleton, spectrin, is composed of two high molecular weight poly-

peptides, bands 1 and 2 (molecular weight 240,000 and 220,000 daltons, respectively) (see 8,146,147,166-168 for review). These subunits are similar in structure but not identical (169-171). Purified bands 1 and 2 may be partially digested with proteolytic enzymes at 0°C; each subunit yields multiple, unique proteolytically resistant domains connected by small protease-sensitive segments (171). The linear alignment of these domains along each subunit has been determined (171), and particular domains serving specific binding functions have been identified (172, see below). Bands 1 and 2 associate in solution to form heterodimers (1+2) and heterotetramers $(1+2)_2$ at low concentration (173-178), although at high concentration large oligomeric species are seen as well (179). Spectrin dimers and tetramers are related through an equilibrium which is readily reversible at 29°C but kinetically trapped at 4°C. The tetramer seems to be the physiological species on the intact membrane (114,180-182), although appreciable amounts of dimer (182) and large oligomeric species (179) are found in low ionic strength extracts.

When examined by electron microscopy after low-angle shadowing, purified spectrin heterodimers appear as long (90-105 nm), slender (5 nm), flexible molecules in which two distinct strands lie partially separated or variably coiled in a loose double helix (183). Associations between the strands appear to be weak except at the ends of the molecule, where sites of tight binding exist.

The electron microscopic finding that spectrin dimers exist as long, thin rods in solution is consistent with the results of some (173,184), but not all (175,177), hydrodynamic studies. Spectrin dimers join end-to-end to form tetramers of length 180-210 nm, but higher aggregates are rarely seen (179,183,185). The latter observation indicates a probable head-to-head binding of the dimers, since head-to-tail binding would be expected to produce an abundance of higher order oligomers as well (183). Head-to-head binding has been recently confirmed by the isolation of an 80,000 dalton proteolytic fragment of band 1 which is involved in tetramer formation and is located near one end of the elongated band 1 subunit (172).

c. Spectrin: Polymerization with Actin and Band 4.1. The rarity with which purified spectrin polymerizes beyond the tetramer in solution suggests that at least one other membrane element may be necessary in order to form the anastomosing cytoskeletal reticulum. Stripping of ghost membranes with hypertonic KCl to spectrin, actin, and bands 4.1 and 4.9 alone leaves an intact cytoskeletal network (151), implicating at least one of the latter three proteins in the role of cross-linking spectrin. A mixture containing purified spectrin heterotetramer, filamentous (polymerized) actin (F-actin), and band 4.1 at physiological ionic strength forms a high molecular weight complex consisting of all three elements (186). Electron microscopy of the ternary complex

shows actin filaments linked by spectrin bridges, suggesting that the actin-binding regions of the tetramer are at the tail ends of the molecule (186). Individual spectrin subunits will not substitute for heterotetramer in this reaction (178). Spectrin dimer is univalent in that it binds to but does not crosslink the actin filaments. Globular (unpolymerized) actin (G-actin) also fails to form extended complexes, as do mixtures of any two of the three purified proteins (186).

Other findings consistent with and extending these observations are the following: 1) a crude spectrin extract consisting of spectrin, actin, and band 4.1 greatly promotes the binding of G-actin to spectrin-actin depleted inside-out membrane vesicles (IOV's) (187) and greatly increases the viscosity of a solution of exogenous G-actin (188); 2) oligomeric complexes of purified spectrin, actin, and band 4.1 cause solutions of exogenous actin to gel at high concentration (189) and increase in viscosity at low concentration (190); 3) spectrin tetramer crosslinks F-actin (but not G-actin) into a highly viscous gel, while spectrin dimer binds to but does not crosslink F-actin (191); 4) spectrin tetramers stimulate the binding of F-actin to IOV's, and this stimulation is enhanced by the addition of band 4.1 (192); 5) IOV's reconstituted with purified spectrin dimer or tetramer induce large increases in the viscosity of exogenous G-actin (193). Electron microscopy of such a preparation reveals an extensive

filamentous meshwork underlying the lipid bilayer similar to that present in the original erythrocyte membrane (194); 6) binary complexes between spectrin and band 4.1 (maximum binding ratio 2 band 4.1 monomers per spectrin tetramer; ref. 195), as well as between spectrin and actin (see 147), can form in solution. Electron microscopy of spectrin-band 4.1 complexes indicates that the binding site for band 4.1 (a 60A sphere) is at the opposite end of the molecule from that involved in the polymerization of dimer spectrin to tetramer (196), while images of actin cross-linked by spectrin suggest that the binding site for actin is at the same end of the molecule as the band 4.1 site (197; see above). Finally, the kinetics of exogenous actin polymerization by a spectrin/actin complex suggest the formation of short actin oligomers (average 10 subunits each) cross-linked by spectrin tetramers (198).

Taken together, these studies provide strong evidence for a basic cytoskeletal network composed mainly of long, flexible, bivalent spectrin tetramers cross-linked at each end by actin and band 4.1 (ref. 116; see fig. 4b). The actin is probably present in the form of short oligomers, since the ratio of spectrin monomer to actin monomer in the membrane is roughly one to one (186, 199; see above). Some nonpolymerized or G-actin may also be present (200), as well as some spectrin tetramers which are unassociated with either actin or band 4.1 (ref. 146).

d. Spectrin: Binding to the Membrane. Several modes of interaction between the spectrin-actin-band 4.1 complex and the overlying lipid bilayer have been demonstrated. Purified spectrin binds specifically to a population (about 100,000 per cell) of high-affinity ($K_D \simeq 10^{-7}M$) sites on the inner surface of ghost membranes (201). The binding is ionic strength-dependent, saturable, and reversible under conditions which favor extraction of spectrin from red cell membranes. Band 2 appears to contain the site on spectrin which is involved in binding (172,178,202). Thus, isolated band 2 both binds to the inner surface of erythrocyte membranes and inhibits the binding of native spectrin, while isolated band 1 is inactive in both respects (202); a 50,000 dalton proteolytic fragment of band 2 also inhibits spectrin binding to inside-out vesicles (172). Chymotryptic digestion of spectrin-depleted, inside-out membrane vesicles releases a 72,000 dalton polypeptide which retains spectrin-binding activity in solution and competitively inhibits ($K_I \simeq 10^{-7}M$) the binding of spectrin to vesicles which have not been treated with chymotrypsin (203). Antibody to purified 72,000 dalton proteolytic fragment cross-reacts only with band 2.1 among the membrane proteins; this reaction is blocked in the presence of the 72,000 dalton fragment (26,204). The extrinsic membrane protein band 2.1 is thus identified as the primary attachment site for spectrin in the membrane, and is named ankyrin (26,

196,204). Peptide maps of bands 2.1,2.2,2.3, and 2.6 are all homologous with the 72,000 dalton fragment (205,206), suggesting that a family of closely related spectrin-binding proteins exists on the membrane. Bands 2.2-2.6 have been shown not to be artifactual breakdown products formed from band 2.1 during ghost preparation (207).

Electron microscopy shows the ankyrin binding site on spectrin to be 200A distal to the end of spectrin involved in the dimer-tetramer interaction (185,196). The electron microscopic localization agrees with the biochemical localization of the dimer-dimer binding region and the ankyrin binding region obtained through alignment of proteolytic fragments of bands 1 and 2 serving particular binding functions (172). The stoichiometry of binding on the membrane is not clear. Ratios of spectrin to ankyrin (2 moles spectrin dimer per mole ankyrin) and spectrin to high-affinity binding sites (2 moles spectrin dimer per mole of binding sites) present on the intact membrane might imply that each spectrin heterotetramer is bound to a single high-affinity membrane attachment site containing band 2.1 (refs 26,205). Supporting this notion is the observation that spectrin heterotetramer binding to inside-out vesicles saturates at a ratio of one tetramer to one ankyrin binding site (208), even though binding of heterodimer to ankyrin in solution saturates at a ratio of one dimer per ankyrin binding site (195,204).

In addition to the 72,000 dalton water-soluble fragment which interacts with spectrin, ankyrin contains a 100,000 dalton domain which does not bind spectrin (26). The larger domain is membrane-bound but not transmembrane, since it cannot be labeled from the extracellular surface of the membrane in intact cells (24) and since it can be eluted from the membrane in dilute acid without detergent (26). Interactions between band 3 and ankyrin, probably involving this 100,000 dalton domain, are discussed below.

It is important to note that the binding studies summarized above are performed under conditions such that associations between spectrin and the membrane with $K_D > 10^{-6}M$ would not be detectable (26). Spectrin may therefore interact in a meaningful way, although with lower affinity, with proteins other than ankyrin or with membrane lipids. Evidence for spectrin-lipid interactions includes the following: 1) spectrin extracts stabilize artificial phospholipid vesicles and prevent calcium-induced vesicle fusion (209); 2) spectrin stabilizes membrane phospholipid asymmetry in that oxidative cross-linking of spectrin allows 30-50% of the inner membrane phospholipids (phosphatidylserine and phosphatidylethanolamine) to become accessible at the outer membrane surface (210); 3) spectrin is easily crosslinked to inner membrane phospholipids in the intact red cell (211); and 4) purified spectrin penetrates synthetic and natural phospholipid monolayers with a

strong preference for negatively charged over zwitterionic or neutral lipids (212). Band 4.1 may be involved in the attachment of spectrin to the membrane, as it binds to inside-out vesicles depleted of spectrin and actin (148) and antibodies to it inhibit the binding of spectrin to such vesicles (202). In addition to spectrin, actin may play a role in attaching the cytoskeleton to the membrane, since F-actin but not G-actin can bind directly to a trypsin-sensitive site on spectrin-depleted inside-out vesicles (187).

One model for the organization of the principal proteins of the cytoskeleton which is consistent with the data available is given by Lux (ref. 147; see fig. 4b).

4. Band 3 - Cytoskeleton Interactions

a. Band 3- Ankyrin. Triton X-100 extracts of spectrin-depleted erythrocyte membranes contain ankyrin tightly linked to band 3 in one-to-one molar ratio (213). This crude complex, which may also include some band 4.2, involves 10-15% of the total band 3 in the membrane. The ankyrin-linked band 3 has a transmembrane orientation and appears to be nearly identical to the remaining band 3 by peptide mapping and immunologic cross-reactivity. Solubilized ankyrin-linked band 3 binds purified spectrin, while free band 3 does not (213). A 43,000 dalton proteolytic fragment of the cytoplasmic domain of band 3 competitively inhibits the binding of ankyrin to

stripped inside-out membrane vesicles (214,215), and the same fragment associates with high affinity in a 1:1 ratio with purified ankyrin in solution (215). There are approximately 100,000 ankyrin binding sites on each ghost membrane, or about 1/10 the number of band 3 monomers present (214,215). Finally, detergent-extracted cytoskeleton preparations are always found to contain a certain amount of firmly bound band 3. Taken together, these data implicate 10-15% of the total band 3 as the ultimate membrane attachment site for spectrin, ankyrin serving as a link between the cytoplasmic portion of band 3 and band 2 of spectrin (213-215).

The stoichiometry of this linkage is as yet unresolved. If ankyrin-linked band 3 has the same tendency as the major portion of band 3 to dimerize in situ (41,111,116,128), then one would expect the ankyrin-linked band 3 oligomer to be arranged with two moles each of band 3 and ankyrin. Such a stoichiometry is supported by the finding that band 2.1, like band 3, is cross-linked in dimeric form (111). On the other hand, ratios of total spectrin to total ankyrin in the membrane suggest the binding of one spectrin tetramer by one band 2.1 monomer, if all the spectrin is linked to ankyrin. Since cross-linking and solubilization studies have consistently failed to demonstrate the presence of spectrin hexamer or octomer on the membrane, it seems unlikely that two spectrin tetramers would be organized in close proximity by (band 3-ankyrin)$_2$ oligomers. Assuming that the spectrin tetramer is symmetric (183), with one

ankyrin binding site per dimer (196), such an arrangement would also leave one end of each spectrin tetramer unattached to ankyrin. One possible resolution to this dilemma stems from the observation that, at physiological ionic strength, approximately 45% of the total spectrin is present as dimers and tetramers which are unassociated with actin or band 4.1 in both ghost extracts (216) and membrane cytoskeletons prepared directly from intact erythrocytes (145,217). If, at any one time, approximately 50% of the spectrin in the intact membrane is also unassociated with ankyrin (perhaps bound to the membrane through interactions with lipid), and 90% of the band 3 is further unbound to ankyrin, complexes involving one spectrin tetramer and one ankyrin dimer-linked band 3 dimer would be consistent with all the available data (see fig. 4b).

b. Band 3 - Spectrin. Information regarding direct band 3 - spectrin interactions on the intact erythrocyte membrane has been gathered using four general techniques: copurification of detergent-extracted band 3 with other membrane componenets; inhibition of spectrin binding to spectrin-depleted inside-out vesicles; perturbation of membrane composition leading to aggregation of intramembranous particles on freeze-fracture electron microscopy; and cross-linking of membrane components in situ under various conditions. No direct associations between band 3 and spectrin or actin are observed in Triton X-100 extracts of ghost membranes, as judged by the ready separation of

these proteins on ion exchange chromatography and rate zonal sedimentation (41,109). If such associations are especially sensitive to dissolution by nonionic detergents, however, they would not be seen in this system. Close proximity between the cytoplasmic segment of band 3 and the membrane binding site(s) for spectrin is demonstrated by experiments showing that antibodies directed against the cytoplasmic segment of band 3 inhibit the binding of spectrin to inside-out vesicles (202).

Evidence has been presented linking band 3 to the intramembranous particles seen on freeze-fracture electron microscopy. In the native erythrocyte membrane, these particles assume a random, dispersed distribution which cannot be perturbed by agents such as multivalent ligands, proteolytic enzymes, or low pH treatments (218,219). When the inner membrane surface is made accessible by hypotonic lysis of erythrocytes, however, low pH (<5.8) (refs. 218-220) or trypsin treatment (124,220,221) causes the particles to become clustered. Incubation of ghost membranes with bivalent but not monovalent antispectrin antibody at the inner membrane surface also causes aggregation of colloidal iron hydroxide-labeled sites (glycophorin) at the outer surface (222). All conditions which favor precipitation of solubilized spectrin-actin extracts (low pH, Ca^{++}, Mg^{++}, polylysine, basic proteins) also induce intramembranous particle aggregation in partially spectrin-depleted ghost membranes (219,223). The same spectrin-aggregating

conditions also cause release from fresh ghosts of small lipid vesicles which are free of both spectrin and integral membrane proteins (223). Low pH -induced clustering of particles reconstituted in egg phosphatidylcholine vesicles is dependent on prior binding of solubilized spectrin-actin extracts (128). Spectrin (visualized by ferritin-conjugated antispectrin) is clustered on the inner membrane surface in patches directly underlying intramembranous particle aggregates (224). Branton and coworkers have synthesized these data into a model in which spectrin and intramembranous particles are involved in strong, specific interactions. The particles are thought to be immobilized by spectrin in the intact membrane. They are therefore incapable of aggregation, a process which must involve lateral movement in the membrane. The particles are mobilized only on partial depletion of spectrin from the membrane, although the presence of some residual spectrin seems to be necessary for particle aggregation. It is the precipitation of this residual spectrin into small patches on the inner membrane surface which is thought to cause the clustering of the particles (128,129,223, 224).

Chemical evidence of <u>in situ</u> interactions between band 3 and spectrin is seen in the results of various cross-linking studies (see 133 for review). Bands 1 and 2 are more readily cross-linked by dimethylmalonimidate in ghosts which have been pretreated with

multivalent Ricinus communis lectin (225), which binds fairly specifically to band 3 on the outer surface of ghost membranes (38). Cross-linking of ghost membrane proteins induced by cleavable bifunctional reagents results in very high molecular weight (>3.5 x 10^6 dalton) complexes which contain spectrin, actin, ankyrin, and band 3 as well as bands 4.2 and 6 (refs. 112-114,226). Unfortunately, it is not possible to determine which of these proteins is cross-linked directly to spectrin. Disulfide-linked complexes involving bands 1+3, bands 2+3, and bands 5+3, as well as heterogeneous aggregates containing bands 1+2+3+4.2+5, are created spontaneously in ghost membranes exposed at low ionic strength to acid pH (pH 4.0-5.5, temperature 0-4°C) or elevated temperature (37°C) (ref. 227). Such complex formation involving spectrin is maximal near its isoelectric point (228) which is also its precipitation point in solution (128,174,219). Furthermore, a complex of bands 1+3 (yield unspecified) results from catalytic oxidation of ghost membranes at pH 7.4 and physiological ionic strength (but not at low ionic strength) (167). These observations suggest to the authors that decreased electrostatic repulsion between adjacent proteins on the membrane may be responsible for changes in cross-linking with pH and ionic strength (167,227). An alternative explanation could involve more specific rearrangements of cytoskeleton structure with pH and ionic strength, such as conformational changes or polymerization of various membrane components.

The data presented in this section support the contention that band 3 interacts rather intimately with spectrin in the erythrocyte membrane. Whether this interaction involves actual binding of band 3 by spectrin or simply entrapment of band 3 in the underlying cytoskeletal network is an unresolved question. High-affinity binding ($K_D < 10^{-7}M$) has been ruled out by several experiments (26,201,203) but lower affinity binding is still a possibility, since the concentration of spectrin inside red cells may be as high as $10^{-5}M$ (ref. 26). More long-range, but nonetheless specific, connections involving other membrane proteins (actin, band 4.1, band 4.2) or even membrane lipids are also conceivable.

B. MEASUREMENTS OF LATERAL DIFFUSION

1. Protein Diffusion: Biological Membranes

Several methods have been devised for the measurement of protein diffusion in the plane of the membrane (reviewed in 2, 229,230). All of the techniques involve labeling of proteins in some way so that their distribution in the membrane may be visualized. Changes in distribution with time imply lateral movement; under appropriate conditions this motion can be shown to be due to diffusion and can be quantified to permit calculation of diffusion coefficients. The overall scheme of these experiments consists of setting up, by some means, a non-uniform distribution of proteins (usually fluorescently labeled) in the membrane. The relaxation of this distribution to its equilibrium state is then observed with the aid of a (fluorescence) microscope. The most widely used methods are cell fusion and, more recently, photobleaching recovery. These have both been applied to lateral diffusion in the erythrocyte membrane, and will be discussed in detail. Several other methods involve observation of the spreading of a patch of fluorescently-labeled anti-membrane protein antibody after application onto a membrane surface (231), study of the kinetics of return to uniform distribution of fluorescently-labeled membrane receptors which have been electrophoretically aggregated at one end of a cell (232,233), and measurement of the relaxation of a dipole moment caused by electric field induced displacement of the

photopigment distribution on a membrane surface (234).

a. Cell Fusion. Frye and Edidin (235) provided the first evidence that rapid lateral diffusion of membrane proteins may occur. They used inactive Sendai virus to fuse human and mouse cells, and observed the intermixing of the human and mouse surface antigens with time by adding human- and mouse-specific antibodies labeled with different colored fluorescent dyes. Total mixing was seen in 90% of the heterokaryons after a forty minute incubation at 37°C (ref. 235). A coefficient of lateral diffusion (D) of approximately 2×10^{-10} cm^2/sec can be estimated from the intermixing rate (229,236). The intermixing process was insensitive to metabolic inhibitors but sensitive to changes in temperature. Further study showed a decrease in the diffusion coefficient with temperature in the ranges 37°C to 21°C and 15°C to 4°C, but a paradoxical increase with decreasing temperature from 21°C to 15°C (ref. 237). This behavior may be a consequence of lateral phase separations in the membrane lipid (238). A more detailed analysis of the intermixing kinetics revealed that a small population of heterokaryons (10-15%) had cell surface antigens which diffused laterally more rapidly ($D=1-4 \times 10^{-9}$ cm^2/sec) than the antigens of the majority of heterokaryons. This heterogeneity was taken as evidence that, in the majority of cells, integral membrane proteins may not be completely free to diffuse on the cell surface (236). Changes in membrane potential (produced by altering the potassium

ion concentration of the medium or by adding drugs such as ouabain, gramicidin, and diphenylhydantoin) were reported to affect the lateral diffusion rates of surface antigens in those cells (80-85%) which restricted diffusion to some extent, but not the rates of the freely diffusing antigens (239).

Lateral mobility of fluorescein-isothiocyanate-labeled integral membrane proteins of human erythrocytes (>70% of label on band 3 and PAS-1) has also been examined by the cell fusion technique (10). A 50/50 mixture of labeled and unlabeled cells in 310 mOsm phosphate-buffered saline, pH 7.6, was treated with Sendai virus to fuse the cells, and redistribution of fluorescence from the labeled to the unlabeled cells was scored with time. A minimum diffusion coefficient of 4×10^{-11} cm^2/sec at 37°C was calculated. Lateral diffusion was found to be highly temperature-dependent and to be two- to three-fold faster in fresh than in aged (ATP-depleted) cells (10). Incubation of virus-treated (hence "leaky") cells with the 72,000 dalton spectrin-binding fragment of ankyrin resulted in a two-fold increase in diffusion coefficient, although standard errors for the control and experimental values were not stated (240).

b. Photobleaching Recovery. Poo and Cone (241) used the natural chromophore present in rhodopsin to measure the lateral diffusion of this integral membrane protein in the disc membrane of rod outer segments. They partially bleached the rhodopsin molecules

in one half of a single rod outer segment with a light flash, and monitored by absorbance the change in the rhodopsin distribution as the bleached and unbleached molecules diffused laterally in the membrane. A uniform distribution was approached exponentially with a half-time of approximately thirty seconds at 20°C, corresponding to a diffusion coefficient of 4-5 x 10^{-9} cm^2/sec.

The first fluorescence photobleaching recovery experiment was performed on fluorescein-isothiocyanate-labeled erythrocyte membrane proteins (9). Single ghosts suspended in 7 mM sodium phosphate buffer, pH 8.0, were observed in a fluorescence microscope at room temperature (20-23°C) and fluorescein on one half of the ghost bleached with an intense light beam. No significant diffusion of fluorescent material into the bleached half of the ghost was detected in a measuring time of 20 minutes. This data apparently set an upper limit on the average lateral diffusion coefficient of the labeled membrane components of 3 x 10^{-12} cm^2/sec at 20-23°C.

More sophisticated versions of the fluorescence photobleaching recovery (FPR) system have been recently developed (242-252). These methods involve observation, generally in a fluorescence microscope using a sharply focused laser beam for excitation, of a single cell membrane containing fluorescently labeled protein or lipid. A small area of the membrane is exposed to a brief intense pulse of laser light, which causes irreversible photochemical bleaching of the fluorophore in that area. The rate and total amount of recovery of the fluorescence in the bleached region, which results

from lateral diffusion of unbleached fluorophore into the bleached area, are monitored using a photomultiplier tube connected to the emission system of the microscope. Appropriate analysis of the fluorescence recovery curves allows estimation of: 1) the type of process which is leading to the recovery, i.e., diffusion vs. flow; 2) the relative amounts of mobile and immobile fluorophore; 3) the lateral diffusion coefficient of the mobile fraction; and 4) the presence or absence of protein or lipid domains in the membrane comparable in size to the bleaching laser beam. One example of the versatility of the FPR system is seen in an experiment involving the lateral motion of fluorescently labeled acetylcholine receptors in cultured rat myotube membranes (253). Two distinct coexisting classes of receptors are found: a mobile, uniformly distributed population of receptors and an immobile, dense, patchy population of receptors. Diffusion coefficients and fractional recoveries (corresponding to the fraction of fluorophore which is mobile) which have been measured for selected membrane proteins in these and other systems are give in table 3.

2. Lipid Diffusion: Biological Membranes

Electron spin resonance (ESR), nuclear magnetic resonance (NMR), and more recently, fluorescence photobleaching recovery (FPR) have all been used to measure lateral diffusion coefficients of lipids in natural membranes (see 2,230 for review). One caveat in inter-

Table 3. Lateral Mobility of Selected Membrane Proteins

Membrane	Label	Method	temp, °C	Dx10^{11}[a]	f(∞)	Ref.
mouse/human heterokaryon	fl.Ab[b]	cell fusion	15	10		237
		"	21	4		237
		"	37	20		235
rat myotube	fl.Ab	spread of fl. spot	0	<1		231
			21	200		"
Xenopus myoblast	fl.conA[c]	electrophoresis	22	510		233
frog disc	retinal	APR[d]	20	350		241,254
		FPR[e]	20	400		255
		dynamic Kerr effect	20	330		234
erythrocyte ghost (human)	FITC[f]	FPR	20	<0.3		9
	"	cell fusion	0	-	0	10
	"	"	23	0.6		"
	"	"	30	3		"
	"	"	37	4		"
	DATF[g]	FPR	30	9.2		256
erythrocyte ghost (normal mouse)	DATF	FPR	24	4.5		257
(sph/sph mouse)	DATF	FPR	24	250		"
mouse fibroblast	FITC	FPR	23	23		246
	fl.conA	FPR	23	<0.1		258
	fl.insulin	FPR	23	40	0.60	259
	"	"	37	<10	<0.10	"
	fl.EGF[h]	"	23	34	0.67	"
	"	"	37	<10	<0.10	"
	fl.T3[i]	FPR	23	28	0.69	260
mouse 3T3 cell	fl.s-conA[j]	FPR		5-10		261
	fl.conA-pl[k]	FPR		22[l]	0.45[l]	262
	"	"		2[m]	0.45[m]	"
mouse lymphocyte	fl.Ab	FPR		30	0.70	263
	fl.α-sIg[n]	FPR	22	53°	0.65°	6
	fl.α-sIg	"	"	8[p]	0.11[p]	"
rat myotube	FITC	FPR		22	0.25	264
	fl.conA	"		3-4	0.67	"
	fl.Ab	"		20	0.50	265

Membrane	Label	Method	temp, °C	Dx10^{a}	f(∞)	Ref.
diffuse	fl.Bgt[q]	"	22	5	0.75	253
patch	"	"	22	<0.1	0	"
diffuse	"	"	37	16	0.75	"
patch	"	"	37	<0.1	0	"
human embryo fibroblast	fl.WGA[r]	FPR	25	2-20	0.80	244
chick embryo fibroblast	fl.CSP[s]	FPR		0.9	0.15	266
rat mast cell	fl.IgE	FPR		21	0.65	267
human PMN[t]	fl.α-HLA[u]	FPR		15		268
	fl.α-C3bR[v]	"		<1		"
human lymphocyte	fl.α-HLA	"		69		"
mouse ovum						
fertilized	fl.Ab	FPR	25	5	0.18	269
unfertilized	"	"	"	14.5	0.40	"
rat tumor	fl.α-RT1[u]	FPR		110	0.73	270
rat macrophage	"	"		130	0.36	"
rat lymphocyte	"	"		150	0.77	270, 271
glial cell	fl.conA	FPR		4		272
neuroblastoma cell	fl.conA	FPR		12		272
	fl.conA	FPR		6	0.35	273
untreated	fl.s-ConA	FPR		13	0.36	274
differentiated	"	"		-	0.07	"

Table 3. continued.

a. diffusion coefficient in cm^2sec^{-1}
b. fluorescent antibody
c. fluorescent concanavalin A
d. absorbance photobleaching recovery (see text)
e. fluorescence photobleaching recovery
f. fluorescein-isothiocyanate
g. dichlorotriazinylaminofluorescein
h. epidermal growth factor
i. 3,3,5-triiodo-L-thyronine
j. fluorescent succinyl-concanavalin A
k. concanavalin A-conjugated platelets
l. platelets covering <3% of cell surface
m. platelets covering >3% of cell surface
n. antibody against surface immunoglobulin
o. conA-platelets covering <10% of cell surface
p. conA-platelets covering >10% of cell surface
q. fluorescent α-bungarotoxin
r. fluorescent wheatgerm agglutinin
s. fluorescent cell surface protein
t. polymorphonuclear leucocyte
u. antibody against histocompatability antigens
v. antibody against C3b (complement) receptor

preting FPR data on lipid diffusion involves the use of various fluorescent lipid analogs as probes of native lipid mobility. It is not clear that these analogs, which are exogenous compounds introduced into the natural membrane, are true models for endogenous membrane lipid. Diffusion coefficients which have been measured for lipids or lipid analogs in natural membranes are given in table 4, for comparison with the protein diffusion coefficients of table 3. In general, it may be noted that lipid diffusion is much faster than protein diffusion and has higher fractional recoveries (fraction of mobile lipid) than protein diffusion. These comparisons are strong evidence for restriction on the lateral mobility of membrane proteins in many biological systems.

Table 4. Lateral Mobility of Selected Membrane Lipid Analogues

Membrane	Label	Method	temp, °C	Dx10^{11}[a]	f(∞)	Ref.
E. coli	^{31}P	NMR[b]	31	1800		275
sciatic nerve	^{1}H	NMR	31	500		276
sarcoplasmic reticulum	^{31}P	NMR	8	600		276
	"	"	25	1800		275
	"	"	50	1000		276
	SLPC[c]	ESR[d]	25	2500		277
			40	6000		"
liver microsome	SLFA[e]	ESR	20	9500		278
	"	"	30	11000		"
	"	"	40	13700		"
electroplax	^{1}H	NMR	33	>100		276
erythrocyte ghost (human)	diI[f]	FPR[g]	7	90		279
	"	"	40[h]	750[h]		"
	diI	FPR	-3[h]	100[h]		280
	"	"	40[h]	230[h]		"
	"	"	-3[i]	60[i]		"
	"	"	40[i]	230[i]		"
erythrocyte ghost (normal mouse)	NBD-PE[j]	FPR	25	1400		281
(sph/sph mouse)	"	"	"	1500		"
mouse 3T3 cell	diI	FPR		800		266
mouse lymphocyte	diI	FPR		1500	1.00	263
rat myotube	diI	FPR	23	>100	1.00	264
	diI	FPR		900	1.00	265
diffuse	diI	FPR	37	150	0.6	282
patch	"	"	37	120	0.7	"
chick myotube	diI	FPR	12	200	0.9	283
	"	"	30	600	0.9	"
chick myoblast during fusion	K-1[f]	FPR		200	0.85	284
	"	"		300	0.85	"

Membrane	Label	Method	temp, °C	Dx10^{11}[a]	f(∞)	Ref.
chick embryo fibroblast	fl.gan.[k]	FPR		45		266
human PMN[l]	diI	FPR		1700		268
	NBD-PE	"		2300		"
human lymphocyte	diI	"		920		"
mouse ovum						
fertilized	diI	FPR	25	200	0.05	269
unfertilized	"	"	"	1900	0.28	"
neuroblastoma	diI	FPR		1010		274
embryonal carcinoma						
undifferentiated	diI	FPR	23	800	0.8	285
differentiated	"	FPR	"	500	0.8	"
teratocarcinoma	"	"	"	500	018	"
S. typhimurium	fl.LPS[m]	FPR		20	0.9	286
human fibroblast	diI	FPR	5	350		287
	"	"	37	1600		"

Table 4. continued.

a. diffusion coefficient in cm^2sec^{-1}
b. nuclear magnetic resonance
c. spin-labeled phosphatidylcholine
d. electron spin resonance
e. spin-labeled fatty acid
f. carbocyanine dye
g. fluorescence photobleaching recovery
h. normal ghost
i. cholesterol-depleted ghost
j. N-4-nitrobenzo-2-oxa-1,3-diazole-phosphatidylethanolamine
k. fluorescent ganglioside
l. polymorphonuclear leucocyte
m. fluorescent lipopolysaccharide

3. Protein and Lipid Diffusion: Artificial Membranes.

Further evidence for the restriction of protein mobility in biological membranes may be seen in the comparisons between protein and lipid lateral mobilities in artificial as opposed to biological membranes. Unlike natural membranes, in which lipid and protein diffusion coefficients may differ by several orders of magnitude (see tables 3,4), artificial membranes exhibit rates of incorporated protein diffusion which are comparable to those of the bulk lipid (table 5). These relationships will be explored further in the Discussion section of this dissertation.

Table 5. Lateral Mobility of Selected Proteins and Lipids in Artificial Membranes[a]

Membrane	Label	temp,°C	Dx10"	Ref.
DMPC[b]	NBD-PE[c]	20	<10	245
	"	30	8000	"
	NBD-PE	25	6000	288
	"	35	8500	"
	NBD-PE	12	2	247
	"	22	20	"
	NBD-PE	24	6300	289
	"	38	9300	"
	NBD-PE	28	6300	290
	fl.α-hapten[d]	28	5700	"
DMPC:chol[e](1:1)	NBD-PE	20	800	245
	"	30	2000	"
EggPC[f]	NBD-PE	25	4000	245
	"	37	8000	"
	NBD-PE	14	4400	289
	"	38	10100	"
EggPC:chol(1:1)	NBD-PE	25	1800	245
	"	37	3500	"
DMPC	FITC-M-13[g]	25	3000	288
	"	35	4500	"
	glycophorin	>15	1000-2000	291
	"	<15	<5	"
EggPC	FIR-M-13	15	2500	292
	apoC-III[h]	20	3000	293
EggPC:chol(1:1)	"	20	140	"

a. all lateral mobilities assessed by fluorescence photobleaching recovery
b. dimyristoylphosphatidylcholine multibilayers or liposomes
c. N-4-nitrobenzo-2-oxa-1,3-diazole-phosphatidylethanolamine
d. fluorescent anti-nitroxide spin label antibody
e. cholesterol
f. egg yolk phosphatidylcholine
g. fluorescent M-13 coat protein
h. fluorescent apolipoprotein C-III

CHAPTER 2. FLUORESCENCE PHOTOBLEACHING RECOVERY

A. THEORY

1. Design of the Experiment

Axelrod et al. (242) have derived a theory to quantitate lateral mobility parameters obtained from fluorescence photobleaching recovery (FPR) measurements using a focused laser beam of Gaussian intensity profile. The design of the experiment is as follows. A sharply focused, circularly symmetric, attenuated laser beam is used to excite fluorescence in a small region of a surface containing fluorescent molecules, e.g., a cell membrane which has been fluorescently labeled. After a measurement of the initial fluorescence (F(-)) is made, the same laser beam is employed, now unattenuated, to deliver a brief, intense pulse of light to the same region of the surface. This pulse causes irreversible photochemical bleaching of the fluorophore in the region. At the end of the bleaching pulse, defined as time zero, periodic measuring pulses are delivered to the labeled surface, using the same laser beam attenuated to the same intensity as that used to measure F(-). A record of the fluorescence excited by these measuring pulses with time (see fig. 5) can be characterized empirically by two parameters: the first is the fractional recovery of fluorescence

$$f(\infty) = (F(\infty)-F(0))/(F(-)-F(0)), \qquad (1)$$

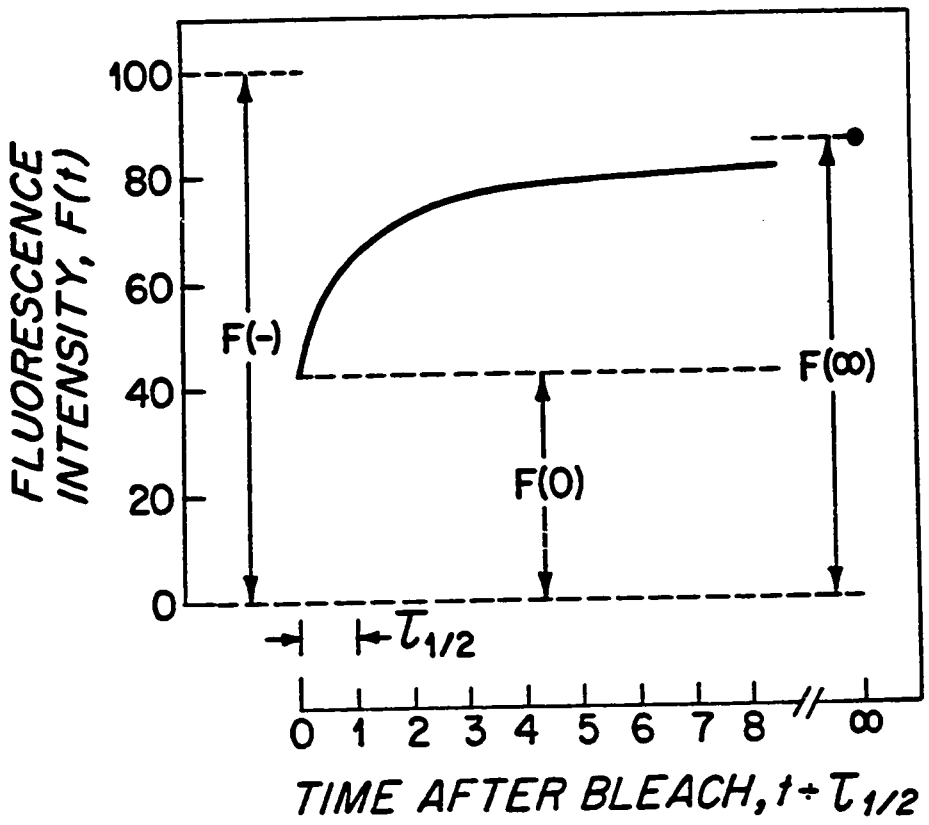

Figure 5. Parameters involved in a typical fluorescence photobleaching recovery experiment. F(-), fluorescence before bleaching; F(0), fluorescence immediately after bleaching; F(∞), fluorescence long after bleaching; $\tau_{1/2}$, half-time for recovery. Diffusion coefficient $D=(w_0^2/4\tau_{1/2})\gamma_D$, in which w_0 is the $1/e^2$ radius of the Gaussian laser beam in the sample plane and γ_D is a small correction factor dependent on the magnitude of the bleaching pulse at time t=0. The fractional recovery, $f(\infty)=(F(\infty)-F(0))/(F(-)-F(0))$, quantitates the fraction of fluorophore that is mobile, i.e., that is free to diffuse laterally with diffusion coefficient D (cm^2sec^{-1}).

where $F(\infty)$ is the fluorescence value attained long after bleaching and $F(0)$ the fluorescence at time zero; the second is the time, $\tau_{1/2}$, required to reach 50% of the final recovery of fluorescence, i.e.,

$$F(\tau_{1/2}) = 1/2\ (F(\infty)-F(0)) + F(0). \qquad (2)$$

Assuming that photochemical recovery of previously bleached fluorophores does not occur and that the measuring pulses do not themselves induce bleaching, recovery of fluorescence in the region of the surface sampled by the laser beam must reflect movement of unbleached fluorophore into the previously bleached region. Such movement could occur either by lateral diffusion or lateral flow; these two cases can be distinguished by the form of the experimental fluorescence recovery curve (242).

2. Photobleaching

The theory for photobleaching on a two-dimensional, uniform distribution of fluorophores (242) assumes that the bleaching of fluorophore to a nonfluorescent compound is an irreversible, first-order reaction characterized by a rate constant $\alpha I(r)$, where α is a proportionality constant and $I(r)$ is the intensity of the bleaching laser beam at distance r from the center of the beam. The instantaneous concentration profile of unbleached fluorophore at distance r immediately after a bleaching pulse which is short compared with the characteristic times for diffusion and/or flow

will then be:

$$C(r) = C_0 \exp(-\alpha T_B I(r)), \tag{3}$$

where C_0 is the initial uniform fluorophore concentration and T_B is the duration of the bleaching pulse. The extent of photobleaching for any given pulse can be completely characterized by the bleaching parameter K:

$$K \equiv \alpha T_B I(0), \tag{4}$$

where I(0) is the intensity of the laser beam at its center. Fluorophore concentration profiles immediately after bleaching for a Gaussian laser beam (i.e., operated in the TEM_{00} mode) at several different values of K are given in fig. 6. Experimentally, K can be determined from the values of the fluorescence immediately before and after the bleaching pulse, according to the relation:

$$F(0)/F(-) = K^{-1}(1-e^{-K}). \tag{5}$$

In fig. 7 this relation is graphically displayed. It should be noted that this method for calculating the bleaching parameter is valid for both diffusion and flow recovery curves, since neither F(0) nor F(-) is dependent on the mode of fluorescence recovery.

3. Fluorescence Recovery Curves

Theoretical recovery curves for diffusion and flow on a two-dimensional surface can be generated from solutions to the differential equations of transport subject to the initial condition caused by photobleaching and characterized by K (derivations in ref. 242).

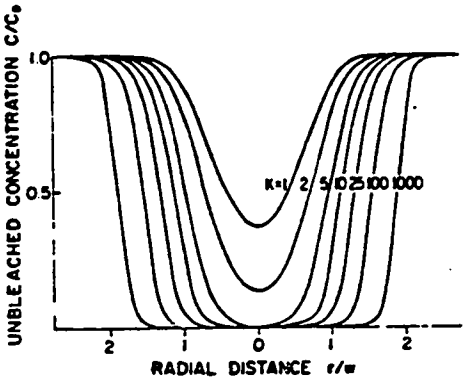

Figure 6. Fluorophore concentration profiles immediately after bleaching with a Gaussian laser beam of $(1/e^2)$ radius w, for various values of bleaching parameter K. (taken from ref. 242)

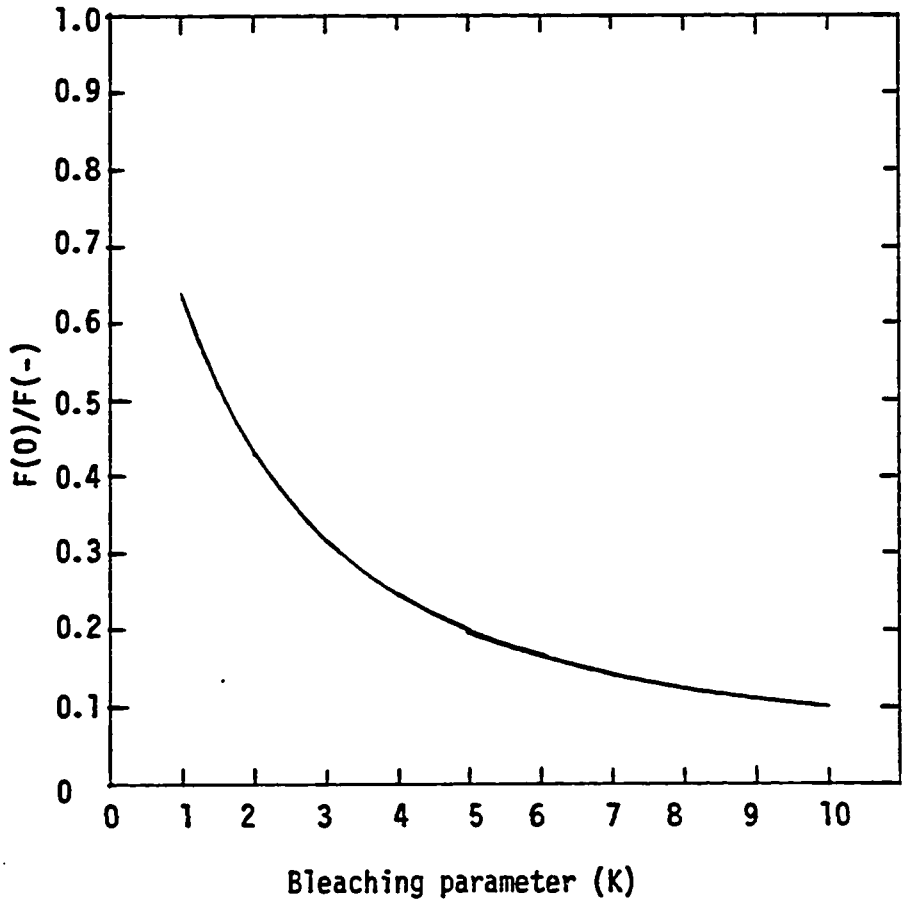

Figure 7. Ratio of fluorescence immediately after bleaching to fluorescence before bleaching *vs.* bleaching parameter. F(0), fluorescence immediately after bleaching. F(-), fluorescence before bleaching.

Such curves have been calculated for a laser beam of Gaussian spatial intensity profile (242) and are reproduced in figs. 8-10. The characteristic time for diffusion is defined as

$$\tau_D \equiv w_o^2/4D, \tag{6}$$

where w_o is the $1/e^2$ radius of the beam at the plane of the fluorescent surface and D is the diffusion coefficient. Similarly, the characteristic time for flow is defined as

$$\tau_F \equiv w_o/V_o, \tag{7}$$

where V_o is the velocity of uniform flow. Calculation of D from experimentally determined values of τ_D requires an independent measurement of w_o, which may be accomplished by the FPR technique itself (242). It should be noted that figs. 9 and 10 are presented in the form of fractional fluorescence recovery f(t) vs. time, where

$$f(t) \equiv [F(t)-F(0)]/[F(\infty)-F(0)], \tag{8}$$

while fig. 8 is given as absolute fluorescence recovery vs. time. The variation in initial fluorescence F(0) with bleaching parameter K can be seen clearly in fig. 8.

More sophisticated versions of the FPR experiment have been recently devised, entailing both theoretical and methodological extensions of the stationary spot photobleaching experiment described above (247-252). Since these methods were not employed in the present work, they will not be discussed further in this dissertation.

Figure 8. Fluorescence recovery F(t) *vs.* t/τ_D for diffusion, with Gaussian laser beam, for various values of K. Fluorescence recovery is normalized to a prebleach value F(-)=1.0. τ_D, characteristic time for diffusion (see text). (taken from ref. 242)

Figure 9. Fractional fluorescence recovery f(t) *vs.* t/τ_D for diffusion, with Gaussian laser beam, for various values of K. $f(t)=(F(t)-F(0))/(F(\infty)-F(0))$. (taken from ref. 242)

Figure 10. Fractional recovery f(t) *vs.* t/τ_F for flow, with Gaussian laser beam, for various values of K. (taken from ref. 242)

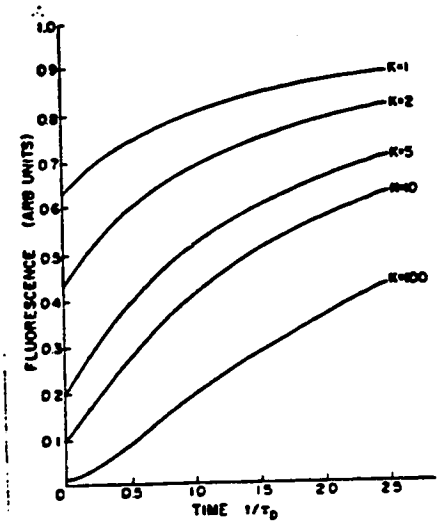

Figure 8.

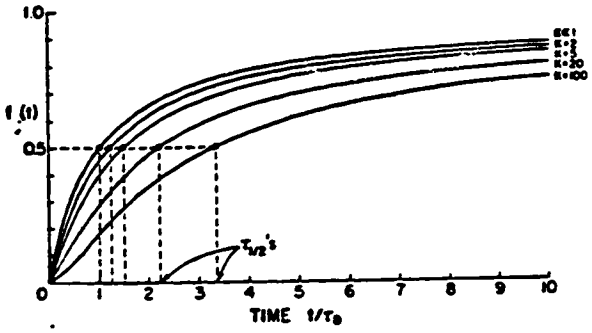

Figure 9.

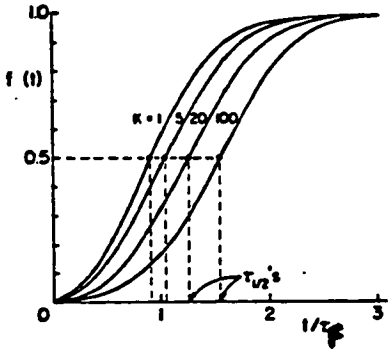

Figure 10.

B. METHODS

1. Optics and Electronics

The design of the optical system for FPR measurements was adapted from Jacobson et al. (244), and is shown in diagrammatic form in fig. 11. Initial studies on the lateral mobility of band 3 as a function of ionic strength and temperature employed the FPR apparatus diagrammed in figs. 11a,b (see chapter 4B), while all of the more recent studies were performed on the same apparatus modified as shown in fig. 11c (see chapters 4C,6-8). A 4W argon-ion laser (Spectra-Physics Model 164-08) tuned to 488 nm was used as the excitation source for a fluorescence microscope (Leitz Ortholux II or Diavert) equipped for incident-light (Ploem) illumination. Operation of the laser in the TEM_{00} mode (Gaussian intensity profile) was checked by expansion of the beam onto a distant surface, where its circular symmetry could be easily appreciated (294), as well as by the form of flow recovery curves obtained on translating a spot bleached in a thin layer of immobile fluorophore through the beam (242). Excitation filters were not needed due to the sharpness of the laser line, so the excitation diaphragm and filter assembly of the conventional Ploem illuminator was removed. The laser output was controlled by an automatic current regulator which stabilized the intensity to $\pm$1%. The beam was focused to a waist (w_{-1}) at the secondary image plane of the microscope (IP_{-1}) by a weak planoconvex lens (f=500 mm, quartz, Melles-

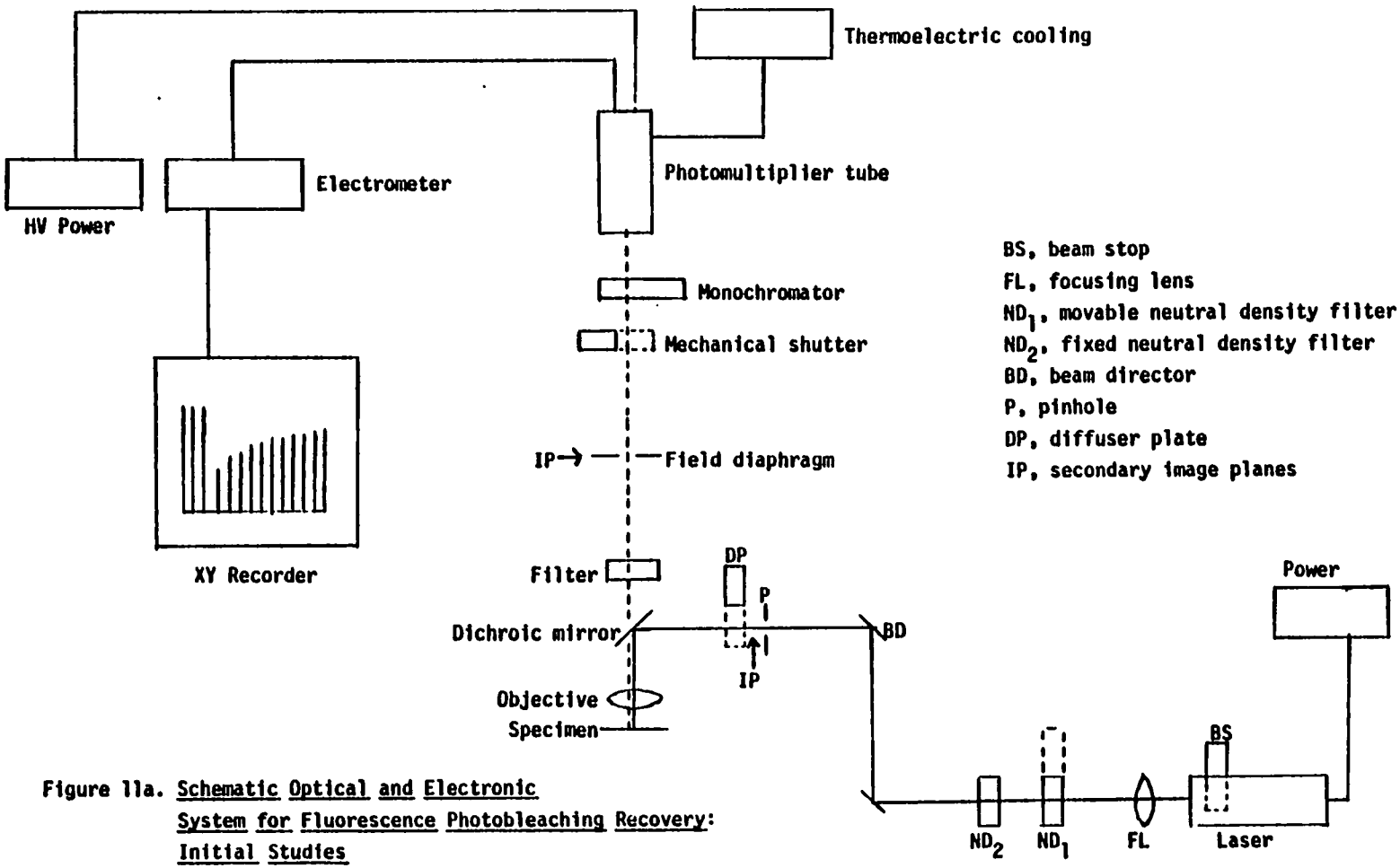

Figure 11a. Schematic Optical and Electronic System for Fluorescence Photobleaching Recovery: Initial Studies

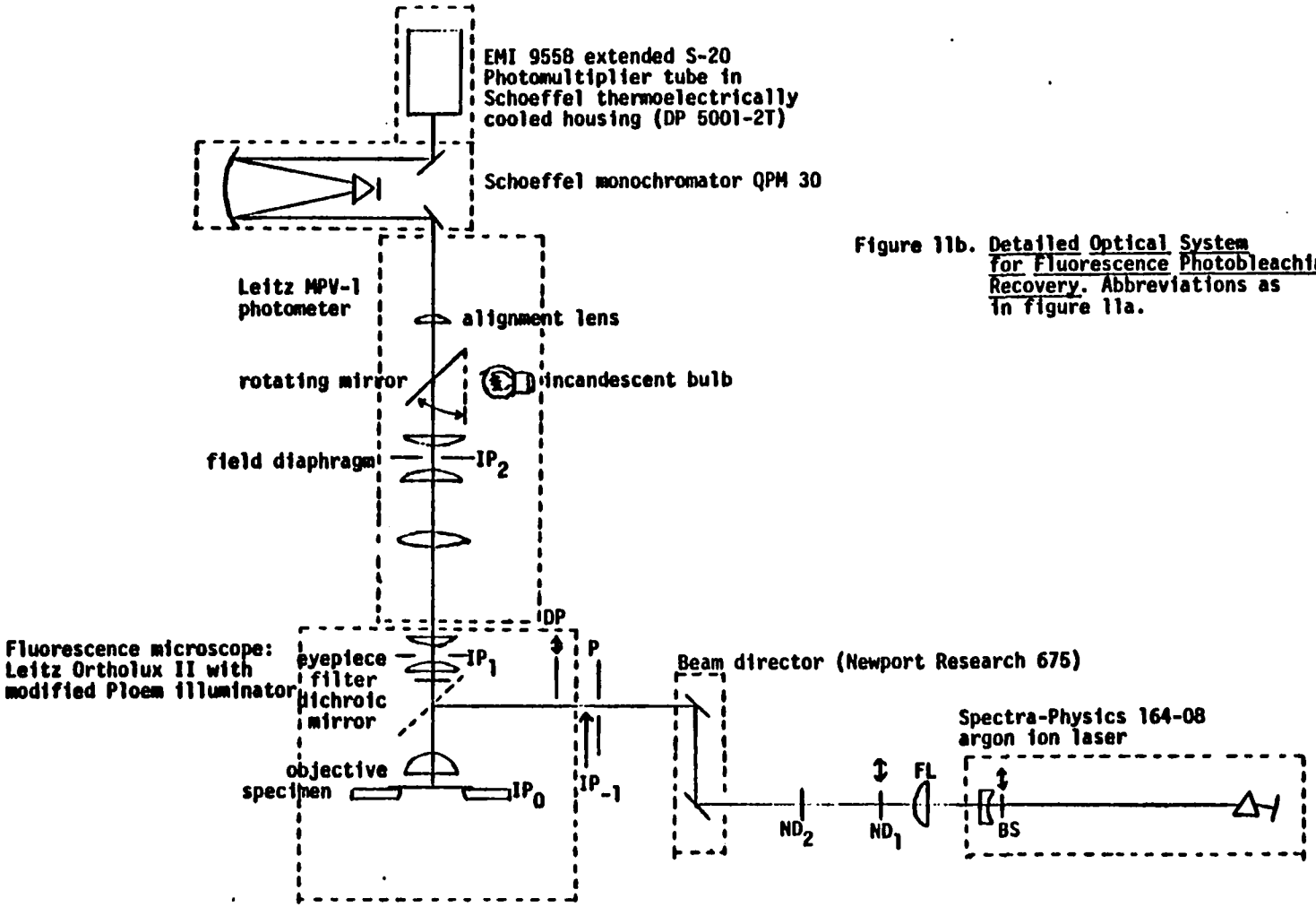

Figure 11b. Detailed Optical System for Fluorescence Photobleaching Recovery. Abbreviations as in figure 11a.

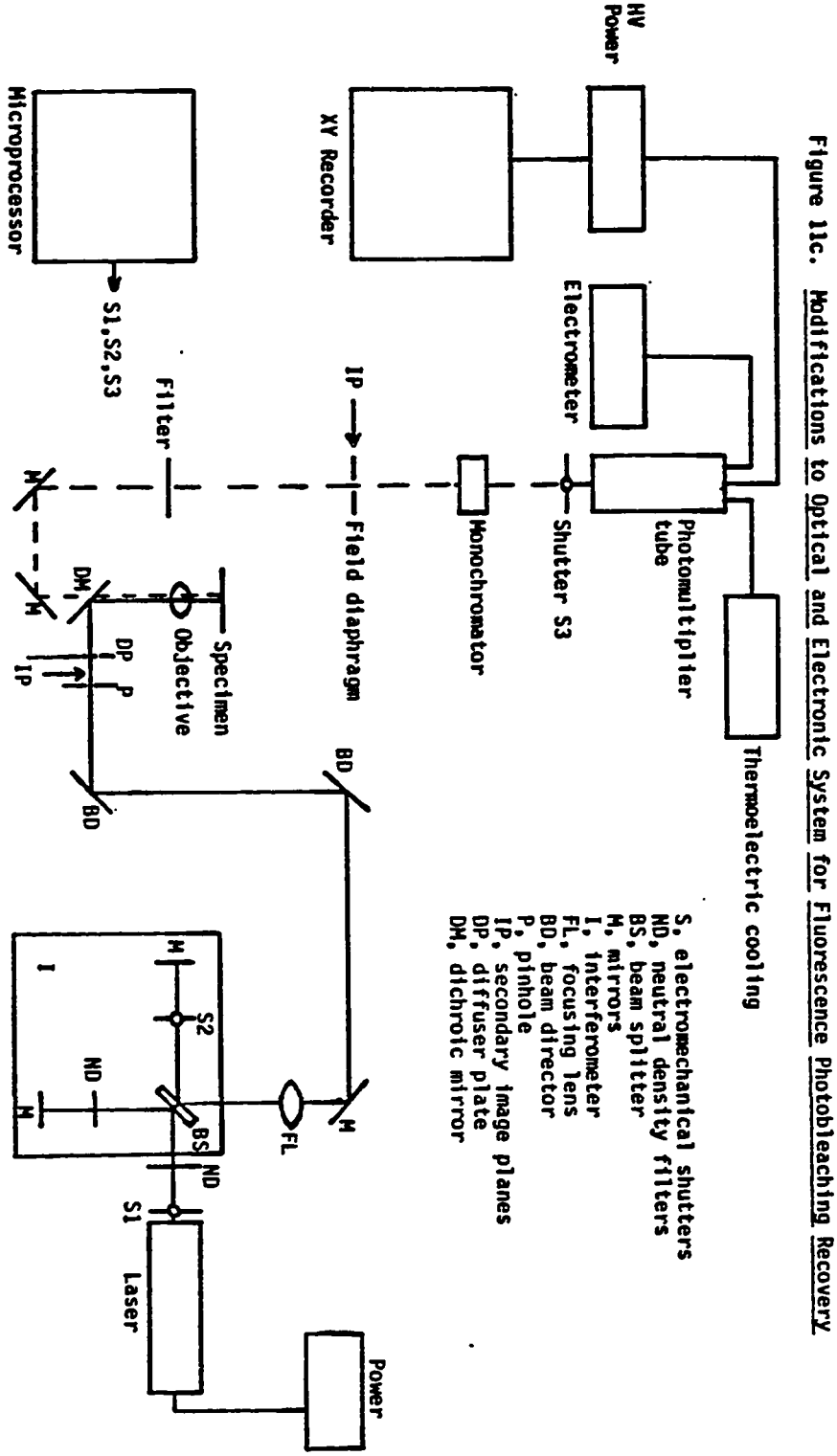

Figure 11c. Modifications to Optical and Electronic System for Fluorescence Photobleaching Recovery

Griot), and to another waist (w_0) at the specimen plane (IP_0) by a 100x oil immersion objective (f=1.9 mm, Leitz Oel 100/1.30) or a 40x achromatic objective (f=4.6mm, Leitz 40/0.65). A beam director (Newport Research Corp. Model 675) was used to change the height of the beam so that it entered the microscope along the direction used by conventional incident excitation sources. Various optical elements between laser and microscope (i.e., focusing lens, mirror, beam director) were mounted on an optical rail (Newport Research Corp. URL-18). A pinhole (0.51 mm diameter) drilled in a brass plate (0.020 inch drill bit, Dixon) and fastened to an XYZ manipulator (Narishige) for fine positioning was placed as close as possible to the secondary image plane of the objective (IP_{-1}) in order to improve the Gaussian beam profile (see below). The illuminated field could be expanded by placement of a diffuser plate (Leitz) in the beam approximately 3 cm after the secondary image plane (IP_{-1}).

Emitted light was collected by the objective and filtered by the dichroic mirror (Leitz TK510) and a suppression filter (Leitz K510) to eliminate most of the back-scattered and reflected excitation light. The emission was then passed through a series of alignment lenses (Leitz, MPV-1) and a monochromator (Schoeffel QPM 30) to an extended S-20 photomultiplier tube (EMI 9558) which was thermoelectrically cooled (Schoeffel Model DP5001-2T) and driven by a stabilized high voltage power supply (Schoeffel Model M600).

An adjustable (square) field diaphragm placed in the image plane (IP_2) was used to discriminate against fluorescence from regions other than the sample plane of interest (243). The photocurrent was fed into an electrometer which formed a single unit with the high voltage power supply and the output read by an XY recorder operated in the time-base mode (Hewlett-Packard 7004B). A dark current of 1×10^{-9} amp at a power of 1100 V was obtained with thermoelectric cooling. The laser, microscope, interposed optical elements, and photomultiplier tube were all mounted on a 22"x72"x4" 750 lb. granite slab (Colonial Marble) which was resting on four rubber inner tubes (Sears) in order to provide vibration isolation.

In the initial studies (fig. 11a,b), a mechanical beam stop within the laser was used to control when the specimen was illuminated for measuring and bleaching pulses. The intensity of illumination for measuring pulses could be adjusted by changing the power output of the laser or the optical density of a neutral density filter (Fish-Schurman) which was fixed in position during the experiment. The bleaching pulse was delivered by mechanical removal of a neutral density filter (O.D. 3.0, Fish-Schurman) as depicted in fig. 12. Coincident with removal of the attenuating filter, the shutter to the photomultiplier tube was mechanically closed to protect the tube from the high level of fluorescence emitted during the bleaching pulse. The shutter was mechanically opened at the same time the attenuating filter was replaced in the

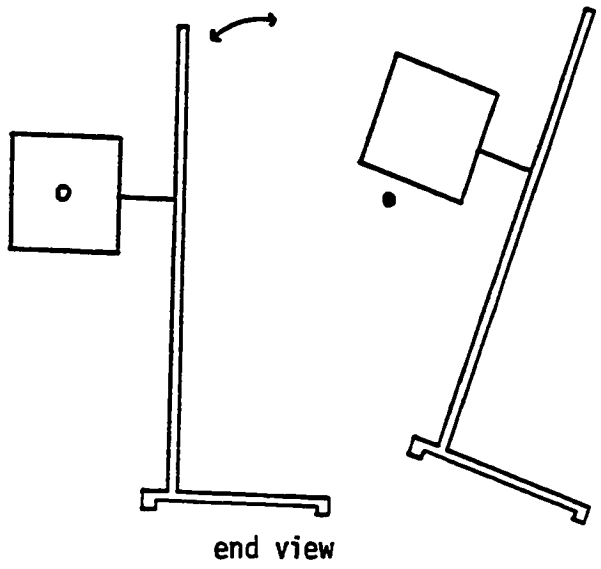

Figure 12. Scheme for Rapid Removal and Replacement of Neutral Density Filter. Neutral density filter (O.D. 3.0) is mounted on triangular-based ring stand which can be rapidly and reproducibly tilted to allow a brief, unattenuated laser pulse to photobleach the specimen.

in the beam, in order to obtain an initial fluorescence value as close as possible to the termination of the bleaching pulse. Periodic measuring pulses were then delivered by mechanically removing and replacing the beam stop within the laser. This was done to avoid excessive bleaching of the sample by excitation light during the recovery period. The entire experiment was conducted in a light-tight room to reduce background noise.

More recent studies employed a series of three microprocessor-controlled (M.O.S. KIM-1) electromechanical shutters (Ilex No. 1 Synchro-electronic) in combination with an interferometer (Ealing) to control the measuring and bleaching pulses (fig. 11c). The interferometer served to split the laser beam into two parts. One part passed twice through a neutral density filter (O.D. 2.0, Fish-Schurman), providing a measuring beam which had been attenuated by 10^4. The other part was normally stopped by a closed shutter, which could be opened on command of the microprocessor to deliver a brief (10-50 msec), unattenuated bleaching pulse. This arrangement allowed the production of bleaching pulses without movement of any optical elements, thus insuring coincidence of bleaching and measuring laser beams to a high degree of precision (248, 295,296). The response time of the electromechanical shutters was less than 10 msec, which enabled the reliable measurement of extremely fast lateral diffusion (τ_D > 250 msec). The machine language program for the KIM-1 microprocessor is reproduced in Appendix A, and the schematic diagram for the electronic interface between microprocessor and shutters is given in Appendix B. This interface served both to transform the microprocessor output into voltages which would open and close the shutters,

and to prevent accidental exposure of the photomultiplier tube to the unattenuated laser beam.

The placement of the weak focusing lens along the optical axis was critical for obtaining the smallest possible beam at the specimen plane. The virtual laser beam waist (w_{-2}) is located near the rear, flat mirror of this laser (specifically, 1.19 m behind the output coupler). Here, the $1/e^2$ radius of the (Gaussian) beam is 0.472 mm. The focusing lens produces another beam waist (w_{-1}) at the secondary image plane of the microscope (IP_{-1}) in accordance with the waist-waist transformation law:

$$(1/w_b^2) = (1/w_a^2)(1-d_1/f)^2 + (1/f^2)(\pi w_a/\lambda)^2 \qquad (9)$$

where w_a is the $1/e^2$ radius of the initial waist, w_b the $1/e^2$ radius of the final waist, d_1 the distance from the initial waist to the lens, f the focal length of the transforming lens, and λ the laser wavelength (297). For the system employed in initial studies (fig. 11a,b), w_a = 0.472 mm, f = 500 mm, d_1 = 1220 mm (including the length of the laser), and $\lambda = 4.88 \times 10^{-4}$ mm, resulting in a $1/e^2$ radius of the beam of 0.145 mm at the secondary image plane. This value was used to calculate the appropriate diameter of the pinhole P (see fig. 11), which should be at least twice the beam diameter in order to avoid truncation errors leading to unwanted diffraction (297). The distance between the secondary image plane (IP_{-1}) and the focusing lens which is appropriate for production of a waist at the image plane was determined by (297):

$$(d_1'-f) = (d_1-f)f^2/[(d_1-f)^2 + (\pi w_a^2/\lambda)^2], \qquad (10)$$

where d_1' is the distance from the transforming lens to the final

waist. Substitution yielded a value for d_1' of 568 mm. A second application of the waist-waist transformation for the microscope objective (d_1=250 mm from the secondary image plane (IP_{-1}) to the objective, f=1.9 mm for 100x oil immersion objective) gave a $1/e^2$ radius of the focused beam in the specimen plane (w_o) of 0.97 μm. For the system employed in more recent studies (fig. 11c), w_a = 0.472 mm, f = 500 mm, d_1 = 1620 mm, and $\lambda = 4.88 \times 10^{-4}$ mm, resulting in a $1/e^2$ radius of the beam of 0.130 mm at IP_{-1} (eq. 9). By eq. 10, d_1' was calculated to be 579 mm. Finally, the $1/e^2$ radius of the focused beam in the specimen plane (w_o) was calculated to be 0.91 μm using the 100x oil immersion objective (f=1.9 mm) and 2.2 μm using the 40x objective (f=4.6 mm) (eq. 9). These values were also checked experimentally (see below).

Alignment of the fluorescent spot in the specimen plane with the excitation and emission systems was accomplished as follows. One drop of a 0.5 mg/ml solution of eosin-5-isothiocyanate (Molecular Probes) in H_2O was placed on a glass slide and covered with a cover slip. An incandescent light bulb above the field diaphragm on the emission system was used to image the field diaphragm (which is also in image plane IP_2) on the region of the specimen plane whose fluorescence was collected by the photomultiplier tube. The center of this region thus defined the axis of the emission system. Adjustments of the horizontal positions of the Ploem illuminator housing and the microscope base were used to bring the fluorescent

spot into the center of the emission axis. Fine adjustment of the position and angle of the upper mirror on the beam director was then employed to line up the fluorescent (green) spot from the eosin with the reflected (blue) spot from the cover glass; perfect alignment indicated that the exciting and emitted light beams were both vertical with respect to the specimen plane. Finally, the pinhole was translated into the beam using the XYZ manipulator; its position with respect to the optical axis was monitored by the appearance or disappearance of the eosin fluorescence on the microscope slide.

2. Experimental Data Analysis

A three-point fit of the data contained in one FPR curve can be used to determine the diffusion coefficient, D, or flow rate, V_0, if the nature of the transport (diffusion vs. flow), the final fluorescence value ($F(\infty)$), and the absolute beam diameter and profile (Gaussian vs. uniform circular disc) are known (242). In general, the nature of transport may be ascertained from the shape of the recovery curve (see figs. 8-10); flow curves are sigmoidal at all K values while diffusion curves are sigmoidal only at very high K values for a Gaussian beam. The shape of the experimental recovery curve can also be compared to the shape of theoretical curves for diffusion and flow at particular K values (figs. 8-10). The final fluorescence value ($F(\infty)$) is simply the asymptote of the experimentally determined recovery curve (fig. 5).

The absolute beam diameter in the specimen plane (w_0) and profile can be experimentally determined (see below).

Once these parameters are known, the analysis for a Gaussian beam profile proceeds as follows:

(1) The time required to reach 50% of the final fluorescence recovery ($\tau_{1/2}$) is determined (eqn. 2).

(2) The bleaching parameter K is calculated from the fluorescence values before bleaching (F(-)) and immediately after bleaching (F(0)) (eqn. 5, fig. 7).

(3) The mobility rates are calculated according to the formulas:

Diffusion coefficient: $$D = (w_0^2/4\tau_{1/2})\gamma_D \qquad (11)$$

Flow rate: $$V_0 = (w_0/\tau_{1/2})\gamma_F, \qquad (12)$$

where γ_D and γ_F are functions of beam shape and K. Fig. 13 gives γ_D and γ_F for diffusion and flow, respectively, with a Gaussian beam (242). The necessity for these correction factors can be seen qualitatively in fig. 6, where it is shown that larger K values lead to bleaching of a wider area on the fluorescent surface. It will thus take longer for the same amount of recovery to occur at higher K, and correction must be made for this in calculating mobility rates. Finally eqn. 1 is used to determine the fractional recovery of fluorescence, which is a measure of the fraction of total fluorophore which is mobile.

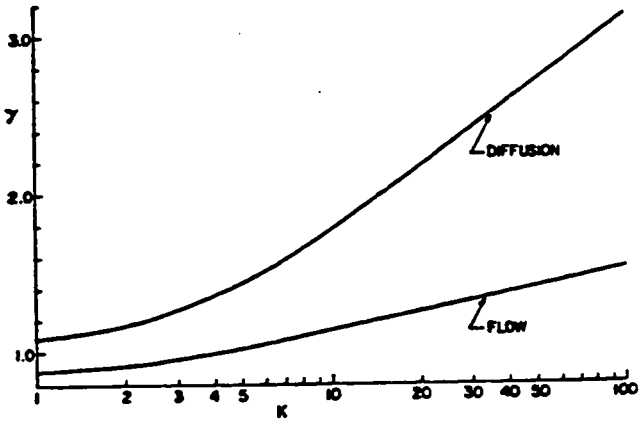

Figure 13. Factor γ (γ_D or γ_F) *vs.* K for a Gaussian beam (taken from ref. 242)

3. Calibration of Beam Size and Profile

The FPR technique itself was used to characterize the profile of the focused laser beam in the plane of the specimen (242). The experiment involved scanning with known velocity V_0 through a spot bleached in a thin layer of immobile fluorophore in order to generate a flow recovery curve which could be matched to a theoretical curve with the same K value. The general shape of the experimental curve provided information about the beam profile (a Gaussian beam gives a sigmoidal curve; a uniform circular disc beam yields a linear curve), while the $\tau_{1/2}$ of the curve could be substituted into eqn. 12 to get the $1/e^2$ beam radius, w_0.

Two methods for the preparation of a thin, immobile layer of fluorophore were employed (adapted from ref. 298). For the calibration of the FPR apparatus used in initial studies (fig. 11a,b), twenty μl of 0.3 mg/ml fluorescein-5-isothiocyanate (FITC, Molecular Probes) in ethanol were dissolved in 0.5 ml of a clear, colorless encapsulating resin (Sylgard 184; Dow-Corning). Two μl of the FITC-resin mixture were placed on a clean glass microscope slide and covered with a cover slip, and pressure was applied to thin the sample as much as possible. The mixture was allowed to set at 60°C for 16 hrs. The final thickness of the set mixture, as measured by a micrometer, was 25 μm. For the calibration of the modified FPR apparatus shown in fig. 11c, ten μl of 0.005 mg/ml FITC in ethanol was allowed to air dry on a cover slip, which was

then placed on a glass microscope slide and sealed around the edges with epoxy (Devcon, "Five-Minute" Epoxy). This method produced an extremely thin ($\sim$ 1 μm) layer of immobile fluorophore.

The FITC-resin or dried FITC slide was placed on the microscope stage of the FPR apparatus. A variable-speed infusion pump drive (B. Braun, Melsungen, W. Germany), to which a long, thin rod was attached in place of the syringe barrel, was used to translate the stage at constant velocity. The slowest translation speed was 0.23 μm/sec as calibrated by a vernier scale on the microscope stage and a stopwatch; this speed was used for the beam size calibration experiments. Prior to bleaching, the infusion pump was started and enough time allowed to elapse for all the slack to be taken out of the translation system. After focusing of the fluorescent spot using the 100x oil immersion objective, the prebleach fluorescence was measured and a brief bleaching pulse (<0.5 sec) administered. As the translation system moved the bleached area out of the (stationary) beam at constant, known velocity, a flow recovery curve was generated. Eqn. 12 and fig. 13 were used to calculate w_0 from the values of $\tau_{1/2}$ and K obtained from the curve, viz.:

$$w_0 = (V_0\tau_{1/2})/\gamma_F. \qquad (13)$$

C. RESULTS: BEAM CALIBRATION

A representative example of a flow recovery curve generated by scanning the focused laser beam at 0.3 μ/sec out of a bleached

spot in a layer of resin-embedded immobile fluorescein-isothiocyanate is given in fig. 14. The nature of transport (i.e., flow) is evident from the sigmoidal shape of the recovery curve. In addition, the experimental points are in good agreement with the theoretical flow recovery curve for a Gaussian beam, calculated for the same K value (242). A series of thirteen such measurements using the FPR apparatus shown in fig. 11a,b, yielded an average $1/e^2$ beam radius of 1.2 ± 0.3 μm. Similarly, a series of thirty-eight such measurements on the dried FITC sample using the modified FPR apparatus shown in fig. 11c yielded an average beam radius of 0.85 ± 0.13 μm. The inference that diffusion and/or spontaneous recovery of fluorescence by previously bleached fluorophore were not contributing to the recovery process was confirmed by an experiment in which FITC-resin or dried FITC was bleached in the absence of translation. In this case, no recovery was observed over several minutes (fig. 14).

D. DISCUSSION

In this chapter the theory, instrumentation, and data analysis involved in performing a fluorescence photobleaching recovery (FPR) experiment are presented. A simple method for calibrating the size and profile of the laser beam used for bleaching and monitoring fluorescence recovery is also given. The results of the calibration experiment show conclusively that the beam has a Gaussian profile.

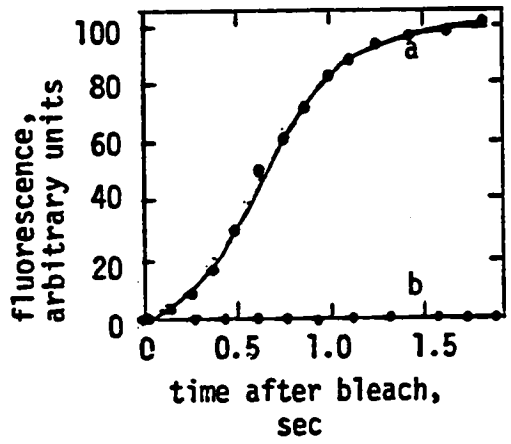

Figure 14. Flow Recovery Curve on Immobile Fluorophore Used for Beam Calibration.
F(-)=100. K=10.
Smooth curve (a) is theoretical recovery curve for flow with a Gaussian beam.
See text for experimental details.
a. Experimental data in presence of translation of beam at 0.23 μ/sec. $\tau_{1/2}$=0.65 sec.
b. Experimental data in absence of translation

The irreversibility of photobleaching for the fluorophore fluorescein-isothiocyanate is also proven. These two conclusions are the two most important assumptions involved in the analysis of an FPR curve, and their confirmation is a necessary prerequisite to accurate data analysis.

The theoretically calculated $1/e^2$ radii of the Gaussian laser beam (0.97 μm for the initial studies, 0.91 μm for more recent studies) are within experimental error of the experimentally measured radii (1.2±0.3 μm and 0.85±0.13 μm, respectively). I shall use the measured values of 1.2 μm and 0.9 μm in the calculation of lateral diffusion coefficients from experimental FPR curves in the initial (chapter 4B) and more recent (chapters 4C,6-8) studies, respectively. Any systematic error which could be incorporated by choosing these or any other values for the beam radius would not affect the major conclusions of this thesis, which are based upon relative differences in FPR parameters between different preparations. In those cases where the absolute value of the diffusion coefficient is of significance (see chapter 9), a systematic overestimation of the diffusion coefficient by less than a factor of two (i.e., by $(1.2/0.97)^2$) would not be great enough to substantially affect the conclusions.

CHAPTER 3. SAMPLE PREPARATIONS

Eosin-5-isothiocyanate was purchased from Molecular Probes. Sodium dodecyl sulfate (SDS), acrylamide, and N,N'-methylene-bis-acrylamide were obtained from Polysciences. Triton X-100 was purchased from New England Nuclear. Neuraminidase (grade IX), sodium ethylenediaminetetraacetate (EDTA), pepstatin A, and dithiothreitol (DTT) were from Sigma. Phenylmethylsulfonylfluoride (PMSF) and 2-mercapto ethanol were purchased from Eastman. α-chymotrypsin was from Worthington Biochemicals. DEAE-cellulose (DE-52) was obtained from Whatman. Sephadex G-25 was from Pharmacia. All other chemicals were reagent grade.

A. EOSIN-ISOTHIOCYANATE LABELING OF BAND 3

1. Methods

a. Labeling of Human Erythrocytes with Eosin-isothiocyanate

The labeling procedure was modified from Cherry et al. (299-301). In the initial studies (chapter 4B), human erythrocytes were isolated from fresh human blood anticoagulated with acid citrate-dextrose by sedimentation at 1 x g in 0.9% NaCl, 0.75% (w/v) dextran 70, at room temperature for 60 min (302). The resulting cells were washed three times in phosphate-buffered saline (10 mM sodium phosphate, 128 mM sodium chloride), pH 7.4 (PBS) at 4°C. Three mg of eosin-5-isothiocyanate (EITC) were dissolved in 6 ml of PBS at room temperature and added to 15 ml of packed, washed erythrocytes.

This mixture was stirred gently at room temperature in the dark for three hours. The erythrocytes were then washed with four to five volumes of PBS three times and subsequently lysed in 750 ml of 5 mM sodium phosphate, pH 7.4, to which 30 nM PMSF had been added, for 30 min. Following lysis the ghosts were pelleted by centrifugation at 21,500 x g for 25 min and washed at least four times with forty volumes of 5 mM sodium phosphate + 30 nM PMSF, pH 7.4. An orange precipitate appeared during the first two to three washes of the labeled ghosts; this was presumed to be EITC which had been noncovalently bound to the membrane and/or trapped inside the erythrocytes during the labeling. Washing was continued until a homogeneous orange-pink ghost pellet with a clear supernatant resulted. All operations except the labeling step were performed at 0-4°C in the dark. The labeled ghosts were stored up to a week in 5 mM sodium phosphate - 30 nM PMSF - 10 mM sodium azide at 4°C in the dark. Unlabeled ghosts were prepared from fresh erythrocytes by an identical procedure, omitting the three hour labeling step at room temperature.

For the more recent studies (chapters 4C,6) the eosin labeling procedure was modified as follows. One mM sodium EDTA was added to the PBS used in the washes of the eosin-labeled erythrocytes. One mM sodium EDTA, 60 μm PMSF (dissolved at 100 mg/ml in dimethylsulfoxide (DMSO)), and 1 μg/ml pepstatin A (dissolved at 10 mg/ml in methanol) were added to the erythrocyte lysis buffer and to all

subsequent ghost washes. Labeled ghosts were stored at 4°C in the dark in 5 mM sodium phosphate, 1 mM EDTA, 60 μM PMSF, 1 μg/ml pepstatin A, 10 mM sodium azide, pH 7.4, and used within four days.

For analytical purposes 150 μl of packed labeled ghosts were dissolved in 1.5 ml 5 mM sodium phosphate + 1% SDS, pH 7.4. The amount of bound eosin was determined spectrophotometrically (303), assuming the maximum molar extinction coefficient of eosin-isothiocyanate to be 8.3×10^4 M^{-1} cm^{-1} (ref. 303; data not shown). The maximum extinction coefficient of this chromophore has been shown to change by <5% upon conjugation to protein (303). The absorption maximum for the solution occurred at 528 nm (Cary 14); the spectrum was identical in shape to that of published EITC spectra (303; data not shown). Protein was determined using the method of Lowry et al. (304).

b. Identification of Labeled Membrane Components

1. SDS-Polyacrylamide Gel Electrophoresis. SDS-polyacrylamide gel electrophoresis was performed using the discontinuous slab gel method of Laemmli (305). The resolving gel was prepared from a solution containing 8.5% acrylamide and 2.6% bis-acrylamide (with respect to acrylamide), the stacking gel from a solution containing 3% acrylamide. Dimensions of the resolving gel were 0.45 x 12 cm. One lane of the gel was 1 cm wide. Packed labeled or unlabeled ghosts as prepared for the initial studies (see above) were solubilized in a solution containing 10 mM Tris chloride, 1 mM EDTA,

3% SDS, 2% sucrose, and 2% 2-mercaptoethanol (final concentrations) at pH 7.4 and incubated for 2 min at 100°C. The solubilized ghosts containing 0.4 mg protein were then loaded onto the gels which were run for 3 hr at a current of 100 mA per gel. Duplicate samples were loaded in a symmetrical fashion about the center lane of the gel in order to facilitate comparison of Coomassie blue and PAS stained bands in the same preparation (see below).

When electrophoresis was complete, the various unstained gel lanes were scanned for eosin absorbance at 515 nm using a spectro-densitometer (Schoeffel Model SD3000). The absorbance from unlabeled ghosts could be subtracted directly from that of labeled ghosts in an adjacent lane by using the double-beam mode of the gel scanner. The gel was then divided in half with a scalpel to create two identical sets of sample lanes. One half was stained with Coomassie blue (25), and the absorbance scanned at 530 nm. The other half was fixed in 10% acetic acid/25% 2-propanol for two days and stained using the periodic acid-Schiff base staining procedure (25); the absorbance was scanned at 560 nm.

2. Selective Extraction Procedures

a. Low Ionic Strength Extraction. One volume of packed labeled ghosts (approximately 5 mg protein/ml) was diluted with nine volumes of warm (37°C) 0.1 mM EDTA, pH 8, and incubated for 20 min at 37°C (ref. 25). The solution was then centrifuged at 35,000 rpm in a SW-41 rotor (Beckman) at 4°C for 30 min. The pellet was resuspended

in 10 volumes of 5 mM sodium phosphate, pH 7.4 + 1% SDS. Eosin was determined spectrophotometrically. Protein was assayed by the Lowry method (304). All operations were performed in the dark.

b. Triton Extraction. One volume of packed labeled ghosts (approximately 5 mg protein/ml) was diluted with 5 volumes of a solution containing 0.5% Triton X-100 (vol/vol) in 56 mM sodium tetraborate, pH 8.0, and incubated for 20 min at 0°C (ref. 47). The solution was then centrifuged at 15,000 rpm in a SS-34 rotor (Sorvall) at 4°C for 30 min. The pellet was resuspended in 5 volumes of 56 mM sodium tetraborate, pH 8.0 + 1% SDS. Eosin and protein were determined as above. All operations were performed in the dark.

c. Chloroform/Methanol Extraction. One volume of packed labeled ghosts was diluted to approximately 2 mg protein/ml in a solution containing 10 mM Tris (hydroxymethyl)aminomethane, 0.1 mM EDTA, pH 7.4. Nine volumes of chloroform/methanol (2/1; vol/vol) were added and the solution incubated with vigorous stirring at room temperature for 30 min (ref. 306). The mixture was then centrifuged at 1500 rpm for 10 min at 4°C and the aqueous layer aspirated off. This layer was recentrifuged at 100,000 x g in a 50-Ti rotor (Beckman) for 60 min at 4°C, in order to remove traces of the insoluble interphase layer remaining in the aspirated aqueous layer. All operations were performed in the dark. Eosin and protein were

determined as above. Sialic acid was determined fluorimetrically by the method of Hammond and Papermaster (307), after sialidase treatment according to Tomita et al. (27).

2. Results and Discussion

a. Eosin Labeling. Packed labeled ghosts prepared by either method (see above) generally contained 4-10 mg protein per ml and 6-15 μg eosinisothiocyanate per ml. The eosin/protein ratio was typically 1.1-2.1 μg eosin per mg total membrane protein.

b. SDS-Polyacrylamide Gel Electrophoresis. Densitometric scans of eosin absorbance, Coomassie blue stain, and PAS stain from gels run on labeled ghosts are given in fig. 15. To reduce background artifacts due to inhomogeneities in the gel, the eosin absorbance scan is a difference scan between adjacent lanes loaded with the same amount of labeled and unlabeled ghost protein, respectively. The same qualitative results were obtained using a single-beam scan of the labeled ghost lane, since the unlabeled ghost lane showed no detectable peaks of absorbance at 515 nm (data not shown).

Most of the eosin absorbance is associated with band 3. A small amount of absorbance is also detected in the region of bands 1 and 2 (spectrin). Only trace amounts, if any, are associated with other proteins stained by Coomassie blue. In the 8.5% gel system the peak of the glycophorin A band (PAS-1) is separated from band 3, although the trailing edge of PAS-1 overlaps the leading edge

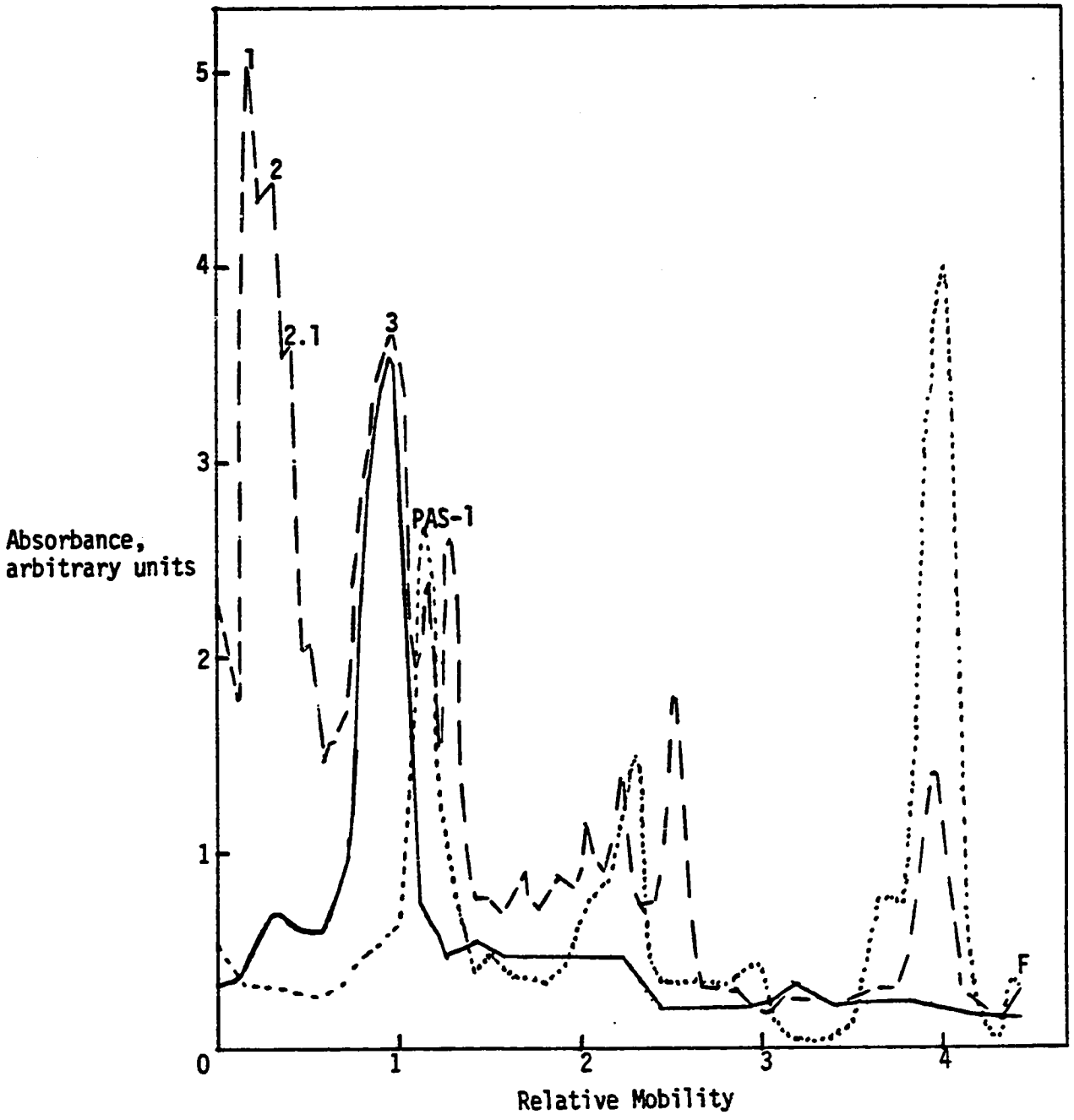

Figure 15. SDS-polyacrylamide gel electrophoresis of eosin-labeled ghost membranes.

– – – : Coomassie blue stained

------: PAS-Schiff base stained

———: Eosin absorbance

Major proteins in high molecular-weight region of the gel are labeled for convenience. F, position of buffer front. See text for experimental details.

of band 3. The peak of eosin absorbance is clearly seen to run with band 3 and not PAS-1; a small amount of glycophorin labeling cannot be excluded from the results of this gel scan, however. Membrane proteins from labeled and unlabeled ghosts appeared identical on Coomassie blue and PAS staining, indicating that no major change in the proteins was caused by either eosin labeling or incubation of the intact erythrocytes at room temperature for 3 hrs (data not shown).

c. Selective Extraction Procedures. Selective extractions of membrane proteins from labeled ghosts were used to confirm the results of the SDS gel scans and to provide a quantitative estimate of the amounts of labeling on proteins other than band 3. The results of these extractions are given in table 6, in addition to literature values for the same extractions on similar preparations of EITC-labeled ghost membranes (300). Low ionic strength treatment of labeled ghosts released 24±6% of the total membrane protein but only 8±2% of the eosin label into the supernatant (N=3). This treatment is reported to selectively solubilize nearly all of bands 1, 2, and 5 (refs. 25, 300). Partial solubilization of band 3 with Triton X-100 resulted in release of 69% of the bound eosin along with 51% of the membrane protein. This experiment was semi-quantitative at best, since Triton extraction is only partially selective for band 3 (the major glycoproteins are released as well),

TABLE 6. SELECTIVE EXTRACTION EXPERIMENTS ON EOSIN-LABELED GHOST MEMBRANES[a]

Extraction procedure	Supernatant				Pellet			
	% eosin		% protein		% eosin		% protein	
	norm[b]	raw	norm[b]	raw	norm[b]	raw	norm[b]	raw
Low ionic strength								
experimental (n=3)	8±2	9±3	24±6	23±8	92±2	105±13	76±6	69±6
literature	7±3[c]		25±7[c]					74[d]
Triton X-100								
experimental (n=1)	69	59	51	42	31	26	49	40
literature	60-80[c]		40[c]					45[e]

	Aqueous			Organic	
	% protein	% eosin	% NANA[f]	% eosin	% protein
Chloroform/Methanol					
experimental (n=1)	5	7	73	0	0
literature	3.7[g]	4[c]	83[g]	0[c]	0[f]

---

[a] see text for detailed methods of extraction

[b] normalized to 100% total for supernatant + pellet

[c] ref. 299; not stated whether normalized or raw values

[d] ref. 25

[e] ref. 47

[f] sialic acid

[g] ref. 306

and not all of the band 3 is released (47). Finally, chloroform/methanol extraction of labeled ghosts resulted in the appearance of 7% of the total eosin, 5% of the total protein, and 73% of the total sialic acid in the aqueous phase; the organic phase contained no detectable protein and no detectable eosin. This extraction is reported to selectively release nearly all of the PAS-staining glycoproteins into the aqueous phase (306), and all of the membrane lipids into the organic phase (299,300).

d. Discussion. In this section a procedure for selective labeling of band 3 with fluorophore in human erythrocyte membranes is presented. SDS-polyacrylamide gel electrophoresis and selective extraction experiments together demonstrate that at least 80% of the eosin-isothiocyanate label is present on band 3, with approximately 8% present on spectrin and 5-10% present on glycophorin. Membrane lipids do not appear to be labeled at all. These values accord well with the literature values for EITC labeling by an almost identical procedure (299-301).

The selective labeling demonstrated in this section and elsewhere (299-301) is in accord with the finding that only glycophorin and band 3 among the major membrane proteins are present on the extracellular surface of the erythrocyte (3,24,25), although the small amount of spectrin labeling must be due to permeation of at least a small percentage of probe through the membrane. Selectivity

of labeling is also consistent with the observation that eosin-isothiocyanate is a potent inhibitor of anion transport (142, 299). Other inhibitors of anion transport such as DIDS bind selectively (>90%) to band 3, labeling glycophorin only to the extent of 7-10% (refs. 50,51). The stoichiometry of eosin binding (1.1-2.1 μg per mg total membrane protein) corresponds to a molar ratio of eosin to band 3 of approximately 0.75 (assuming 100% binding of eosin to band 3, a molecular weight for band 3 of 90,000 daltons, and a ratio of band 3 to total membrane protein of 0.24), which is close to the theoretical limit as well as the experimental values found for anion transport inhibitors (50,51,56,140,141).

B. 72,000 DALTON ANKYRIN FRAGMENT

1. Methods. The 72,000 dalton proteolytic fragment of ankyrin which contains the high-affinity binding site for spectrin on the inner membrane surface was purified according to Bennett (203,204). Human erythrocytes were isolated from fresh human blood anticoagulated with acid citrate-dextrose by sedimentation at 1 x g in 0.9% NaCl, 0.75% (w/v) dextran 70, at room temperature for 60 min. The resulting cells were washed three times in 4 volumes of PBS (see above) to which 1 mM EDTA and 10 μg/ml PMSF had been added, lysed in 25 volumes of 5 mM sodium phosphate, pH 7.4, to which 1 mM EDTA, 10 μg/ml PMSF, and 1 μg/ml pepstatin A had been added, and washed four times in the lysis buffer. Spectrin-depleted inside-out vesicles

were prepared from the erythrocyte ghosts (25 ml in first preparation, 16.6 ml in second) by incubation for 30 min at 37°C in 30 volumes of 0.3 mM sodium phosphate, pH 7.4, to which 0.2 mM DTT and 10 μg/ml PMSF had been added. The resulting vesicles were pelleted at 25,498 x g for 68 min and resuspended in 27.5 ml or 18.7 ml (first or second preparations, respectively) of 7.5 mM sodium phosphate, pH 7.4, to which 0.2 mM DTT had been added. Chymotrypsin was added to a final concentratin of 1 μg/ml. After a 30 min incubation at 0°C, PMSF dissolved in DMSO was added to final concentrations 50 μg/ml and 0.5% (v/v), respectively, and the suspension centrifuged at 193,000 x g for 24 min. The supernatants from two such preparations were combined with 0.09 volumes of packed DE-52 beaded cellulose equilibrated with 7.5 mM sodium phosphate, 0.2 mM DTT, pH 7.5, and mixed gently at 0°C for 30 min. The DE-52 was packed into a column at 4°C and the supernatant collected. The column was washed with 12 column volumes of 7.5 mM $NaPO_4$, 0.2 mM DTT, pH 7.5, followed by 3 column volumes of 80 mM KCl, 7.5 mM $NaPO_4$, 0.2 mM DTT, pH 7.5. The column was then eluted with 200 mM and 400 mM KCl dissolved in 7.5 mM $NaPO_4$, 0.2 mM DTT, pH 7.5, and the fractions (0.67 ml) collected. All fractions were monitored for protein (A_{280}) and selected fractions were assayed for protein by the Lowry procedure (304). The first protein peak (fractions 24 and 25, see below) was dialyzed against two changes of 7.5 mM sodium phosphate, 0.5 mM EDTA, 0.2 mM DTT, pH 7.5 and

stored frozen in this buffer.

Protein was assayed by the method of Lowry (304). Discontinuous SDS-polyacrylamide gel electrophoresis was performed by the Laemmli procedure (305), using a 1.5 mm thick 3% polyacrylamide stacking gel and a 6% polyacrylamide resolving gel. Gels were stained with Coomassie blue (25) and scanned at 550 nm with a spectrodensitometer (Schoeffel SD3000).

2. Results and Discussion. Low ionic strength treatment of erythrocyte ghosts (147 mg, 3.5 mg protein/ml) yielded 22 mg of spectrin-depleted inside-out vesicles. Chymotrypsin treatment of these vesicles resulted in 9.6 mg of solubilized polypeptides of which 3.7 mg adsorbed to DEAE-cellulose. Elution of the adsorbed protein with 200 mM KCl yielded 1.3 mg present in DEAE peak #1, while elution with 400 mM KCl yielded 1.8 mg present in DEAE peak #2. The elution profile from the DEAE-cellulose column is shown in fig. 16. Analysis of the fractions by SDS-polyacrylamide gel electrophoresis (fig. 17) indicated that DEAE peak #1 consists primarily of a 72,000 dalton polypeptide (66% by densitometer scan) with traces of higher molecular weight polypeptides, while peak #2 contains primarily a 45,000 dalton polypeptide.

In general, the yields from various steps in the preparation, the DEAE-cellulose column elution profile, and SDS-polyacrylamide gels of the two main column peaks closely resemble literature results (203,204). It was therefore assumed that the 72,000 dalton

Figure 16. Elution profile from DEAE-cellulose column used to purify 72,000 dalton ankyrin fragment. The supernatant from a chymotryptic digest of spectrin-depleted inside-out vesicles was combined with DE-52 beaded cellulose equilibrated with 7.5 mM $NaPO_4$, 0.2 mM DTT, pH 7.5 and packed into a column. The column was washed successively with buffers containing 7.5 mM $NaPO_4$, 0.2 mM DTT, pH 7.5 and nothing else (fractions 1-14), 80 mM KCl (fractions 15-18), 200 mM KCl (fractions 19-56), and 400 mM KCl (fractions 57-70). Each fraction (0.67 ml) was monitored for protein (A_{280}). Fractions 23-26 are designated DEAE peak #1 (1.3 mg protein); fractions 61-63 are designated DEAE peak #2 (1.8 mg protein).

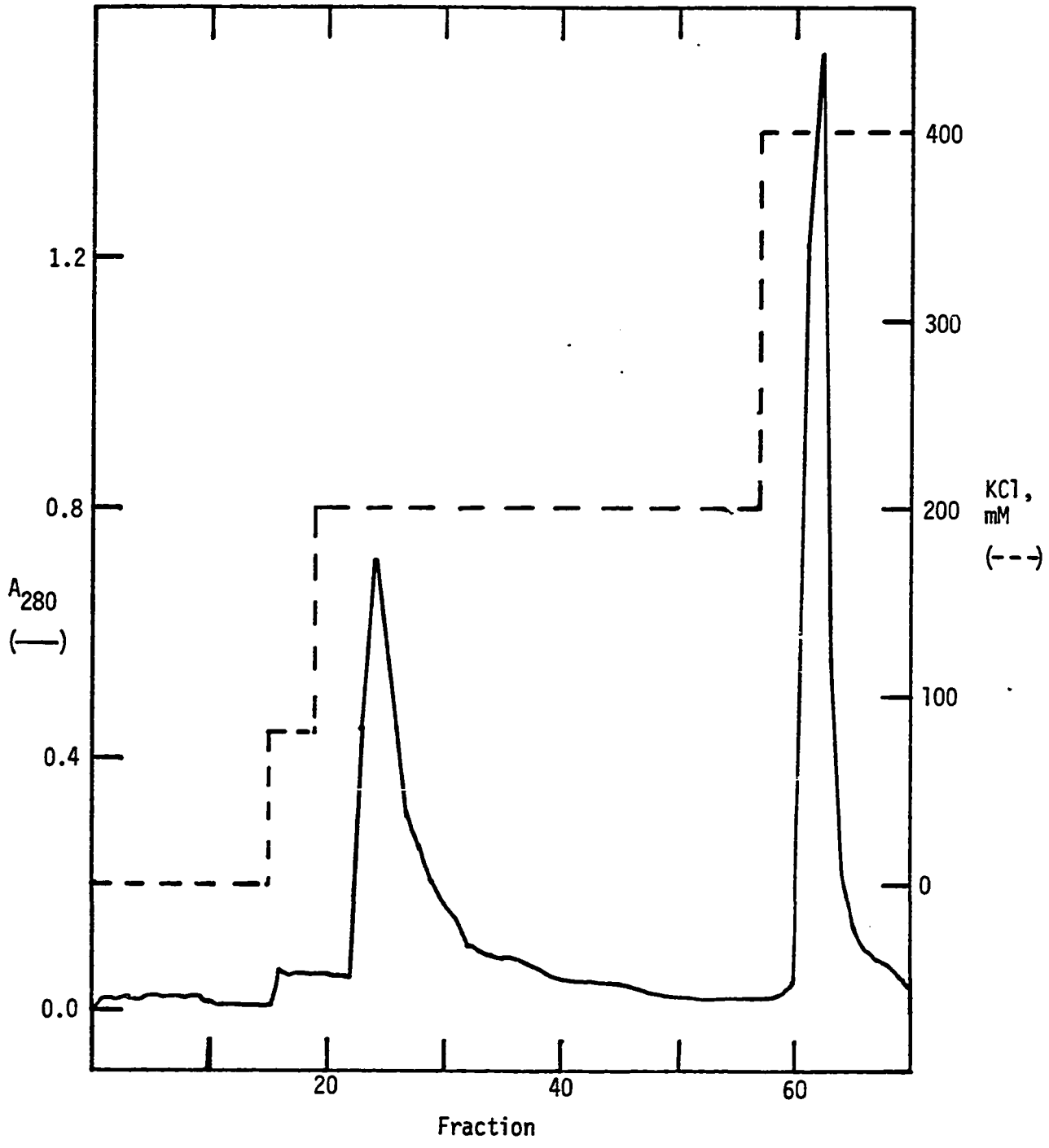

Figure 16.

Figure 17. SDS-polyacrylamide gel analysis of purification of 72,000 dalton ankyrin fragment. Discontinuous SDS-polyacrylamide gel electrophoresis was performed using a 3% polyacrylamide stacking gel and a 6% polyacrylamide resolving gel. (A) Human erythrocyte ghost membranes (33 μg protein). (B) Spectrin-depleted inside-out vesicles (25 μg). (C) Chymotryptic digest of spectrin-depleted inside-out vesicles (13 μg). (D) DEAE peak #1 (18 μg). (E) DEAE peak #2 (17 μg). DEAE peak #1 consists primarily of a 72,000 dalton polypeptide (66% by densitometer scan) with traces of several higher molecular weight polypeptides.

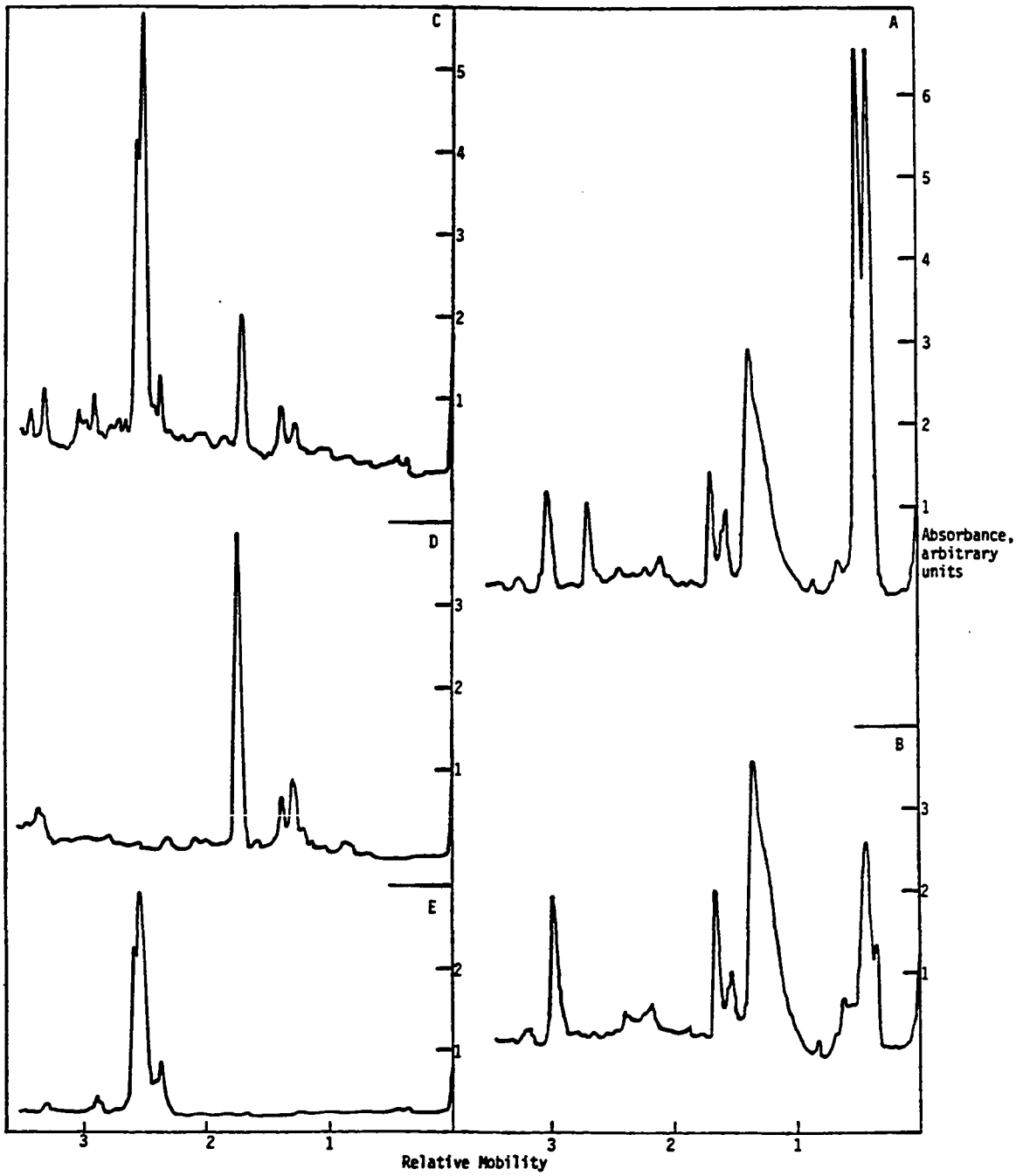

Figure 17.

chymotryptic fragment purified in the above manner was in fact identical with the proteolytic fragment of ankyrin which serves as the spectrin binding site on the membrane, and this fragment was used in FPR experiments without further characterization.

C. 80,000 DALTON SPECTRIN FRAGMENT

1. Methods. A sample of purified 80,000 dalton tryptic fragment of spectrin band 1 involved in the polymerization of dimer to tetramer spectrin (171,172) was generously provided by Dr. Jon S. Morrow, Dept. of Pathology, Yale University School of Medicine, New Haven, CT. The sterile sample (8.5 ml) was received in isotonic KCl, pH 7.6, at a concentration of 0.25 mg protein/ml by the Lowry procedure (304), and stored at 0°C. This sample was dialyzed twice at 4°C against 1000 ml of 20 mM sodium phosphate, 1 mM EDTA, 10 μg/ml PMSF, 3 mM sodium azide, pH 7.4, and the dialyzed sample concentrated at 4°C by pressure dialysis through Diaflo PM10 ultrafilters at a pressure of 15-20 psi of nitrogen. The concentrated solution was then redialyzed against the same buffer for 24 hr at 4°C, and stored for two weeks at 0°C in the course of FPR experiments. In addition, the dialysis chamber was rinsed with PBS and 1 mM EDTA, pH 7.4, to remove a small amount of precipitate remaining on the walls of the chamber.

Protein was assayed by the Lowry procedure (304). Discontinuous SDS-polyacrylamide gel electrophoresis was performed (305) using

1.5 mm thick gels with 6% polyacrylamide in the resolving gel and 3% polyacrylamide in the stacking gel. Gels were stained with Coomassie blue (25) and scanned with a spectrodensitometer (Schoeffel SD3000).

2. Results and Discussion. Of the original 2.0 mg of protein, 0.70 mg remained in the dialysis chamber at a concentration of 1.55 mg/ml, 0.65 mg passed into the filtrate during pressure dialysis at a concentration of 0.08 mg/ml, and 0.55 mg was solubilized by PBS during the final rinse of the dialysis chamber. SDS-polyacrylamide gel scans of the starting material and of all three fractions were virtually identical (fig. 18), with at least 70% of the protein present as a homogeneous band at 80,000 daltons and smaller bands present at approximately 70,000 daltons (20%) and 50,000 daltons (5-10%). The precipitation of some of the 80,000 dalton sample on concentration in 20 mM sodium phosphate buffer was taken as an indication that further attempts at concentration would be futile, and the concentrated sample (1.55 mg protein/ml) was therefore used without further purification in FPR experiments.

D. NBD-PE AND NBD-CHOL LABELING OF ARTIFICIAL AND ERYTHROCYTE MEMBRANES

All experiments involving the lipid probes NBD-PE and NBD-chol were designed and executed in full collaboration with Drs. M. Robert

Figure 18. SDS-polyacrylamide gel electrophoresis of purified 80,000 dalton spectrin fragment. Discontinuous SDS-polyacrylamide gel electrophoresis was performed using a 3% polyacrylamide stacking gel and a 6% polyacrylamide resolving gel. At least 70% of the protein is present as a homogeneous band at 80,000 daltons.

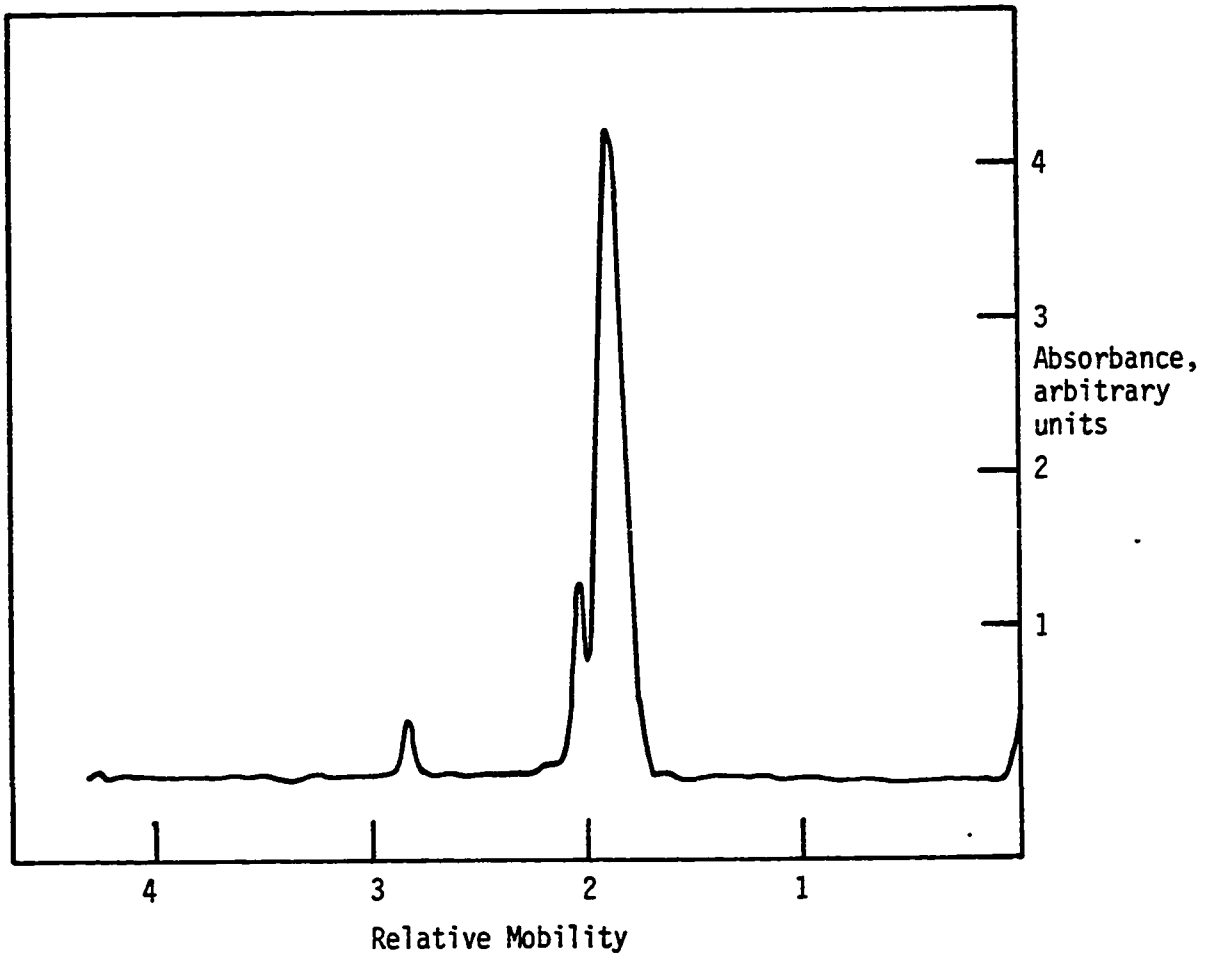

Figure 18.

Alecio and Robert R. Rando, Department of Pharmacology, Harvard Medical School, Boston, MA. The preparation and analysis of the various membrane samples described in this section were performed in their laboratory, while the FPR experiments themselves were carried out by the author.

1. Materials and Methods. Dimyristoylphosphatidylcholine (DMPC), egg yolk phosphatidylcholine (egg PC), and N-4-nitrobenzo-2-oxa-1,3-diazole-phosphatidylethanolamine (NBD-PE) were purchased from Avanti Biochemicals. Choesterol was from Sigma. NBD-chol (8(N-cholesterylcarbamylamino-3,6-dioxaoctyl-1-amino-(N-4-nitrobenzo-2-oxa-1,3-diazole))) was prepared by Drs. Alecio and Rando as described (308). Unless otherwise indicated, the buffer for hydration was composed of 10 mM sodium phosphate, 150 mM NaCl, pH 7.2, which had been purged with nitrogen for at least 20 min.

a. Labeling of DMPC-cholesterol and egg PC-cholesterol multilamellar liposomes. The labeling procedure was modified from that of Smith et al. (292) as follows. Solutions of DMPC or egg PC and cholesterol (if required) in chloroform were mixed to give a total of 1.5 μmole of lipid. A solution of either NBD-PE or NBD-chol (2.2 nmole, 0.15 mole%) in chloroform was added. After thorough mixing, the solvent was removed at 20°C using a rotary evaporator. The lipids were then redissolved in fresh chloroform (200 μl) and again roto-evaporated to a thin film. Traces of solvent were removed by

keeping the sample under a pressure of approximately 0.5 torr at 20°C for at least 8 hr. The thin lipid film was handled under nitrogen at all times to prevent oxidation of lipids.

After thorough solvent removal the lipid mixture was hydrated under nitrogen in 1 ml of buffer for 15 min at 40°C and then vortexed vigorously for 15 sec. This procedure produced large multilamellar liposomes which were stored on ice and used in FPR experiments within several hours.

b. Preparation and labeling of multilamellar liposomes from extracted erythrocyte membrane lipids. Erythrocyte membrane lipids were extracted and purified as described by Rouser and coworkers (309, 310). Briefly, white erythrocyte ghosts in 5 mM sodium phosphate, 1 mM EDTA, 10 μg/ml PMSF, 1 μg/ml pepstatin A, pH 7.4, were extracted twice with chloroform:methanol (2:1,v:v), once with chloroform:methanol (1:2,v:v), and finally with chloroform:methanol (7:1,v:v) saturated with aqueous ammonium hydroxide, and all four extracts pooled. The product was chromatographed on a washed Sephadex G-25 column using mixtures of chloroform:methanol:water to elute as described (310). After chromatography the solvent was removed by rotary evaporation and the residue stored in fresh chloroform under nitrogen at -20°C. Total lipid phosphate (311) and total cholesterol (312,313) were assayed as described.

Solutions of total extracted erythrocyte membrane lipids (3.4 μmole total lipid) in chloroform and either NBD-PE or NBD-chol

(2.2 nmole, 0.06 mole%) in chloroform were mixed, and the solvent removed at 20°C using a rotary evaporator. The labeled thin lipid film was then washed once in chloroform, dried, hydrated, and vortexed as described above, and the large unilamellar liposomes used in FPR experiments within several hours. Buffers for hydration included phosphate-buffered saline, pH 7.2 (see above) and 14 mM sodium phosphate, 1 mM EDTA, 10 μg/ml PMSF, 1 μg/ml pepstatin, pH 7.4.

c. Labeling of erythrocyte ghosts. White human erythrocyte ghosts were prepared as described above with a final wash in 40 mM sodium phosphate, 1 mM EDTA, 10 μg/ml PMSF, 1 μg/ml pepstatin, pH 7.4. Unless otherwise indicated, this buffer was used for all experiments with labeled ghosts.

1. NBD-PE labeling. NBD-PE (110 nmole) was dried from a stock solution in chloroform, 200 μl of sodium phosphate buffer was added to the thin film, and the mixture sonicated briefly at 10°C until clarified. Packed ghosts (200 μl, 7.1 mg protein/ml) were added and the sample stirred gently at 20°C for 20 min. The labeled ghosts were washed twice in approx. 75 volumes of the phosphate buffer, resulting in uniformly fluorescent biconcave discs which were used immediately in FPR experiments or stored under nitrogen at 0°C for up to two days before use. For analytical purposes, a small amount of labeled ghost sample was incubated at 4°C in 50 volumes of 10 mM triethanolamine, pH 7.6 for 30 min and washed twice in the same

buffer, to remove all traces of inorganic phosphate. Total lipid phosphate (311) and total cholesterol (312,313) were then assayed as described. Incorporated fluorophore was estimated from the absorbance at 462 nm of an ethanol extract of the labeled ghosts which had been dried for 5 hrs at 20°C under vacuum, assuming an extinction coefficient of 19,500 $cm^{-1}M^{-1}$ for the fluorophore in ethanol at 462 nm (Alecio, R.,unpublished data).

2. NBD-chol labeling. NBD-chol (410 nmole) was mixed with 80 µl of the total extracted erythrocyte membrane lipid solution (2.7 µmole total lipid) in chloroform, and the solvent removed at 20°C using a rotary evaporator. The labeled lipid film was washed once in chloroform and dried, and then hydrated and vortexed in 400 µl of phosphate buffer. The resulting labeled liposomes were stirred gently at 20°C for 2 hr with packed white erythrocyte ghosts in 40 mM sodium phosphate (400 µl, 7.1 mg protein/ml), and the suspension washed twice in approx. 75 volumes of phosphate buffer. This procedure yielded faintly fluorescent biconcave discs which were used immediately in FPR experiments.

2. Results and Discussion: Composition of Samples. As mentioned above, DMPC-cholesterol or egg PC-cholesterol multilamellar liposomes were prepared with fluorophore (NBD-PE or NBD-chol) at a final concentration of 0.15 mole%. Multilamellar liposomes from extracted erythrocyte membrane lipids contained fluorophore at a final concentration of 0.06 mole%; these liposomes had a cholesterol/

phospholipid (C/P) molar ratio of 0.75. Erythrocyte ghosts labeled with NBD-PE were found to have a fluorophore concentration of 6.7 mole% and a C/P molar ratio of 0.99. Corrected for addition of the exogenous fluorophore, the C/P molar ratio in the labeled erythrocyte ghosts was 1.17, which compares favorably with that found in unlabeled ghosts (1.11). It thus appears that labeling with fluorophore does not change the overall lipid composition of the erythrocyte membrane.

Several points should be noted concerning the labeling of the erythrocyte membrane by fluorescent lipid probes. First, in order to obtain a fluorescent signal great enough to allow performance of the FPR experiment, it was necessary to label the erythrocyte ghosts with a much larger concentration of NBD-PE than that required for the multilamellar liposome samples. It is hoped that such a perturbation does not affect long-range interactions on the membrane such as those required in lateral diffusion over μm distances. Second, it was surprisingly difficult to label the erythrocyte ghosts with a large enough concentration of NBD-chol to perform the FPR experiment. Sonication of a suspension of the probe in phosphate buffer followed by incubation with ghosts did not result in detectable labeling (data not shown). Exchange of NBD-chol from liposomes prepared from extracted erythrocyte lipids, a procedure employed with this probe in several other cell types with great success (Rando, R.R. and F.W. Bangerter, in preparation),

proceeded only slowly and erratically in erythrocyte ghosts. It was therefore decided to concentrate on NBD-PE labeled ghosts for the FPR experiments, with only one series of experiments on NBD-chol labeled ghosts for comparison. Finally, the C/P molar ratio and final concentration of fluorophore in NBD-chol labeled ghosts could not be determined quantitatively, given the necessity of adding the probe in the presence of exogenous lipid. It is expected, however, that exchange of the probe from erythrocyte lipids to ghosts would proceed without significant change in the C/P molar ratio of the resultant labeled ghosts. The final NBD-chol concentration can be estimated to be 1-2 mole% in the labeled ghosts, from a comparison of the fluorescence intensity of a typical NBD-chol labeled ghost with that of a typical NBD-PE labeled ghost in the fluorescence microscope (data not shown).

CHAPTER 4. LATERAL MOBILITY OF BAND 3: EFFECT OF LOW IONIC STRENGTH

Abundant indirect evidence exists implicating the erythrocyte cytoskeleton in restriction of integral membrane protein mobility (see chapter 1). In designing the experiments reported in this and succeeding chapters, it was thought desirable to measure directly the lateral mobility of band 3 both in the presence and in the absence of cytoskeletal forces. The usual conditions for complete dissociation of the cytoskeleton from the membrane, however, lead to extensive vesiculation of erythrocyte ghosts (219). The resultant vesicles are comparable in size to the focused laser beam used in the FPR experiment; when subjected to a bleaching pulse, an entire vesicle will be bleached, leaving no unbleached fluorophore which is capable of lateral diffusion. For technical reasons, then, FPR cannot be used on such a system. It was hypothesized that the same experimental parameters important in complete dissociation of the cytoskeleton - i.e., low ionic strength, high temperature, and time - might also be involved in a rearrangement of cytoskeletal membrane proteins which would precede both complete cytoskeletal dissociation and ghost vesiculation. Such a rearrangement could involve a metastable state of cytoskeleton structure intermediate between tight binding to and complete dissociation from the membrane. The lateral mobility of band 3 might also be

expected to change dramatically under such conditions. This chapter, then, examines the effects of low ionic strength, temperature and time on the lateral mobility of eosin-labeled band 3 in erythrocyte ghost membranes. All three parameters are found to affect greatly both the diffusion rate of the mobile band 3 and the fraction of total band 3 which is free to diffuse in the plane of the membrane.

A. METHODS

1. Fluorescence Photobleaching Recovery System

The optics and electronics for the FPR system are described in chapter 2. In the initial studies (chapter 4B), control of sample temperatures above room temperature was achieved with an air stream stage incubator (Nicholson Precision Instruments, Model C300) placed 4-6 inches from the microscope stage. A microprobe thermometer (YSI model 423 probe, model 42SC meter) was taped to the microscope slide to monitor the temperature at the sample. Once the system was equilibrated (10-15 min), temperature was controlled to $\pm$1°C. One experiment involved FPR measurements at 10°C. This temperature was achieved by blowing cold nitrogen gas (cooled by being passed through a coil of copper tubing submerged in a dry ice/acetone mixture) onto the microscope stage and monitoring the sample temperature as described above. Temperature was controlled by this method to $\pm$2°C.

In the later studies (chapter 4C), sample temperatures were controlled both above and below room temperature by fastening the microscope slide in an aluminum sample holder fitted with copper tubing and connected to a precision water bath (Lauda RC3) as diagrammed in fig. 19. Sample temperatures were again monitored by a microprobe thermometer taped to the microscope slide, and could be controlled to $\pm$0.5°C over the entire temperature range employed in these studies (10°-37°C).

2. Preparation of the Sample

Thirty µl of packed, eosin-labeled erythrocyte ghosts (4-10 mg protein/ml, 1.1-2.1 µg eosin/mg protein) in 5 mM sodium phosphate, 10 mM NaN_3, 30 nM PMSF, pH 7.4 (initial studies) or 5 mM sodium phosphate, 1 mM EDTA, 60 µM PMSF, 1 µg/ml pepstatin A, 10 mM NaN_3, pH 7.4 (later studies) were diluted to 300 µl with various concentrations of sodium phosphate buffer, pH 7.4, to which EDTA, PMSF, and pepstatin A had been added as noted. The diluted ghost suspension was deoxygenated in a sealed, purged glove bag (Ventron, model X-27-17) by a stream of argon for 30 min (5.2 mM $NaPO_4$ sample), nitrogen for 3 hrs (all other samples in the initial studies) or nitrogen for 1 hr (all samples in the later studies) at room temperature in the dark. The nitrogen and argon were first bubbled through water to prevent excessive evaporation of the suspension.

Photoinduced oxidation of erythrocyte membrane proteins leading to extensive cross-linking has been shown in the presence of oxygen

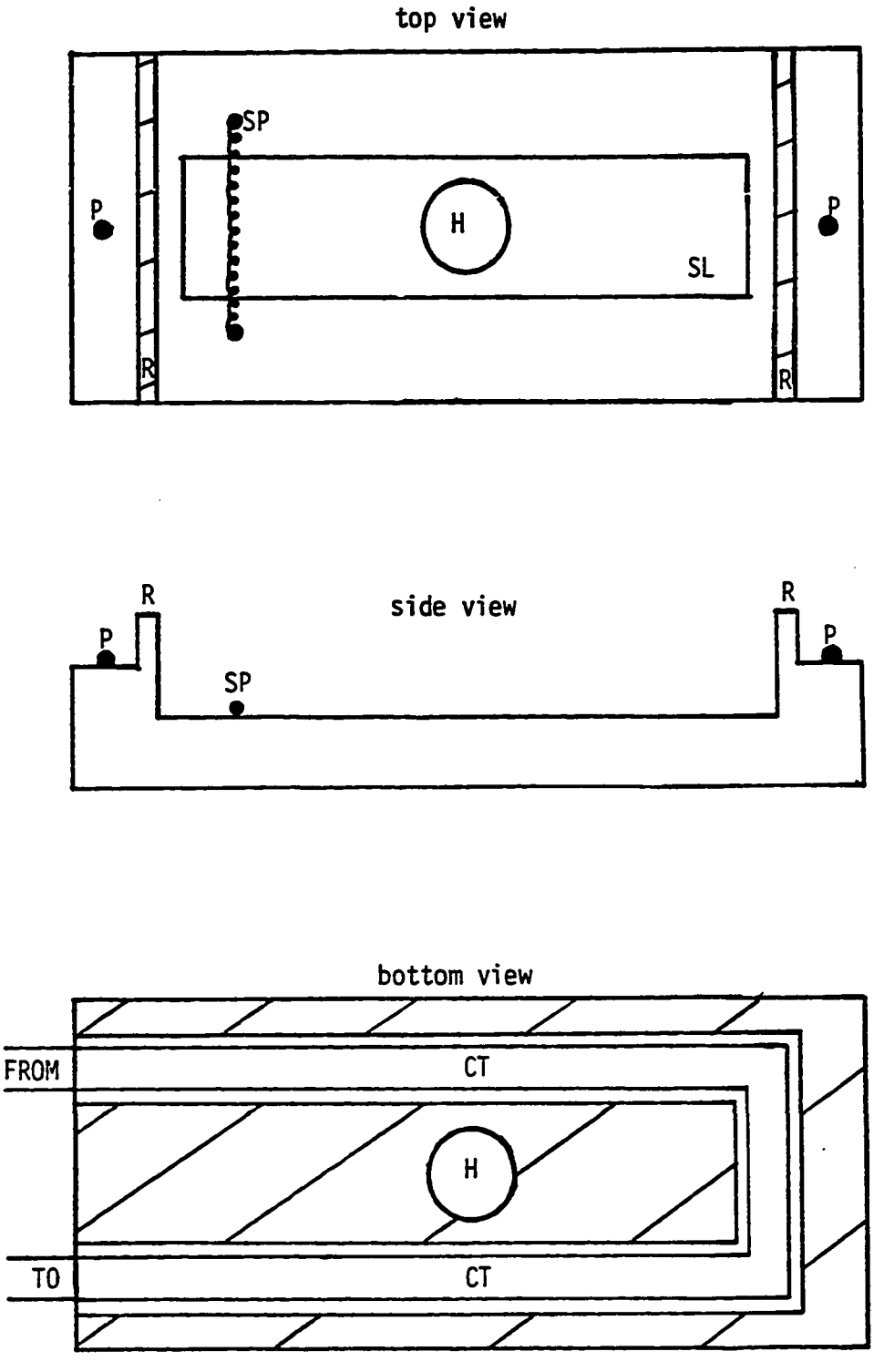

Figure 19. Aluminum sample holder outfitted for precise temperature regulation. P,pin; R,ridge; SP, spring; SL,slide; H,hole; CT,copper tubing; FROM,from water bath; TO,to water bath.

and fluorescein (314,315) or eosin (142), but not in the absence of oxygen (142,314,315). This finding implies that purging cell suspensions of oxygen prior to FPR experiments should eliminate the possibility of photosensitized cross-linking. These photo-oxidation experiments are performed on macroscopic suspensions of ghosts using large doses of diffuse laser light, though, and their applicability to the microscopic situation of an FPR experiment is questionable. For example, the extent of cross-linking decreases with shorter exposure times to the same total irradiation dose of exciting light (315), suggesting that the bleaching pulses involved in FPR experiments (<1 sec duration) may induce only minimal cross-linking (see also 316,317). In addition, various control experiments comparing lateral mobility parameters determined by FPR experiments with those determined by other techniques in the same system (255,318) have not shown any deleterious effect of photobleaching on the measurement of these parameters. Both irreversible dye bleaching (necessary for FPR measurements) and photosensitized oxidation (leading to production of singlet oxygen with subsequent cross-linking of membrane proteins) may proceed by so-called type II mechanisms in which electronically excited dye triplet state interacts with molecular oxygen to produce singlet oxygen and either bleached (irreversibly oxidized) or ground-state dye (315). If this is the case, then removal of oxygen from the system should mean that a greater number of photons must be directed at the sample

in order to get the same amount of fluorophore bleaching. This hypothesis was in fact borne out in the present studies, and the success of purging could be determined by the rapidity with which bleaching of fluorophore occurred at a given laser intensity (data not shown). It is likely, moreover, that photochemical bleaching of fluorophore can proceed by mechanisms which do not involve oxygen, while photoinduced cross-linking of membrane proteins almost certainly involves a diffusible oxygen intermediate. Purging the eosin-labeled ghosts of oxygen prior to FPR experiments was thus deemed the best method for eliminating possible adverse cross-linking effects mediated by excited state molecular oxygen.

One to two μl of the purged ghost suspension was placed on a microscope slide, covered with a 22 mm x 22 mm cover glass (No. 1 thickness), and sealed with epoxy (Devcon, "Five-Minute" Epoxy), all inside the glove bag. The ghost suspension spread spontaneously between the slide and cover glass, yielding a sample of average thickness 2-4 μm (calculated from the volume applied and the area occupied). This geometry oriented the ghosts parallel to the microscope slide and maintained them in a fixed position on the slide, a necessary prerequisite for measurements of diffusion by FPR. Defocusing effects in bleaching and fluorescence measurements due to the small depth of field of the 100x objective were also almost entirely eliminated with a sample of this thinness (see ref. 244). Thus, it can be calculated that the focused laser beam

irradiated both the top and bottom ghost membranes with a maximum difference in beam area of 14% between the two membranes, if the membranes were separated by 2 μm (see ref. 244). This difference was well within the experimental error of the apparatus. The volume of the ghost suspension after purging was compared to the volume before purging, in order to determine the exact concentration of phosphate buffer in the sample which was sealed on the microscope slide.

In a control experiment, 300 μl of human hemoglobin in distilled H_2O (prepared by lysis of intact erythrocytes and centrifugation to pellet the membranes, as described in chapter 3) was deoxygenated with nitrogen for one to three hours and sealed on a microscope slide with epoxy, all in the glove bag. The absorbance spectrum (Cary 14) of all of the samples showed only deoxyhemoglobin immediately after deoxygenation and sealing. No spectrophotometrically detectable oxyhemoglobin was regenerated on standing at room temperature for 24 hrs, confirming that the epoxy was impermeable to oxygen over a period of at least 24 hrs (data not shown).

3. Fluorescence Photobleaching Recovery Experiment

The deoxygenated eosin-labeled ghost sample was placed either directly on the microscope stage of the FPR apparatus (initial studies) or in the aluminum sample holder which was itself on the microscope stage (later studies). Individual ghosts were located either by transmitted light or by incident-light fluorescence.

The latter mode used the fully attenuated laser beam as the excitation source, with the diffuser plate placed in the beam in order to expand the area of the microscope field which was illuminated (see fig. 11). The cells appeared disc-like to cup-shaped and were uniformly fluorescent with a bright green perimeter; they were fairly homogeneous in size with diameter 5-9 μm. A single cell was centered in the field so that the focused laser spot fell in the center of the cell. The field diaphragm (fig. 11) was adjusted to an area approximately ten times larger in the specimen plane than that of the ghost. The laser power output was adjusted so that a measuring light pulse would produce a convenient signal as measured by the photomultiplier tube. Typical settings were: laser power, 100 mW (attenuated by 5×10^4 to 1×10^5 by neutral density filters before the beam reached the sample); voltage to photomultiplier, 1100 V; electrometer, 10-30 $\times 10^{-9}$ amp full scale. The XY recorder was started in the time-base mode with a 0.25 sec filter and several values of the pre-bleach fluorescence from the laser-illuminated spot were measured. A brief (<1 sec in initial studies, 10-100 msec in later studies) intense bleaching pulse (approximately 1 mW) was delivered as described in chapter 2. Periodic measuring pulses (duration 1 sec) were delivered until a stable post-bleach fluorescence level was reached. Under certain circumstances the fluorescence recovery was seen to proceed with extreme rapidity ($\tau_{1/2}$<5 sec); in these cases, the beam stop

(initial studies) or measuring electromechanical shutters (later studies) were left open for the entire recovery period and a smooth recovery curve was obtained. Sometimes a ghost was bleached two to four times in succession in the same spot, in order to compare diffusion coefficients and fractional recoveries of fluorescence when some of the (immobile) fluorophore in a given region of the cell was already bleached. At the conclusion of the experiment, a very long bleaching pulse was delivered (90-120 sec) in order to bleach all of the fluorophore in the illuminated area. The residual fluorescence value after this bleaching pulse (usually <5% of the fluorescence of an unbleached spot) was a measure of the background light level in the system. This value was taken to be the zero level in calculating the K parameter from the immediate pre- and post-bleach fluorescence values (eqn. 5).

In a control experiment a single cell was centered in the field and, with the diffuser plate in the beam and the field diaphragm wide open, the fluorescence produced on the illumination of the entire cell was measured. The whole cell was then bleached in the usual manner by the unattenuated laser beam while keeping the diffuser plate in the beam. No recovery of fluorescence was observed over a period of 15 min, indicating that spontaneous photochemical recovery of eosin fluorescence was not contributing to the recovery process in the normal FPR experiment, i.e., that bleaching

was in fact an irreversible process (data not shown).

B. RESULTS: INITIAL STUDIES.

The results of the initial series of fluorescence photobleaching recovery experiments on eosin-labeled erythrocyte ghosts are summarized in table 7. Incubation conditions ranged from 5.2 mM to 46 mM sodium phosphate buffer at pH 7.4 (all sample buffers also contained 1 mM NaN_3 and 30 nM PMSF) and from 21°C to 37°C in temperature. Typical experimental recovery curves under the extremes of these incubation conditions are given in fig. 20 and compared to theoretical FPR curves for diffusion with a Gaussian beam (242). In general the fit is excellent, implying that lateral diffusion is the only process which is contributing significantly to fluorescence recovery. This notion was confirmed, albeit in a qualitative way, by the visual observation that the cell which had been bleached was immobile over the time course of the FPR experiment, retaining the same position in the microscope field at all times. The experimental data tended to be more scattered under conditions of high ionic strength and low temperature, where fractional recoveries of fluorescence were low (fig. 20C). This was mainly a signal-to-noise problem, since the percentage contribution of noise to the experimental data was greater with smaller changes in signal. This scatter was also reflected in the relatively large error in fractional recovery at 46 mM phosphate and 21°C (table 7). Nonetheless, even under these conditions the data fit a theoretical diffusion curve well.

TABLE 7. EFFECT OF LOW IONIC STRENGTH ON LATERAL MOBILITY OF BAND 3: INITIAL STUDIES

	21°C[b]			30°C[c]			37°C[d]		
$[PO_4]$, mM[a]	$Dx10^{11}$, cm^2/sec	f(∞)	N	D	f(∞)	N	D	f(∞)	N
5.2	5.0 ± 2.2[e]	0.72 ± 0.02[e]	4	11 ± 1	0.69 ± 0.08	2	---[f]	---	
9.4	9.5 ± 2.3	0.51 ± 0.14	5				---	---	
13.3	6.7 ± 0.2	0.34 ± 0.05	3	14 ± 5	0.60 ± 0.12	4	65 ± 40	0.83 ± 0.06	3
18.8	8.7 ± 1.8	0.37 ± 0.09	3	7.9 ± 1.2	0.79 ± 0.05	3	58 ± 8	0.73 ± 0.11	2
21.4	8.2 ± 1.2	0.36 ± 0.09	6				29 ± 10	0.75 ± 0.11	7
26[g]	7.0 ± 3.0	0.38 ± 0.09	4	7.0 ± 3.0	0.71 ± 0.10	2	14 ± 4	0.75 ± 0.13	2
46	4.3 ± 0.2	0.11 ± 0.08	2				4.6 ± 0.8	0.41 ± 0.12	3

[a]All samples also buffered in 1 mM NaN_3, 30 nM PMSF, pH 7.4

[b]4-5 hr incubation, except 5.2 mM PO_4 which was 1-2 hr incubation

[c]0.5-1 hr incubation, except 5.2 mM PO_4 which was 0.25-0.5 hr

[d]0.5-1 hr incubation

[e]All values expressed as mean ± S.D.

[f]Experiment prevented by 100% ghost vesiculation

[g]Approximate concentration

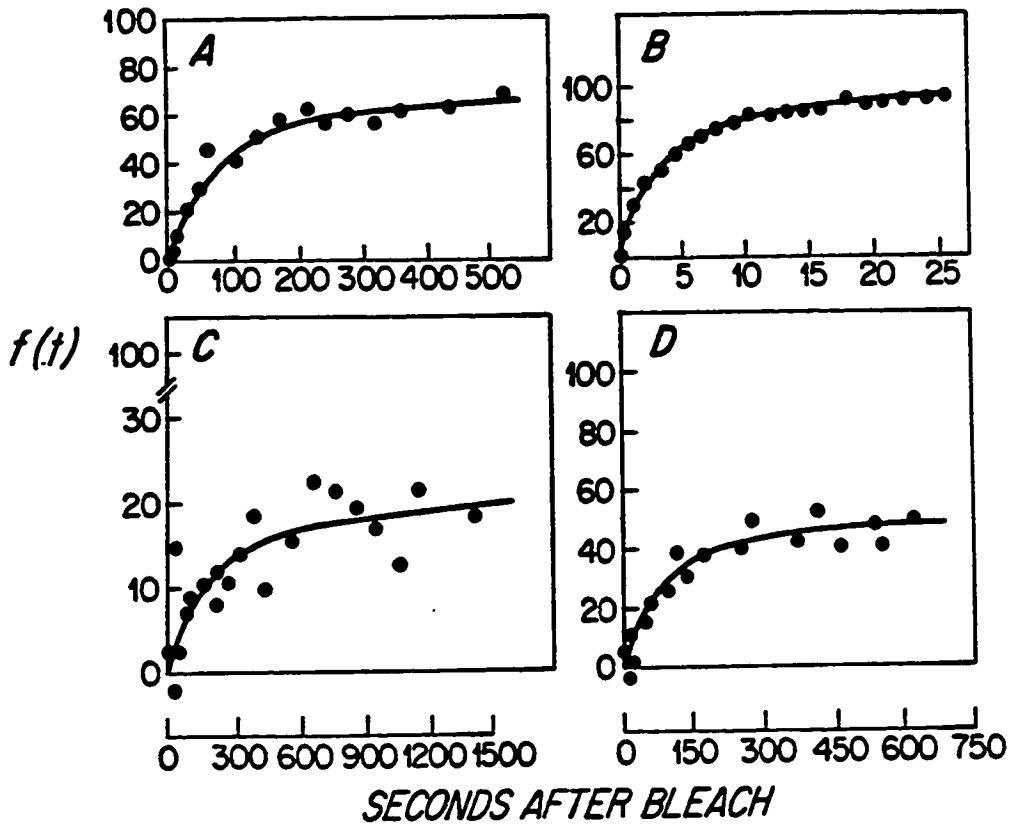

Figure 20. Experimental FPR curves on eosin-labeled erythrocyte ghosts at the extremes of ionic strength and temperature used in this study. Theoretical curves for diffusion with a Gaussian beam were fit to experimental points by hand. The good agreement between FPR data and theoretical curves demonstrates that lateral diffusion is responsible for the observed fluorescence recovery under all conditions of ionic strength and temperature. The parameter f(t) represents the fractional recovery of fluorescence at time t; $f(t)=(F(t)-F(0))/(F(-)-F(0))$. Curves on left, 21°C; curves on right, 37°C. Curves at top, low ionic strength; curves at bottom, high ionic strength. Note large differences in time scale (i.e., diffusion coefficient) and fractional recovery (i.e., mobile fraction) under various conditions.

(A) 5 mM $NaPO_4$, 21°C; $D=6.2 \times 10^{-11}$ cm^2sec^{-1}, $f(\infty)=0.65$.

(B) 13 mM $NaPO_4$, 37°C; $D=130 \times 10^{-11}$ cm^2sec^{-1}, $f(\infty)=0.94$.

(C) 46 mM $NaPO_4$, 21°C; $D=2.1 \times 10^{-11}$ cm^2sec^{-1}, $f(\infty)=0.20$.

(D) 46 mM $NaPO_4$, 37°C; $D=4.4 \times 10^{-11}$ cm^2sec^{-1}, $f(\infty)=0.50$.

1. Effect of Ionic Strength. Low temperature (21°C) and high ionic strength (46 mM phosphate) favored immobilization of band 3 (11±8% fractional recovery) as well as slow diffusion of the mobile fraction ($D=4.3\pm0.2 \times 10^{-11}$ cm^2/sec) (table 7). Decreasing the ionic strength at the same temperature caused little if any change in diffusion coefficient ($D=5\text{-}10 \times 10^{-11}$ cm^2/sec at all phosphate concentrations) but a marked increase in fractional recovery ($f(\infty)=72\pm2\%$ at 5 mM phosphate) (fig. 21).

At 37°C much of the band 3 was mobile even at high ionic strength (41±12% fractional recovery at 46 mM phosphate), although diffusion of the mobile fraction was still slow ($D=4.6\pm0.8 \times 10^{-11}$ cm^2/sec). Decreasing ionic strength led first to a rapid increase in fractional recovery to 75±13%, followed by a sharp rise in diffusion coefficient to $65\pm40 \times 10^{-11}$ cm^2/sec (fig. 21). It should be noted that the sharp increase in diffusion coefficient occurred over an ionic strength range in which the fractional recovery was not changing at all. Measurement of lateral mobility at phosphate buffer concentrations less than 10 mM at 37°C was prevented by rapid (<15 min) and total vesiculation of ghost membranes. The 1-2 μm diameter vesicles produced were easily identified in the fluorescence microscope. In addition, cells containing endocytotic vesicles showed no fluorescence recovery after bleaching, since the vesicles which were bleached were approximately the same size as the bleaching laser beam (data not shown).

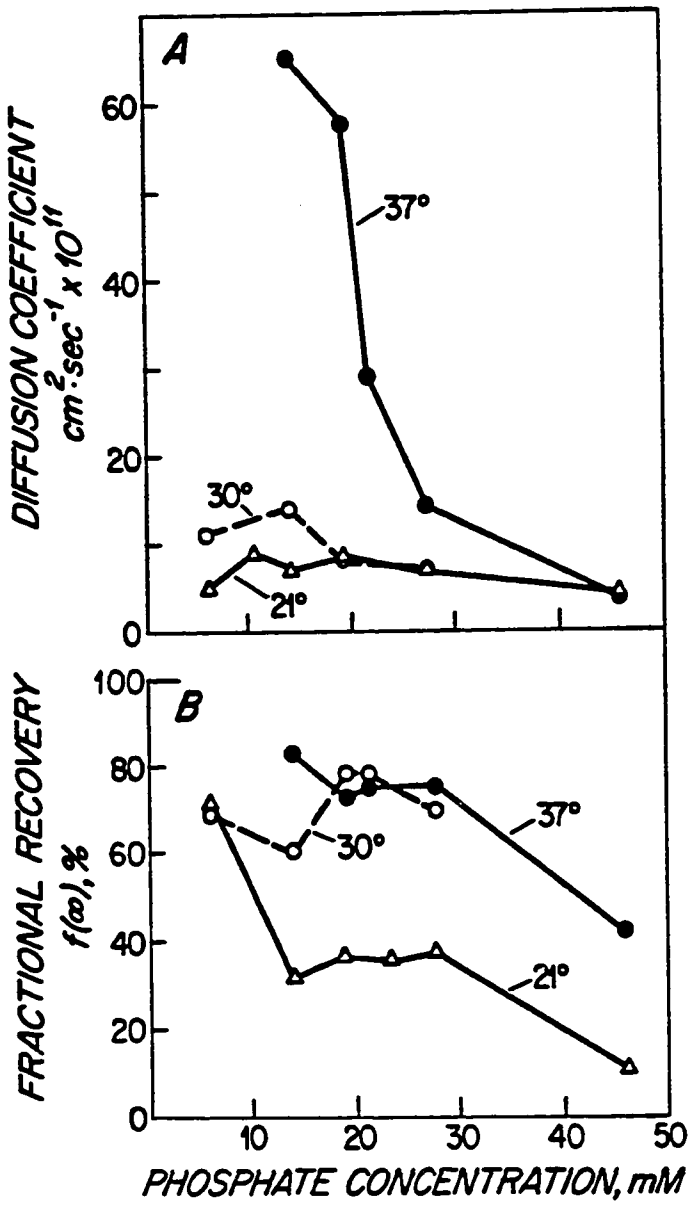

Figure 21. Diffusion coefficients (A) and fractional recoveries of fluorescence (B) obtained from FPR experiments on eosin-labeled erythrocyte ghosts as functions of ionic strength, at various temperatures. The fractional recovery represents the fraction of band 3 molecules that is free to diffuse laterally. Each point represents the mean of two to seven independent determinations on separate ghosts (see Table 7).

2. Effect of Temperature. Increasing temperature led to increases in both diffusion coefficient and fractional recovery. These changes occurred over different ranges of ionic strength and temperature, however, and were thus dissociated from one another (fig. 21). At 46 mM phosphate, for example, increasing temperature from 21°C to 37°C caused a significant increase in the fractional recovery (11±8% to 41±12%) but no change in the (still slow) diffusion coefficient. Conversely, at 5 mM phosphate increasing temperature from 21°C to 30°C led to an increase in the diffusion coefficient (5±2 to 11±1 x 10^{-11} cm^2/sec) but no change in the (already high) fractional recovery. At intermediate phosphate concentrations, increasing temperature resulted first in an increase in fractional recovery (from 30-40% to 60-80%), followed by a sharp rise in diffusion coefficient (fig. 21). In all cases the fractional recovery increased to 60-80% before the diffusion coefficient began to rise.

The ability of the two FPR parameters to change with decreases in temperature provided further evidence of their dissociation (fig. 22). At ionic strengths of 13 mM and 21 mM phosphate, incubation of ghosts at 37°C for 2.5 hr produced large increases in both diffusion coefficient and fractional recovery when compared to the initial values at 21°C. Cooling of the samples back to 21°C for two hours resulted in a return of the diffusion coefficients to the initial values, while the fractional recoveries remained elevated on cooling

Figure 22. Reversibility of diffusion coefficients and fractional recoveries of fluorescence. Eosin-labeled ghost samples were incubated at 21°C for 4.5 hrs after which time FPR measurements were taken. The temperature was then increased to 37°C for 2.5 hrs and FPR experiments again performed. Finally the temperature was lowered back to 21°C for 2 hrs and FPR parameters were again measured.
(a) ghost sample prepared in 13 mM $NaPO_4$
(b) ghost sample prepared in 21 mM $NaPO_4$

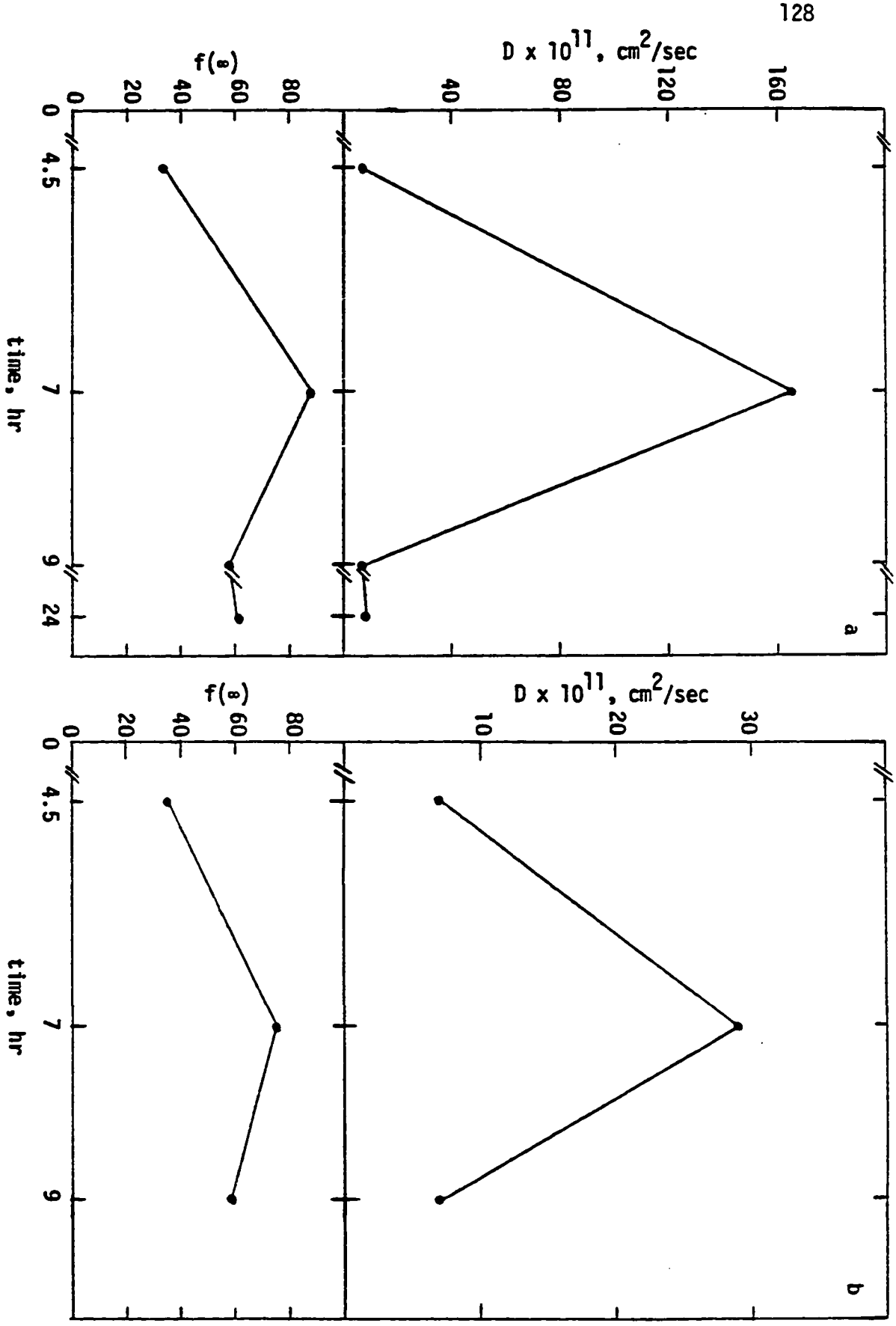

Figure 22.

even at 24 hrs (fig. 22a). The molecular interpretation of this reversibility data is far from clear, however (see below).

It was possible to inhibit completely the lateral mobility of band 3 in the membrane. A sample of labeled ghosts was prepared in the usual manner (see Methods) and incubated for 24 hrs at 4°C in the dark. The slide was then placed on the precooled microscope stage (10°C) and the FPR experiment performed at 10±2°C. No fluorescence recovery was detected in 30 min after bleaching. Warming of the sample to 21°C for 60 min resulted in a recovery curve whose parameters (diffusion coefficient, fractional recovery) were within experimental error of those from a sample at the same ionic strength and temperature which had not been incubated in the cold (data not shown).

3. Effect of Time. Under the proper conditions of ionic strength and temperature, the diffusion coefficient and fractional recovery of fluorescence were extremely sensitive to the time of incubation. Figure 23 presents the results of an experiment in which the FPR parameters were determined every 15 minutes for 3 hours after raising the temperature of the sample from 21°C to 37°C. A different cell was used for each point to avoid bleaching an area in a cell which had been bleached previously in the experiment. Within 50 minutes the fractional recovery increased to a maximum value of 88±10% and remained at that value for the duration of the experiment. On the other hand, the diffusion coefficient increased slowly for the

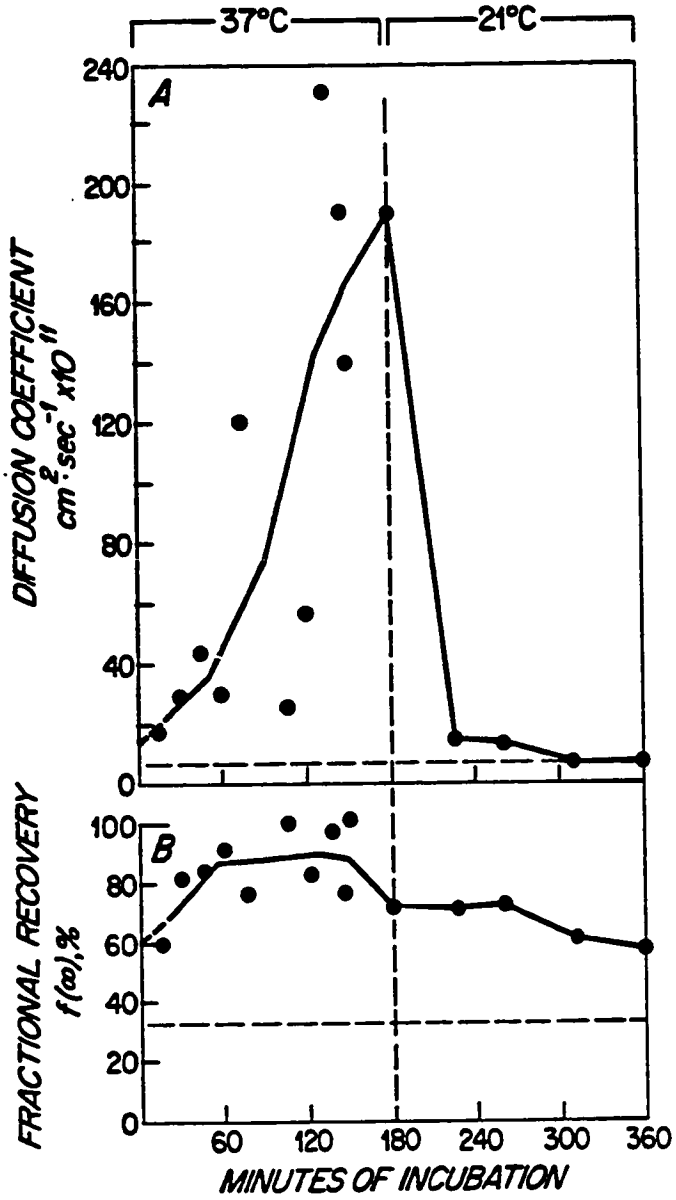

Figure 23. Diffusion coefficients (A) and fractional recoveries of fluorescence (B) as functions of incubation time at 37°C in 13 mM $NaPO_4$ buffer. Horizontal broken lines represent initial values at 21°C, before temperature had been increased to 37°C. Smoothed curves are drawn through the experimental points by pairwise averaging of adjacent data points. At t=0, curves are extrapolated back to the values obtained at 30°C in the same buffer (probably a slight underestimate for the initial values at 37°C). The vertical broken line represents return of temperature to 21°C. Temperature equilibration time was 10-15 min. Each experimental point was obtained from a separate erythrocyte ghost in the sample.

first hour and much more rapidly over the following two hours, reaching an average value of $1.9 \pm 0.3 \times 10^{-9}$ cm^2/sec (N=4) at the end of three hours. Reversal of the incubation temperature resulted in prompt reversibility of the diffusion coefficient but only minimal reversibility of the fractional recovery (fig. 23; but see Chapter 4C).

4. Rebleaching Experiments. Successive bleaches of the same fluorescently-labeled region on a cell membrane should theoretically result in increasingly greater fractional recoveries of fluorescence with each bleach (264,265). This is because the fractional recovery of fluorescence reflects the ratio of unbleached mobile to immobile fluorophore in the region prior to bleaching, and successive bleaches lead to progressively greater increases in this ratio. If the mobile fluorophore is only free to diffuse within discrete membrane domains significantly smaller than the size of the cell but comparable in size to the bleaching laser beam, however, a limiting fractional recovery which is considerably less then 100% would eventually be reached no matter how many bleaches are delivered (273).

To test this in the eosin-labeled band 3 system, successive rebleachings were performed under a variety of ionic strength and temperature conditions (table 8). In all cases the fractional recovery increased with each succeeding bleach, reaching a value of 80-100% after the third or fourth bleach. Unless the fractional

TABLE 8. REBLEACHING EXPERIMENTS ON EOSIN-LABELED GHOST MEMBRANES

$[PO_4]$, mM[a]	temp, °C	bleach #	K[b]	$Dx10^{11}$, cm^2/sec	f(∞)
46	21	1	1.9	---	0.07
		2	1.9	4.4	0.50
	37	1	1.6	5.7	0.50
		2	2.6	5.8	0.60
		3	2.7	5.1	0.68
		4	4.5	16.	0.81
21.4	21	1	1.9	9.6	0.32
		2	1.6	2.9	0.73
		3	1.8	2.3	0.94
	37	1	2.1	22.	0.68
		2	2.0	9.6	1.06
18.8	37	1	0.7	66.	0.64
		2	1.4	57.	0.92
9.4	21	1	1.5	7.9	0.50
		2	2.9	8.5	0.73
5[c]	21	1	2.4	7.9	0.45
		2	2.7	8.6	0.59
		3	1.5	7.2	0.66
		4	3.3	4.9	0.87
	21	1	2.3	5.4	0.44
		2	5.0	9.2	0.50
		3	3.4	6.2	0.67
		4	3.0	6.7	0.86

[a] +1 mM NaN_3, 30 nM PMSF

[b] bleaching parameter

[c] +10 mM NaN_3, 30 nM PMSF

recovery was very high on the first bleach (60-70%), it did not reach 80-100% after the second bleach because the bleaching of immobile fluorophore by two laser pulses with K parameters of 2-5 was still incomplete. Subsequent bleaches approached 100% recovery in all cases.

C. RESULTS: ADDITION OF PROTEASE INHIBITORS.

A variety of erythrocyte membrane-associated proteases have been characterized in the past several years (319-330). The functional importance of these proteases has been demonstrated in several recent experiments concerning the stability and integrity of various cytoskeletal proteins (152,204,330). For example, endogenous proteases which attack membrane-bound ankyrin were found to be inhibited by a combination of the calcium chelator EDTA with the sulfonyl fluoride PMSF (326), while the yield of purified ankyrin from erythrocyte ghosts was greatly increased by the inclusion of EDTA, PMSF, and the acid-protease inhibitor pepstatin A in lysis, washing, and storage buffers (204). Of perhaps the most relevance to the present study is the finding, in rat erythrocytes, of a calcium-activated (EDTA-inhibited) thiol-containing protease which degrades various membrane proteins (probably including spectrin, ankyrin, and band 3) and leads to increased freedom of lateral motion of intramembranous particles (330). In the light of this evidence, it was deemed prudent to examine the effect of protease inhibitors on the low ionic strength-induced increase

in band 3 lateral mobility. The reader is reminded that all FPR experiments in this section and, indeed, in the remainder of this dissertation were performed on the improved, recalibrated apparatus described in chapter 2.

1. Effect of PMSF Alone.

Eosin-labeled erythrocyte ghosts were prepared as for the initial studies in chapter 4B, except that PMSF was added to a final concentration of 30 μM (instead of 30 nM) in all washing, lysis, and storage buffers. The ghosts were then incubated in 16.2 mM sodium phosphate, pH 7.4, containing final concentrations of PMSF from 3 to 130 μM. Results of a series of FPR experiments on such ghosts are given in table 9 and reproduced in graphical form in fig. 24. Above 30 μM PMSF, there was little change in either the diffusion coefficient or the fractional recovery of the eosin-labeled band 3. Below 30 μM PMSF, however, there were sharp increases in both lateral mobility parameters which are especially evident at high temperature.

These data were taken as evidence for a PMSF-sensitive process, most likely proteolysis, contributing to the low ionic strength-induced increase in band 3 lateral mobility reported in the previous section. It was decided to pursue the problem in two complementary manners. First, the low ionic strength dependence of band 3 lateral mobility was re-examined in the presence of three protease inhibitors known to be effective on erythrocyte membrane-

TABLE 9. EFFECT OF PMSF ON LATERAL MOBILITY OF BAND 3[a]

	21°C[b]			30°C[c]			37°C[d]		
[PMSF], μM[e]	$Dx10^{11}$, cm^2sec^{-1}	f(∞)	N	D	f(∞)	N	D	f(∞)	N
3	2.8 ± 0.3	0.36 ± 0.11	2	3.5 ± 0.6	0.62 ± 0.07	2	26 ± 11	0.85 ± 0.06	7
31	1.7 ± 1.2	0.16 ± 0.07	3	3.0 ± 0.8	0.56 ± 0.14	3	6.6 ± 1.5	0.50 ± 0.09	3
130	1.6 ± 0.6	0.24 ± 0.01	3	2.6 ± 0.7	0.23 ± 0.15	2	3.5 ± 2.0	0.32 ± 0.06	3

[a]All values expressed as mean ± S.D.

[b]2-3 hr incubation

[c]0.5-1 hr incubation

[d]0.67-1.33 hr incubation

[e]All samples also buffered in 16.2 mM $NaPO_4$, 1 mM NaN_3, pH 7.4

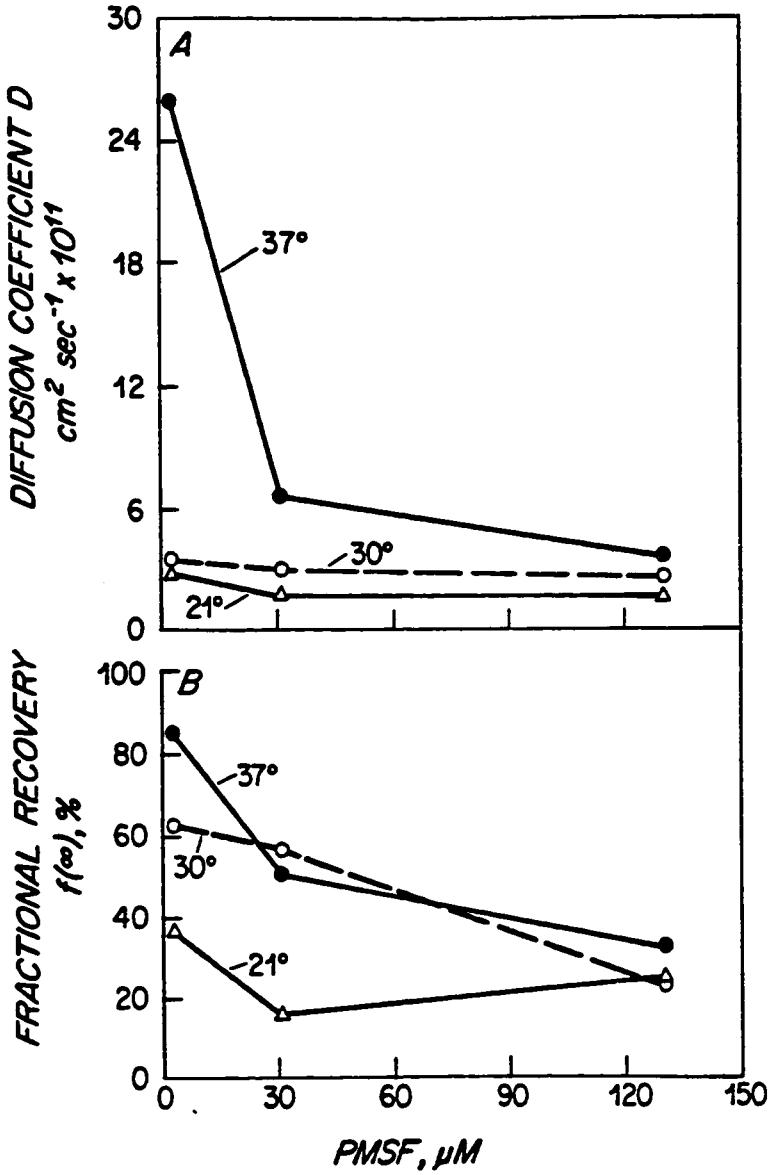

Figure 24. Diffusion coefficients (A) and fractional recoveries of fluorescence (B) obtained from FPR experiments on eosin-labeled erythrocyte ghosts in 16.2 mM $NaPO_4$ buffer as functions of the concentration of PMSF, at various temperatures. Each point represents the mean of two to seven independent determinations on separate ghosts (see Table 9).

associated proteases (i.e., PMSF, EDTA, and pepstatin A). Concentrations of protease inhibitor were chosen in accord with literature values (204,326) and in consideration of the results shown in table 9. Second, dissociation and proteolysis of various membrane protein components under the incubation conditions of the FPR experiment were investigated directly by SDS-polyacrylamide gel electrophoresis. The results of the former set of experiments are reported in the remaining sections of this chapter, those of the latter series of experiments in the following chapter.

2. Effect of Ionic Strength and Temperature.

Even in the presence of the protease inhibitors PMSF, EDTA, and pepstatin A, the lateral mobility of band 3 was strongly dependent on ionic strength and temperature (table 10, fig. 25). These dependencies were similar to those seen in the presence of a small concentration of PMSF alone (table 7, fig. 21), in that low ionic strength (13.9 mM $NaPO_4$) and high temperature (37°C) favored large increases in both diffusion coefficient ($24\pm7 \times 10^{-11}$ cm^2/sec^{-1}) and fractional recovery (0.66 ± 0.08) over high ionic strength (42 mM $NaPO_4$) or low temperature (21°C) values. Further, the increases in fractional recovery were somewhat dissociated from those in diffusion coefficient, although this dissociation was less striking than that seen in the absence of protease inhibitors. The lateral mobility increases appeared at lower ionic strength in the presence of protease inhibitors than in their

TABLE 10. EFFECT OF LOW IONIC STRENGTH ON LATERAL MOBILITY OF BAND 3: ADDITION OF PROTEASE INHIBITORS[a]

	21°C[b]			30°C[c]			37°C[d]		
$[PO_4]$, mM[e]	$Dx10^{11}$, cm^2sec^{-1}	f(∞)	N	D	f(∞)	N	D	f(∞)	N
13.9	1.3 ± 0.5	0.17 ± 0.06	5	1.9 ± 0.8	0.40 ± 0.11	4	24 ± 7	0.66 ± 0.08	6
17.9	1.3 ± 0.1	0.20 ± 0.01	2	2.1 ± 0.8	0.28 ± 0.11	2	5.1 ± 0.6	0.57 ± 0.14	2
23.9	1.5 ± 0.4	0.20 ± 0.01	2	2.1 ± 0.4	0.19 ± 0.00	2	0.95 ± 0.10	0.40 ± 0.12	3
42.0	1.3 ± 0.5	0.12 ± 0.09	6	1.9 ± 0.9	0.16 ± 0.07	5	1.3 ± 0.4	0.21 ± 0.13	8

[a]All values expressed as mean ± S.D.

[b]2-3 hr incubation

[c]0.5-1 hr incubation

[d]0.67-1.33 hr incubation

[e]All samples also buffered in 1 mM NaN_3, 60 μM PMSF, 1 mM EDTA, 1 μg/ml pepstatin A, pH 7.4

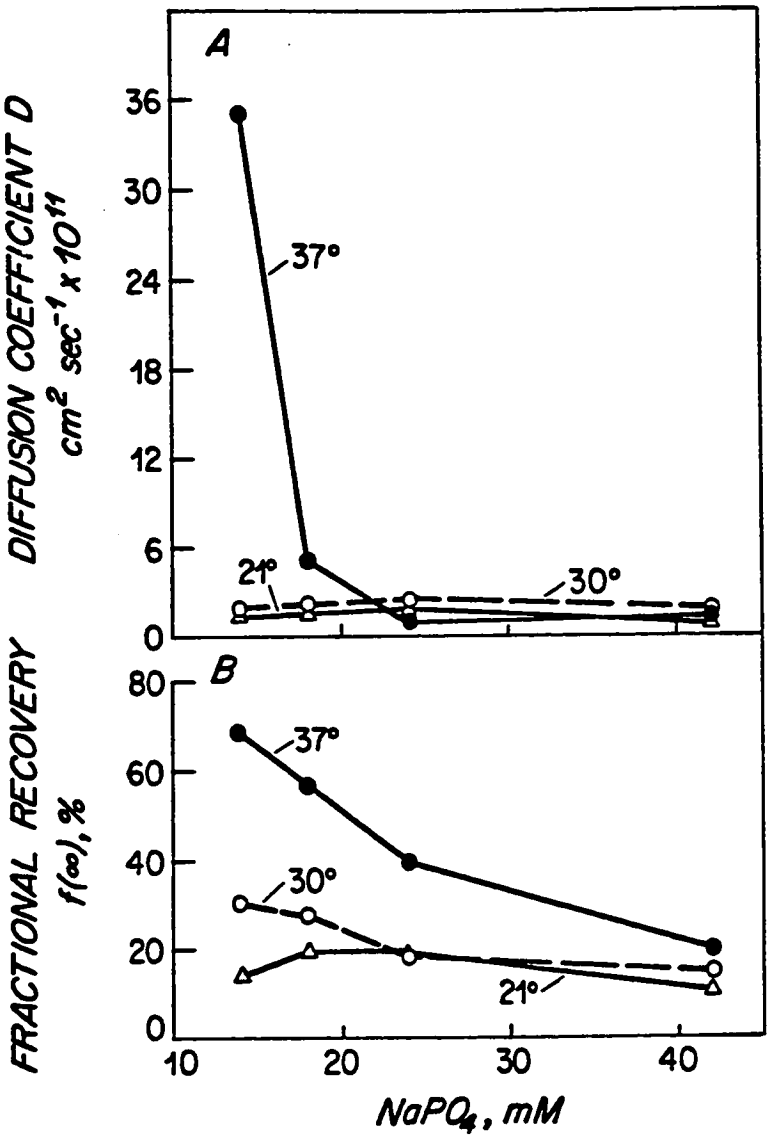

Figure 25. Diffusion coefficients (A) and fractional recoveries of fluorescence (B) obtained from FPR experiments on eosin-labeled erythrocyte ghosts, in the presence of the protease inhibitors PMSF (60 μM), EDTA (1 mM), and pepstatin A (1 μg/ml), as functions of ionic strength, at various temperatures. Individual points represent the average of two to eight independent measurements (see Table 10).

absence, as expected from the results of the previous section (table 9). Nonetheless, as we shall see in the next chapter, these increases at relatively short incubation times were not associated with the specific proteolysis of any major membrane component.

3. Effect of Time.

The effect of incubation time on band 3 lateral mobility under very low ionic strength (13.9 mM $NaPO_4$), high temperature (37°C) conditions was not substantially changed by the addition of the protease inhibitors PMSF, EDTA, and pepstatin A to the incubation medium. Figure 26 presents the results of two such kinetic experiments, in which a FPR measurement was taken every 15 min after increasing the temperature of each sample from 21°C to 37°C. Some variability may be seen in the data, especially in the measurement of diffusion coefficient at long incubation times and in the length of the lag period preceding large increases in lateral mobility. Several consistent findings should be noted, however. First, as seen in the absence of protease inhibitors (fig. 23), there was an approximately 50-fold difference between the lateral diffusion coefficient of band 3 at room temperature ($D=1.3\pm0.5 \times 10^{-11}$ cm^2sec^{-1}, N=5) and the fastest diffusion coefficient at long times of incubation at 37°C ($D = 54\pm19 \times 10^{-11}$ cm^2sec^{-1}, N=9). These extremes are both approximately 4-fold lower than comparable measurements in the

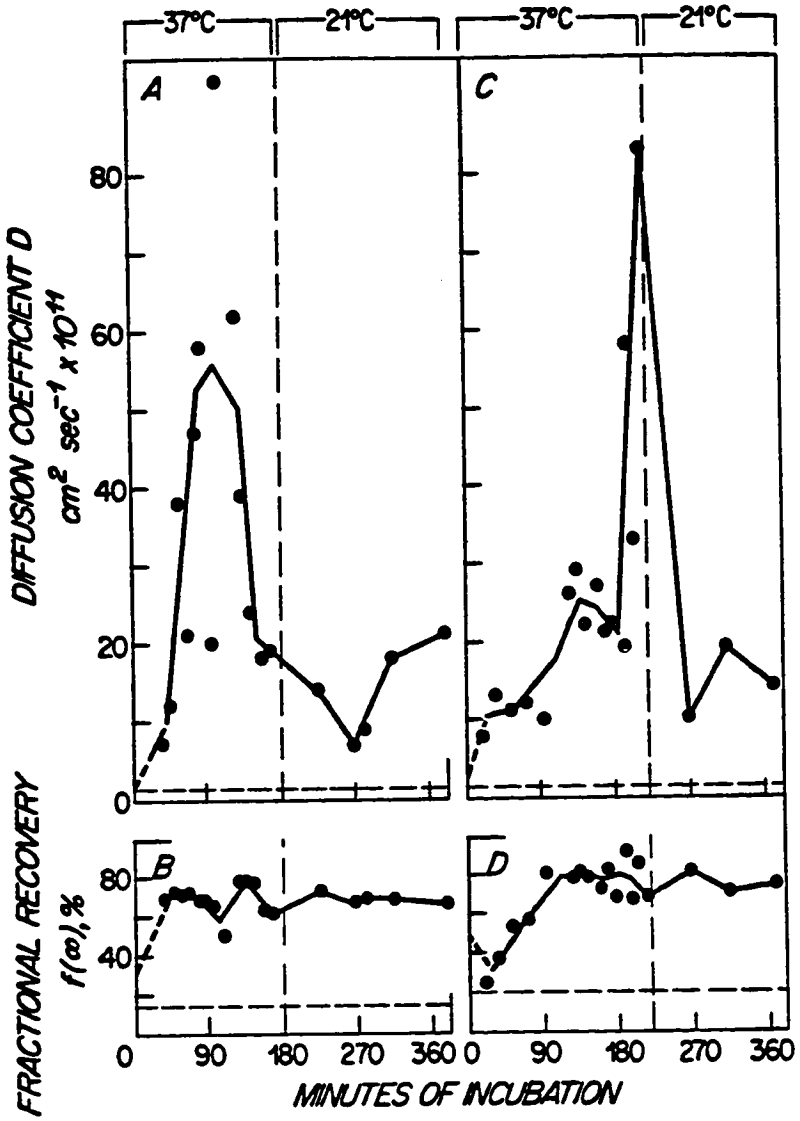

Figure 26. Diffusion coefficients (A,C) and fractional recoveries of fluorescence (B,D) obtained from two independent FPR experiments on eosin-labeled erythrocyte ghosts, in the presence of the protease inhibitors PMSF (60 μM), EDTA (1 mM), and pepstatin A (1 μg/ml), as functions of incubation time at 37°C, in 13.9 mM $NaPO_4$ buffer. Panels A,B and C,D represent the results of experiments performed on separate ghost samples, on different days. Horizontal broken lines represent initial values at 21°C, before the temperature had been increased to 37°C. Smoothed curves are drawn through the experimental points by pairwise averaging of adjacent data points. At t=0, curves are extrapolated back to the values obtained at 30°C in the same buffer. Vertical broken lines represent return of temperature to 21°C. Temperature equilibration time was approximately 10 min. Each experimental point was obtained from a separate erythrocyte ghost in the sample.

absence of protease inhibitors (fig. 23), although some of this difference may simply be due to the more accurate calibration of the FPR apparatus employed in gathering the data shown in fig. 26 (see chapter 2). Second, there was a 1-2 hr lag period preceding very large increases in diffusion coefficient, again paralleling results seen in the absence of protease inhibitors. Third, in both sets of kinetic measurements the fractional recovery increased to maximal values (70-80%) before very large changes in diffusion coefficient occurred, although this dissociation was less striking than that observed in fig. 23. Finally, both kinetic experiments showed only partial reversibility of diffusion coefficient, and no reversibility of fractional recovery,upon return of the sample temperature to 21°C following 3 hr incubations at 37°C. This is not surprising in the light of experiments reported in chapter 5, which demonstrate the specific proteolysis of the particular cytoskeletal protein ankyrin under the conditions of low ionic strength, high temperature, and long incubation time.

D. DISCUSSION

This chapter presents the results of fluorescence photobleaching recovery experiments on eosin-labeled band 3 in erythrocyte ghost membranes under various conditions of ionic strength, temperature, and time, both in the presence and absence of the protease inhibitors EDTA, PMSF, and pepstatin A. Experimental recovery curves were closely fit by theoretical curves for diffusion, proving that

fluorescence recovery after photobleaching represented lateral diffusion in the plane of the membrane with negligible contribution from any systematic flow process. Low ionic strength and high temperature promoted rapid diffusion of band 3 and a high proportion of mobile to total band 3 molecules; high ionic strength and low temperature favored slow diffusion of band 3 and immobilization of band 3 molecules on the time scale of the experiment. This generalization was true both in the presence and absence of protease inhibitors, even though at least one of these inhibitors (PMSF) was shown to have an effect on band 3 mobility at moderate ionic strength. It was repeatedly demonstrated, moreover, that the diffusion and the immobilization processes have different dependencies on ionic strength, temperature, and time. In all cases, increases in the diffusion coefficient occurred at lower ionic strength, higher temperature, or longer incubation times than comparable increases in fractional recovery. An important consequence of this result is that very large increases in the diffusion coefficient occurred only when the fractional recovery was already high, i.e., when nearly all the band 3 molecules were free to diffuse in the plane of the membrane. Furthermore, changes in the diffusion coefficient over almost two orders of magnitude were at least partially reversible, while two- to three-fold changes in the fractional recovery were, under some conditions at least, irreversible. Any model for erythrocyte membrane structure must take

these observations into account; several such models are presented and discussed in chapter 9.

The question of reversibility of lateral mobility parameters will be more fully discussed at the end of chapter 5, after various biochemical correlates between changes in lateral mobility and in the protein composition of the erythrocyte cytoskeleton have been explored.

Several qualifications must be placed on the theoretical limits of the experimental data obtainable by the actual FPR experiment, due to both the finite size of the erythrocyte membrane and the finite length of time in which a single FPR curve is obtained. As noted in chapter 2, the $1/e^2$ radius of the Gaussian laser beam used for bleaching is approximately 1 μm. The percentage of the total erythrocyte membrane surface (top and bottom) which is illuminated by the beam is approximately 6%, assuming a surface area for the membrane of 150 μm^2. A bleaching pulse characterized by a K value of 2-5 therefore bleaches approximately 4-6% of the total fluorophore present on the membrane surface (see fig. 6), and the maximum possible fractional recovery of fluorescence is 94-96% rather than 100%. After correcting for the finite size of the cell, then, the maximum mobile fraction of fluorophore observed in these FPR experiments (fig. 23) is (88/10)/95, or 93±10%. Unfortunately, the experimental error precludes a definitive statement as to whether all the band 3, or simply most of the band 3, is free to diffuse

under these conditions. If it is assumed that eosin labeling of spectrin occurs to the extent of 8% (see chapter 3), and that most if not all of the spectrin is immobile on the membrane (see chapter 1), then the experimentally observed maximum mobile fraction of band 3 is probably 100±10%. If the ankyrin-linked band 3 (10-15% of total band 3) is ever free to diffuse in the plane of the membrane, then either band 3-ankyrin, ankyrin-spectrin, or some other spectrin-membrane bonds must be broken. The implications of this statement are discussed more fully in chapter 9.

The finite length of time for which fluorescence recovery after bleaching is monitored leads to an estimate of the maximum possible diffusion coefficient for the fraction of fluorophore which is immobile on the time scale of the experiment. Assuming an observation time of 20 minutes after bleaching and a bleaching parameter (K) of 2, and taking a 20% change in fluorescence to be the minimum significant difference observable, a maximum diffusion coefficient for the immobile fraction of 1×10^{-12} cm^2/sec can be calculated (see fig. 9, eqn. 11). This number is at least an order of magnitude less than the minimum diffusion coefficient determined for the fraction of fluorophore which is mobile on the time scale of these experiments.

Under all conditions of ionic strength and temperature tested, successive bleachings on the same region of the ghost membrane resulted in 80-100% fractional recovery of fluorescence after the

third or fourth bleach. This is the result expected if mobile fluorophore is capable of diffusing over distances on the membrane much greater than the size of the laser beam (265). In particular, this result implies that bounded domains of protein or lipid were not responsible for the restricted lateral mobility of band 3 under various conditions of ionic strength and temperature in these FPR experiments. As noted above, a typical bleaching pulse leads to irreversible bleaching of approximately 5% of the total fluorophore on the membrane. Since the fractional recovery of fluorescence on repetitive bleaching is greater than 80%, the membrane area in which the fluorophore is freely diffusing can be no smaller than 5%/(100-80%), or at least 1/4 the area of the intact erythrocyte. Large domains of this size are highly unlikely.

The technical aspects of the experiments reported in this chapter are very reassuring in that the internal strucutre and consistency of the data excludes many potential artifacts from playing a major role in the results. The large dynamic range of values observed for both diffusion coefficients and fractional recoveries under various conditions implies that all the values are meaningful, especially in comparison with one another. In addition, as noted above, relative differences between diffusion coefficients under various conditions are independent of the diameter of the laser beam used for bleaching, and a slightly smaller or larger value for the beam size would not affect these

comparisons. Indeed, although a 4-fold difference was observed between the extreme values of the absolute lateral diffusion coefficient of band 3 in the experiments reported in chapter 4B and those in chapter 4C, the same relative difference between the extreme values was obtained in both cases.

CHAPTER 5. MEMBRANE PROTEIN DISSOCIATION AND PROTEOLYSIS: EFFECT OF LOW IONIC STRENGTH

The lateral mobility of band 3 in the erythrocyte membrane is highly dependent on the same experimental parameters which favor complete dissociation of the cytoskeleton from the membrane (see chapter 4). In this and the following chapter attempts are made to elucidate the molecular basis for changes in the lateral mobility of band 3. Biochemical evidence for the role of the erythrocyte cytoskeleton, and in particular the cytoskeletal protein ankyrin, in the control of band 3 mobility is presented in this chapter. First, the ionic strength dependence of dissociation of spectrin, the major cytoskeletal protein, from the ghost membrane is examined. While spectrin dissociation is indeed found to be dependent on ionic strength, complete dissociation of spectrin occurs over a range of ionic strengths much lower than that over which dramatic changes in lateral mobility are seen. This is true even under the high temperature, long incubation time conditions which lead to the largest changes in band 3 mobility. Similarly, specific proteolysis of no major erythrocyte membrane protein is associated with large changes in fractional mobility and moderate (10-fold) increases in lateral diffusion coefficient of band 3. Large (50-fold) increases in the lateral diffusion rate of band 3 under low ionic strength, high temperature, long incubation time

conditions are, however, found to be associated with specific proteolysis of the particular cytoskeletal protein ankyrin.

A. IONIC STRENGTH - DEPENDENT DISSOCIATION OF SPECTRIN

1. Methods. The method used for analysis of spectrin dissociation was taken from Bennett and Branton (201). In the initial experiment, four µl of packed, eosin-labeled erythrocyte ghosts (10.9 mg protein/ml; 1.1 µg eosin/mg protein) in 5 mM sodium phosphate, 10 mM sodium azide, 30 nM PMSF, pH 7.4 were suspended in a 200 µl volume containing 1 mM sodium azide, 30 nM PMSF, and various concentrations of sodium phosphate, pH 7.4. After incubation for 60 min at 37°C, the samples were sonicated 15 times for 1 sec at 30 W (Ultrasonics model W-225R, microprobe tip), gently shaken, layered onto 200 µl of 20% sucrose in 500 µl microfuge tubes, and centrifuged (Eppendorf model 5412) at 4°C for 40 min at 15600 x g. The sonication and shaking steps were used to facilitate release into free solution of any solubilized protein molecules which had been entrapped within the ghosts. The resulting supernatants were carefully removed and discarded, and the orange-pink pellets dissolved in 50 µl of 10 mM Tris chloride, 1 mM EDTA, 3% SDS, 2% sucrose, 2% 2-mercaptoethanol, pH 7.4. The composition of the dissolved pellets was analyzed by discontinuous slab gel electrophoresis according to Laemmli (305). The stacking gel was 3% in acrylamide, the resolving gel 7.5% in acrylamide and 2.7% in bis-acrylamide (with respect to acrylamide).

Dimensions of the gel were 0.15 x 12 cm. Following staining with Coomassie blue (25), the gel lanes were scanned at 550 nm (Schoeffel spectrodensitometer, model SD3000). The amount of spectrin (bands 1 and 2) remaining in the membrane pellets relative to band 3 (which was presumed inextractable without detergent) was estimated by the comparison of the heights of or the areas under the peaks corresponding to bands 1, 2, and 3. A control sample was maintained at 0°C in 16 mM sodium phosphate, pH 7.4 for 60 min and then subjected to the same analytical procedures as the experimental samples. The percent dissociation of band 1 was calculated as $\frac{(\text{height band 1/height band 3})_{\text{experimental}}}{(\text{height band 1/height band 3})_{\text{control}}}$; the percent dissociation of band 2 was obtained from a similar equation. The average dissociation of spectrin (bands 1+2) was calculated either as $\frac{[(\text{height band 1 + height band 2})/\text{height band 3}]_{\text{experimental}}}{[(\text{height band 1 + height band 2})/\text{height band 3}]_{\text{control}}}$; or as $\frac{(\text{area bands 1+2/area band 3})_{\text{experimental}}}{(\text{area bands 1+2/area band 3})_{\text{control}}}$. These two methods of calculation for the average dissociation of spectrin yielded the same results within experimental error ($\pm$10%). Using an identical procedure, Bennett and Branton (201) have shown that less than 4% of the extracted spectrin is pelleted through 20% sucrose when centrifuged in the absence of membranes.

It may be noted that the assay for spectrin dissociation described above relies on the ability of spectrin, a heterodimer of

approximate molecular weight 430,000 daltons, to penetrate the erythrocyte membrane upon sonication and shaking of the ghosts incubated at 37°C for 60 min. To further test this assumption, the ionic strength dependent dissociation of spectrin was examined in the presence of saponin, a permeabilizing agent which may interact with cholesterol (331-2) and which allows the entry of ferritin (a particle 110A in diameter) into erythrocytes at concentrations as low as 30 μg/ml (333-337). Four μl of packed, eosin-labeled erythrocyte ghosts (20.1 mg protein/ml; 1.1 μg eosin/mg protein) in 5 mM $NaPO_4$, 10 mM NaN_3, 30 mM PMSF, pH 7.4 were suspended in a 200 μl volume containing either 0 or 100 μg/ml saponin (U.S. Biochemical), 1 mM NaN_3, 30 nM PMSF, and various concentrations of $NaPO_4$, pH 7.4. Samples were incubated and assayed for spectrin dissociation as described above. Control samples were maintained at 0°C in 20 mM $NaPO_4$, pH 7.4 for 60 min and assayed as described. Ratios of bands 1+2 to band 3 were not significantly different between the control samples with and without saponin addition, so these two samples were pooled as a single 0°C control.

2. Results and Discussion. The ionic strength dependence of spectrin dissociation from eosin-labeled ghosts on incubation without saponin at 37°C for 60 minutes is presented in figure 27. At phosphate concentrations greater than 5 mM, approximately 15-20% of bands 1 and 2 were dissociated; this amount did not change with increasing

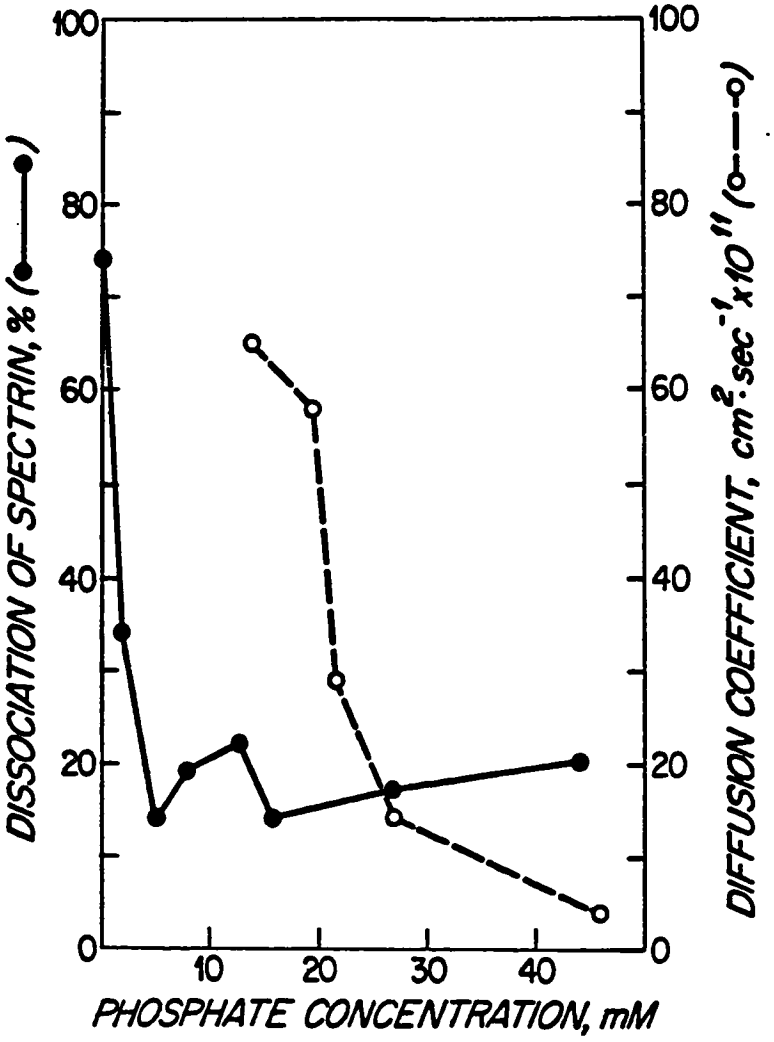

Figure 27. Dissociation of spectrin from eosin-labeled erythrocyte ghosts with decreasing phosphate concentrations. Eosin-labeled erythrocyte ghosts were suspended in various concentrations of $NaPO_4$, pH 7.4, and incubated for 60 min at 37°C. Dissociation of spectrin from the ghost membranes was assayed as described by Bennett and Branton (201). The percent dissociation is expressed relative to a control sample maintained at 0°C in 16 mM $NaPO_4$, pH 7.4, for 60 min.

ionic strength at least up to 44 mM phosphate. Below 5 mM phosphate there was an abrupt transition in the stability of the spectrin-membrane complex leading to 74% dissociation of spectrin (band 1:80%; band 2: 64%) at 0.1 mM phosphate. At 2 mM phosphate the degree of dissociation of band 1 (45%) was significantly greater than that of band 2 (18%); at all other buffer concentrations the extents of dissociation of the two components of spectrin were not significantly different.

The addition of 100 μg/ml saponin to the incubation medium did not significantly alter the dependence of spectrin dissociation on low ionic strength as assayed by the Bennett and Branton procedure (fig. 28). Although more spectrin was released into the supernatant at very low ionic strengths (0.3-2 mM $NaPO_4$) in the presence than in the absence of saponin, the amounts of spectrin dissociation under these two conditions were not significantly different in the ionic strength range of interest (5-40 mM $NaPO_4$).

Figures 27 and 28 are in agreement with previous reports of spectrin elution from erythrocyte ghosts at low ionic strength (25,26,174,201,219,338-341). Quantitative measurements of spectrin elution *vs.* KCl concentration (pH 7.6, incubation for 30 min at 37°C) showed a relationship very similar to that found in this report for spectrin dissociation *vs.* phosphate concentration. Thus, ≈20% dissociation at KCl concentrations greater than 10 mM was found, with a sharp increase in elution below 10 mM KCl leading to

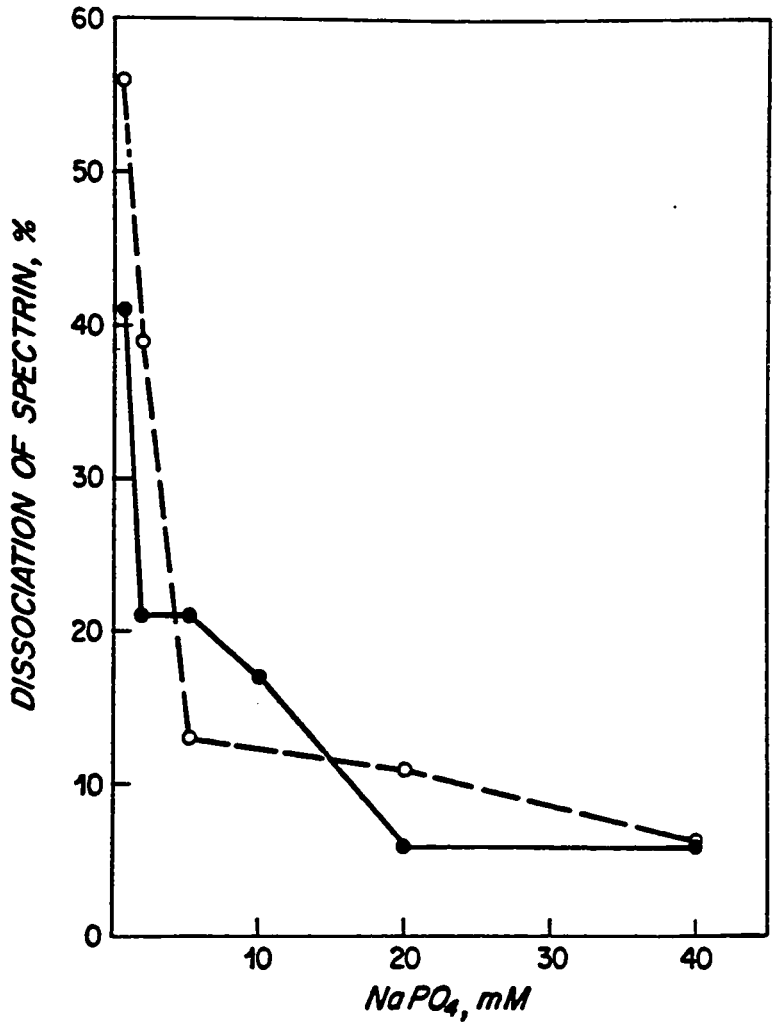

Figure 28. Dissociation of spectrin from eosin-labeled erythrocyte ghosts with decreasing phosphate concentrations in the presence (o--o) and absence (o—o) of 100 μg/ml saponin. Eosin-labeled erythrocyte ghosts were suspended in various concentrations of $NaPO_4$, pH 7.4, in the presence or absence of saponin, and incubated for 60 min at 37°C. Dissociation of spectrin from the ghost membranes was assayed as described by Bennett and Branton (201). The percent dissociation is expressed relative to control samples maintained at 0°C in 20 mM $NaPO_4$, pH 7.4, for 60 min.

a maximum of 60-80% dissociation of 0 mM KCl (ref. 201). The buffer concentration at which 50% dissociation occurred was 5 mM KCl (ionic strength (μ) = 5 mM, ref. 201) compared with 2 mM $NaPO_4$ ($\mu \simeq 5$ mM, this study).

Figure 27 also presents a comparison of the ionic strength dependence of spectrin dissociation with that of the diffusion coefficient for eosin-labeled band 3 in ghost membranes. In both cases, the ghosts were incubated for 60 minutes at 37°C, eliminating the effects of temperature and time from the comparison. It is readily apparent that changes in spectrin dissociation occurred only at very low ionic strengths whereas increases in the diffusion coefficient occurred at much higher phosphate concentrations. The elution of 10-20% of the total spectrin at high ionic strengths is an interesting observation in its own right, and may indicate heterogeneity of spectrin binding to the membrane (ref. 201; see chapter 9). This is especially noteworthy because the 20% dissociation seen on incubation at 37°C did not occur in the control samples, which were incubated at 0°C. Nonetheless, this degree of spectrin dissociation was nearly constant over the ionic strength range in which the lateral mobility of band 3 changed greatly, and complete spectrin dissociation alone cannot explain the increases in diffusion coefficient.

The relationship between spectrin elution and ghost membrane vesiculation is intriguing. As noted in chapter 4, photobleaching

recovery experiments at 37°C at phosphate buffer concentrations less than 10 mM were prevented due to rapid and total membrane vesiculation. Extensive ghost membrane vesiculation was also seen at 37°C in 8 mM $NaPO_4$ buffer in another study (219). In this section, however, it was shown that significant (>20%) elution of spectrin from the ghost membrane did not occur until the buffer concentration was decreased below 5 mM phosphate. From these data, it would appear that membrane vesiculation occurs just before complete dissociation of spectrin, the major cytoskeletal protein. This is yet another indication that significant changes in membrane structure are possible without total removal of the cytoskeleton.

B. TIME-DEPENDENT DISSOCIATION OF SPECTRIN

In the preceeding section it was shown that complete spectrin dissociation cannot be the molecular explanation for ionic strength-dependent changes in the lateral mobility of band 3 on incubation of erythrocyte ghost membranes at 37°C for 60 min (as seen in fig. 21). The time-dependent dissociation of spectrin at 37°C under both low and high ionic strength conditions is investigated in this section; complete spectrin dissociation is found not to correlate with even the largest changes in band 3 mobility.

1. Methods. Ten µl of packed, eosin-labeled erythrocyte ghosts

(4.9 mg protein/ml; 1.4 μg eosin/mg protein) in 5 mM $NaPO_4$, 10 mM NaN_3, 1 mM EDTA, 60 μM PMSF, 1 μg/ml pepstatin, pH 7.4 were suspended in a 200 μl volume containing 100 μg/ml saponin, 1 mM EDTA, 60 μM PMSF, 1 μg/ml pepstatin, 0.1 mM NaN_3, and either 14 mM or 40 mM $NaPO_4$, pH 7.4 (final concentrations). Samples were incubated at 37°C for 0, 1, 2, or 3 hours, and analyzed for spectrin release into the supernatant as described above (chapter 5A). The percent dissociation of spectrin at 1, 2, and 3 hours was expressed relative to that at zero time for each ionic strength series.

2. Results and Discussion. The time dependence of spectrin dissociation from eosin-labeled ghost membranes under low (14 mM $NaPO_4$) and high (40 mM) ionic strength conditions, in the presence of the protease inhibitors PMSF, EDTA, and pepstatin A and of the permeabilizing agent saponin, is shown in fig. 29. At all times of incubation there was a small (<20%) degree of spectrin dissociation, in accordance with previous results (figs. 27,28). Moreover, as seen by others investigating spectrin dissociation as a function of KCl concentration (201), the amount of dissociation at each ionic strength reached a plateau by the one hour time point. The time dependence of spectrin dissociation may be compared with that of band 3 lateral mobility at low ionic strength (14 mM $NaPO_4$) and 37°C (fig. 26). It is evident that complete spectrin dissociation from ghost membranes cannot explain the largest observed changes in

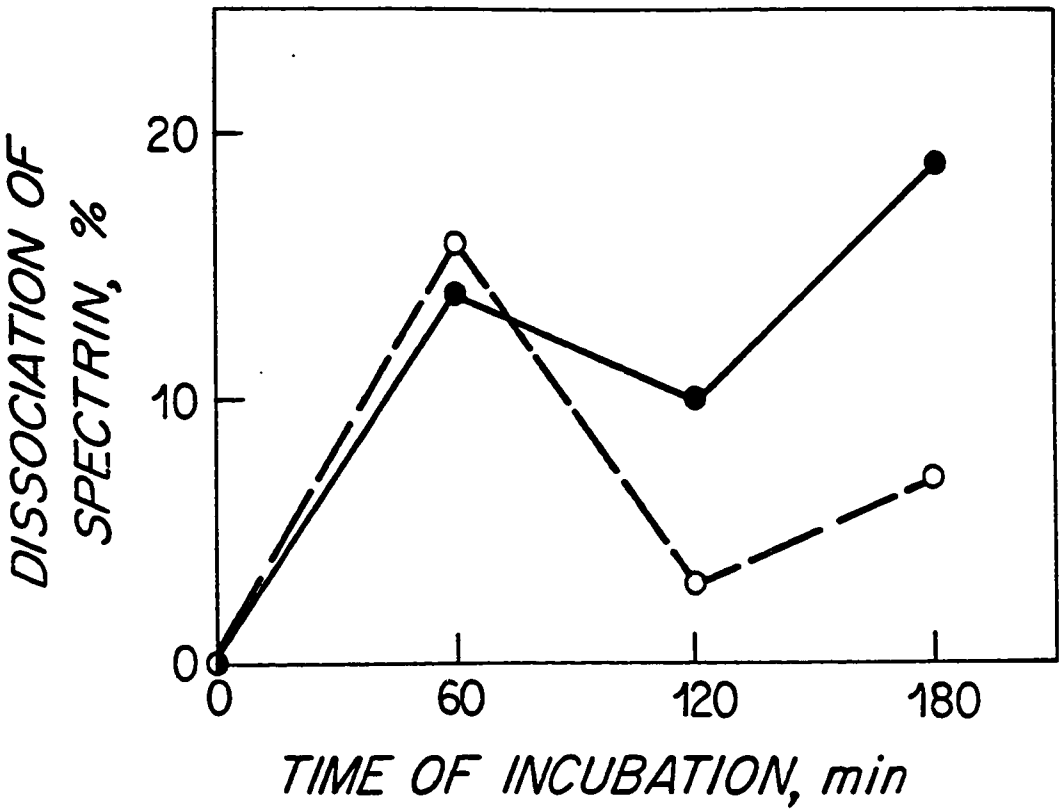

Figure 29. Dissociation of spectrin from eosin-labeled erythrocyte ghosts with increasing time of incubation under low and high ionic strength conditions. Eosin-labeled erythrocyte ghosts were suspended in 14 (o--o) or 40 (o—o) mM $NaPO_4$, pH 7.4, in the presence of 60 μM PMSF, 1 mM EDTA, 1 μg/ml pepstatin A, and 100 μg/ml saponin, and incubated for 60-180 min at 37°C. Dissociation of spectrin from the ghost membranes was assayed as described by Bennett and Branton (201). The percent dissociation is expressed relative to that at t=0 for each ionic strength series.

band 3 diffusion rate under low ionic strength, high temperature, long incubation time conditions.

C. IONIC STRENGTH- AND TIME-DEPENDENT PROTEOLYSIS OF MEMBRANE PROTEINS

As noted above, there are several proteases which have been associated with the erythrocyte membrane (319-330). Although the protease inhibitors PMSF, EDTA, and pepstatin A were added during eosin-labeled ghost preparation and incubation for FPR experiments (chapter 4C), it was decided to test their efficacy directly. Macroscopic samples of eosin-labeled erythrocyte ghosts were incubated at low and high ionic strengths under conditions identical to those employed in FPR experiments, and membrane protein integrity over time was assayed by SDS-polyacrylamide gel eletrophoresis. The results implicate the specific cytoskeletal protein ankyrin as a key mediating element in the restraint on the lateral mobility of band 3.

1. Methods. Sixty-four μl of eosin-labeled erythrocyte ghost membranes (4.5 mg protein/ml; 1.7 μg eosin/mg protein) in 5 mM $NaPO_4$, 10 mM NaN_3, 1 mM EDTA, 60 μM PMSF, 1 μg/ml pepstatin, pH 7.4 were mixed at 0°C with 336 μl of buffer containing 1 mM EDTA, 60 μM PMSF, 1 μg/ml pepstatin, and either 40 or 14 mM $NaPO_4$, pH 7.4. The ghost suspensions were then incubated at 37°C; 50 μl aliquots were taken at 0, 1, 2, and 3 hr and mixed immediately with SDS gel sample buffer (comprising 10 mM Tris chloride, 1 mM EDTA, 3% SDS, 2% sucrose,

and 2% 2-mercaptoethanol, final concentrations) at 0°C to stop any reaction. SDS-polyacrylamide gel electrophoresis was performed using the discontinuous slab gel procedure (305); the resolving gel was 6% and the stacking gel 3% in acrylamide. The gel lanes were stained with Coomassie blue (25) and scanned at 550 nm with a spectrodensitometer (Schoeffel SD3000). The amount of protein in bands 1+2 (spectrin), 2.1 (ankyrin), 3, 4.1, 4.2, and 5 (actin) in each sample was quantitated as the area under the appropriate peak of the gel scan, and expressed relative to the amount present at zero time.

2. Results and Discussion. The results of gel scans analyzing membrane protein integrity over time during 37°C incubations at low and high ionic strengths are presented in table 11 and reproduced in fig. 30. There is no significant proteolysis of band 3, spectrin, band 4.1, or band 4.2 under either low or high ionic strength conditions during the 3 hr incubation period. Although there is a significant degree of proteolysis of band 5 (actin), the amount of proteolysis (30-40%) is the same under low and high ionic strength conditions. Actin proteolysis alone, therefore, cannot be responsible for band 3 lateral mobility changes which are observed only at low ionic strength (cf. figs. 25,26). The one striking difference in membrane protein integrity between low and high ionic strength incubations is the stability of ankyrin (band 2.1). While

Table 11. Proteolysis of Membrane Proteins[a]

$NaPO_4$, mM[b]	Time, hr[c]	Band[d] 1+2	2.1	3	4.1	4.2	5
40	0	100	100	100	100	100	100
	1	94	82	93	100	101	64
	2	92	94	93	94	92	61
	3	93	109	103	112	85	62
14	0	100	100	100	100	100	100
	1	104	85	90	84	93	75
	2	109	67	97	85	90	68
	3	92	27	88	78	77	55

[a]All values are normalized to 100% at zero time of incubation.

[b]All samples were also incubated in 1 mM EDTA, 60 μM PMSF, 1 μg/ml pepstatin, 1.5 mM NaN_3, pH 7.4.

[c]All incubations were at 37°C.

[d]Quantitation of protein bands was by gel scans of Coomassie blue stained SDS-polyacrylamide gels.

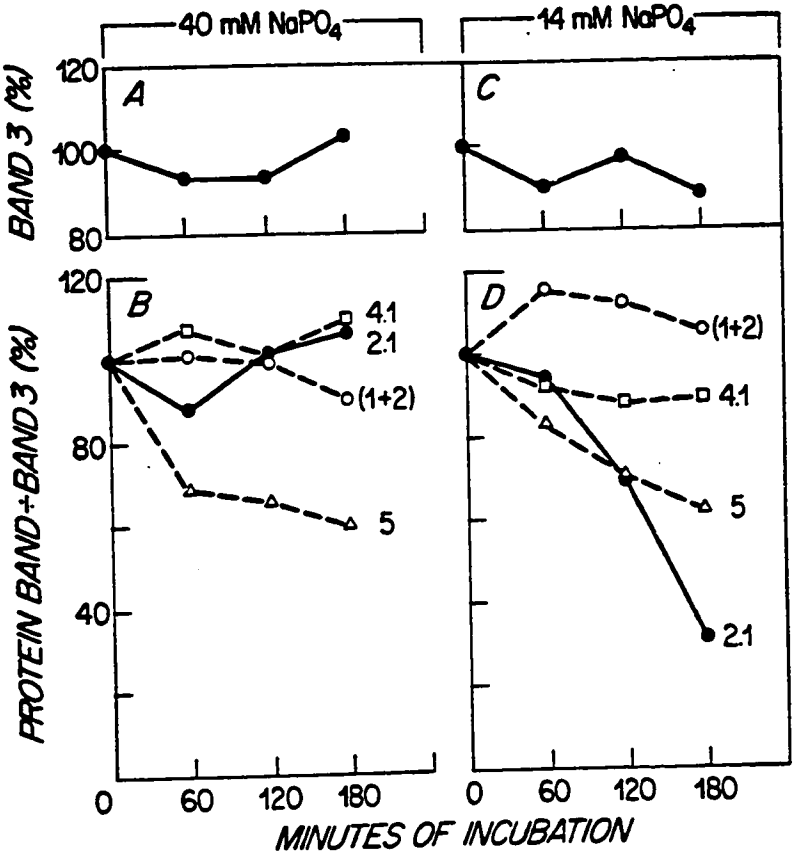

Figure 30. Integrity of erythrocyte membrane proteins as a function of incubation time at 37°C under low and high ionic strength conditions. Eosin-labeled erythrocyte ghosts were incubated in 14 (C,D) or 40 (A,B) mM $NaPO_4$, pH 7.4, in the presence of the protease inhibitors PMSF (60 μM), EDTA (1 mM), and pepstatin A (1 μg/ml), at 37°C. Aliquots were taken at 0,1,2 and 3 hr and analyzed by SDS-polyacrylamide gel electrophoresis for membrane protein integrity. (A) and (C), amount of band 3 remaining relative to that at t=0 for each ionic strength series. (B) and (D), amount of membrane protein remaining in each band relative to that at t=0 for each ionic strength series, normalized to the amount of band 3 present at each time of incubation.

this protein remains intact when erythrocyte ghosts are incubated at 37°C for 3 hr in high ionic strength buffer, it undergoes significant and systematic proteolysis in low ionic strength buffer. The time course of ankyrin proteolysis at 37°C in low ionic strength medium (fig. 30) may be compared with that of band 3 lateral mobility under identical incubation conditions (fig. 26; see also fig. 23). Large changes in the fractional mobility of band 3, as well as moderate increases in the lateral diffusion coefficient, occur over a time range (1 hr) during which the bulk of ankyrin remains intact. The largest increases in diffusion coefficient (at 2-3 hr) do correlate, however, with the specific and substantial (∿70%) proteolysis of this critical cytoskeletal protein.

The association between large increases in the lateral diffusion rate of band 3 and specific proteolysis of ankyrin may serve to explain results both in the literature and in the present study. It has already been noted (204,326) that ankyrin is a protein especially sensitive to membrane-associated proteolysis; indeed, this finding was the original impetus behind the addition of various protease inhibitors in the FPR experiments reported in chapters 4C and 6. The correlation between significant ankyrin proteolysis and extremely rapid transmembrane protein diffusion may imply that such proteolysis occurs only under conditions leading to a "loosened" state of the cytoskeleton, in which ankyrin becomes increasingly

exposed to some endogenous membrane protease. This notion is supported by the observation that band 3 lateral mobility increases somewhat before ankyrin undergoes proteolysis, but that band 3 lateral mobility increases to a maximum only after a significant percentage of ankyrin has been proteolytically cleaved. The former changes may be due to some cytoskeletal rearrangement or relaxation, the latter to complete loss of cytoskeletal restraint.

The proteolysis of ankyrin at long incubation times under low ionic strength, high temperature conditions may explain the data on reversibility of changes in band 3 lateral mobility depicted in figs. 22,23, and 26. Cytoskeletal protein proteolysis might be expected to lead, not only to increased lateral mobility of constrained transmembrane proteins, but also to overall membrane instability and eventual vesiculation. Indeed, such vesiculation was often observed in the present study under conditions leading to rapid band 3 diffusion. If there were present a population of erythrocyte ghosts heterogeneous in cytoskeletal fragility and/or deformability, one might expect the least stable erythrocyte membranes to undergo the sequence of events, characterized by progressive release of constraints on transmembrane protein mobility accompanied by specific proteolysis of a critical cytoskeletal protein and culminating in ghost vesiculation, at a faster rate than the more stable membranes. As such a ghost population was incubated under destabilizing conditions for various lengths of time

(e.g., 37°C incubation at low ionic strength) and then returned to more stabilizing conditions (e.g., 21°C incubation), a spectrum of possible results would obtain. First, under all destabilizing conditions an increased standard deviation of diffusion coefficients would accompany the general increase in lateral mobility; this was observed in the present study (figs. 23,26). Second, under mild destabilizing conditions not resulting in significant ankyrin proteolysis, the lateral mobility changes at 37°C would be totally reversible; this also may have been observed (fig. 22b), although membrane protein integrity under the incubation conditions of fig. 22b was not assayed directly. Third, under severe destabilizing conditions subtle differences between ghost populations would be manifest in the exact kinetics of lateral mobility changes, as well as in the time required for all of the least stable cells to vesiculate while leaving intact the more stable ghosts; this too was seen in the present study (fig. 23, 26). Finally, under all conditions destabilizing enough to result in significant ankyrin proteolysis, lateral mobility changes would not be totally reversible; this was observed for increases in both fractional mobility (figs. 22,23, and 26) and diffusion coefficient (fig. 26). The apparent total reversibility in diffusion coefficient seen in fig. 23 may be secondary to a mechanism alluded to above, in which vesiculation of an entire population of destabilized erythrocyte membranes leaves remaining a few extremely stable ghosts with intact cytoskeletons.

CHAPTER 6. LATERAL MOBILITY OF BAND 3: EFFECT OF SPECIFIC CYTOSKELETAL PERTURBATIONS

In the preceding chapters it has been demonstrated that conditions similar to those which destabilize several associative interactions in the erythrocyte cytoskeleton (e.g., spectrin dimer-tetramer association, spectrin-actin association, spectrin-ankyrin association; see chapter 9) also result in progressive, large increases in the lateral mobility of the transmembrane protein band 3. Moreover, the greatest changes in band 3 mobility have been correlated with specific proteolysis of the particular cytoskeletal protein ankyrin. The putative role of ankyrin in mediating cytoskeletal restraint of band 3 lateral mobility is further explored in this chapter, in which the effects of several cytoskeletal perturbants on band 3 mobility are examined. Conditions affecting cytoskeletal perturbation include hypertonic ionic strength, which destabilizes both the ankyrin-band 3 (196,204,214) and ankyrin-spectrin (151,204,213) linkages while leaving intact the spectrin-actin-band 4.1 complex; and proteolytic fragments of particular cytoskeletal proteins containing "univalent" binding sites which would be expected to compete, on the intact ghost membrane, with "bivalent" cytoskeletal proteins.

Four proteolytic fragments were considered as potential agents of cytoskeletal destabilization: a 72,000 dalton fragment of ankyrin

involved in binding band 2 of spectrin (26,171,172,202,206); an 80,000 dalton fragment of band 1 of spectrin important in the association of spectrin dimers to tetramers (171,172); a 43,000 dalton fragment of band 3 which binds ankyrin (213-215); and a 50,000 dalton fragment of band 2 of spectrin which binds ankyrin (172). The effect of the latter two fragments on band 3 mobility was not examined, because these fragments are reported to have significantly lower affinities for their respective binding sites on ankyrin than those of the native protein molecules from which they are derived. Effective competition for binding sites on the intact ghost membrane would have therefore required prohibitively high concentrations of the proteolytic fragments. The former two fragments, however, are reported to have approximately the same affinities for their membrane attachment sites as the proteins from which they are derived, making the likelihood greater that they would be able to compete effectively on the intact membrane. Thus, the 72,000 dalton ankyrin fragment inhibits binding of purified spectrin to inside-out vesicles with $K_i \simeq 10^{-7}M$ (203), while the 80,000 dalton band 1 fragment binds to dimer spectrin in solution with $K_a \simeq 2.7 \times 10^{-6}M$ (172).

In this chapter, then, the effects of hypertonic ionic strength, the 72,000 dalton ankyrin fragment, and the 80,000 dalton spectrin fragment on the lateral mobility of band 3 are reported. The results confirm the central role of ankyrin in the mediation of

band 3 mobility restriction.

A. METHODS

The FPR apparatus employed in these studies was the improved, recalibrated system described in chapter 2 (fig. 11c). Sample temperature was controlled to ±0.5°C with the thermostatted aluminum sample holder (fig. 19), and monitored by means of a microprobe thermometer. Eosin-labeled erythrocyte ghosts were prepared in the presence of PMSF, EDTA, and pepstatin A, and stored in 5 mM $NaPO_4$, 1 mM EDTA, 60 μM PMSF, 1 μg/ml pepstatin, 10 mM NaN_3, pH 7.4, at 4°C in the dark, until use (see chapter 3). Samples were mixed and incubated as described below; they were then deoxygenated by a stream of nitrogen for 1 hr and sealed on a microscope slide with epoxy, all inside a pre-purged glove bag, as described in chapter 4A. The FPR experiment was performed as noted above (chapter 4A).

1. Hypertonic KCl Incubation. Thirty μl of eosin-labeled ghosts was diluted to 300 μl with buffer comprising various concentrations of potassium chloride (approximately 0-1 M), 40 mM sodium phosphate, 1 mM EDTA, 60 μM PMSF, 1 μg/ml pepstatin A, and 1 mM NaN_3, pH 7.4 (final concentrations), and the suspension incubated on ice for 15 min. Samples were then deoxygenated at room temperature and sealed on a glass slide as described above.

2. 72,000 Dalton Ankyrin Fragment Incubation. Four μl of eosin-

labeled ghosts (4.5 mg protein/ml; 2.1 μg eosin/mg protein) was added to 76 μl of a solution of purified 72,000 dalton fragment in 7.5 mM $NaPO_4$, 0.5 mM EDTA, 0.2 mM DTT, pH 7.5 (i.e., pooled fractions 24 and 25 from DEAE-cellulose column chromatography; 0.3 mg protein/ml, 66% pure 72,000 dalton fragment by densitometer scan), and the suspension incubated on ice for 30 min. This preincubation at 0°C, under low ionic strength conditions, in the presence of EDTA, was designed to maximize the likelihood that the ankyrin fragment would be able to penetrate freely the ghost membrane. Sixteen μl of buffer was then added to bring the solution to 40 mM sodium phosphate, 1 mM EDTA, 60 μM PMSF, 1 μg/ml pepstatin A, 0.5 mM NaN_3, 0.2 mM DTT, pH 7.4 (final concentrations), and the mixture incubated on ice an additional 15 min. The final concentration of 72,000 dalton fragment in the solution was 2.6×10^{-6} M, and the excess of fragment molecules to competing ankyrin molecules on the membrane was 40:1. Samples were prepared for FPR experiments as described above.

3. 80,000 Dalton Spectrin Fragment Incubation. In the first experiment, 2.5 μl of eosin-labeled ghosts (4.0 mg protein/ml; 1.8 μg eosin/mg protein) was added to 50 μl of a stock solution of concentrated 80,000 dalton fragment in 20 mM $NaPO_4$, 1 mM EDTA, 60 μM PMSF, 3 mM NaN_3, pH 7.4 (i.e., concentrated by pressure dialysis; 1.55 mg protein/ml, 67% pure 80,000 dalton fragment by densitometer scan), and the suspension incubated on ice for 60 min. One-half μl of a stock solution of pepstatin was added to bring its concentration to 1 μg/ml, and the sample was immediately prepared for the FPR

experiment. The final concentration of 80,000 dalton fragment in this solution was 1.2×10^{-5} M, and the excess of fragment molecules to competing spectrin dimers on the membrane was 90:1. In all other experiments, 3.5 µl of eosin-labeled ghosts (5.6 mg protein/ml; 2.1 µg eosin/mg protein) was mixed with 41.5 µl of 1 mM EDTA in H_2O and 25 µl of the stock solution of concentrated 80,000 dalton fragment, and the suspension incubated on ice for 1-64 hr (see below). As above, these long preincubations at 0°C under conditions of low ionic strength were designed to allow maximum diffusion of the fragment across the ghost membranes. Final concentrations of constituents in this pre-incubation medium were: $NaPO_4$, 7.4 mM; EDTA, 1 mM; PMSF, 24 µM; pepstatin, 0.05 g/ml; NaN_3, 1.6 mM; and 80,000 dalton fragment, 4.7×10^{-6} M. The excess of fragment molecules to spectrin dimers on the membrane was 23:1. Small amounts (10-15 µl) of buffer were then added to bring the solution to various concentrations of sodium phosphate (23-45 mM), 1 mM EDTA, 60 µM PMSF, 1 µg/ml pepstatin, 1.6 mM NaN_3, pH 7.4 (final concentrations), and the mixture incubated on ice an additional 15 min.

B. RESULTS

1. Hypertonic Ionic Strength. The results of a series of fluorescence photobleaching recovery experiments on eosin-labeled erythrocyte ghosts under hypertonic conditions are summarized in table 12 and reproduced in fig. 31. These results are compared to those at 40 mM $NaPO_4$ with no added KCl, under which conditions there was, as

TABLE 12. EFFECT OF HYPERTONIC KCl ON LATERAL MOBILITY OF BAND 3[a]

	21°C[b]			30°C[c]			37°C[d]		
KCl, mM[e]	$D \times 10^{11}$, $cm^2 sec^{-1}$	f(∞)	N	D	f(∞)	N	D	f(∞)	N
945	2.1 ± 0.6	0.13 ± 0.04	2	---[f]	---[f]		---[f]	---[f]	
589	---[g]	0.08 ± 0.08	2	1.1 ± 0.1	0.35 ± 0.08	2	---[f]	---[f]	
320	1.7 ± 0.6	0.24 ± 0.14	9	1.7 ± 0.7	0.42 ± 0.15	6	12 ± 9	0.68 ± 0.16	8
0	1.3 ± 0.5	0.12 ± 0.09	6	1.9 ± 0.9	0.16 ± 0.07	5	1.3 ± 0.4	0.21 ± 0.13	8

[a] All values expressed as mean ± S.D.

[b] 2-3 hr incubation

[c] 0.5-1 hr incubation

[d] 0.7-1.3 hr incubation

[e] All samples also buffered in 40 mM $NaPO_4$, 1 mM EDTA, 60 μM PMSF, 1 μg/ml pepstatin A, 1 mM NaN_3, pH 7.4

[f] Experiments prevented by 100% ghost vesiculation

[g] Not determined

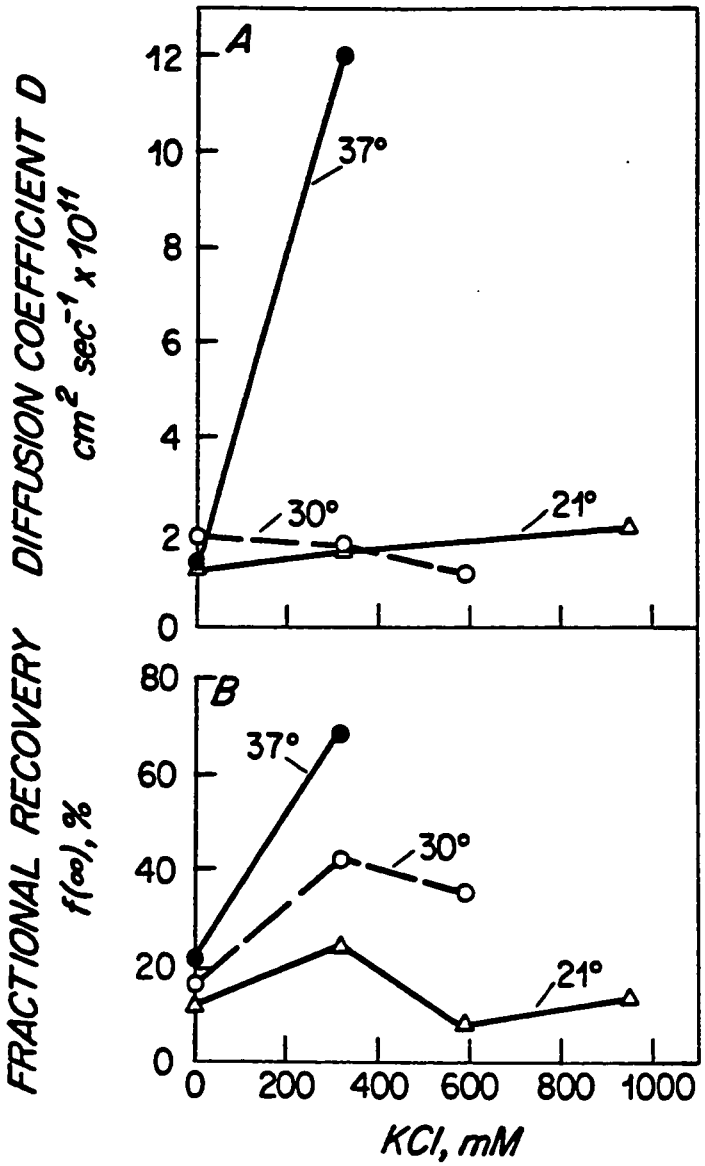

Figure 31. Diffusion coefficients (A) and fractional recoveries of fluorescence (B) obtained from FPR experiments on eosin-labeled erythrocyte ghosts, as functions of ionic strength, at various temperatures. All experiments were performed in the presence of 40 mM $NaPO_4$, 60 μM PMSF, 1 mM EDTA and 1 μg/ml pepstatin A at pH 7.4. Individual points represent the average of two to nine independent measurements (see Table 12).

expected, a high degree of band 3 immobilization (10-20% mobile) as well as slow diffusion of the mobile fraction ($D \cong 1.5 \times 10^{-11}$ cm^2sec^{-1}) at all temperatures. In many respects the hypertonic KCl results parallel those observed on low ionic strength incubation of eosin-labeled ghosts (chapter 4; figs. 21, 25). At very high KCl concentrations as at very low ionic strengths, FPR measurements were prevented by rapid and total ghost vesiculation, especially at elevated temperatures. As the KCl concentration was decreased from these very high levels, significant increases over control values in both fractional recovery and diffusion coefficient were observed. These changes were dissociated from one another, as in the low ionic strength experiments, in that fractional recovery increases occurred at lower temperature than diffusion coefficient increases. For example, at 30°C the fractional mobility of band 3 was significantly greater in 320 mM or 589 mM KCl buffer than in control buffer while the diffusion coefficient remained unchanged.

The only hypertonic condition under which FPR measurements could be obtained at 37°C was 320 mM KCl buffer. A detailed comparison between results obtained in this vs. control buffer is shown in fig. 32C,D. Significant differences in band 3 diffusion coefficient at 37°C ($p < 0.02$) and fractional mobility at both 30°C ($p < 0.01$) and 37°C ($p < 0.001$) are evident.

As in the low ionic strength experiment (figs. 23, 26), the lateral mobility of band 3 was sensitive to incubation time at 37°C under hypertonic conditions. Figure 33 presents the results of a kinetic experiment in 320 mM KCl buffer, in which FPR parameters

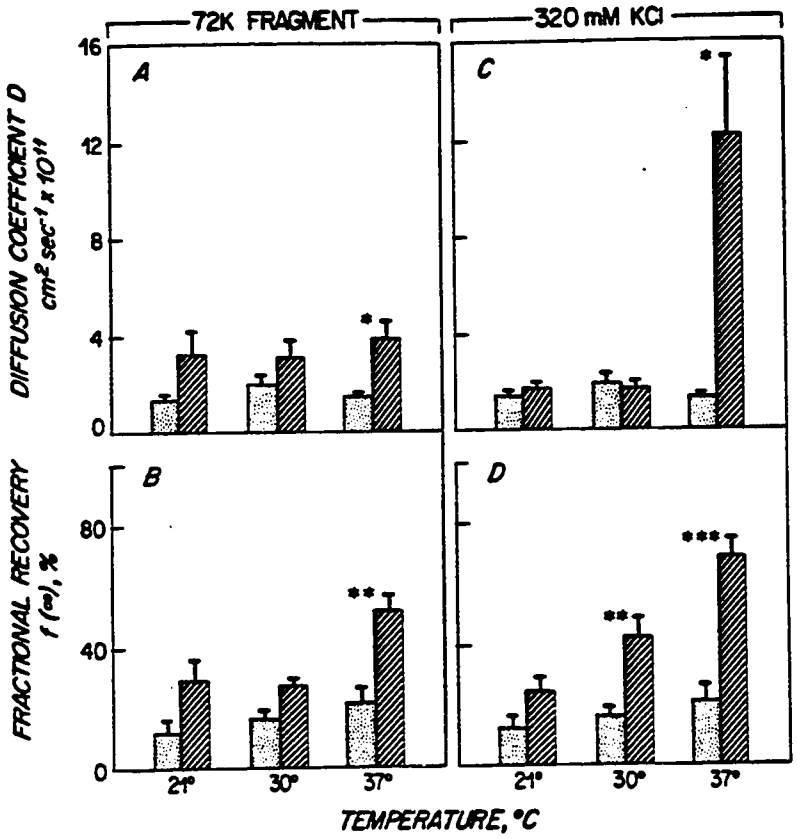

Figure 32. Effect of specific cytoskeletal perturbation on diffusion coefficients (A,C) and fractional recoveries of fluorescence (B,D) obtained from FPR experiments on eosin-labeled erythrocyte ghosts. (A,B) Ghosts were incubated in 40 mM $NaPO_4$ buffer, pH 7.4 containing 60 μM PMSF, 1 mM EDTA, and 1 μg/ml pepstatin A, in the presence (hatched bars) or absence (stippled bars) of a 2.6×10^{-6} M concentration of purified 72,000 dalton ankyrin fragment containing the high-affinity spectrin attachment site. Incubations were carried out for 1 (30°C, 37°C) or 3 (21°C) hr. Individual points represent the average of two to eight independent measurements; error bars represent mean ± S.E.M. Significant differences (*, $p<0.02$; **, $p<0.01$) between values in the presence and in the absence of the ankyrin fragment were found for both diffusion coefficients and fractional recoveries at 37°C. (C,D) Ghosts were incubated in 40 mM $NaPO_4$ buffer, pH 7.4 containing 60 μM PMSF, 1 mM EDTA, and 1 μg/ml pepstatin A, in the presence (hatched bars) or absence (stippled bars) of 320 mM KCl. Incubations were carried out for 1 (30°C, 37°C) or 3 (21°C) hr. Individual points represent the average of five to nine independent measurements (see Table 12); error bars represent mean ± S.E.M. Significant differences (*, $p<0.02$; **, $p<0.01$; ***, $p<0.001$) between values in the presence and in the absence of hypertonic KCl were found for diffusion coefficients at 37°C and fractional recoveries at 30°C and 37°C.

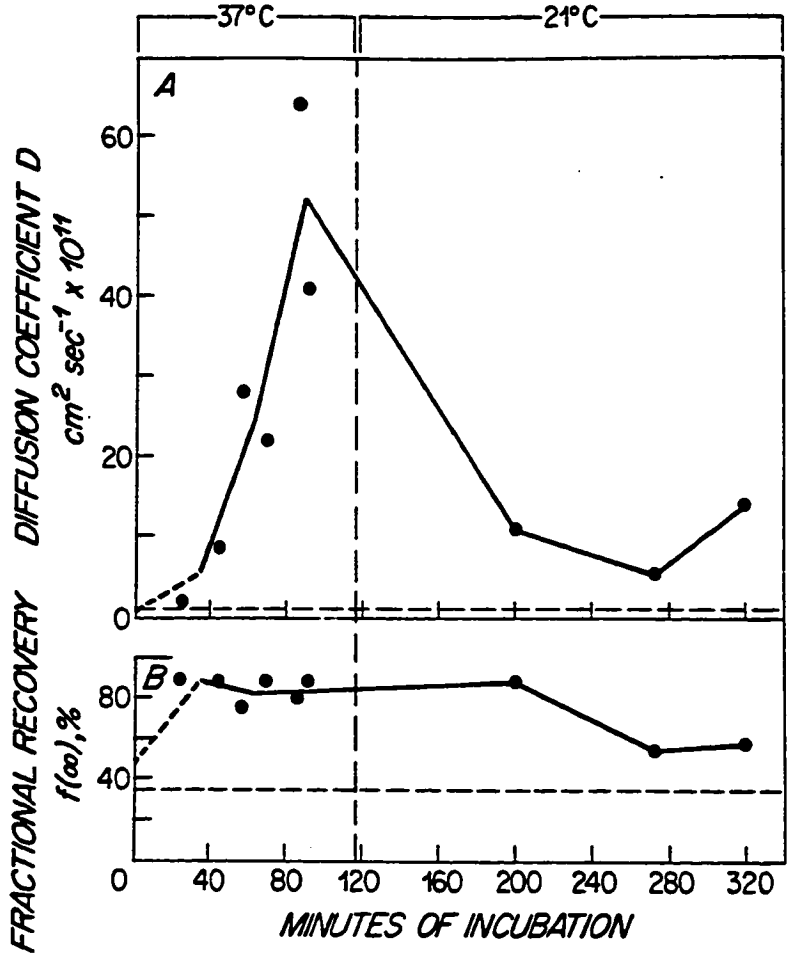

Figure 33. Diffusion coefficients (A) and fractional recoveries of fluorescence (B) obtained from FPR experiments on eosin-labeled erythrocyte ghosts as functions of incubation time at 37°C. The buffer comprised 40 mM $NaPO_4$, 320 mM KCl, 60 μM PMSF, 1 mM EDTA, 1 μg/ml pepstatin A, pH 7.4. Horizontal broken lines represent initial values at 21°C, before the temperature had been increased to 37°C. Smoothed curves are drawn through the experimental points by pairwise averaging of adjacent data points. At t=0, curves are extrapolated back to the values obtained at 30°C in the same buffer. Vertical broken lines represent return of temperature to 21°C. Temperature equilibration time was approximately 10 min. Each experimental point was obtained from a separate erythrocyte ghost in the sample.

were determined every 10-20 min after increasing the incubation temperature to 37°C. An immediate increase in fractional recovery to 85-90% (probably maximal under these conditions; see chapter 4) was followed by a more gradual increase in diffusion coefficient to $52 \pm 12 \times 10^{-11}$ cm^2sec^{-1} (N=2), or about 50 times the room temperature value. Reversal of the incubation temperature to 21°C resulted in partial reversibility of both diffusion coefficient and fractional recovery. All of these features of the kinetic experiment have their parallels in the low ionic strength case (figs. 23, 26). It should be noted that, while large fractional recoveries were always observed under hypertonic (320 mM) KCl, 37°C, long incubation time conditions, 50-fold increases in diffusion coefficient were only observed in two out of four eosin-labeled ghost preparations examined. This variability was manifested statistically by the relatively large standard deviation of the diffusion coefficient under these conditions (table 12). The reason for the variability is unknown; it may relate to subtle biochemical differences among the various ghost preparations. In particular, different ghost membrane preparations might have different susceptibilities to endogenous proteases (or even different numbers of active protease molecules) whose action in the specific proteolytic degradation of ankyrin is necessary prior to complete release of band 3 from cytoskeletal restraint (see chapter 9).

2. 72,000 Dalton Ankyrin Fragment. The lateral mobility of eosin-labeled band 3 in the presence and absence of a 72,000 dalton

proteolytic fragment of ankyrin which serves as the high-affinity binding site for spectrin on the membrane is shown in fig. 32A,B. All samples were buffered in 40 mM $NaPO_4$, pH 7.4, in the presence of the protease inhibitors EDTA, PMSF, and pepstatin A. In the presence of the 72,000 dalton fragment both the diffusion coefficient and fractional recovery were increased over control values at all temperatures, but the differences reached statistical significance only at 37°C ($p < 0.02$ for diffusion coefficient, $p < 0.01$ for fractional recovery). Under these conditions the fractional mobility of band 3 was increased 2½-fold, and the diffusion coefficient of the mobile fraction 3-fold, over control values.

3. 80,000 Dalton Spectrin Fragment. The lateral mobility of eosin-labeled band 3 was apparently unaffected by the presence of an 80,000 dalton fragment of band 1 involved in the dimer-tetramer interaction of spectrin, under a variety of pre-incubation and incubation conditions (table 13; cf. control values in table 10). The bulk of the pre-incubations of ghosts with concentrated 80,000 dalton fragment was performed in 7.5 mM $NaPO_4$ buffer at 0°C, under which conditions a substantial amount of the 72,000 dalton ankyrin fragment was apparently able to penetrate the ghost membrane (as assessed by its positive effect on band 3 lateral mobility; cf. fig. 32). Even upon incubation at relatively low ionic strength (23 mM $NaPO_4$), however, the diffusion coefficient and fractional mobility of band 3 were not significantly changed by the addition of the spectrin fragment.

TABLE 13. EFFECT OF 80K SPECTRIN FRAGMENT ON LATERAL MOBILITY OF BAND 3[a]

	21°C[b]			30°C[c]			37°C[d]		
$NaPO_4$,[e] mM	$D \times 10^{11}$, $cm^2 sec^{-1}$	f(∞)	N	D	f(∞)	N	D	f(∞)	N
23[f]	1.1	0.06 ± 0.06	2	1.2 ± 0.0	0.32 ± 0.03	2	1.4 ± 0.8	0.46 ± 0.09	5
26[g]	1.9	0.13 ± 0.01	2				1.3 ± 0.4	0.23 ± 0.07	4
32[h]	---[i]	0.05 ± 0.04	2				1.7 ± 0.6	0.26 ± 0.07	5
45[h]	1.6	0.08 ± 0.07	2	0.87	0.21 ± 0.11	2	1.5 ± 0.4	0.23 ± 0.05	3
24[j]	---[i]	0.04 ± 0.02	2				1.8 ± 0.3	0.36 ± 0.06	4

[a]All values expressed as mean ± S.D. Concentration of 80K fragment was 4.7×10^{-6} M in all preparations, except 24 mM $NaPO_4$ where concentration was 1.2×10^{-5} M

[b]2-3 hr incubation

[c]0.5-1 hr incubation

[d]0.5-3 hr incubation

[e]All samples also buffered in 1 mM EDTA, 60 μM PMSF, 1 μg/ml pepstatin, 1.6 mM NaN_3, pH 7.4

[f]Sample was pre-incubated at 0°C for 64 hr in 7.4 mM $NaPO_4$

[g]Sample was pre-incubated at 0°C for 42 hr in 7.4 mM $NaPO_4$

[h]Sample was pre-incubated at 0°C for 1 hr in 7.4 mM $NaPO_4$

[i]Not determined

[j]Sample was pre-incubated at 0°C for 1 hr in 19 mM $NaPO_4$

C. DISCUSSION

This chapter presents a series of fluorescence photobleaching recovery experiments in which the lateral mobility of eosin-labeled band 3 in erythrocyte ghost membranes was measured as a function of various treatments known to perturb specifically interactions with the erythrocyte cytoskeleton. Incubation in hypertonic KCl buffer led to large increases in both the fraction of mobile band 3 (90% mobile) and the diffusion rate of the mobile fraction (50×10^{-11} cm^2sec^{-1}). The increase in the fraction of mobile band 3 was dissociated from that in the diffusion coefficient, under conditions of varying ionic strength (fig. 31), temperature (fig. 32), and incubation time (fig. 33). These features of the hypertonic KCl experiments all had close parallels in the low ionic strength experiments (chapter 4); this in turn may imply a common, or at least overlapping, biochemical basis for the observed lateral mobility changes under both sets of conditions. In particular, it suggests that specific proteolysis of ankyrin might be the universal biochemical correlate of extremely rapid band 3 diffusion (see chapter 9). It may be noted that, as in the low ionic strength experiments, hypertonic conditions identical to those employed conventionally to achieve a particular biochemical effect (e.g., the extraction of ankyrin from erythrocyte cytoskeletons (204) or spectrin-actin depleted vesicles (196) with 1 M KCl) were too strong for the FPR experiments in the sense that they led to rapid and complete ghost vesiculation. Milder but qualitatively similar conditions (e.g.,

320 mM KCl) were, however, very effective in producing large lateral mobility changes without immediate vesiculation.

Treatment of eosin-labeled erythrocyte ghosts with a 72,000 dalton proteolytic fragment of ankyrin containing the high affinity binding site for spectrin on the inner membrane surface led to approximately 3-fold increases over control values in both diffusion coefficient and fractional mobility of band 3. The concentration of 72,000 dalton fragment was approximately 25 times greater in this experiment than that needed to produce its in vitro biochemical effect (see above). Using the cell fusion technique for lateral mobility measurement (see chapter 1), Fowler and Bennett (240) showed a two-fold increase in the lateral diffusion of fluorescein-labeled erythrocyte transmembrane proteins (chiefly band 3 and glycophorin) in the presence of the 72,000 dalton fragment. The concentration of fragment required to achieve this effect was within a factor of two of that used in the present study. These experiments implicate the ankyrin-spectrin linkage as one controlling element in band 3 lateral mobility. It is evident that other forces must be involved as well, however, since the increase in lateral mobility achieved by the ankyrin fragment alone was still an order of magnitude less than that observed under both low and hypertonic ionic strength conditions (see above and chapter 9).

In contrast to the 72,000 dalton ankyrin fragment, the 80,000 dalton band 1 fragment involved in the polymerization of dimer spectrin was unable to produce increases in band 3 lateral mobility. For technical reaons it was possible to incubate eosin-labeled ghosts

with a concentration of 80,000 dalton fragment only 2- to 4-fold greater than that which binds to dimer spectrin in solution (172, see above). The inability of such a low concentration of fragment to compete effectively with its binding site on the membrane may verywell be the explanation for the lack of change in band 3 lateral mobility. In particular, it may <u>not</u> be concluded from this data that the spectrin polymerization process is not involved in the regulation of mobility of the transmembrane protein band 3.

CHAPTER 7. LATERAL MOBILITY OF PHOSPHOLIPID AND CHOLESTEROL: MODEL SYSTEMS

It has been shown that, in both low and hypertonic ionic strength medium, the lateral diffusion coefficient of band 3 in the erythrocyte ghost membrane may reach a maximum value which is approximately 50-fold greater than that seen under more physiologic conditions. The hypothesis was conceived that this rapid lateral mobility might signify the "diffusion limit" for band 3 in the ghost membrane, i.e., that a diffusion coefficient of 50×10^{-11} cm^2sec^{-1} might represent the fastest possible rate of lateral mobility for a 90,000 dalton transmembrane protein in a lipid bilayer composed of the mixture of phospholipids and cholesterol given in Table 1. The most direct experimental approach to test this hypothesis, it was thought, would be to measure the lateral diffusion, under the same membrane under the same conditions, of an object whose mobility was governed only by the viscosity of the lipid bilayer. Such an object is present in abundance in the erythrocyte membrane in the form of phospholipid or cholesterol. The phospholipid probe employed in these FPR studies was NBD-phosphatidylethanolamine (NBD-PE); the cholesterol probe was NBD-cholesterol (NBD-chol). Since the latter is a fluorescent cholesterol derivative newly synthesized in the laboratory of Dr. Robert R. Rando, Dept. of Pharmacology, Harvard Medical School (308), it was thought desirable to compare its lateral mobility with that of the conventional phospholipid probe NBD-PE in several

model systems before incorporating the probes into erythrocyte ghost membranes. In this chapter, the lateral mobilities of NBD-PE and NBD-chol as functions of temperature and composition are compared in multilamellar liposomes composed of pure dimyristoylphosphatidylcholine (DMPC), DMPC + 0-40 mole % cholesterol, pure egg phosphatidylcholine (egg PC), and egg PC + 0-50 mole % cholesterol. Studies of these probes in the erythrocyte ghost membrane appear in the following chapter.

A. METHODS

The FPR apparatus employed in these studies was the improved, recalibrated system diagrammed in fig. 11c. Sample temperatures were controlled to ± 0.5°C with the thermostatted sample holder shown in fig. 19. Solutions of DMPC or egg PC and cholesterol (if required) were labeled with 0.15 mole % NBD-PE or NBD-chol and multilamellar liposomes prepared as described (chapter 3). Many such liposomes were in excess of 20 μm in diameter, making possible the use of the 40 X objective ($1/e^2$ radius (w) = 2.2 μm; see chapter 2) instead of the 100 X objective (w = 0.9 μm) for more accurate measurement of extremely rapid lateral diffusion. Three hundred μl solutions of liposomes were deoxygenated for an additional hr and samples sealed on a microscope slide with epoxy as described (chapter 4A). The FPR experiment was performed as noted in chapter 4A, except that the XY recorder filter was switched to 0.00 sec for experiments in which extremely rapid lateral diffusion ($\tau_{\frac{1}{2}}$ = 0.25 - 2 sec) was measured.

B. RESULTS

1. Lateral Mobility of NBD-PE and NBD-chol in DMPC Liposomes: Temperature Dependence. Lateral diffusion coefficients for NBD-PE and NBD-chol as a function of temperature in pure DMPC multilamellar liposomes are presented in fig. 34. Both probes manifested a sharp, 50-fold change in diffusion coefficient at 24°C, the main phase transition temperature (Tm) for the bulk phospholipid. Diffusion coefficients for the two probes were not significantly different from each other at temperatures both above and below Tm. There was some variability in measurements of diffusion coefficients below Tm, which may reflect subtle differences in phospholipid packing resulting from small variations in sample preparation (e.g., degree of hydration; see ref. 342) from day to day. When careful comparisons between lateral mobility parameters of NBD-PE and NBD-chol were made in identical DMPC multilamellar liposome preparations on the same day, however, diffusion coefficients for the two probes were within experimental error of one another both above and below Tm (fig. 34; table 14). Fractional recoveries averaged 0.85 for both probes at all temparatures examined (data not shown).

2. Lateral Mobility of NBD-PE and NBD-chol in Binary Mixtures of DMPC and Cholesterol: Composition Dependence. Lateral diffusion coefficients for both lipid probes were strongly dependent on the mole fraction of cholesterol (X_{chol}) in multilamellar liposomes prepared from mixtures of DMPC and cholesterol (fig. 35; table 15). Below the main phase

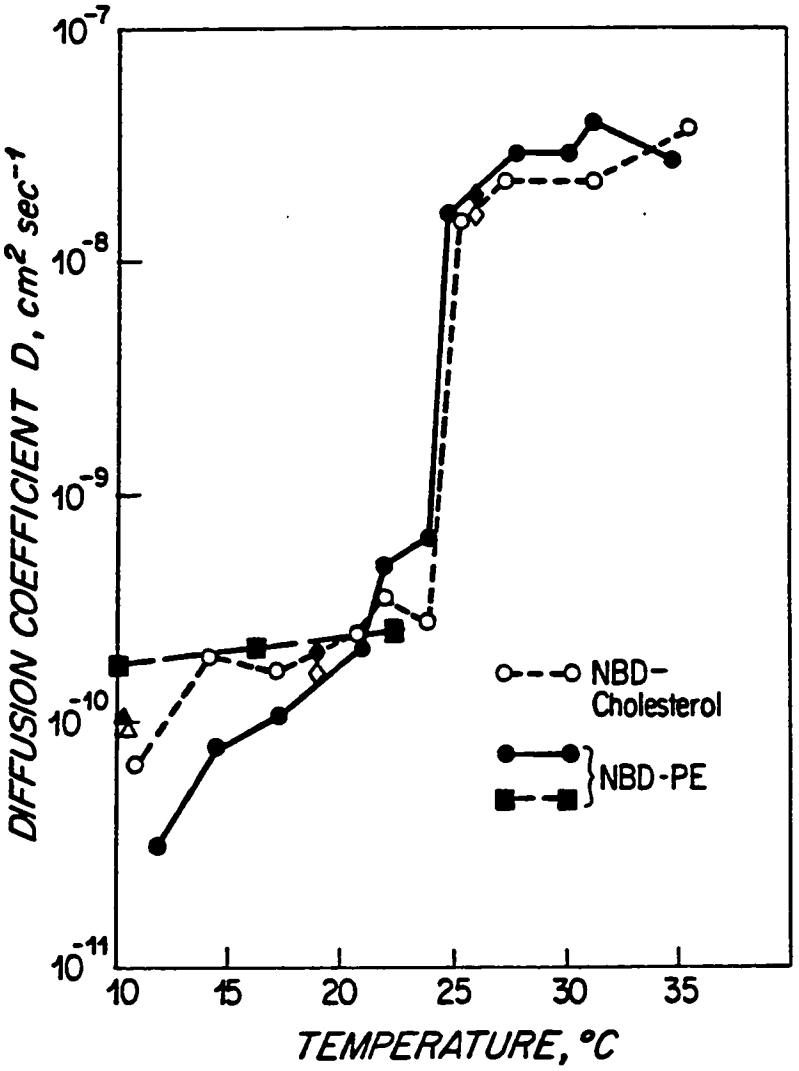

Figure 34. Lateral diffusion coefficient of NBD-phosphatidylethanolamine (closed symbols) and NBD-cholesterol (open symbols) in dimyristoylphosphatidylcholine multilamellar liposomes, as a function of temperature. Lipid probes were added to a final mole fraction of 0.15%. Points connected by curves represent measurements performed on a single liposome preparation by scanning temperature from lowest to highest. Identical symbols (triangles, diamonds) represent direct comparisons between the two fluorescent lipid probes in identical liposome preparations measured on the same day. Each point represents the average of 2 (○,●), 4 (◇,◆) or 6 (△,▲,■) independent measurements. There is no significant difference between the diffusion coefficients of the two probes at any temperature examined. Fractional recoveries of fluorescence averaged 0.85 for both probes at all temperatures.

Table 14. LATERAL MOBILITY OF NBD-PE AND NBD-CHOL IN DMPC MULTILAMELLAR LIPOSOMES: DIRECT COMPARISONS[a]

Probe	Temp, °C	$Dx10^{10}$, cm^2sec^{-1}	f(∞)	N
NBD-PE	10.3	1.1 ± 0.1	0.89 ± 0.05	6
NBD-chol	10.5	1.0 ± 0.4	0.89 ± 0.04	6
NBD-PE	19.0	2.1 ± 0.2	0.79 ± 0.04	4
NBD-chol	19.0	1.7 ± 0.6	0.77 ± 0.04	5
NBD-PE	26.0	180 ± 20	0.91 ± 0.06	4
NBD-chol	26.0	160 ± 30	0.91 ± 0.04	4

[a] Measurements at a given temperature were performed on identical liposome preparations on the same day. Measurements are reported as mean ± SD.

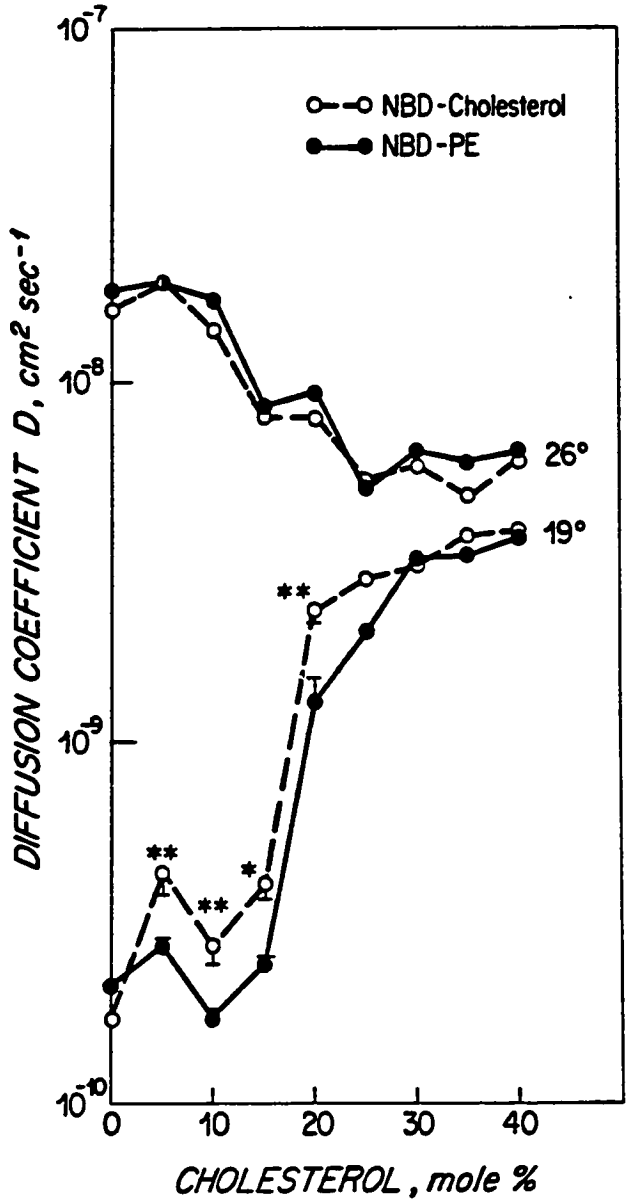

Figure 35. Lateral diffusion coefficient of NBD-phosphatidylethanolamine (closed symbols) and NBD-cholesterol (open symbols) in binary mixtures of dimyristoylphosphatidylcholine and cholesterol, as a function of cholesterol mole fraction, at temperatures above and below the main phase transition temperature for the pure phospholipid (24°C). Measurements at any given lipid composition were performed on identical liposome preparations on the same day. Individual points represent the average of three to six independent measurements. Error bars (mean ± S.E.M.) are shown for comparisons in which there are significant differences (*, $p<0.03$; **, $p<0.02$) between diffusion coefficients of the phospholipid and cholesterol probes. The sample temperature was measured to an accuracy of ± 0.5°C with a thermistor. There are significant differences between diffusion coefficients of the two probes only for cholesterol mole fractions between 5% and 20% at the temperature below the phase transition temperature for the pure phospholipid.

TABLE 15a. LATERAL MOBILITY OF NBD-PE AND NBD-CHOL IN DMPC/CHOLESTEROL MULTILAMELLAR LIPOSOMES; $T < Tm$[a]

	NBD-PE			NBD-CHOL			
X^b_{chol}	$Dx10^{11}$ cm^2sec^{-1}	$f(\infty)$	N	D	$f(\infty)$	N	P^c
0.00	2.1 ± 0.2	0.79 ± 0.04	4	1.7 ± 0.6	0.77 ± 0.04	5	NS[d]
0.05	2.7 ± 0.3	0.75 ± 0.05	5	4.3 ± 1.0	0.78 ± 0.05	6	<0.02
0.10	1.7 ± 0.2	0.85 ± 0.01	4	2.7 ± 0.7	0.84 ± 0.02	6	<0.02
0.15	2.4 ± 0.1	0.86 ± 0.03	3	4.0 ± 0.7	0.91 ± 0.02	4	<0.03
0.20	13 ± 6	0.91 ± 0.06	6	23 ± 3	0.93 ± 0.04	4	<0.02
0.25	20 ± 3	0.93 ± 0.10	3	28 ± 5	0.86 ± 0.04	3	NS
0.30	32 ± 4	0.86 ± 0.05	4	31 ± 3	0.93 ± 0.02	4	NS
0.35	33 ± 2	0.91 ± 0.05	6	37 ± 6	0.92 ± 0.06	6	NS
0.40	37 ± 6	0.95 ± 0.04	4	38 ± 1	0.95 ± 0.03	4	NS

[a]Measurements at a given cholesterol mole fraction were performed on identical liposome preparations on the same day. Temperature was 19°C. Measurements are reported as mean ± SD.

[b]cholesterol mole fraction

[c]Test of significance between diffusion coefficients of NBD-PE and NBD-chol (Student's two-tailed t test)

[d]Not significant ($P > 0.03$)

TABLE 15b. LATERAL MOBILITY OF NBD-PE AND NBD-CHOL IN DMPC/CHOLESTEROL MULTILAMELLAR LIPOSOMES: T > Tm[a]

	NBD-PE			NBD-CHOL			
X^b_{chol}	$Dx10^9$ cm^2sec^{-1}	f(∞)	N	D	f(∞)	N	p^c
0.00	18 ± 2	0.91 ± 0.06	4	16 ± 3	0.91 ± 0.04	4	NS
0.05	19 ± 4	0.84 ± 0.08	6	19 ± 3	0.88 ± 0.04	6	NS
0.10	17 ± 1	0.88 ± 0.04	4	14 ± 1	0.95 ± 0.01	4	NS
0.15	8.6 ± 0.4	0.92 ± 0.03	4	8.0 ± 0.5	0.92 ± 0.03	4	NS
0.20	9.4 ± 1.2	0.86 ± 0.04	4	7.9 ± 1.8	0.92 ± 0.05	4	NS
0.25	5.1 ± 0.9	0.87 ± 0.02	3	5.3 ± 0.3	0.88 ± 0.03	3	NS
0.30	6.4 ± 0.6	0.92 ± 0.04	4	5.8 ± 0.9	0.94 ± 0.01	4	NS
0.35	5.9 ± 0.7	0.92 ± 0.02	4	4.8 ± 0.8	0.95 ± 0.03	4	NS
0.40	6.4 ± 0.5	0.94 ± 0.02	4	6.0 ± 0.7	0.97 ± 0.02	4	NS

[a]Measurements at a given cholesterol mole fraction were performed on identical liposome preparations on the same day. Temperature was 26°C. Measurements are reported as mean ± SD.

[b]Cholesterol mole fraction.

[c]Test of significance between diffusion coefficients of NBD-PE and NBD-chol (Student's two-tailed t test)

[d]Not significant ($p > 0.03$)

transition temperature for the bulk phospholipid (T < Tm), there was a sharp 10-fold increase in the diffusion coefficient of both NBD-PE and NBD-chol at X_{chol} = 0.20; at T > Tm, there was a more gradual 3-fold decrease in the diffusion coefficients of both probes over the range X_{chol} = 0.10 - 0.25. The diffusion coefficients of NBD-PE and NBD-chol were within experimental error of one another except under the conditions of T < Tm, X_{chol} = 0.05 - 0.20, where the cholesterol probe consistently diffused 60-80% faster than the phospholipid probe. Fractional recoveries for the two probes were not significantly different from one another under any conditions of temperature and composition (table 15).

3. Lateral Mobility of NBD-PE and NBD-chol in Egg PC Liposomes: Temperature Dependence. The two lipid probes manifested identical lateral mobility behavior in egg PC multilamellar liposomes (fig. 36; table 16). The lateral diffusion coefficients showed a very weak temperature dependence, as expected for diffusion in a heterogeneous mixture of various phosphatidylcholines. In particular, there was no recognizable phase transition over the temperature range 10°-37°C, and diffusion was rapid over the entire range of temperatures (fig. 36). NBD-PE and NBD-chol diffusion coefficients in egg PC liposomes were identical to those in DMPC liposomes at temperatures greater than Tm, the main phase transition temperature for this homogeneous saturated phospholipid (fig. 36).

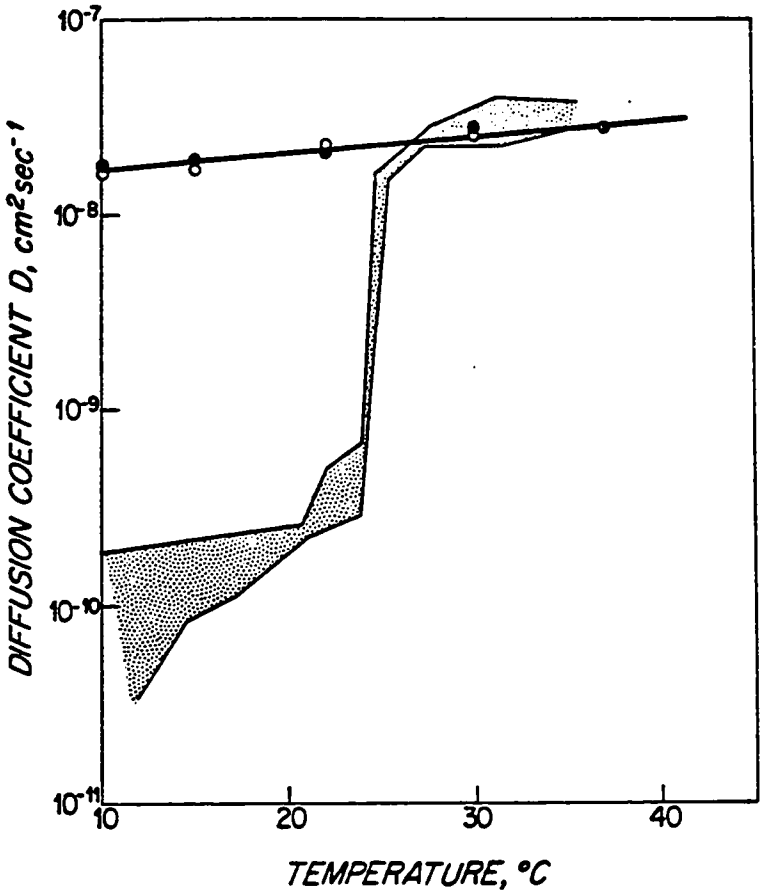

Figure 36. Lateral diffusion coefficient of NBD-phosphatidylethanolamine (closed symbols) and NBD-cholesterol (open symbols) in egg phosphatidylcholine multilamellar liposomes, as a function of temperature. Lipid probes were added to a final mole fraction of 0.15%. Measurements at a given temperature were performed on identical liposome preparations on the same day. Each point represents the average of three to five independent measurements (see Table 16). There is no significant difference between the diffusion coefficients of the two probes at any temperature examined. Fractional recoveries of fluorescence averaged 0.88 for NBD-phosphatidylethanolamine and 0.93 for NBD-cholesterol; these were not significantly different at any temperature. For comparison the range of values of the lateral diffusion coefficient of the lipid probes in dimyristoylphosphatidylcholine multilamellar liposomes is shown (stippled area; see Figure 34).

TABLE 16. LATERAL MOBILITY OF NBD-PE AND NBD-CHOL IN EGG PC MULTILAMELLAR LIPOSOMES[a]

Probe	Temp, °C	$Dx10^8$, cm^2sec^{-1}	f(∞)	N
NBD-PE	10	1.8 ± 0.2	0.84 ± 0.09	4
NBD-chol	10	1.7 ± 0.2	0.90 ± 0.02	4
NBD-PE	15	1.9 ± 0.3	0.88 ± 0.08	4
NBD-chol	15	1.7 ± 0.3	0.92 ± 0.03	5
NBD-PE	22	2.1 ± 0.3	0.91 ± 0.04	4
NBD-chol	22	2.3 ± 0.1	0.93 ± 0.08	4
NBD-PE	30	2.8 ± 0.3	0.89 ± 0.04	3
NBD-chol	30	2.6 ± 0.4	0.97 ± 0.01	4
NBD-PE	37	2.8 ± 0.3	0.87 ± 0.04	3
NBD-chol	37	2.8 ± 0.2	0.94 ± 0.01	4

[a]Measurements at a given temperature were performed on identical liposome preparations on the same day. Measurements are reported as mean ± SD.

4. Lateral Mobility of NBD-PE and NBD-chol in Mixtures of Egg PC and Cholesterol: Composition Dependence. As in egg PC multilamellar liposomes, the phospholipid and cholesterol probes manifested identical lateral mobility behavior in multilamellar liposomes composed of egg PC and cholesterol over the entire composition range from X_{chol} = 0.0 to X_{chol} = 0.5 (fig. 37; table 17). Diffusion coefficients showed a gradual two-fold decrease with increasing cholesterol mole fraction at both 15°C and 37°C (fig. 37); this may be compared with the three-fold decrease exhibited by the two probes in binary mixtures of DMPC and cholesterol above the main phase transition temperature for the bulk phospholipid (fig. 35).

C. DISCUSSION

In this chapter the lateral mobilities of the phospholipid analog NBD-PE and the cholesterol analog NBD-chol in various model membrane systems have been examined. Both probes exhibited relatively slow diffusion ($D < 10^{-9}$ cm^2sec^{-1}) in membranes comprised mainly of "solid" lipid regions (i.e., DMPC/cholesterol liposomes at $X_{chol} < 0.20$ and $T < Tm$), and relatively fast diffusion ($D > 10^{-9}$ cm^2sec^{-1}) in membranes containing large amounts of "fluid" phase lipid (i.e., DMPC/cholesterol liposomes at $X_{chol} \geq 0.20$ and/or $T > Tm$, and all egg PC/cholesterol liposomes). Increasing temperature led to increases in the lateral diffusion coefficient of both probes in all liposome systems, with sharp 50-fold changes at the main phase transition temperature of the bulk phospholipid (Tm) in DMPC liposomes. The

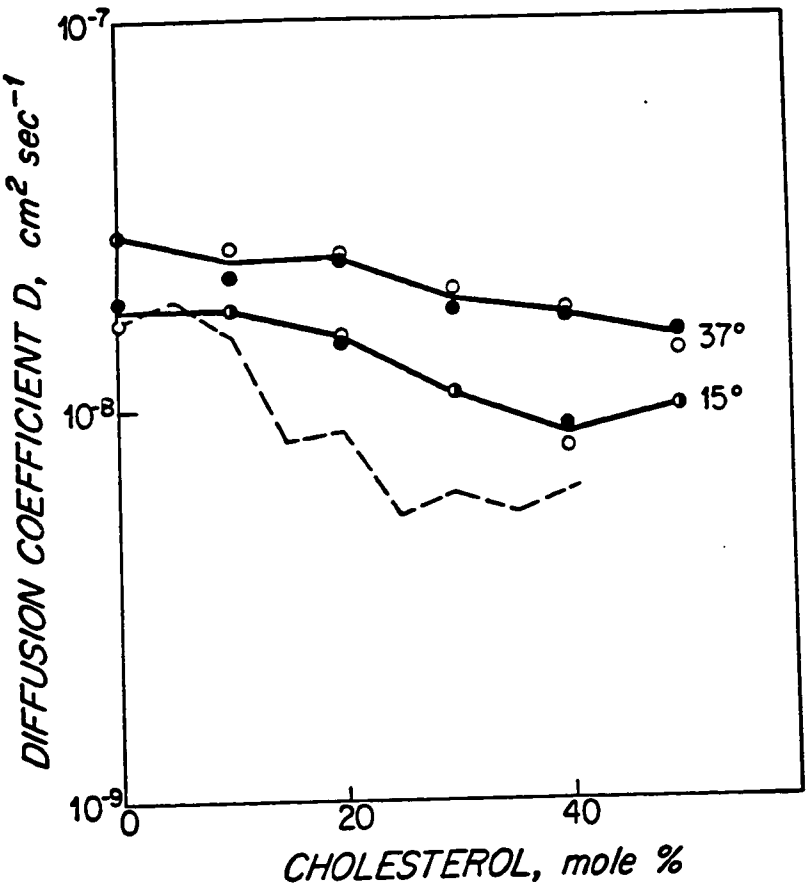

Figure 37. Lateral diffusion coefficient of NBD-phosphatidylethanolamine (closed symbols) and NBD-cholesterol (open symbols) in mixtures of egg phosphatidylcholine and cholesterol, as a function of cholesterol mole fraction, at two different temperatures. Measurements at any given lipid composition were performed on identical liposome preparations on the same day. Individual points represent the average of two to five independent measurements (see Table 17). There is no significant difference between the diffusion coefficients of the two probes at any lipid composition at either temperature. For comparison the mean value of the lateral diffusion coefficient of the lipid probes in binary mixtures of dimyristoylphosphatidylcholine and cholesterol above the main phase transition temperature for the bulk phospholipid is shown (dashed line; see Figure 35).

TABLE 17. LATERAL MOBILITY OF NBD-PE AND NBD-CHOL IN EGG PC/CHOLESTEROL MULTILAMELLAR LIPOSOMES[a]

		NBD-PE			NBD-CHOL		
Temp, °C	X^b_{chol}	$Dx10^8$, cm^2sec^{-1}	f(∞)	N	D	F	N
10	0.0	1.8 ± 0.2	0.84 ± 0.09	4	1.7 ± 0.2	0.90 ± 0.02	4
	0.1	1.8 ± 0.2	0.88 ± 0.03	4	1.6 ± 0.2	0.84 ± 0.01	4
15	0.0	1.9 ± 0.3	0.88 ± 0.08	4	1.7 ± 0.3	0.92 ± 0.03	5
	0.1	1.8 ± 0.2	0.98 ± 0.01	4	1.8 ± 0.2	0.87 ± 0.02	4
	0.2	1.5 ± 0.2	0.90 ± 0.08	4	1.6 ± 0.2	0.89 ± 0.06	4
	0.3	1.1 ± 0.1	0.94 ± 0.02	4	1.1 ± 0.1	0.97 ± 0.02	3
	0.4	0.9 ± 0.1	0.94 ± 0.11	2	0.8 ± 0.0	0.91 ± 0.07	2
	0.5	1.0 ± 0.1	0.83 ± 0.14	3	1.0 ± 0.1	0.87 ± 0.04	4
21	0.0	2.1 ± 0.3	0.91 ± 0.04	4	2.3 ± 0.1	0.93 ± 0.08	4
	0.5	1.0 ± 0.1	0.95 ± 0.3	3	0.9 ± 0.1	0.97 ± 0.03	4
37	0.0	2.8 ± 0.3	0.87 ± 0.04	3	2.8 ± 0.2	0.94 ± 0.01	4
	0.1	2.2 ± 0.4	0.97 ± 0.01	4	2.6 ± 0.2	0.87 ± 0.01	3
	0.2	2.4 ± 0.3	0.94 ± 0.02	4	2.5 ± 0.6	0.87 ± 0.03	4
	0.3	1.8 ± 0.1	0.92 ± 0.01	4	2.0 ± 0.1	0.96 ± 0.04	3
	0.4	1.7 ± 0.1	0.90 ± 0.05	2	1.8 ± 0.5	0.96 ± 0.03	3
	0.5	1.6 ± 0.3	0.93 ± 0.04	3	1.4 ± 0.2	0.98 ± 0.02	4

Table 17 (continued)

[a]Measurements at a given cholesterol mole fraction were performed on identical liposome preparations, on the same day. Measurements are reported as mean ± SD.

[b]Cholesterol mole fraction.

mole fraction of cholesterol (X_{chol}) in binary mixtures of phospholipid (DMPC or egg PC) and cholesterol was directly related to the lateral diffusion coefficient (D) of both probes at temperature (T) below Tm and inversely related to D at temperatures above Tm; sharp 10-fold increases in diffusion rate at $X_{chol} \sim 0.20$, $T < Tm$, in DMPC/cholesterol liposomes were also observed. NBD-PE and NBD-chol manifested identical lateral mobilities in all model systems except DMPC liposomes to which 5-20 mole % cholesterol had been added, at temperatures below Tm. Under these conditions the cholesterol probe consistently diffused 60-80% faster than the phospholipid probe. Lateral mobility parameters for the phospholipid probe NBD-PE obtained in the present study agree, both qualitatively and quantitatively, with those presented in the literature for model membrane systems composed of pure DMPC liposomes (290) or multibilayers (245,247,289), egg PC multibilayers (245,289), DMPC/cholesterol liposomes (290) or multibilayers (245,343), and egg PC/cholesterol multibilayers (245,289) (see table 5).

The concordance between the lateral mobilities of NBD-chol and NBD-PE in model membranes under nearly all conditions implies that this novel fluorescent cholesterol analog functions as a true probe of lipid (and more specifically, cholesterol) mobility. Further, this agreement suggests that any significant difference between diffusion coefficients of NBD-chol and NBD-PE in a particular membrane system reflects a real distinction between the environments of the bulk (unlabeled) cholesterol and phospholipid. Such a difference was found

in the present study for DMPC/cholesterol liposomes at cholesterol mole fractions between 5 and 20% and temperatures less than the main phase transition temperature for the phospholipid (fig. 35). That this difference was due to the addition of bulk cholesterol to DMPC and not to temperature alone is evident from the observation that tracer quantities of NBD-PE and NBD-chol have identical lateral mobilities in pure DMPC liposomes at temperatures both above and below Tm (fig. 34, table 14). Low concentrations of cholesterol (5-20 mole %), when added to gel-phase DMPC, thus appear to partition in the membrane such that the bulk of the cholesterol is in a different physical environment from the bulk of the phospholipid. Two models for the molecular packing in binary mixtures of DMPC and cholesterol have recently appeared in the literature; both suggest a lateral phase separation between "solid" regions containing pure phospholipid and "fluid" regions containing phospholipid + 20 mole % cholesterol, under the conditions $T < Tm$, $X_{chol} < 0.20$ (refs. 344, 345). The first model postulates a separation based on alternating parallel bands of solid and fluid lipid (344) and is supported by freeze-fracture electron microscopic studies (346); the second hypothesizes unoriented islands of solid and fluid lipid (345). From the present data it is impossible to choose between these competing models, since they both would predict only a small difference between the measured diffusion coefficients of cholesterol and phospholipid in DMPC/cholesterol multilamellar liposomes using the FPR technique. Thus, the large discrepancy between the size of the putative lipid

domains (0.01 - 0.1 μm width) and the diameter of the bleaching laser beam (2 μm), as well as the spatial averaging over all possible domain orientations in a multilamellar system, both tend to minimize the measured difference between the diffusion coefficients of the two probes (see, for example, fig. 7 of ref. 344).

In contrast to the results obtained in DMPC/cholesterol liposomes at $X_{chol} < 0.20$, $T < Tm$ (in which lipid lateral mobility is greatly slowed by significant amounts of "solid"-phase lipid), cholesterol and phospholipid have the same lateral mobility in all model membranes composed of "fluid"-phase lipid only. This result is of interest in light of the hypothesis that coexisting, immiscible fluid domains may be present in model membranes under certain conditions (347). The present observations would imply either that cholesterol is present to the same extent in all of the fluid domains, that lipids in all of the domains have the same lateral mobility, or that the FPR technique is not sensitive enough to detect small differences in microenvironment between adjacent fluid lipid domains.

CHAPTER 8. LATERAL MOBILITY OF PHOSPHOLIPID AND CHOLESTEROL: ERYTHROCYTE MEMBRANE

In the preceding chapter the utility of the fluorescent phospholipid and cholesterol analogs, NBD-PE and NBD-chol respectively, in the measurement of phospholipid and cholesterol lateral mobility has been demonstrated. Based on the model system studies, it might be predicted that cholesterol and phospholipid should have identical lateral mobilities in the erythrocyte ghost membrane, which contains a heterogeneous mixture of lipids (table 1) that are not organized into laterally separated domains (see chapter 4). Studies in the present chapter address this question directly. In addition, the relationships between band 3 and lipid mobility in the human erythrocyte ghost membrane, and between lipid mobility in the ghost membrane and in liposomes prepared from whole lipid extracts of the ghost membrane, are explored.

A. METHODS

The improved, recalibrated FPR apparatus diagrammed in fig. 11c was employed in these studies. Sample temperatures were controlled to ± 0.5°C with a thermostatted sample holder (fig. 19).

As described in chapter 3, multilamellar liposomes were prepared from extracted erythrocyte membrane lipids (cholesterol/phospholipid (C/P) molar ratio of 0.75) and either NBD-PE or NBD-chol (final fluorophore concentration of 0.06 mole %). Erythrocyte ghosts (C/P molar ratio of 1.11)

were labeled directly using a sonicated solution of pure NBD-PE (final fluorophore mole fraction of 0.067), then washed twice in one of several phosphate buffers (see Results). Ghosts were also labeled by exchange using a suspension of NBD-chol labeled liposomes prepared from total extracts of erythrocyte membrane lipid. The final mole fraction of NBD-chol in these ghosts was estimated to be 0.01 - 0.02.

As noted in chapter 3, NBD-chol exchange into ghost membranes proceeded slowly and erratically. Such exchange most likely involves a water-soluble intermediate rather than a fusion event between liposome and ghost membrane (348-350), implying that the problem with exchange in the present case occurs in either the release of NBD-chol from the liposome or the insertion of the solubilized probe into the ghost membrane. The latter possibility is made less likely by the observation that the cholesterol content of erythrocyte ghost membranes can be varied markedly by equilibration with phospholipid dispersions containing the appropriate level of cholesterol (351). Since NBD-chol does, in fact, readily exchange from simple phospholipid/cholesterol dispersions into cell membranes of several other types (Rando, R.R. and F.W. Bangerter, in preparation), there may well be a unique interaction between the probe and the particular mixture of lipids in the erythrocyte membrane which prevents efficient solubilization (release) of the cholesterol derivative from the erythrocyte lipid liposomes.

Three hundred μl solutions of labeled liposomes or ghosts were deoxygenated and the samples sealed on a microscope slide with epoxy, as

described in chapter 4A. The FPR experiment was performed as described (chapter 4A).

B. RESULTS

In multilamellar liposomes prepared from total lipid extracts of erythrocyte ghost membranes, NBD-PE and NBD-chol manifested identical lateral mobilities within the temperature range 15°C to 37°C. Diffusion coefficients and fractional recoveries of fluorescence had no dependence on ionic strength for either probe (table 18). As seen in the model systems egg PC and egg PC:cholesterol (1:1, mol:mol), the temperature dependence of the diffusion coefficient was small (less than two-fold increase from 15°C to 37°C); fractional mobilities of the probes were greater than 0.90 in all cases (fig. 38, table 18).

Because of the difficulties involved in the incorporation of NBD-chol into erythrocyte ghost membranes (see chapter 3), comparisons between lateral mobility parameters for NBD-PE and NBD-chol were possible only in 40 mM $NaPO_4$ buffer. Under these conditions the cholesterol and phospholipid probes exhibited identical lateral mobility between 15°C and 37°C (fig. 38, table 19). Again the temperature dependence of the diffusion coefficient was small; fractional recoveries of fluorescence averaged 0.79 for NBD-PE and 0.75 for NBD-chol in this buffer system.

There was no significant ionic strength dependence of the lateral mobility parameters of NBD-PE in erythrocyte ghost membranes. Buffers employed in this study included isotonic phosphate-buffered

TABLE 18. LATERAL MOBILITY OF NBD-PE AND NBD-CHOL IN EXTRACTED ERYTHROCYTE LIPID MULTILAMELLAR LIPOSOMES[a]

		NBD-PE			NBD-CHOL		
Buffer	Temp, °C	$Dx10^9$, cm^2sec^{-1}	f(∞)	N	D	f(∞)	N
b	15	4.8 ± 0.2	0.91 ± 0.05	3	4.9 ± 0.4	0.98 ± 0.01	4
	21	5.6 ± 0.5	0.92 ± 0.04	2	5.2 ± 0.8	0.95 ± 0.02	4
	37	7.1 ± 1.4	0.88 ± 0.03	4	8.5 ± 0.7	0.88 ± 0.02	3
c	15	5.8 ± 0.4	0.90 ± 0.04	4	5.4 ± 0.1	0.93 ± 0.06	4
	21	5.7 ± 0.3	0.94 ± 0.02	4	5.4 ± 0.3	0.91 ± 0.04	4
	37	8.5 ± 0.7	0.95 ± 0.01	4	7.8 ± 0.6	0.94 ± 0.01	4

[a]Measurements are reported as mean ± SD.

[b]PBS; 10 mM $NaPO_4$, 150 mM NaCl, pH 7.2

[c]14 mM $NaPO_4$, 1 mM EDTA, 10 μg/ml PMSF, 1 μg/ml pepstatin A, pH 7.4

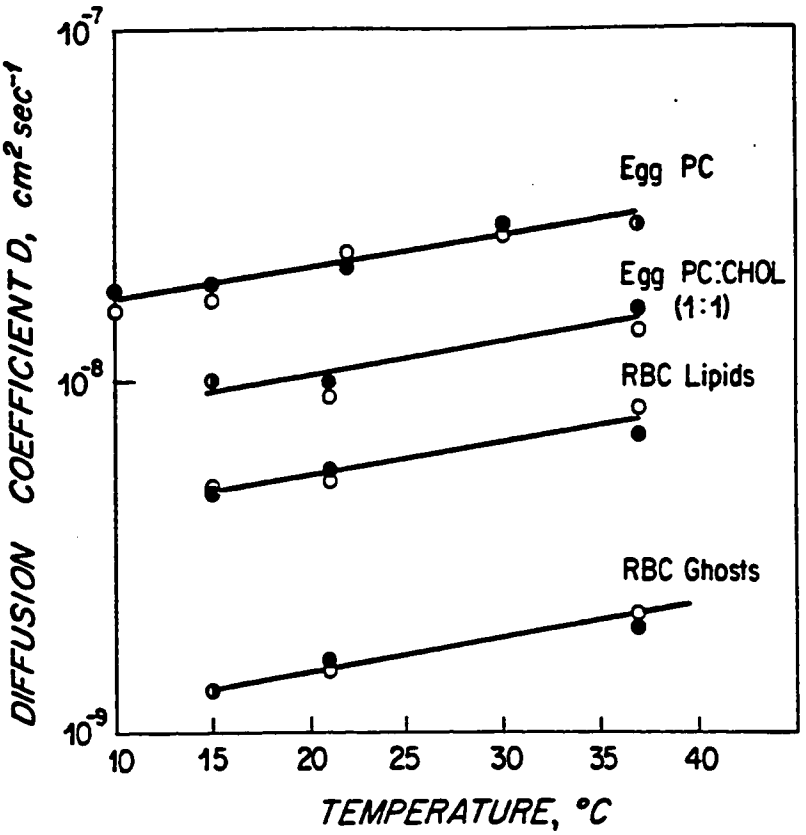

Figure 38. Lateral diffusion coefficient of NBD-phosphatidylethanolamine (closed symbols) and NBD-cholesterol (open symbols) in egg phosphatidylcholine multilamellar liposomes (Egg PC); egg phosphatidylcholine:cholesterol (1:1, mol:mol) multilamellar liposomes (Egg PC:CHOL (1:1)); multilamellar liposomes prepared from total lipid extracts of erythrocyte ghost membranes (RBC Lipids); and erythrocyte ghost membranes (RBC Ghosts); as a function of temperature. Lipid probes were added to final mole fractions of 0.15% in the Egg PC and Egg PC:CHOL (1:1) samples, 0.06% in the RBC Lipids sample, and 6.7% (NBD-PE) or approximately 1.5% (NBD-chol) in the RBC Ghosts sample (see text). Measurements at a given temperature were performed on identical liposome or ghost preparations on the same day. Buffers comprised 10 mM $NaPO_4$, 150 mM NaCl, pH 7.2 for all samples except RBC ghosts for which the buffer comprised 40 mM $NaPO_4$, 60 μM PMSF, 1 mM EDTA, 1 μg/ml pepstatin A, pH 7.4. Each point represents the average of two to five independent measurements (see Tables 16, 17, 18, 19). There is no significant difference between the diffusion coefficients of the two lipid probes under any conditions.

TABLE 19. LATERAL MOBILITY OF NBD-PE AND NBD-CHOL IN ERYTHROCYTE GHOST MEMBRANES[a,b]

	NBD-PE			NBD-CHOL		
Temp, °C	$Dx10^9$, cm^2sec^{-1}	f(∞)	N	D	f(∞)	N
15	1.3 ± 0.2	0.79 ± 0.06	5	1.3 ± 0.1	0.81 ± 0.06	4
21	1.6 ± 0.4	0.77 ± 0.06	5	1.5 ± 0.1	0.75 ± 0.04	3
37	2.0 ± 0.3	0.80 ± 0.02	4	2.2 ± 0.7	0.68 ± 0.10	4

[a]Measurements are reported as mean ± SD.

[b]Buffer comprised 40 mM $NaPO_4$, 1 mM EDTA, 10 μg/ml PMSF, 1 μg/ml pepstatin A, pH 7.4

saline, pH 7.2, as well as 14 and 40 mM $NaPO_4$ to which 1 mM EDTA, 10 μg/ml PMSF, and 1 μg/ml pepstatin A, pH 7.4, had been added (table 20).

C. DISCUSSION

Phospholipid and cholesterol probes have identical lateral mobilities in the erythrocyte ghost membrane, under all conditions of ionic strength and temperature examined. There is a small dependence of the lipid lateral diffusion coefficient on temperature over the range 15°C to 37°C, with no suggestion of a "break point" that would signify a membrane lipid phase transition in this temperature range. At 37°C the diffusion coefficient of the lipid probes is 2.1×10^{-9} cm^2sec^{-1}, or approximately four-fold greater than the band 3 "rapid diffusion limit." This comparison will be discussed in greater detail in the following chapter.

Lipid diffusion data obtained in the present study agree, both quantitatively and qualitatively, with those available from the literature. Thompson and Axelrod (180) and Kapitza and Sackmann (279) independently measured the lateral mobility of the lipid probe diI (3,3'-dioctadecylindocarbocyanine) in the human erythrocyte ghost membrane, the former over the temperature range -3°C to 40°C and the latter over the range 10°C to 45°C. Both groups reported a small temperature dependence of diffusion coefficient (1½ to 2-fold change between 15°C and 37°C measurements); the diI diffusion coefficient at 20°C was approximately $1.0 - 1.5 \times 10^{-9}$ cm^2sec^{-1} in both cases.

TABLE 20. EFFECT OF IONIC STRENGTH ON LATERAL MOBILITY OF NBD-PE IN ERYTHROCYTE GHOST MEMBRANES[a]

Buffer	Temp, °C	$Dx10^9$, cm^2sec^{-1}	f(∞)	N
b	15	1.0 ± 0.3	0.82 ± 0.03	4
	21	1.4 ± 0.2	0.82 ± 0.05	4
	30	2.1 ± 0.3	0.84 ± 0.00	3
	37	2.2 ± 0.4	0.84 ± 0.02	3
c	15	1.1 ± 0.2	0.88 ± 0.04	4
	21	1.4 ± 0.3	0.83 ± 0.02	5
	30	2.0 ± 0.5	0.86 ± 0.02	4
	37	2.2 ± 0.3	0.86 ± 0.04	5
d	15	1.3 ± 0.2	0.79 ± 0.06	5
	21	1.6 ± 0.4	0.77 ± 0.06	5
	37	2.0 ± 0.3	0.80 ± 0.02	4

[a]Measurements are reported as mean ± SD.

[b]PBS; 10 mM $NaPO_4$, 150 mM NaCl, pH 7.2

[c]14 mM $NaPO_4$, 1 mM EDTA, 10 μg/ml PMSF, 1 μg/ml pepstatin A, pH 7.4

[d]40 mM $NaPO_4$, 1 mM EDTA, 10 μg/ml PMSF, 1 μg/ml pepstatin A, pH 7.4

More recently, Koppel et al. (281) observed a diffusion coefficient for NBD-PE lateral mobility of 1.4×10^{-8} cm^2sec^{-1} in the mouse. erythrocyte ghost membrane at 23°C. The order-of-magnitude difference between this and the results described for the hyman erythrocyte ghost may reflect a real interspecies difference in membrane fluidity; experiments on both human and mouse cells using the same FPR apparatus would have to be performed, however, in order to exclude inter-laboratory variation in apparatus calibration as the cause for this apparent discrepancy (see chapter 2).

Both NBD-PE and NBD-chol diffuse four-fold faster in liposomes prepared from chloroform/methanol extracts of erythrocyte ghost membranes ($D = 8.0 \times 10^{-9}$ cm^2sec^{-1}) than in the ghost membranes themselves. As noted in chapter 3, the mole fraction of cholesterol in the extracted lipid liposomes (0.43) differed only slightly from that in the ghost membranes (0.53). Based on the model system studies, such a small difference in membrane composition would not be sufficient to account for a four-fold change in lipid diffusion coefficient (see fig. 37). It appears, rather, that the presence of membrane proteins partially restricts the lateral mobility of both phospholipid and cholesterol in the erythrocyte ghost membrane. This restriction could be mediated through a nonspecific reduction in membrane "fluidity" by the addition of membrane proteins to a pure lipid bilayer (see, for example, refs. 352-355), analogous to the "solidifying" effect of cholesterol on pure phospholipid bilayers above the main phase transition temperature (see fig. 35). Alternatively, a specific interaction between both phospholipid and cholesterol and some slowly

diffusing or immobile integral membrane protein might exist, leading to a slowing of the lipid diffusion rate (see ref. 287). It is unlikely, however, that molecules as different as phospholipid and cholesterol should interact in exactly the same manner with membrane protein to produce the same degree of slowing of both lipid components.

Restriction of lipid lateral mobility by membrane protein has also been shown by Jacobson et al. (287), who compared the diffusion of the lipid probe diI in plasma membranes of human fibroblasts with that in multibilayers reconstituted from fibroblast plasma membrane lipids. Between 25°C and 40°C diI diffusion was four times faster in the extracted lipid multibilayers than in the plasma membranes themselves, a difference identical to that observed in the present study. Qualitatively similar results were also obtained in studies of fluorescence polarization of the membrane probe diphenylhexatriene, in which greater anisotropy changes (interpreted as faster rotation) were observed in extracted membrane lipid bilayers from mouse LM cells (356) and human lymphocytes (357) in the plasma membranes themselves.

Phospholipid and cholesterol diffusion in liposomes prepared from extracted erythrocyte lipids ($X_{cholesterol} = 0.43$) is very similar to that in the model liposome system egg PC + 50 mole % cholesterol (fig. 38). Phospholipid and cholesterol mobilities are identical within each membrane system, and the lateral diffusion coefficients exhibit the same small temperature dependence in the two membranes. The absolute diffusion coefficient of the lipid probes is approximately two-fold greater in the egg PC/cholesterol membrane

than in the extracted erythrocyte lipid membrane; this difference can probably be ascribed to the unusual lipid composition of the erythrocyte membrane (see Table 1).

CHAPTER 9. DISCUSSION

The data reported in this dissertation describe a wide range of phenomena concerning the lateral mobility of band 3, phospholipid, and cholesterol in the human erythrocyte membrane. Within a fairly narrow range of temperatures and ionic strengths, conditions are described under which fifty-fold changes in diffusion coefficient and nearly maximal changes in the mobile fraction of band 3 occur. Under the same conditions, in contrast, phospholipid and cholesterol diffusion rates change by less than two-fold. Clearly the lateral mobility of this integral membrane protein is regulated in some systematic way. In this discussion six possible models for intramembranous forces capable of restricting translational diffusion of band 3 are presented. Careful consideration of the present data, as well as other observations from the literature, leads to a rejection of all but two of the models as likely options. Both of these involve an intimate association between the cytoplasmic portion of band 3 and the cytoskeleton of the erythrocyte membrane: one proposes a specific complex between the bulk of band 3 and some immobile cytoskeletal component (most likely spectrin or ankyrin); the other postulates a nonspecific entanglement of band 3 in the cytoskeletal reticulum formed by spectrin, actin, and various other peripheral membrane proteins. Although it cannot be determined from the present data which model is, in fact, the correct one, it is clear that the cytoskeletal protein ankyrin plays a crucial role in mediating the restriction on band 3 lateral mobility.

A. COMPARISONS WITH MEASUREMENTS OF TRANSLATIONAL AND ROTATIONAL DIFFUSION

Before considering specific models of erythrocyte membrane structure, it is relevant to compare the lateral mobility data obtained in this work with various measurements of translational and rotational diffusion for integral membrane proteins (including band 3) and lipids in the literature. Peters *et al.* (9) reported a maximum translational diffusion coefficient of 3×10^{-12} cm^2/sec for fluorescein-isothiocyanate (FITC)-labeled human erythrocyte membrane proteins in ghosts suspended in 7 mM $NaPO_4$ buffer, pH 8.0 (μ = 25 mM) at 20-23°C. This value is in apparent disagreement with the results of the present study, in which a diffusion coefficient for band 3 in ghost membranes of $9.5 \pm 2.3 \times 10^{-11}$ cm^2/sec (with a fractional recovery of 51 ± 14%) in 9 mM $NaPO_4$ buffer, pH 7.4 (μ = 23 mM) at 21°C was observed. In hindsight, however, there were several erroneous assumptions made in the paper of Peters *et al.* which led to an artificially low estimate of the diffusion coefficient of the integral membrane proteins. An SDS-polyacrylamide gel scan of FITC-labeled ghosts (see fig. 3b of ref. 9) shows approximately 40% of the label on band 3 or glycophorin, with about 10% on spectrin and about 50% either bound to lipid or noncovalently attached to the membrane in some way. The label on spectrin would presumably be immobile, while the lipid-bound or noncovalently bound fluorophore would probably exhibit extremely rapid diffusion. The authors took

their first measurement of fluorescence recovery at 3 to 3.5 minutes after bleaching, however, by which time all the rapidly diffusing fluorophore could have recovered. It can also be calculated that, within this time period, about 40% of the maximum band 3-associated fluorescence recovery would have already occurred, given a lateral diffusion coefficient of 9.5×10^{-11} cm^2/sec (see figure 2 of ref. 9). Since the fractional recovery of band 3 fluorescence at this ionic strength is only about 50% (table 7), the expected overall recovery of fluorescence between 3 and 23 minutes after bleaching is 40% x 60% x 50%, or about 12%. In fact, Peters et al. estimated a fluorescence recovery during this time period of 9 ± 7%, indicating actual agreement with the present study.

Fowler and Branton (10) used inactivated Sendai virus to fuse a 50/50 mixture of unlabeled and FITC-labeled erythrocytes (> 70% of label on band 3 or PAS-1) in 310 mOsm phosphate-buffered saline, pH 7.6, at 0°, 23°, 30°, and 37°C. Translational diffusion coefficients for the integral membrane proteins were determined from the rate of appearance of fused cell pairs with "uniform" distribution of fluorescence, based on a model for diffusion from one half of a spherical shell into the other (see table 3). Given the uncertainties concerning the (possibly temperature-dependent) effects of Sendai virus fusion, the unknown influence of immobile fluorophore on the scoring system used to determine the percentage of fused cells which are "uniformly fluorescent" (see fig. 3 of ref. 10), and the fact that a spherical-shell model for diffusion will only approximate the

actual diffusion coefficient in an hourglass-shaped system (see fig. 2b of ref. 10), the cell fusion results compare favorably with the FPR measurements at high ionic strength of this work (see tables 7, 10).

Sheetz, Koppel and coworkers (256,358,359) pretreated human erythrocytes with diisopropylfluorophosphate (DFP), labeled the surface glycoproteins (primarily band 3 and glycophorin) with dichlorotriazinylaminofluorescein (DTAF), and measured protein lateral mobility using a combination of cell fusion and fluorescence photobleaching techniques(see table 3). In buffers comprising 5 (ref. 359) to 6 (refs. 256,358) mM sodium phosphate, 46 (ref. 359) to 72 (refs. 256,358) mM NaCl, and 1 (ref. 359) to 5 (refs. 256,358) mM EDTA, pH 7.4, average diffusion coefficients for membrane protein lateral mobility of 4 - 9 x 10^{-11} cm^2sec^{-1} at 30-37°C were obtained. Fractional recoveries of 0.87 on overnight incubation of membrane samples at 37°C were also reported (358). Differences in sample preparation and data analysis are probably great enough to explain discrepancies between these data and those of the present study. Thus, the methods of Sheetz et al. include prolonged incubation of erythrocytes in pH 10.1 buffer, a treatment which may have a deleterious effect on the membrane cytoskeleton. Many of the fusion measurements were made after treatment with polyethylene glycol, which may have secondary effects on observed diffusion coefficients and fractional mobilities of membrane components. DTAF labeling is only approximately 60% specific for band 3; the remainder is found on glycophorin and other,

unidentified, high molecular weight membrane proteins (256). Analysis of data from cell fusion experiments yields approximate diffusion coefficients, owing to the complex geometry of the fused cell system (9,248,256). Finally, estimation of glycoprotein fractional mobilities after prolonged incubation of erythrocytes at elevated temperatures, without full biochemical characterization of the membranes after such treatment, may result in values which do not reflect the physiologic condition (see chapter 5).

Two laboratories have measured lateral diffusion coefficients for the lipid analogue diI in the human erythrocyte ghost membrane (279,280). Over the temperature range of interest in the present study, diI diffusion coefficients increased from 1.4 - 1.6 x 10^{-9} cm^2sec^{-1} at 15°C to 2.2-3.0 x 10^{-9} cm^2sec^{-1} at 37°C. These values are in excellent agreement with those reported in chapter 8.

Comparing lateral mobility data obtained for band 3, phospholipid, and cholesterol in the human erythrocyte ghost membrane with those found for other membrane proteins and lipid analogues (tables 3, 4,5), it is evident that both protein and lipid mobilities are slower in the human erythrocyte membrane than in many other natural membranes, and much slower than in artificial membrane systems. For example, the fastest diffusion coefficient observed for band 3 under certain conditions (54 ± 19 x 10^{-11} cm^2sec^{-1}) is still nearly an order of magnitude less than that of rhodopsin in the frog disc membrane (D = 350 ± 150 x 10^{-11} cm^2sec^{-1}), a molecule whose mobility is believed to be restricted only by the bilayer viscosity (2,241).

Similarly, diffusion coefficients for both phospholipid and cholesterol in the human erythrocyte ($210 \pm 40 \times 10^{-9}$ $cm^2 sec^{-1}$ at 37°C) are up to an order of magnitude less than those of diI and NBD-PE in several biological membranes (table 4). These observations may imply that, due to its unique lipid composition (table 1) and cytoskeleton structure, the human erythrocyte is less "fluid" than most other biological membranes.

It is instructive in this regard to estimate the viscosity of the erythrocyte membrane at 37°C, assuming that a translational diffusion coefficient of 5.4×10^{-10} cm^2/sec represents unrestricted lateral mobility for band 3, and that a diffusion coefficient of 2.1×10^{-9} cm^2/sec represents unrestricted mobility for phospholipid and cholesterol. There are two models for diffusion in a viscous medium which can be employed for such a calculation. The Einstein-Sutherland diffusion equation (cited in ref. 241) relates the translational diffusion coefficient D_T of a large spherical particle of radius r in an isotropic (three-dimensional) medium to the viscosity of the medium η:

$$\eta = (kT)/(6\pi D_T r), \qquad (14)$$

where k is the Boltzmann constant and T is the absolute temperature. An approximate radius for the intramembranous portion of the band 3 dimer (mol. wt. approximately 100,000 daltons) of 40A is assumed, as this value is approximately twice the radius estimated by Poo and Cone (241) for the rhodopsin monomer (38,000 daltons) in the

disc membrane and approximately half the diameter of the intramembranous particles in the erythrocyte membrane (which may be an overestimate). The resultant viscosity for a translational diffusion coefficient of $5.4 \pm 1.9 \times 10^{-10}$ cm^2/sec (n=9) at 37°C is 11 ± 4P. This value compares rather favorably with previous estimates of erythrocyte membrane viscosity based on measurements of fluorescence polarization (360-365) and methanol diffusion (366), and with estimates of membrane viscosity in other systems (see table 21).

The Saffman-Delbruck equation (ref. 367) considers the translational diffusion of a cylinder of radius a and height h through a two-dimensional viscous medium of viscosity η (i.e., the lipid bilayer) which is bounded on either side by a much less viscous medium of viscosity η' (i.e., the intracellular and extracellular aqueous fluid):

$$D_T = \frac{kT}{4\pi\eta h}\left(\ln\frac{\eta h}{\eta' a} - \gamma\right), \qquad (15)$$

where γ is Euler's constant (0.5772). Again assuming the radius of the band 3 dimer to be 40A, and taking values for the thickness of the hydrophobic membrane core of 40A and for the aqueous phase viscosity of 1×10^{-2}P, the bilayer viscosity implied for $D_T = 5.4 \pm 1.9 \times 10^{-10}$ cm^2/sec at 37°C is 140 ± 60P. Similarly, assuming a radius for phospholipid or cholesterol in the membrane of 4A (see ref. 281), and assuming that lipids in one leaflet of the bilayer diffuse independently of lipids in the other leaflet (i.e., that the effective thickness of the hydrophobic membrane core is 20A for

Table 21. Estimates of Membrane Viscosity

Membrane	Temp. °C	Viscosity (poise)	Method	Label	Ref.
erythrocyte ghosts	20	1.2	fl. pol.[a]	perylene	360
"	37	1.7	"	"	"
"	21	1-10	fl. pol.	retinol	361
"	20	5-7	fl. pol.	DPH[b]	362
"	37	2-4	"	"	"
"	25	2.6	fl. pol.	perylene	363
"	4	16.0	fl. pol.	DPH	364
"	25	6.3	"	"	"
"	37	4.0	"	"	"
"	10	1.0	fl. pol.	DPH	365
"	35	0.4	"	"	"
"	20	1.7	methanol diff.	methanol	366
"	21	25-100	rot.diff.band 3	EITC[c]	299
"	37	25-100	rot.diff.band 3	EITC	116
"	37	7-15[d]	lat.diff.band 3	EITC	this study
		80-200[e]	"	"	"
		60-100[e]	lat.diff.lipid	NBD-PE NBD-chol	"
frog disc	21	0.6-6.0[d]	rot.diff.rhodopsin	retinol	368
amphibian disc	21	1-4[d]	lat.diff.rhodopsin	retinol	368
mouse-human heterokaryon	37	8-10[d]	lat.diff.surface antigens	fl.antibody	2,235

[a] fluorescence polarization

[b] 1,6-diphenyl-1,3,5-hexatriene

[c] eosin-5-isothiocyanate

[d] calculated according to eqn. 14

[e] calculated according to eqn. 15

[f] average of all data for NBD-PE, NBD-chol (n=20)

an individual phospholipid or cholesterol molecule (see ref. 383)), the bilayer viscosity obtained for $D_T = 2.1 \pm 0.4 \times 10^{-9}$ cm^2/sec (n=20) at 37°C is 80 ± 20P. It should be noted that these estimates of viscosity are inversely proportional to the value chosen for the membrane thickness but relatively insensitive to even large changes in particle radius, while the viscosities estimated from the Einstein-Sutherland relation are linearly related to particle radius but (of necessity) independent of membrane thickness.

The bilayer viscosity as estimated by the two-dimensional diffusion equation from measured diffusion coefficients of band 3, phospholipid, or cholesterol differs by an order of magnitude from that calculated assuming diffusion in an isotropic three-dimensional medium. It is in agreement, however, with the estimate of viscosity based on rotational diffusion of eosin-labeled band 3 in the ghost membrane (table 7). It is not at all clear that the bilayer viscosity sampled by small molecular probes such as diphenylhexatriene and methanol is the same effective viscosity governing the motion of larger membrane proteins or lipids, nor is it obvious that a three-dimensional diffusion equation has any quantitative bearing on a two-dimensional diffusion process. Furthermore, it is not unreasonable to image a considerably greater viscosity for the cholesterol-rich, sphingomyelin-rich erythrocyte membrane than for other biological membranes which do not contain as much cholesterol and sphingomyelin. The agreement between viscosity etsimates based

on models for both translational and rotational diffusion of band 3, and for translational diffusion of phospholipid and cholesterol, in a two-dimensional viscous medium is striking, and suggests that the effective viscosity of the erythrocyte bilayer sampled by this integral membrane protein and by various membrane lipids may be considerably higher than previously estimated. Further, the concordance between viscosity estimates calculated from lateral diffusion rates of band 3, phospholipid, and cholesterol in the same membrane implies strongly that the lateral diffusion coefficient of band 3 employed in this calculation represents unrestricted mobility (i.e., restricted only by the viscosity of the bilayer) for this integral membrane protein.

Rotational diffusion of eosin-labeled band 3 has been studied by observing the decay of flash-induced absorption or phosphorescence anisotropy of the eosin probe (116,131,299-301,369-373). A single rotational correlation time of about 0.5 msec at both 21°C (299-301) and 37°C (116) in 5 mM $NaPO_4$ buffer, pH 7.4 was originally estimated. More recently, two components of the decay of flash-induced anisotropy have been reported (369-371,373), but their relationship to any physical model (such as rapidly and slowly rotating forms of band 3) cannot be unambiguously stated. In particular it is difficult from this data to implicate any particular membrane-associated process in restriction of the rotational mobility of band 3, since the physical meaning of the anisotropy decay components is highly

uncertain. In the rapid translational diffusion limit, however, a comparison between the translational and rotational diffusion coefficients is instructive. In low ionic strength (5 mM sodium phosphate, pH 7.4), high temperature (37°C) buffer, the average rotational correlation time of eosin-labeled band 3 is between 0.5 (116) and 1.0 (370) msec. This corresponds to a rotational diffusion coefficient about the membrane normal (D_R) of between 200 sec^{-1} (ref. 370) and 500-2000 sec^{-1} (ref. 116). The theoretical relationship between translational and rotational diffusion coefficients for protein embedded in a lipid bilayer (367) can be used to estimate the translational diffusion coefficient which should be supported by the lipid viscosity at 37°C:

$$\frac{D_T}{D_R} = a^2 \left(\ln \frac{\eta h}{\eta' a} - \gamma\right). \qquad (16)$$

For a bilayer viscosity of approx. 100P (see above), a maximum translational diffusion coefficient of 3-30 x 10^{-10} cm^2/sec would be expected. The agreement between the predicted value and the value obtained in the present study (5.4 ± 1.9 x 10^{-10} cm^2/sec) is striking, suggesting that in the rapid (or unrestricted) mobility limit at least, rotation and translation of band 3 are governed by identical forces. It should be noted that rotational diffusion of band 3 has only been measured at low ionic strength, where the fraction of band 3 which is free to diffuse laterally is very high. Measurements of rotational mobility under high ionic strength, low temperature conditions

would be very instructive in deciding whether the membrane-associated process which causes translational immobilization of band 3 (i.e., low fractional recovery) also induces rotational immobilization of band 3.

B. MODELS OF ERYTHROCYTE MEMBRANE STRUCTURE

From the data presented in this dissertation, it appears that there are at least two separate processes restricting the lateral mobility of band 3 in the human erythrocyte membrane. One process regulates the fraction of band 3 which is free to diffuse in the plane of the membrane; the other controls the rate at which the mobile fraction of band 3 diffuses. Both processes are dependent on ionic strength and temperature, in that high ionic strength (40 mM phosphate) and low temperature (21°C) favor immobilization (10% mobile) and slow diffusion ($D = 1 \times 10^{-11}$ cm^2/sec) of band 3, while low (13 mM phosphate) or hypertonic (320 mM KCl + 40 mM phosphate) ionic strength and high temperature (37°C) favor mobilization (> 75% mobile) and fast diffusion ($D = 5 \times 10^{-10}$ cm^2/sec) of band 3. Detailed analysis of the ionic strength and temperature dependencies of these two experimental parameters reveals, however, that they are clearly dissociated and therefore must result from at least two different membrane-associated processes. Thus, increases in the fraction of mobile band 3 to near maximal levels (> 75%) always precede (i.e., occur at more moderate ionic strengths and lower temperatures than)

large increases in the diffusion coefficient. Similarly, prolonged incubation of ghosts at constant low or hypertonic ionic strength and high temperature leads to rapid increases in mobile fraction; the diffusion rate of the mobile fraction increases more slowly and gradually. Further evidence for the dissociation of the processes responsible for regulating immobilization and diffusion is the difference in reversibility of these two parameters: changes in the diffusion rate of band 3 with temperature are at least partially reversible whereas increases in the mobile fraction of band 3 are minimally if at all reversible.

There are at least six theoretical membrane-associated processes capable of regulating the lateral mobility of band 3 to some degree. In increasing order of likelihood, these include: 1) electrostatic repulsion between putative band 3-glycophorin complexes; 2) lipid domain formation on the membrane; 3) planar aggregation of band 3 dimers; 4) lipid viscosity; 5) specific complex formation between band 3 and some immobile cytoskeletal component; and 6) nonspecific entanglement of the cytoplasmic portion of band 3 in the cytoskeletal network.

An association between band 3 and glycophorin in the intramembranous particles revealed on freeze-fracture of the erythrocyte membrane has been postulated for some time (see chapter 1). Such a complex might render band 3 mobility susceptible to ionic strength changes, since the electrostatic repulsion between such particles (due to the very large amount of negatively-charged sialic acid

present on each glycophorin monomer) would become accentuated at low ionic strength. One would not expect the lateral mobility of the putative band 3-glycophorin complex to be especially temperature-sensitive, however, if electrostatic repulsion were the major factor governing restriction of mobility. Electrostatic effects would be expected to become manifest instantaneously upon changes of ionic strength or other conditions; the slow rise in diffusion coefficient on prolonged incubation at 37°C (figs. 23,26,33) argues strongly against the importance of such effects in causing these diffusion rate changes. Finally, the effect of low ionic strength on electrostatic repulsion should be opposite to that of hypertonic ionic strength; that these two treatments are, in fact, similar in effect on lateral mobility is inconsistent with the postulate that an electrostatic mechanism causes large changes in lateral mobility.

The likelihood of domain formation in the erythrocyte membrane is low on several accounts, including the results of the present study. X-ray diffraction studies indicate that there is negligible liquid-crystalline phase lipid present in the erythrocyte membrane above 0°C (ref. 374). Differential scanning calorimetry could not detect a phase transition below 40°C (ref. 375), and the present study failed to demonstrate a phase transition by fluorescence photobleaching recovery over the temperature range 15°C to 37°C (see fig. 38). All of these studies are consistent with the high cholesterol content and heterogeneous lipid composition of the membrane. In

chapter 4 the presence of domains smaller in area than about 1/4 of the total membrane surface was explicitly ruled out over a wide range of ionic strengths and temperatures, since rebleaching laser pulses delivered to the same area of eosin-labeled ghost membrane consistently resulted in 80-100% fractional recovery of fluorescence after the third or fourth bleach. Had bounded domains comparable in size to the focused laser spot been present, fractional recoveries on rebleaching would never have reached these high levels. The identity between the lateral mobility parameters of NBD-PE and NBD-chol in the erythrocyte membrane further suggests that lateral phase separations between phospholipid and cholesterol do not exist in this membrane. This conclusion is strengthened by the observation that the slopes of the curves of log (diffusion coefficient) vs. temperature^{-1} (i.e., the activation energies for diffusion) for both NBD-PE and NBD-chol are similar in intact erythrocyte ghost membranes and in multibilayers composed of extracted erythrocyte lipids (data from fig. 38; see also ref. 287).

Self-aggregation of band 3 dimers has been postulated as the physical explanation for the temperature dependence of the two components of rotational diffusion of eosin-labeled band 3 (ref. 369). Large aggregates are highly unlikely, since crosslinking and solubilization studies show mainly dimers of band 3 (with some trimers and tetramers, but no higher aggregates) and since no temperature-dependent aggregation of band 3-associated intramembranous particles

in the erythrocyte membrane has ever been seen. The increased trypsin susceptibility of band 3 at low ionic strength (74) may imply a conformational change in band 3 structure with ionic strength; there is no a priori reason to suppose, however, that such a change would necessarily be associated with aggregation of band 3 dimers. Nigg and Cherry (369) invoke microaggregates of 5-10 band 3 dimers as sufficient to explain the temperature dependence of the data on rotational diffusion. Assuming a dependence of translational diffusion coefficient on particle size of $D \propto 1/r$, where r is the radius of the particle, however, an aggregation of at least 2500 band 3 dimers would be necessary to explain a 50-fold change in diffusion coefficient. Even this is probably an underestimate, since D may actually have a log (1/r) rather than a 1/r dependence on particle size (cf. eqn. 15 vs. eqn. 14). Clearly the large changes in diffusion coefficient seen in the present study under various conditions of ionic strength and temperature cannot be explained on the basis of planar aggregation alone. It is at least theoretically possible, however, that microaggregates of 2-10 band 3 dimers could be tightly bound to individual ankyrin monomers through a single high-affinity ankyrin-band 3 bond, providing a mechanism for low band 3 fractional mobility under physiologic ionic strength or low temperature conditions (see below).

Lipid viscosity appears not to be a major mediator of large changes in the lateral mobility of band 3. Obviously lipid viscosity plays a crucial role in setting a "baseline" level of lateral mobility

for integral membrane proteins (see eqn. 14,15); it is interesting that this viscosity, as assessed for the erythrocyte membrane by the lateral mobility of fluorescent phospholipid and cholesterol analogues, may be quite high compared to that of other biological membranes and various model membrane systems (cf. tables 4,5,21; fig. 38; ref. 280). There are several pieces of evidence, however, against this factor as a regulator of changes in lateral mobility in the erythrocyte membrane. Much data has accumulated indicating that the lateral diffusion coefficient of the lipid probes in erythrocyte ghosts changes little between 0°C and 40°C (refs. 279, 280; chapter 8), implying that the membrane viscosity also changes little over this wide range of temperatures. Similarly, ionic strength affects the lateral mobility of the probe NBD-PE not at all (table 20). Finally, we have shown temperature effects on the diffusion coefficient of band 3 to be highly time-dependent, with a lag of more than 60 minutes between warming up to temperature and achieving of the maximum rate of diffusion at that temperature. Viscosity effects should become manifest almost instantaneously on warming up to a given temperature. It is highly unlikely, therefore, that large changes in lipid viscosity are responsible for major alterations in the lateral mobility of band 3.

There are now several systems in which cytoskeletal elements have been shown to be important in controlling the distribution and dynamics of integral membrane proteins (e.g., refs. 6,262,376-9). In particular, there is a great deal of experimental evidence to

support the contention that band 3 interacts intimately with the cytoskeleton of the human erythrocyte membrane. It would be surprising on steric grounds alone if such associations did not occur, since the anastomosing cytoskeletal reticulum covers approximately 1/3 of the inner membrane surface (146) and a considerable portion of the band 3 molecule is entirely intracellular. Much of this data is summarized in chapter 1, and will not be repeated here. Of particular interest are the observations that: 1) cross-linking between band 1 of spectrin and band 3 at pH 7.4 is ionic strength dependent (occurring in isotonic KCl but not in 10 mM KCl) (167); 2) antibodies directed against the cytoplasmic portion of band 3 inhibit spectrin binding to inside-out vesicles (8); 3) approximately 10-15% of the total band 3 is tightly linked to ankyrin, a cytoskeletal protein (213); and 4) enhanced clustering of concanavalin A receptors (i.e., band 3; see ref. 37) occurs in domains of neonatal human erythrocyte and reticulocyte membranes which are deficient in spectrin (380). None of these findings, however, is conclusive proof that the major portion of band 3 forms a specific complex with the cytoskeleton in a manner which could restrict lateral mobility. Although up to 40% of band 3 remains with the cytoskeleton upon Triton X-100 extraction of erythrocyte ghosts in isotonic buffer (151), band 3 cannot be solubilized with the major cytoskeletal proteins (spectrin, actin) in low ionic strength medium and it does not serve as a high-affinity binding site ($K_D < 10^{-7}M$) for spectrin on the inner membrane surface (201).

Correlations between changes in the lateral mobility of band 3 induced by various experimental perturbations and the biochemical effects of these treatments on the erythrocyte membrane provide strong evidence for cytoskeletal control of band 3 lateral mobility. Low ionic strength incubation of ghost membranes at 37°C for one hour leads to a twenty-fold increase in the lateral diffusion coefficient of band 3 (from 1.3×10^{-11} to 24×10^{-11} cm^2sec^{-1}) and a three-fold increase in fractional mobility (from 21% to 66%); at three hours even greater mobility is seen ($D = 54 \times 10^{-11}$ cm^2sec^{-1}, $f(\infty) = 75\%$). Effects of low ionic strength on erythrocyte membrane structure include disruption of ankyrin-spectrin bonds with eventual formation of spectrin-depleted inside-out vesicles (e.g., ref. 196), disruption of spectrin-actin (e.g., ref. 25) and spectrin-band 4.1 (e.g., ref. 196) bonds with dissolution of the cytoskeletal shell, shift of the spectrin dimer-tetramer equilibrium toward the dimer form (181-2), and possibly disruption of ankyrin-band 3 bonds (215) although the latter effect has not been observed by all investigators (214). In addition, low ionic strength changes the susceptibility of membrane-bound band 3 to proteolysis (98) and to cross-linking with spectrin (167), presumably through protein conformational changes. At the ionic strengths employed in the present study, there is less than 20% dissociation of spectrin from the ghost membrane. Low ionic strength incubation of ghosts at 37°C for one hour does not result in the specific proteolysis of any major membrane component; at three hours, ankyrin alone undergoes specific (70%) proteolysis.

Hypertonic ionic strength treatment of ghost membranes at 37°C also results in large increases in both the lateral diffusion coefficient (from 1.3 x 10^{-11} to 52 x 10^{-11} cm^2sec^{-1}) and fractional mobility (from 21% to 90%) of band 3. Biochemical effects of such treatment include disruption of bonds between ankyrin and band 3 (refs. 196, 204,214,215) and between ankyrin and spectrin (151,204,213); the spectrin-actin-band 4.1 cytoskeletal shell remains intact under hypertonic conditions (151). Finally, incubation of ghost membranes with the 72,000 dalton proteolytic fragment of ankyrin which serves as the high-affinity binding site for spectrin on the membrane causes a two- to three-fold change in both diffusion coefficient (fig. 32, ref. 240) and fractional mobility of band 3. This fragment presumably acts by disrupting specifically ankyrin-spectrin bonds, although treatment of intact erythrocyte ghost membranes with the ankyrin fragment alone does not release spectrin from the membranes into the supernatant (240).

The similarity between the effects of low and hypertonic ionic strength on both the diffusion coefficient and fractional mobility of band 3 is striking, and suggests that these two treatments may affect erythrocyte membrane structure in the same way to cause changes in band 3 mobility. For example, both of these incubation conditions result in disruption of ankyrin-spectrin and (perhaps) ankyrin-band 3 bonds, while hypertonic ionic strength does not shift the spectrin dimer-tetramer equilibrium or disrupt the spectrin-

actin-band 4.1 cytoskeletal shell. The 72,000 dalton ankyrin fragment, like low and hypertonic ionic strength treatments, causes disruption of ankyrin-spectrin bonds; changes in band 3 lateral mobility upon incubation with this fragment are not nearly as great, however, as those achieved with ionic strength perturbations. Taken together, these observations imply that the breakage of ankyrin-spectrin linkages may be sufficient to cause relatively modest increases in band 3 mobility, but that disruption of high-affinity ankyrin-band 3 bonds is necessary for large changes in lateral mobility. The notion that direct connections between at least some of the band 3 and other cytoskeletal components are involved in restricting the lateral mobility of the bulk of band 3 is further supported by the finding that band 3 conformation itself may be significantly altered at low ionic strength (see above). The increased susceptibility of ankyrin to proteolysis under conditions which favor rapid diffusion of band 3 is a final piece of evidence that ankyrin linkages are directly involved in the control of band 3 lateral mobility.

It is claimed that the rotational diffusion of band 3 has the same characteristics (rate, temperature dependence, etc.) in spectrin-depleted membrane vesicles as in native ghost membranes, and that this evidence excludes the spectrin-actin network from any possible role in restriction of rotational diffusion (299,369). These experiments were performed in low ionic strength buffer (5 mM $NaPO_4$), however, under which conditions we find the (laterally) mobile fraction of band 3 to be high (> 70%). Unless the cytoskeleton is

free to diffuse laterally on the membrane (which is unlikely but not impossible), one would expect specific band 3-cytoskeleton bonds to immobilize totally the band 3 involved. Such interactions would surely decrease the fraction of band 3 which is mobile but might not affect the diffusion coefficient of the mobile fraction. Since the rotational diffusion measurements were gathered under ionic strength and temperature conditions such that the (laterally) mobile fraction of band 3 is already high, they can tell us nothing about any process responsible for changing the percentage of total band 3 which is mobile. If specific band 3-cytoskeleton complexes were the physical explanation behind a decreased fractional recovery of fluorescence at low temperature and/or high ionic strength, then any change in rotational diffusion due to such complex formation would not have been seen by Cherry et al., even in intact ghosts. Thus, although specific interactions between the major portion of band 3 and the cytoskeleton have never been conclusively demonstrated, they have not been ruled out either. In particular, a low-affinity ($K_D \cong 10^{-5} - 10^{-6}$M) complex between band 3 and spectrin would not be inconsistent with any available data. If such a complex were to form at physiologic ionic strength and/or low temperature, then it could easily lead to total immobilization of the band 3 involved and hence a decreased fractional recovery of fluorescence in FPR experiments (see below). Similarly, a process involving increased aggregation of band 3 dimers, of which one per aggregate is coupled through a

high-affinity band 3-ankyrin bond to the cytoskeletal shell, would also lead to immobilization of the bulk of band 3 in the membrane.

While formation of a stable, long-lived complex between band 3 and some immobile cytoskeletal element could explain changes in fractional recovery under various conditions, it could not explain variations in the diffusion coefficient of the mobile fraction of band 3. A satisfactory explanation for the large changes observed in diffusion coefficient in this study must involve more dynamic membrane forces affecting the long-range environment in which the individual band 3 molecules are diffusing. As noted above, lipid viscosity, domain formation, planar aggregation, and electrostatic repulsion are unlikely candidates for this dynamic membrane force. Nonspecific entanglement of the cytoplasmic portion of band 3 in the cytoskeletal reticulum in a manner which is dependent on ionic strength, temperature, and time is one possible explanation for the data on diffusion coefficients. This mechanism has been named the "polymer matrix model" for control of protein diffusion in membranes (281,381); it has been invoked as the dominant force regulating lipopolysaccharide diffusion in multibilayer membranes reconstituted from E. coli outer membrane components (381) and transmembrane protein diffusion in mouse erythrocyte ghost membranes (281). In brief, the model proposes that a membrane cytoskeleton can function as a labile polymer network capable of sterically hindering the long-range lateral diffusion of trans-

membrane proteins but not of membrane lipids. The network is envisioned to be dynamic, with cross-links that can continually break and reform, thus allowing hindered diffusion of entrapped membrane proteins. Measured diffusion coefficients, according to this model, are functions of the density of matrix cross-links on the membrane and their rate of breaking down (281). In the human erythrocyte membrane system, it is not difficult to imagine a metastable state of cytoskeleton structure intermediate between tight binding to and complete dissociation from the membrane which would allow rapid lateral diffusion of band 3. Indeed, heterogeneity of spectrin binding to the membrane in the form of high-affinity interactions with ankyrin as well as low-affinity interactions with other membrane proteins or membrane lipid has been postulated by at least one author (201; see below). The stabilities of the lipid-free cytoskeleton formed on Triton extraction of ghosts and of the pure spectrin-actin-band 4.1 shell produced after hypertonic treatment of the intact cytoskeletal reticulum (151) are further indications that, under some conditions at least, the cytoskeleton may be attached to the membrane by very tenuous forces without involving actual membrane fragmentation.

An alternative mechanism for the restriction of transmembrane protein mobility by a membrane cytoskeleton involves specific, reversible binding of the transmembrane protein to some immobile cytoskeletal component. If the binding interaction is long-lived compared to the characteristic time for diffusion, the transmembrane

component will appear to be immobile on the time scale of the FPR experiment (see above); if many binding encounters can occur within the diffusion half-time, the diffusing protein will appear to be mobile. The diffusion coefficient of the mobile species is a function of the density of binding sites on the membrane and the equilibrium constant for the binding interaction, according to the following relation (ref. 7; E. Elson, personal communication):

$$D_{measured} = \frac{D_{free}}{1 + Kc_{cyto}} \qquad (17),$$

where $D_{measured}$ and D_{free} are lateral diffusion coefficients in the presence and absence, respectively, of the hindering cytoskeleton; K is the equilibrium constant for association between the transmembrane protein and the immobile cytoskeletal component; and $\bar{c}_{cyto}$ is the total concentration of cytoskeletal binding sites on the membrane. This model has already been offered as a plausible alternative to the polymer matrix model in explaining the control of lipopolysaccharide diffusion in reconstituted E. coli outer membrane (382). With reference to the human erythrocyte ghost membrane, it is instructive to calculate the equilibrium constant for a putative band 3-spectrin interaction which would account for a 50-fold change in the diffusion coefficient of the mobile band 3 upon removal of the cytoskeletal (spectrin-binding) constraint. From eq. 17 we find that $K\bar{c}_{cyto} \cong 50$ for $D_{free}/D_{measured} = 50$. The effective concentration of hypothetical band 3 binding sites on spectrin, assuming

one site per spectrin heterodimer, can be determined from the total number of heterodimers per erythrocyte membrane (approx. 200,000), the inner membrane surface area of the erythrocyte (approx. 150 μm^2), and the thickness of the sub-lipid bilayer space within which spectrin and band 3 would be expected to interact (approx. 25 nm; see fig. 2a of ref. 12). This concentration is approximately 8×10^{-5} M; it implies a maximum dissociation constant (1/K) for the putative band 3-spectrin complex of 2×10^{-4} M. As has been noted (chapter 1; ref. 26), interactions of such low affinity between spectrin and other erythrocyte membrane components have not been heretofore amenable to analysis. It is quite possible, then, that the lateral mobility of mobile band 3 in the intact erythrocyte membrane is controlled by specific, low-affinity, rapidly reversible binding to some immobile cytoskeletal component, most likely spectrin.

In summary, then, the model for erythrocyte membrane structure most consistent with the data presented in this dissertation is as follows. Under conditions of high ionic strength and low temperature, nearly all of the band 3 is totally immobilized on the membrane, either through specific, low-affinity complexes between the band 3 molecules and some immobile cytoskeletal component(s) (most likely spectrin in addition to ankyrin), or through severe restriction within very small domains (molecular size) by entrapment in a tightly bound cytoskeletal net. As various cytoskeletal interactions are perturbed by changes in ionic strength and temperature or by

the addition of cytoskeletal fragments, two sequential processes occur which progressively lift the restrictions on band 3 lateral mobility. The first process allows a greater and greater proportion of band 3 molecules to diffuse over large distances (at least 4μ) on the membrane. This process probably involves either the breaking of low-affinity bonds between the cytoskeleton and band 3 (if such are actually formed), the disruption of low-affinity bonds between spectrin and other membrane elements such as lipid, the disruption of some high-affinity bonds between spectrin and ankyrin, or the disaggregation of band 3 microaggregates from their high-affinity ankyrin binding sites. While the first membrane-associated process is sufficient for increases in the percentage of the total band 3 which is mobile on the membrane surface, it does not allow that mobile fraction to diffuse much faster. For this a second, separate process is required, which is more difficult to set in motion than the first process but which is at least partially reversible on a change of conditions back to the original. The second process almost certainly involves disruption of some spectrin-membrane bonds, as it occurs to an appreciable degree only under conditions which approach (but do not include) complete spectrin dissociation from the membrane and vesiculation of ghost membranes. It may also involve disruption of high-affinity ankyrin-band 3 linkages (see above). Disruption of these bonds would lead to a very loose but metastable state of cytoskeleton structure which would allow

unrestricted lateral mobility of band 3 in the plane of the membrane, either through decreased binding of band 3 to some immobile cytoskeletal component or through decreased influence of the cytoskeletal matrix on band 3 mobility. Parenthetically, it would also result in a state of cytoskeleton structure in which ankyrin is sensitive to one or another membrane-associated protease. Cleavage of ankyrin in this loosened cytoskeletal state would further result in at least partial irreversibility of the ionic strength- and temperature-induced changes in band 3 lateral mobility.

C. CONCLUDING REMARKS

This thesis describes a series of phenomena concerning the restriction of lateral mobility of band 3 in the human erythrocyte membrane. Possible molecular bases for these phenomena are discussed, but further experimental work is needed to elucidate more definitively the mechanisms underlying the control of lateral mobility. Such work would include studies of glycophorin and even spectrin mobility on the membrane, using specifically labeled endogenous proteins or labeled exogenous protein fragments. Direct comparisons between lateral and rotational diffusion of band 3 molecules under the same experimental conditions would be informative in deciding between the matrix control model and the specific low-affinity binding model of band 3 mobility regulation.

It is highly likely that changes in cytoskeletal structure are responsible for part or all of the changes in lateral mobility observed in the present study. If this is the case, then a detailed analysis of changes in lateral mobility should help answer the as yet unresolved questions relating to molecular interactions both within the cytoskeleton and between the cytoskeleton and various other membrane components. Such interactions are important in maintaining red cell shape and flexibility, and may be governed by dynamic equilibria regulating the state of phosphorylation of membrane elements such as spectrin and band 3. The study of these interactions is important not only for its clinical relevance to various diseases of erythrocyte membrane structure (e.g., hereditary spherocytosis), but also for its basic implications concerning the structure and function of cytoskeleton-containing membrane systems more complex than the erythrocyte.

REFERENCES

1. Singer, S.J. and G.L. Nicolson. 1972. The Fluid Mosaic Model of the Structure of Cell Membranes. Science 175:720-731.

2. Edidin, M. 1974. Rotational and Translational Diffusion in Membranes. Ann. Rev. Biophys. Bioeng. 3:179-201.

3. Bretscher, M.S. 1973. Membrane Structure: Some General Principles. Science 181:622-629.

4. Nicolson, G.L. 1976. Transmembrane Control of the Receptors on Normal and Tumor Cells. Biochim. Biophys. Acta 457:57-108.

5. Edelman, G.M. 1976. Surface Modulation in Cell Recognition and Cell Growth. Science 192:218-226.

6. Henis, Y.I. and E.L. Elson. 1981. Inhibition of the Mobility of Mouse Lymphocyte Surface Immunoglobulins by Locally Bound Concanavalin A. Proc. Natl. Acad. Sci. USA 78:1072-1076.

7. Elson, E.L. and J.A. Reidler. 1979. Analysis of Cell Surface Interactions by Measurements of Lateral Mobility. J. Supramolec. Struct. 12:481-489.

8. Marchesi, V.T. 1979. Functional Proteins of the Human Red Blood Cell Membrane. Semin. Hematol. 16:3-20.

9. Peters, R., J. Peters, K.H. Tews and W. Bahr. 1974. A Microfluorimetric Study of Translational Diffusion in Erythrocyte Membranes. Biochim. Biophys. Acta 367:282-294.

10. Fowler, V. and D. Branton. 1977. Lateral Mobility of Human Erythrocyte Integral Membrane Proteins. Nature 268:23-26.

11. Marchesi, V.T., H. Furthmayr, and M. Tomita. 1976. The Red Cell Membrane. Ann. Rev. Biochem. 45:667-698.

12. Tsukita, S., S. Tsukita, and H. Ishikawa. 1980. Cytoskeletal Network Underlying the Human Erythrocyte Membrane: Thin-section Electron Microscopy. J. Cell Biol. 85:567-576.

13. Op den Kamp, J.A.F. 1979. Lipid Asymmetry in Membranes. Ann. Rev. Biochem. 48:47-71.

14. Barenholz, Y. and T.E. Thompson. 1980. Sphingomyelins in Bilayers and Biological Membranes. Biochim. Biophys. Acta 604:129-158.

15. Fisher, K.A. 1976. Analysis of Membrane Halves: Cholesterol. Proc. Natl. Acad. Sci. USA 73:173-177.

16. Blau, L. and R. Bittman. 1978. Cholesterol Distribution between Two Halves of Lipid Bilayer of Human Erythrocyte Ghost Membranes. J. Biol. Chem. 253:8366-8368.

17. Lange, Y. and J.S. D'Alessandro. 1978. Exchangeability of Human Erythrocyte-Membrane Cholesterol. J. Supramol. Struct. 8:391-397.

18. Lange, Y., J. Dolde, and T.L. Steck. 1981. The Rate of Transmembrane Movement of Cholesterol in the Human Erythrocyte. J. Biol. Chem. 256:5321-5323.

19. Hanahan, D.J. 1969. Characterization of Erythrocyte Membrane. IN: G.A. Jamieson and T.J. Greenwalt (editors), Red Cell Membrane Structure and Function, p. 84. Philadelphia: J.B. Lippincott Co.

20. Rouser, G., C.J. Nelson, S. Fleischer, and G. Simon. 1968. Lipid Composition of Animal Cell Membranes, Organelles and Organs. IN: D. Chapman (editor), Biological Membranes, p. 5. New York: Academic Press.

21. Guidotti, G. 1972. Membrane Proteins. Ann. Rev. Biochem. 41: 731-752.

22. Wallach, D.F.H. 1972. The Dispositions of Proteins in the Plasma Membranes of Animal Cells: Analytical Approaches Using Controlled Peptidolysis and Protein Labels. Biochim. Biophys. Acta 265:61-83.

23. Juliano, R.L. 1973. The Proteins of the Erythrocyte Membrane. Biochim. Biophys. Acta 300:341-378.

24. Steck, T.L. 1974. The Organization of Proteins in the Human Red Blood Cell Membrane. J. Cell Biol. 62:1-19.

25. Fairbanks, G., T.L. Steck, and D.F.H. Wallach. 1971. Electrophoretic Analysis of the Major Polypeptides of the Human Erythrocyte Membrane. Biochem. 10:2606-2617.

26. Bennett, V. and P.J. Stenbuck. 1979. Identification and Partial Purification of Ankyrin, the High Affinity Membrane Attachment Site for Human Erythrocyte Spectrin. J. Biol. Chem. 254:2533-2541.

27. Tomita, M.,H. Furthmayr, and V.T. Marchesi. 1978. Primary Structure of Human Erythrocyte Glycophorin A: Isolation and Characterization of Peptides and Complete Amino Acid Sequence. Biochem. 17:4756-4770.

28. Tilney, L.G. and P. Detmers. 1975. Actin in Erythrocyte Ghosts and Its Association with Spectrin. J. Cell Biol. 66:508-520.

29. Cabantchik, Z.I., P.A. Knauf, and A. Rothstein. 1978. The Anion Transport System of the Red Blood Cell: The Role of Membrane Protein Evaluated by the Use of "Probes." Biochim. Biophys. Acta 515: 239-302.

30. Rothstein, A. 1978. The Functional Roles of Band 3 Protein of the Red Blood Cell. IN: A.K. Solomon and M. Karnovsky (editors), Molecular Specialization and Symmetry in Membrane Function, pp. 128-159. Cambridge, Mass: Harvard University Press.

31. Knauf, P.A. 1979. Erythrocyte Anion Exchange and the Band 3 Protein: Transport Kinetics and Molecular Structure. Curr. Topics Memb. Transp. 12:249-363.

32. Juliano, R.L. and A. Rothstein. 1971. Properties of an Erythrocyte Membrane Lipoprotein Fraction. Biochim. Biophys. Acta 249:227-235.

33. Steck, T.L. and G. Dawson. 1974. Topographical Distribution of Complex Carbohydrates in the Erythrocyte Membrane. J. Biol. Chem. 249:2135-2142.

34. Drickamer, L.K. 1978. Orientation of the Band 3 Polypeptide from Human Erythrocyte Membranes: Identification of NH_2-Terminal Sequence and Site of Carbohydrate Attachment. J. Biol. Chem. 253:7242-7248.

35. Markowitz, S. and V.T. Marchesi. 1981. The Carboxyl-terminal Domain of Human Erythrocyte Band 3. J. Biol. Chem. 256:6463-6468.

36. Golovtchenko-Matsumoto, A.M. and T. Osawa. 1980. Heterogeneity of Band 3, the Major Intrinsic Protein of Human Erythrocyte Membranes. J. Biochem. 87:847-854.

37. Furthmayr, H., I. Kahane, and V.T. Marchesi. 1976. Isolation of the Major Intrinsic Transmembrane Protein of the Human Erythrocyte. J. Membrane Biol. 26:173-187.

38. Adair, W.L. and S. Kornfeld. 1974. Isolation of Receptors for Wheat Germ Agglutinin and the Ricinus communis Lectins from Human Erythrocytes Using Affinity Chromatography. J. Biol. Chem. 249:4676-4704.

39. Findlay, A. 1974. The Receptor Proteins for Concanavalin A and Lens culinaris Phyto-hemagglutinin in the Membrane of the Human Erythrocyte. J. Biol. Chem. 249:4378-4403.

40. Tanner, M.J.A. and D.H. Boxer. 1972. Separation and Some Properties of the Major Proteins of the Human Erythrocyte Membrane. Biochem. J. 129:333-347.

41. Yu,J. and T.L. Steck. 1975. Isolation and Characterization of Band 3, the Predominant Polypeptide of the Human Erythrocyte Membrane. J. Biol. Chem. 250:9170-9175.

42. Ross, A.H. and H.M. McConnell. 1977. Reconstitution of Band 3, the Erythrocyte Anion Exchange Protein. Biochem. Biophys. Res. Commun. 74:1318-1325.

43. Lukacovic, M.J., M.B. Feinstein, R.I. Sha'afi, and S. Perrie. 1981. Purification of Stabilized Band 3 Protein of the Human Erythrocyte Membrane and Its Reconstitution into Liposomes. Biochemistry 20:3145-3151.

44. Cabantchik, A.I., D.J. Volsky, H. Ginsburg, and A. Loyter. 1980. Reconstitution of the Erythrocyte Anion Transport System: In Vitro and In Vivo Approaches. Ann. N.Y. Acad. Sci. 341:444-454.

45. Wolosin, J.M. 1980. A Procedure for Membrane-Protein Reconstitution and the Functional Reconstitution of the Anion Transport System of the Human Erythrocyte. Biochem. J. 189:35-44.

46. Ho, M.K. and G. Guidotti. 1975. A Membrane Protein from Human Erythrocytes Involved in Anion Exchange. J. Biol. Chem. 250: 675-683.

47. Yu, J., A. Fischman, and T.L. Steck. 1973. Selective Solubilization of Proteins and Phospholipids from Red Blood Cell Membranes by Nonionic Detergents. J. Supramol. Struct. 1:233-248.

48. Clarke, S. 1975. The Size and Detergent Binding of Membrane Proteins. J. Biol. Chem. 250:5459-5469.

49. Cabantchik, Z.I. and A. Rothstein. 1972. The Nature of the Membrane Sites Controlling Anion Permeability of Human Red Blood Cells as Determined by Studies with Disulfonic Stilbene Derivatives. J. Membrane Biol. 10:311-330.

50. Cabantchik, Z.I. and A. Rothstein. 1974. Membrane Proteins Related to Anion Permeability of Human Red Blood Cells. I. Localization of Disulfonic Stilbene Binding Sites in Proteins Involved in Permeation. J. Membrane Biol. 15:207-226.

51. Cabantchik, Z.I. and A. Rothstein. 1974. Membrane Proteins Related to Anion Permeability of Human Red Blood Cells. II. Effects of Proteolytic Enzymes on Disulfonic Stilbene Sites of Surface Proteins. J. Membrane Biol. 15:227-248.

52. Rothstein, A., Z.I. Cabantchik, M. Balshin, and R. Juliano. 1975. Enhancement of Anion Permeability in Lecithin Vesicles by Hydrophobic Proteins Extracted from Red Blood Cell Membranes. Biochem. Biophys. Res. Commun. 64:144-150.

53. Zaki, L., H. Fasold, B. Schulmann, and H. Passow. 1975. Chemical modification of Membrane Proteins in Relation to Inhibition of Anion Exchange in Human Red Blood Cells. J. Cell. Physiol. 86:471-494.

54. Rothstein, A., Z.I. Cabantchik, and P.A. Knauf. 1976. Mechanism of Anion Transport in Red Blood Cells: Role of Membrane Proteins. Fed. Proc. 35:3-10.

55. Passow, H., H. Fasold, S. Lepke, M. Pring, and B. Schulmann. 1977. Chemical and Enzymatic Modification of Membrane Proteins and Anion Transport in Human Red Blood Cells. IN: M. Miller and A.E. Shamoo (editors), Membrane Toxicity, pp. 353-379. New York: Plenum Press.

56. Lepke, S., H. Fasold, M. Pring, and H. Passow. 1976. A Study of the Relationship between Inhibition of Anion Exchange and Binding to the Red Blood Cell Membrane of 4, 4'-diisothiocyanostilbene-2,2'-disulfonic acid (DIDS) and its Dihydro Derivative (H_2DIDS). J. Membrane Biol. 29:147-177.

57. Avruch, J. and G. Fairbanks. 1972. Demonstration of a Phosphopeptide Intermediate in the Mg^{++}-dependent Na^{+}-and K^{+}-stimulated Adenosine Triphosphatase Reaction of the Erythrocyte Membrane. Proc. Natl. Acad. Sci. USA 69:1216-1220.

58. Knauf, P.A., F. Proverbio, and J. Hoffman. 1974. Chemical Characterization and Pronase Susceptibility of the Na:K Pump-associated Phosphoprotein of Human Red Blood Cells. J. Gen. Physiol. 63:305-323.

59. Brown, P.A., M.B. Feinstein, and R.I. Sha'afi. 1975. Membrane Proteins Related to Water Transport in Human Erythrocytes. Nature 254:523-535.

60. Bellhorn, M.B., O.O. Blumenfeld, and P.M. Gallop. 1970. Acetylcholinesterase of the Human Erythrocyte Membrane Labeled with Tritiated Diisopropylfluorophospate. Biochem. Biophys. Res. Commun. 39:267-273.

61. Young, J.D., S.E.M. Jones, and J.C. Ellory. 1981. Amino Acid Transport Via the Red Cell Anion Transport System. Biochim. Biophys. Acta 645:157-160.

62. Sachs, J.R., P.A. Knauf, and P.B. Dunham. 1974. Transport through Red Cell Membranes. IN: D.M. Surgenor (editor), The Red Blood Cell, 2nd edition, vol. 2, pp. 613-705. New York: Academic Press.

63. Taverna, R.D. and R.G. Langdon. 1973. D-glucosyl-isothiocyanate: An Affinity Label for the Glucose Transport Proteins of the Human Erythrocyte Membrane. Biochem. Biophys. Res. Commun. 54:593-599.

64. Lin, S. and J.A. Spudich. 1974. Binding of Cytochalasin B to a Red Cell Membrane Protein. Biochem. Biophys. Res. Commun. 61: 1471-1476.

65. Kahlenberg, A. 1976. Partial Purification of a Membrane Protein from Human Erythrocytes Involved in Glucose Transport. J. Biol. Chem. 251:1582-1590.

66. Batt, E.R., R.E. Abbott, and D. Schachter. 1976. An Exofacial Component of Glucose Transport Mechanism of Human Erythrocyte. Fed. Proc. 5:606a.

67. Goldin, S. and V. Rhoden. 1978. Reconstitution and "Transport Specificity Fractionation" of the Human Erythrocyte Glucose Transport System. J. Biol. Chem. 253:2575-2583.

68. Kasahara, M. and P.C. Hinkle. 1977. Reconstitution and Purification of the D-glucose Transporter from Human Erythrocytes. J. Biol. Chem. 252:7384-7390.

69. Lundahl, P., F Acevedo, G. Froman, and S. Phutrakul. 1981. The Stereospecific D-Glucose Transport Activity of Cholate Extracts from Human Erythrocyte Membranes. Biochim. Biophys. Acta 644: 101-107.

70. Jones, M.N. and J.K. Nickson. 1981. Monosaccharide Transport Proteins of the Human Erythrocyte Membrane. Biochim. Biophys. Acta 650:1-20.

71. Anselstetter, V. and J.H. Horstmann. 1975. Two-dimensional Polyacrylamide Gel Electrophoresis of the Proteins and Glycoproteins of the Human Erythrocyte Membrane. Eur. J. Biochem. 56:259-269.

72. Conrad, M.J. and J.T. Penniston. 1976. The Resolution of Erythrocyte Membrane Proteins by Two-dimensional Electrophoresis. J. Biol. Chem. 251:253-255.

73. Drickamer, L.K. Fragmentation of the 95,000-Dalton Transmembrane Polypeptide in Human Erythrocyte Membranes: Arrangement of the Fragments in the Lipid Bilayer. J. Biol. Chem. 251:5115-5123.

74. Jenkins, R.E. and M.J.A. Tanner. 1977. The Structure of the Major Protein of the Human Erythrocyte Membrane: Characterization of the Intact Protein and Major Fragments. Biochem. J. 161: 139-147.

75. Steck, T.L., G. Fairbanks, and D.F.H. Wallach. 1971. Disposition of the Major Proteins in the Isolated Erythrocyte Membrane: Proteolytic Dissection. Biochem. 10:2617-2624.

76. Bretscher, M.S. 1971. A Major Protein Which Spans the Human Erythrocyte Membrane. J. Mol. Biol. 59:351-357.

77. Bretscher, M.S. 1971. Human Erythrocyte Membranes: Specific Labelling of Surface Proteins. J. Mol. Biol. 58:775-781.

78. Arrotti, J.J. and J.E. Garvin. 1972. Selective Labelling of Human Erythrocyte Membrane Components with Tritiated Trinitrobenzesulfonic Acid and Picryl Chloride. Biochem. Biophys. Res. Commun. 49:205-211.

79. Staros, J.W. and F.M. Richards. 1974. Photochemical Labelling of the Surface Proteins of Human Erythrocytes. Biochem. 13: 2720-2726.

80. Berg, H.C. 1969. Sulfanilic Acid Diazonium Salt: A Label for the Outside of the Human Erythrocyte Membrane. Biochim. Biophys. Acta 183:65-78.

81. Whiteley, H.M. and H.C. Berg. 1974. Amidation of the Outer and Inner Surfaces of the Human Erythrocyte Membrane. J. Mol. Biol. 87:541-561.

82. Cabantchik, Z.I., M. Balshin, W. Breuer, H. Markus, and A. Rothstein. 1975. A Comparison of Intact Human Red Blood Cells and Resealed and Leaky Ghosts with Respect to their Interactions with Surface Labelling Agents and Proteolytic Enzymes. Biochim. Biophys. Acta 382:621-633.

83. Cabantchik, Z.I., M. Balshin, W. Breuer, and A. Rothstein. 1975. Pyridoxal Phosphate: an Anionic Probe for Protein Amino Groups Exposed on the Outer and Inner Surfaces of Intact Human Red Blood Cells. J. Biol. Chem. 250:5130-5136.

84. Bender, W.W., H. Garen, and H.C. Berg. 1971. Proteins of the Human Erythrocyte Membrane as Modified by Pronase. J. Mol. Biol. 58:783-797.

85. Jenkins, R.E. and M.J.A. Tanner. 1975. The Major Human Erythrocyte Membrane Protein: Evidence fo an S-Shaped Structure which Traverses the Membrane Twice and has Duplicated Sets of Sites. Biochem. J. 147:393-399.

86. Phillips, D.R. and M. Morrison. 1971. Exterior Proteins on the Human Erythrocyte Membrane. Biochem. Biophys. Res. Commun. 45:1103-1108.

87. Steck, T.L., B. Ramos, and E. Strapazon. 1976. Proteolytic Dissection of Band 3, the Predominant Transmembrane Polypeptide of the Human Erythrocyte Membrane. Biochem. 15:1154-1161.

88. Triplett, R.B. and K.L. Carraway. 1972. Proteolytic Digestion of Erythrocytes, Resealed Ghosts and Isolated Membranes. Biochem. 11:2897-2903.

89. Reichstein, E. and R. Blostein. 1973. Asymmetric Iodination of the Human Erythrocyte Membrane. Biochem. Biophys. Res. Commun. 54:494-500.

90. Reichstein, E. and R. Blostein. 1975. Arrangement of Human Erythrocyte Membrane Proteins. J. Biol. Chem. 250:6256-6263.

91. Boxer, D.H., R.E. Jenkins, and M.J.A. Tanner. 1974. The Organization of the Major Protein of the Human Erythrocyte Membrane. Biochem. J. 137:531-534.

92. Hubbard, A.L. and Z.A. Cohn. 1972. The Enzymatic Iodination of the Red Cell Membrane. J. Cell. Biol. 55:390-415.

93. Mueller, T.J. and M. Morrison. 1974. The Transmembrane Proteins in the Plasma Membrane of Normal Human Erythrocytes. J. Biol. Chem. 249:7568-7573.

94. Shin, B.C. and K.L. Carraway. 1974. Lactoperoxidase Labelling of Erythrocyte Membranes from the Inside and Outside. Biochim. Biophys. Acta 345:141-153.

95. Drickamer, L.K. 1977. Fragmentation of the Band 3 Polypeptide from Human Erythrocyte Membranes. J. Biol. Chem. 252:6909-6917.

96. Abbott, R.E. and D. Schachter. 1976. Impermeant Maleimides: Oriented Probes of Erythrocyte Membrane Proteins. J. Biol. Chem. 251:7176-7183.

97. Rao, A. 1979. Disposition of the Band 3 Polypeptide in the Human Erythrocyte Membrane: the Reactive Sulfhydral Groups. J. Biol. Chem. 254:3503-3511.

98. Jenkins, R.E. and M.J.A. Tanner. 1977. Ionic-Strength-Dependent Changes in the Structure of the Major Protein of the Human Erythrocyte Membrane. Biochem. J. 161:131-138.

99. Rao, A. and R.A.F. Reithmeier. 1979. Reactive Sulfhydral Groups of the Band 3 Polypeptide from Human Erythrocyte Membranes: Location in the Primary Structure. J. Biol. Chem. 254:6144-6150.

100. Steck, T.L., J.J. Koriarz, M.J. Singh, G. Reddy, and H. Kohler. 1978. Preparation and Analysis of Seven Major, Topographically Defined Fragments of Band 3, the Predominant Transmembrane Polypeptide of Human Erythrocyte Membranes. Biochem. 17:1216-1222.

101. Fukuda, M., Y. Eshdat, G. Tarone, and V.T. Marchesi. 1978. Isolation and Characterization of Peptides Derived from the Cytoplasmic Segment of Band 3, the Predominant Intrinsic Membrane Protein of the Human Erythrocyte. J. Biol. Chem. 243:2419-2428.

102. Grinstein, S., S. Ship, and A. Rothstein. 1978. Anion Transport in Relation to Proteolytic Dissection of Band 3 Protein. Biochim. Biophys. Acta 507:294-304.

103. Knauf, P.A., W. Breuer, L. McCulloch, and A. Rothstein. 1978. N-(4-Azido-2-Nitrophenyl)-2-Aminoethylsulfonate (NAP-Taurine) as a Photoaffinity Probe for Identifying Membrane Components Containing the Modifier Site of the Human Red Blood Cell Anion Exchange System. J. Gen. Physiol. 72:631-649.

104. Ramjeesingh, M., A. Gaarn, and A. Rothstein. 1980. The Location of a Disulfonic Stilbene Binding Site in Band 3, The Anion Transport Protein of the Red Blood Cell Membrane. Biochim. Biophys. Acta 599:127-139.

105. Ramjeesingh, M., A. Gaarn, and A. Rothstein. 1981. The Amino Acid Conjugate Formed by the Interaction of the Anion Transport Inhibitor 4,4'-Diisothiocyano-2,2'-Stilbenedisulfonic Acid (DIDS) with Band 3 Protein from Human Red Blood Cell Membranes. Biochim. Biophys. Acta 641:173-182.

106. Shami, Y., A. Rothstein, and P.A. Knauf. 1978. Identification of Cl Transport Site of Human Red Blood Cells by a Kinetic Analysis of Inhibitory Effects of a Chemical Probe. Biochim. Biophys. Acta 508:357-363.

107. Grinstein, S., L. McCullough, and A. Rothstein. 1979. Transmembrane Effects of Irreversible Inhibitors of Anion Transport in Red Blood Cells: Evidence for Mobile Transport Sites. J. Gen. Physiol. 73:493-514.

108. Haest, C.W.M., D. Kamp, and B. Deuticke. 1981. Topology of Membrane Sulfhydryl Groups in the Human Erythrocyte. Biochim. Biophys. Acta 643:319-326.

109. Yu, J. and T.L. Steck. 1975. Associations of Band 3, the Predominant Polypeptide of the Human Erythrocyte Membrane. J. Biol. Chem. 250:9176-9184.

110. Nakashima, H., Y. Nakagawa, and S. Makino. 1981. Detection of the Associated State of Membrane Proteins by Polyacrylamide Gradient Gel Electrophoresis with Non-Denaturing Detergents. Biochim. Biophys. Acta 643:509-518.

111. Steck, T.L. 1972. Cross-linking the Major Proteins of the Isolated Erythrocyte Membrane. J. Mol. Biol. 66:295-305.

112. Wang, K. and F.M. Richards. 1974. An Approach to Nearest Neighbor Analysis of Membrane Proteins. J. Biol. Chem. 249:8005-8018.

113. Wang, K. and F.M. Richards. 1975. Reaction of dimethyl-3,3'-dithiobispropionimidate with Intact Human Erythrocytes. J. Biol. Chem. 250:6622-6626.

114. Kiehm, D.J. and T.H. Ji. 1977. Photochemical Cross-Linking of Cell Membranes. J. Biol. Chem. 252:8524-8531.

115. Staros, J.V., D.G. Morgan, and D.R. Appling. 1981. A Membrane-Impermeant, Cleavable Cross-linker. J. Biol. Chem. 256:5890-5893.

116. Nigg, E. and R.J. Cherry. 1979. Dimeric Association of Band 3 in the Erythrocyte Membrane Demonstrated by Protein Diffusion Measurements. Nature 277:493-494.

117. Macara, I.G. and L.C. Cantley. 1981. Interactions between Transport Inhibitors at the Anion Binding Sites of the Band 3 Dimer. Biochemistry 20:5095-5105.

118. Reithmeier, R.A.F. and A. Rao. 1979. Reactive Sulfydral Groups of the Band 3 Polypeptide from Human Erythrocyte Membranes. J. Biol. Chem. 254:6151-6155.

119. Tillack, T.W. and V.T. Marchesi. 1970. Demonstration of the Outer Surface of Freeze-etched Red Blood Cell Membranes. J. Cell. Biol. 45:649-653.

120. Pinto da Silva, P. and D. Branton. 1970. Membrane Splitting in Freeze-etching: Covalently Bound Ferritin as a Membrane Marker. J. Cell Biol. 45:598-605.

121. Branton, D. 1971. Freeze-etching Studies of Membrane Structure. Phil. Trans. Roy. Soc. Lond. B 261:133-138.

122. Pinto da Silva, P., S.D. Douglas, and D. Branton. 1971. Location of A Antigen Sites on Human Erythrocyte Ghosts. Nature 232: 194-195.

123. Marchesi, V.T., T.W. Tillack, R.L. Jackson, J.P. Segrest, and R.E. Scott. 1972. Chemical Characterization and Surface Orientation of the Major Glycoprotein of the Human Erythrocyte Membrane. Proc. Natl. Acad. Sci. USA 69:1445-1449.

124. Tillack, T.W., R.E. Scott, and V.T. Marchesi. 1972. The Structure of Erythrocyte Membranes Studied by Freeze-etching. J. Exp. Med. 135:1209-1227.

125. Pinto da Silva, P., P.S. Moss and H.H. Fudenberg. 1973. Anionic Sites on the Membrane Intercalated Particles of Human Erythrocyte Ghost Membranes: Freeze-Etch Localization. Exp. Cell Res. 81: 127-138.

126. Pinto da Silva, P. and G.L. Nicolson. 1974. Freeze-Etch Localization of Concanavalin A Receptors to the Membrane Intercalated Particles of Human Erythrocyte Ghost Membranes. Biochim. Biophys. Acta 363:311-319.

127. Wolosin, J.M., H. Ginsburg, and Z.I. Cabantchik. 1977. Functional Characterization of Anion Transport System Isolated from Human Erythrocyte Membranes. J. Biol. Chem. 252:2419-2427.

128. Yu, J. and D. Branton. 1976. Reconstitution of Intramembrane Particles in Recombinants of Erythrocyte Protein Band 3 and Lipid: Effects of Spectrin-Actin Association. Proc. Natl. Acad. Sci. USA 73:3891-3895.

129. Bachi, T., K. Whiting, M.J.A. Tanner, M.N. Metaxas, and D.J. Anstee. 1977. Freeze-fracture Electron Microscopy of Human Erythrocytes Lacking the Major Membrane Sialoglycoprotein. Biochim. Biophys. Acta 464:635-639.

130. Grant, C.W.M. and H.M. McConnell. 1974. Glycophorin in Lipid Bilayers. Proc. Natl. Acad. Sci. USA 71:4653-4657.

131. Nigg, E.A., C. Bron, M. Girardet, and R.J. Cherry. 1980. Band 3-Glycophorin A Association in Erythrocyte Membranes Demonstrated by Combining Protein Diffusion Measurements with Antibody-Induced Cross Linking. Biochemistry 19:1887-1893.

132. Phillips, D.R. and M. Morrison. 1973. Changes in Accessibility of Plasma Membrane Protein as the Result of Tryptic Hydrolysis. Nature New Biol. 242:213-215.

133. Ji, T.H. 1979. The Application of Chemical Crosslinking for Studies on Cell Membranes and the Identification of Surface Receptors. Biochim. Biophys. Acta 559:39-69.

134. Kant, J.A. and T.L. Steck. 1973. Specificity in the Association of Glyceraldehyde-3-Phosphate Dehydrogenase with Isolated Human Erythrocyte Membranes. J. Biol. Chem. 248:8457-8464.

135. Strapazon, E. and T.L. Steck. 1976. Binding of Rabbit Muscle Aldolase to Band 3, the Predominant Polypeptide of the Human Erythrocyte Membrane. Biochem. 15:1421-1424.

136. Strapazon, E. and T.L. Steck. 1977. Interaction of Aldolase and the Membrane of Human Erythrocytes. Biochem. 16:2966-2971.

137. Fossel, E.T. and A.K. Solomon. 1977. Membrane-Mediated Link Between Ion Transport and Metabolism in Human Red Cells. Biochim. Biophys. Acta 464:82-92.

138. Gunn, R.B. in press. Transport of Anions Across Red Cell Membranes. IN: G. Giebisch, D.C. Tosteson, and H. Ussing (editors), Transport Across Biological Membranes.

139. Hokin, L.E. 1981. Reconstitution of "Carriers" in Artificial Membranes. J. Membrane Biol. 60:77-93.

140. Halestrap, A.P. 1976. Transport of Pyruvate and Lactate into Human Erythrocytes. Biochem. J. 156:193-207.

141. Ship, S., Y. Shami, and A. Rothstein. 1977. Synthesis of Tritiated 4,4'-diisothiocyano-2,2'-stilbene disulfonic acid ([^{3}H]DIDS) and its Covalent Reaction with Sites Related to Anion Transport in Human Red Blood Cells. J. Memb. Biol. 33:311-324.

142. Nigg, E., M. Kessler, and R.J. Cherry. 1979. Labeling of Human Erythrocyte Membranes with Eosin Probes used for Protein Diffusion Measurements. Biochim. Biophys. Acta 550:328-340.

143. Cabantchik, Z.I., P.A. Knauf, T. Ostwald, H. Markus, L. Davidson, W. Breuer, and A. Rothstein. 1976. The Interaction of an Anionic Photoreactive Probe with the Anion Transport System of the Human Red Blood Cell. Biochim. Biophys. Acta 455:526-537.

144. Kohne, W., C.W.M. Haest, and B. Deuticke. 1981. Mediated Transport of Anions in Band 3-Phospholipid Vesicles. Biochim. Biophys. Acta 664:108-120.

145. Sheetz, M.P., D. Sawyer, and S. Jacowski. 1978. The ATP-Dependent Red Cell Membrane Shape Change. IN: G. Brewer (editor), The Red Cell, pp. 431-450. New York: Liss.

146. Lux, S.E. 1979. Spectrin-Actin Membrane Skeleton of Normal and Abnormal Red Blood Cells. Semin. Hematol. 16:21-51.

147. Lux, S.E. 1979. Dissecting the Red Cell Membrane Skeleton. Nature 281:426-429.

148. Branton, D., C.M. Cohen, and J. Tyler. 1981. Interaction of Cytoskeletal Proteins on the Human Erythrocyte Membrane. Cell 24:24-32.

149. Palek, J. and S.C. Liu. 1980. Red Cell Membrane Skeleton: Structure-Function Relationsihps. IN: Immunobiology of the Erythrocyte, pp. 21-44. New York: Alan R. Liss, Inc.

150. Lux, S.E., K.M. John, and M.J. Karnovsky. 1976. Irreversible Deformation of the Spectrin-Actin Lattice in Irreversibly Sickled Cells. J. Clin. Invest. 58:955-963.

151. Sheetz, M.P. 1979. Integral Membrane Protein Interaction with Triton Cytoskeletons of Erythrocytes. Biochim. Biophys. Acta 557:122-134.

152. Sheetz, M.P. 1979. DNase I-Dependent Dissociation of Erythrocyte Cytoskeletons. J. Cell. Biol. 81:266-270.

153. Nicolson, G.L., V.T. Marchesi, and S.J. Singer. 1971. The Localization of Spectrin on the Inner Surface of Human Red Blood Cell Membranes by Ferritin-Conjugated Antibodies. J. Cell Biol. 51:265-272.

154. Hainfeld, J.F. and T.L. Steck. 1977. The Sub-Membrane Reticulum of the Human Erythrocyte: A Scanning Electron Microscope Study. J. Supramol. Struct. 6:301-311.

155. Tsukita, S., S. Tsukita, H. Ishikawa, S. Sato, and M. Nakao. 1981. Electron Microscopic Study of Reassociation of Spectrin and Actin with the Human Erythrocyte Membrane. J. Cell Biology 90:70-77.

156. Kirkpatrick, F.H. 1979. New Models of Cellular Control: Membrane Cytoskeletons, Membrane Curvature Potential, and Possible Interactions. Biosystems 11:93-109.

157. Sheetz, M.P. and S.J. Singer. 1977. On the Mechanism of ATP-Induced Shape Changes in Human Erythrocyte Membranes. I. The Role of the Spectrin Complex. J. Cell Biology 73:638-646.

158. Birchmeier, W. and S.J. Singer. 1977. On the Mechanism of ATP-Induced Shape Changes in Human Erythrocyte Membranes. II. The Role of ATP. J. Cell Biology 73:647-659.

159. Johnson, R.M. and J. Robinson. 1976. Morphological Changes in Asymmetric Erythrocyte Membranes Induced by Electrolytes. Biochem. Biophys. Res. Commun. 70:925-931.

160. Johnson, R.M., T. Gregory, and D.B. Meyer. 1980. Shape and Volume Changes in Erythrocyte Ghosts and Spectrin-Actin Networks. J. Cell Biology 86:371-376.

161. Patel, V.P. and G. Fairbanks. 1981. Spectrin Phosphorylation and Shape Change of Human Erythrocyte Ghosts. J. Cell Biology 88:430-440.

162. Wildenauer, D.B., H. Reuther, and J. Remier. 1981. Reactions of the Alkylating Agent Tris (2-Chloroethyl)-Amine with the Erythrocyte Membrane. Biochim. Biophys. Acta 603:101-116.

163. Ott, P., M.J. Hope, A.J. Verkleij, B. Roelofsen, Y. Brodbeek, and L.L.M. VanDeenen. 1981. Effect of Dimyristoyl Phosphatidylcholine on Intact Erythrocytes. Biochim. Biophys. Acta 641: 79-87.

164. Lange, Y., H.B. Cutler, and T.L. Steck. 1980. The Effect of Cholesterol and Other Intercalated Amphipaths on the Contour and Stability of the Isolated Red Cell Membrane. J. Biol. Chem. 255:9331-9337.

165. Tomaselli, M.B., K.M. John, and S.E. Lux. 1981. Elliptical Erythrocyte Membrane Skeletons and Heat-Sensitive Spectrin in Hereditary Elliptocytosis. Proc. Natl. Acad. Sci. USA 78:1911-1915.

166. Kirkpatrick, F.H. 1976. Spectrin: Current Understanding of its Physical, Biochemical, and Functional Properties. Life Sci. 19:1-18.

167. Palek, J. and S.-C. Liu. 1979. Dependence of Spectrin Organization in Red Blood Cell Membranes on Cell Metabolism: Implications for Control of Red Cell Shape, Deformability, and Surface Area. Semin. Hematol. 16:75-93.

168. Marchesi, V.T. 1979. Spectrin: Present Status of a Putative Cyto-Skeletal Protein of the Red Cell Membrane. J. Membrane Biol. 51:101-131.

169. Anderson, J.M. 1979. Structural Studies on Human Spectrin: Comparison of Subunits and Fragmentation of Native Spectrin. J. Biol. Chem. 254:939-944.

170. Hsu, C.J., A. Lemay, Y. Eshdat, and V.T. Marchesi. 1979. Substructure of Human Erythrocyte Spectrin. J. Supramolec. Structure 10:227-239.

171. Speicher, D.W., J.S. Morrow, W. Knowles, and V.T. Marchesi. 1980. Identification of Proteolytically Resistant Domains of Human Erythrocyte Spectrin. Proc. Natl. Acad. Sci. USA 77: 5673-5677.

172. Morrow, J.S., D.W. Speicher, W.J. Knowles, C.J. Hsu, and V.T. Marchesi. 1980. Identification of Functional Domains of Human Erythrocyte Spectrin. Proc. Natl. Acad. Sci. USA 77:6592-6596.

173. Schechter, N.M., M. Sharp, J.A. Reynolds, and C. Tanford. 1976. Erythrocyte Spectrin: Purification in Deoxycholate and Preliminary Characterization. Biochem. 15:1897-1904.

174. Gratzer, W.B. and G.H. Beaven. 1975. Properties of the High-Molecular-Weight Protein (Spectrin) from Human-Erythrocyte Membranes. Eur. J. Biochem. 58:403-409.

175. Ralston, G.B. 1976. Physico-Chemical Characterization of the Spectrin Tetramer from Bovine Erythrocyte Membranes. Biochim. Biophys. Acta 455:163-172.

176. Ralston, G.B., J. Dunbar, and M. White. 1977. The Temperature-Dependent Dissociation of Spectrin. Biochim. Biophys. Acta 491:345-348.

177. Kam, Z., R. Josephs, H. Eisenberg, and W.B. Gratzer. 1977. Structural Study of Spectrin from Human Erythrocyte Membranes. Biochem. 16:5568-5572.

178. Calvert, R., P. Bennett, and W. Gratzer. 1980. Properties and Structural Role of the Subunits of Human Spectrin. Eur. J. Biochem. 107:355-361.

179. Morrow, J.S. and V.T. Marchesi. 1981. Self-Assembly of Spectrin Oligomers In Vitro: A Basis for a Dynamic Cytoskeleton. J. Cell Biology 88:463-468.

180. Ji, T.H., D.J. Kiehm, and C.R. Middaugh. 1980. Presence of Spectrin Tetramer on the Erythrocyte Membrane. J. Biol. Chem. 255:2990-2993.

181. Liu, S.C. and J. Palek. 1980. Spectrin Tetramer-Dimer Equilibrium and the Stability of Erythrocyte Membrane Cytoskeletons. Nature 285:586-588.

182. Ungewickell, E., and W.B. Gratzer. 1978. Self-Association of Human Spectrin. Eur. J. Biochem. 88:379-385.

183. Shotton, D.M., B.E. Burke and D. Branton. 1979. The Molecular Structure of Human Erythrocyte Spectrin. J. Mol. Biol. 131: 303-329.

184. Stokke, B.T. and A. Elgsaeter. 1981. Human Spectrin. VI. A Viscometric Study. Biochim. Biophys. Acta 640:640-645.

185. Tyler, J.M., B.N. Reinhardt, and D. Branton. 1980. Associations of Erythrocyte Membrane Proteins: Binding of Purified Bands 2.1 and 4.1 to Spectrin. J. Biol. Chem. 255:7034-7039.

186. Ungewickell, E., P.M. Bennett, R. Calvert, V. Ohanian, and W.B. Gratzer. 1979. In Vitro Formation of a Complex between Cytoskeletal Proteins of the Human Erythrocyte. Nature 280: 811-814.

187. Cohen, C.M., P.L. Jackson, and D. Branton. 1978. Actin-Membrane Interactions: Association of G-Actin with the Red Cell Membrane. J. Supramolec. Struct. 9:113-124.

188. Lin, D.C. and S. Lin. 1979. Actin Polymerization Induced by a Motility-Related High-Affinity Cytochalasin Binding Complex from Human Erythrocyte Membrane. Proc. Natl. Acad. Sci. USA 76: 2345-2349.

189. Fowler, V. and D.L. Taylor. 1978. Actin-Binding Proteins from Human Erythrocyte Membranes. J. Cell Biol. 79:222a.

190. Fowler, V. and D.L. Taylor. 1980. Spectrin Plus Band 4.1 Cross-Link Actin. J. Cell Biology 85:361-376.

191. Brenner, S.L. and E.D. Korn. 1979. Spectrin-Actin Interaction. J. Biol. Chem. 254:8620-8627.

192. Cohen, C.M. and S.F. Foley. 1980. Spectrin-Dependent and -Independent Association of F-Actin with the Erythrocyte Membrane. J. Cell Biology 86:694-698.

193. Fowler, V.M., E.J. Luna, W.R. Hargreaves, D.L. Taylor, and D. Branton. 1981. Spectrin Promotes the Association of F-Actin with the Cytoplasmic Surface of the Human Erythrocyte Membrane. J. Cell Biology 88:388-395.

194. Tsukita, S., Sh. Tsukita, H. Ishikawa, S. Sato, and M. Nakao. 1981. Electron Microscopic Study of Reassociation of Spectrin and Actin with the Human Erythrocyte Membrane. J. Cell Biology 90:70-77.

195. Tyler, J.M., B.N. Reinhardt, and D. Branton. 1980. Associations of Erythrocyte Membrane Proteins. J. Biol. Chem. 255:7034-7039.

196. Tyler, J.M., W.R. Hargreaves, and D. Branton. 1979. Purification of Two Spectrin-Binding Proteins. Proc. Natl. Acad. Sci. USA 76:5192-5196.

197. Cohen, C.M., J.M. Tyler, and D. Branton. 1980. Spectrin-Actin Associations Studied by Electron Microscopy of Shadowed Preparations. Cell 21:875-883.

198. Brenner, S.L. and E.D. Korn. 1980. Spectrin/Actin Complex Isolated from Sheep Erythrocytes Accelerates Actin Polymerization by Simple Nucleation. J. Biol. Chem. 255:1670-1676.

199. Cohen, C.M. and D. Branton. 1979. The Role of Spectrin in Erythrocyte Membrane-Stimulated Actin Polymerization. Nature 279:163-165.

200. Dunbar, J.C. and G.B. Ralston. 1978. The Incorporation of ^{32}P into Spectrin Aggregates Following Incubation of Erythrocytes in ^{32}P-Labelled Inorganic Phosphate. Biochim. Biophys. Acta 510:283-291.

201. Bennett, V. and D. Branton. 1977. Selective Association of Spectrin with the Cytoplasmic Surface of Human Erythrocyte Plasma Membranes. J. Biol. Chem. 253:2753-2763.

202. Litman, D., C.J. Hsu, and V.T. Marchesi. 1980. Evidence that Spectrin Binds to Marcomolecular Complexes on the Inner Surface of the Red Cell Membrane. J. Cell Sci. 42:1-22.

203. Bennett, V. 1978. Purification of an Active Proteolytic Fragment of the Membrane Attachment Site for Human Erythrocyte Spectrin. J. Biol. Chem. 253:2292-2299.

204. Bennett, V. and P.J. Stenbuck. 1980. Human Erythrocyte Ankyrin. J. Biol. Chem. 255:2540-2548.

205. Yu, J. and S.R. Goodman. 1979. Syndeins: The Spectrin-Binding Protein(s) of the Human Erythrocyte Membrane. Proc. Natl. Acad. Sci. USA 76:2340-2344.

206. Luna, E.J., G.H. Kidd, and D. Branton. 1979. Identification by Peptide Analysis of the Spectrin-Binding Protein in Human Erythrocytes. J. Biol. Chem. 254:2526-2532.

207. Siegel, D.L., S.R. Goodman, and D. Branton. 1980. The Effect of Endogenous Proteases on the Spectrin Binding Proteins of Human Erythrocytes. Biochim. Biophys. Acta 598:517-527.

208. Goodman, S.R. and S.A. Weidner. 1980. Binding of Spectrin α_2-β_2 Tetramers to Human Erythrocyte Membranes. J. Biol. Chem. 255: 8082-8086.

209. Mombers, C., P.W.M. Van Dijck, and L.L.M. Van Deenen. 1977. The Interaction of Spectrin-Actin and Synthetic Phospholipids. Biochim. Biophys. Acta 470:152-160.

210. Haest, C.W.M., G. Plasa, D. Kamp, and B. Deuticke. 1978. Spectrin as a Stabilizer of the Phospholipid Asymmetry in the Human Erythrocyte Membrane. Biochim. Biophys. Acta 509:21-32.

211. Marinetti, G.V. and R.C. Crain. in press. Topology of Amino-Phospholipids in the Red Cell Membrane. IN: S.E. Lux, V.T. Marchesi, and C.F. Fox (editors), Normal and Abnormal Red Cell Membranes. New York: Liss.

212. Mombers, C., J. DeGier, R.A. Demel, and L.L.M. Van Deenen. 1980. Spectrin-Phospholipid Interaction: A Monolayer Study. Biochim. Biophys. Acta 603:52-62.

213. Bennett, V. and P.J. Stenbuck. 1979. The Membrane Attachment Protein for Spectrin is Associated with Band 3 in Human Erythrocyte Membranes. Nature 280:468-473.

214. Hargreaves, W.R., K.N. Giedd, A. Verkleij, and D. Branton. 1980. Reassociation of Ankyrin with Band 3 in Erythrocyte Membranes and in Lipid Vesicles. J. Biol. Chem. 255:11965-11972.

215. Bennett, V. and P.J. Stenbuck. 1980. Association between Ankyrin and the Cytoplasmic Domain of Band 3 Isolated from the Human Erythrocyte Membrane. J. Biol. Chem. 255:6424-6432.

216. Lux, S.E., K.M. John, and B. Pease. 1978. Functional Heterogeneity of Spectrin: Effect on Interactions with Actin. Fed. Proc. 37: 1507.

217. Sheetz, M.P. and D. Sawyer. in press. Triton Shells of Intact Erythrocytes. IN: S.E. Lux, V.T. Marchesi, and C.F. Fox (editors), Normal and Abnormal Red Cell Membranes. New York: Liss.

218. Pinto da Silva, P. 1972. Translational Mobility of the Membrane Intercalated Particles of Human Erythrocyte Ghosts. J. Cell Biol. 53:777-787.

219. Elgsaeter, A. and D. Branton. 1974. Intramembrane Particle Aggregation in Erythrocyte Ghosts. I. The Effects of Protein Removal. J. Cell Biol. 63:1018-1030.

220. Nicolson, G.L. 1973. Anionic Sites of Human Erythrocyte Membranes. I. Effects of Trypsin, Phospholipase C, and pH on the Topography of Bound Positively Charged Colloidal Particles. J. Cell Biol. 57:373-387.

221. Speth, V., D.F.H. Wallach, E. Weidekamm, and H. Knufermann. 1972. Micromorphologic Consequences Following Perturbation of Erythrocyte Membranes by Trypsin, Phospholipase A, Lysolecithin, Sodium Dodecyl Sulfate, and Saponin. Biochim. Biophys. Acta 255:386-394.

222. Nicolson, G.L. and R.G. Painter. 1973. Anionic Sites of Human Erythrocyte Membranes. II. Antispectrin-Induced Transmembrane Aggregation of the Binding Sites for Positively Charged Colloidal Particles. J. Cell Biol. 59:395-406.

223. Elgsaeter, A., D.M. Shotton, and D. Branton. 1976. Intramembrane Particle Aggregation in Erythrocyte Ghosts. II. The Influence of Spectrin Aggregation. Biochim. Biophys. Acta 426:101-122.

224. Shotton, D., K. Thompson, L. Wofsy, and D. Branton. 1978. Appearance and Distribution of Surface Proteins of the Human Erythrocyte Membrane. J. Cell Biol. 76:512-531.

225. Ji, T.H. and G.L. Nicolson. 1974. Lectin Binding and Perturbation of the Outer Surface of the Cell Membrane Induces a Transmembrane Organizational Alteration at the Inner Surface. Proc. Natl. Acad. Sci. USA 71:2212-2216.

226. Huang, C.-K. and F.M. Richards. 1977. Reaction of a Lipid-Soluble Unsymmetrical, Cleavable, Cross-Linking Reagent with Muscle Aldolase and Erythrocyte Membrane Proteins. J. Biol. Chem. 252:5514-5521.

227. Liu, S.-C., G.Fairbanks, and J. Palek. 1977. Spontaneous, Reversible Protein Cross-Linking in the Human Erythrocyte Membrane. Biochem. 16:4066-4074.

228. Bhakdi, S., H. Knufermann, and D.F.H. Wallach. 1974. Separation of EDTA-Extractable Erythrocyte Membrane Proteins by Isoelectric Focusing Linked to Electrophoresis in Sodium Dodecyl Sulfate. Biochim. Biophys. Acta 345:448-457.

229. Cherry, R.J. 1975. Protein Mobility in Membranes. FEBS Lett. 55:1-7.

230. Cherry, R.J. 1979. Rotational and Lateral Diffusion of Membrane Proteins. Biochim. Biophys. Acta 559:289-327.

231. Edidin, M., and D. Fambrough. 1973. Fluidity of the Surface of Cultured Muscle Fibers. J. Cell Biol. 57:27-37.

232. Poo, M.-M. and K.R. Robinson. 1977. Electrophoresis of Concanavalin-A Receptors Along Embryonic Muscle Cell Membrane. Nature 265:602-605.

233. Poo, M.-M., J.W. Lam, N. Orida, and A.W. Chao. 1979. Electrophoresis and Diffusion in the Plane of the Cell Membrane. Biophys. J. 26:1-21.

234. Takezoe, H. and H. Yu. 1981. Lateral Diffusion of Photopigments in Photoreceptor Disk Membrane Vesicles by the Dynamic Kerr Effect. Biochemistry 20:5275-5281.

235. Frye, L.D. and M. Edidin. 1970. The Rapid Intermixing of Cell Surface Antigens After Formation of Mouse-Human Heterokaryons. J. Cell Sci. 7:319-335.

236. Edidin, M., and T. Wei. 1977. Diffusion Rates of Cell Surface Antigens of Mouse-Human Heterokaryons. I. Analysis of the Population. J. Cell Biol. 75:475-482.

237. Petit, V.A. and M. Edidin. 1974. Lateral Phase Separation of Lipids in Plasma Membranes: Effect of Temperature on the Mobility of Membrane Antigens. Science 184:1183-1185.

238. Linden, C.D., K.L. Wright, H.M. McConnell, and C.F. Fox. 1973. Lateral Phase Separations in Membrane Lipids and the Mechanism of Sugar Transport in Escherichia coli. Proc. Natl. Acad. Sci. USA 70:2271-2275.

239. Edidin, M. and T. Wei. 1977. Diffusion Rates of Cell-Surface Antigens of Mouse-Human Heterokaryons. II. Effect of Membrane Potential on Lateral Diffusion. J. Cell Biol. 75:483-489.

240. Fowler, V. and V. Bennett. 1978. Association of Spectrin with its Membrane Attachment Site Restricts Lateral Mobility of Human Erythrocyte Integral Membrane Proteins. J. Supramol. Struct. 8:215-221.

241. Poo, M.-M. and R.A. Cone. 1974. Lateral Diffusion of Rhodopsin in the Photoreceptor Membrane. Nature 247:438-441.

242. Axelrod, D., D.E. Koppel, J. Schlessinger, E. Elson, and W. Webb. 1976. Mobility Measurement by Analysis of Fluorescence Photobleaching Recovery Kinetics. Biophys. J. 16:1055-1069.

243. Koppel, D.E., D. Axelrod, J. Schlessinger, E. Elson, and W. Webb. 1976. Dynamics of Fluorescence Marker Concentrations as a Probe of Mobility. Biophys. J. 16:1315-1329.

244. Jacobson, K., Z. Derzko, E.-S. Wu, Y. Hou, and G. Poste. 1976. Measurement of the Lateral Mobility of Cell Surface Components in Single, Living Cells by Fluorescence Recovery After Photobleaching. J. Supramol. Struct. 5:565-576.

245. Wu, E.-S., K. Jacobson, and D. Papahadjopoulos. 1977. Lateral Diffusion in Phospholipid Multibilayers Measured by Fluorescence Recovery After Photobleaching. Biochem. 16:3936-3941.

246. Edidin, M., Y. Zagyansky, and T.J. Lardner. 1976. Measurement of Membrane Protein Lateral Diffusion in Single Cells. Science 191:466-468.

247. Smith, B.A. and H.M. McConnell. 1978. Determination of Molecular Motion in Membranes Using Periodic Pattern Photobleaching. Proc. Natl. Acad. Sci. USA 75:2759-2763.

248. Koppel, D.E. 1979. Fluorescence Redistribution After Photobleaching: A New Multipoint Analysis of Membrane Translational Dynamics. Biophys. J. 28:281-292.

249. Koppel, D. 1980. Lateral Diffusion in Biological Membranes: A Normal-Mode Analysis of Diffusion on a Spherical Surface. Biophys. J. 30:187-192.

250. Smith, L.M., H.M. McConnell, B.A. Smith, and J.W. Parce. 1981. Pattern Photobleaching of Fluorescent Lipid Vesicles Using Polarized Laser Light. Biophys. J. 33:139-146.

251. Thompson, N.L., T.P. Burghardt, and D. Axelrod. 1981. Measuring Surface Dynamics of Biomolecules by Total Internal Reflection Fluorescence with Photobleaching Recovery or Correlation Spectroscopy. Biophys. J. 33:435-454.

252. Burghardt, T.P. and D. Axelrod. 1981. Total Internal Reflection/ Fluorescence Photobleaching Recovery Study of Serum Albumin Adsorption Dynamics. Biophys. J. 33:455-465.

253. Axelrod, D., P. Ravdin, D.E. Koppel, J. Schlessinger, W. Webb, E. Elson, and T.R. Podleski. 1976. Lateral Motion of Fluorescently Labeled Acetylcholine Receptors in Membranes of Developing Muscle Fibers. Proc. Natl. Acad. Sci. USA 73:4594-4598.

254. Liebman, P.A. and G. Entine. 1974. Lateral Diffusion of Visual Pigment in Photoreceptor Disk Membranes. Science 185:457-459.

255. Wey, C., R. Cone, and M. Edidin. 1981. Lateral Diffusion of Rhodopsin in Photoreceptor Cells Measured by Fluorescence Photobleaching and Recovery. Biophys. J. 33:225-232.

256. Schindler, M., D.E. Koppel, and M.P. Sheetz. 1980. Modulation of Membrane Protein Lateral Mobility by Polyphosphates and Polyamines. Proc. Natl. Acad. Sci. USA 77:1457-1461.

257. Sheetz, M.P., M. Schindler, and D.E. Koppel. 1980. The Lateral Mobility of Integral Membrane Proteins is Increased in Spherocytic Erythrocytes. Nature 285:510-512.

258. Zagyansky, Y. and M. Edidin. 1976. Lateral Diffusion of Concanavalin A Receptors in the Plasma Membrane of Mouse Fibroblasts. Biochim. Biophys. Acta 433:209-214.

259. Schlessinger, J., Y. Schechter, P. Cuatrecasas, M.C. Willingham, and I. Pastan.. 1978. Quantitative Determination of the Lateral Diffusion Coefficients of the Hormone-Receptor Complexes of Insulin and Epidermal Growth Factor on the Plasma Membrane of Cultured Fibroblasts. Proc. Natl. Acad. Sci. USA 75:5353-5357.

260. Maxfield, F.R., M.C. Willingham, I. Pastan, P. Dragsten, and S.-Y. Cheng. 1981. Binding and Mobility of the Cell Surface Receptors for 3,3',5-Triiodo-L-Thyronine. Science 211:63-65.

261. Jacobson, K., E. Wu, and G. Poste. 1976. Measurement of the Translational Mobility of Concavalin A in Glycerol-Saline Solutions and on the Cell Surface by Fluorescence Recovery After Photobleaching. Biochim. Biophys. Acta 433:215-222.

262. Schlessinger, J., E.L. Elson, W.W. Webb, I. Yahara, U.Rutishauser, and G.M. Edelman. 1977. Receptor Diffusion on Cell Surfaces Modulated by Locally Bound Concavalin A. Proc. Natl. Acad. Sci. USA 74:1110-1114.

263. Dragsten, P., J. Schlessinger, P. Henkart, J.N. Weinstein, and R. Blumenthal. 1979. Lateral Diffusion of Membrane Antigens and a Lipid Probe in Lymphocytes. Biophys. J. 25:294a.

264. Schlessinger, J., D.E. Koppel, D. Axelrod, K. Jacobson, W. Webb, and E. Elson. 1976. Lateral Transport on Cell Membranes: Mobility of Concavalin A Receptors on Myoblasts. Proc. Natl. Acad. Sci. USA 73:2409-2413.

265. Schlessinger, J., D. Axelrod, D.E. Koppel, W. Webb, and E. Elson. 1977. Lateral Transport of a Lipid Probe and Labeled Proteins on a Cell Membrane. Science 195:307-309.

266. Schlessinger, J., L.S. Barak, G.G. Hammes, K.M. Yamada, I. Postan, W. Webb, and E. Elson. 1977. Mobility and Distribution of a Cell Surface Glycoprotein and its Interaction with Other Membrane Components. Proc. Natl. Acad. Sci. USA 74: 2909-2913.

267. Schlessinger, J., W.W. Webb, E.L. Elson, and H. Metzger. 1976. Lateral Motion and Valence of Fc Receptors on Rat Peritoneal Mast Cells. Nature 264:550-552.

268. Petty, H.R., L.M. Smith, D.T. Fearon, and H.M. McConnell. 1980. Lateral Distribution and Diffusion of the C3b Receptor of Complement, HLA Antigens, and Lipid Probes in Peripheral Blood Leucocytes. Proc. Natl. Acad. Sci. USA 77:6587-6591.

269. Johnson, M. and M. Edidin. 1978. Lateral Diffusion in Plasma Membrane of Mouse Egg is Restricted After Fertilization. Nature 272:448-450.

270. Woda, B.A., J. Yguerabide, and J.D. Feldman. 1981. Mobility of Surface Proteins on Normal Rat Macrophages and on a "Macrophagelike" Rat Tumor. J. Cell Biol. 90:705-710.

271. Woda, B.A., J. Yguerabide, and J.D. Feldman. 1979. Mobility and Density of AgB, "Ia," and Fc Receptors on the Surface of Lymphocytes from Young and Old Rats. J. Immunol. 123:2161-2167.

272. Zagyansky, Y.A., P. Benda, and J.C. Bisconte. 1977. Restricted Lateral Diffusion of Concavalin A Receptors of Different Malignant Cells of the Nervous System. FEBS Lett. 77:206-208.

273. Zagyansky, Y.A. and S. Jard. 1979. Does Lectin-Receptor Complex Formation Produce Zones of Restricted Mobility within the Membrane? Nature 280:591-593.

274. Fishman, M.C., P.R. Dragsten, and I. Spector. 1981. Immobilization of Concanavalin A Receptors during Differentiation of Neuroblastoma Cells. Nature 290:781-783.

275. Davis, D.G. 1972. Phosphorus Nuclear Magnetic Resonance in Egg Yolk Lecithin: Field-Dependent Line Widths and Phosphate Group Mobility. Biochem. Biophys. Res. Commun. 49:1492-1497.

276. Lee, A.G., N.J.M. Birdsall, and J.C. Metcalfe. 1973. Measurement of Fast Lateral Diffusion of Lipids in Vesicles and in Biological Membranes by 'H Nuclear Magnetic Resonance. Biochem. 12:1650-1659.

277. Scandella, C.J., P. Devaux, and H.M. McConnell. 1972. Rapid Lateral Diffusion of Phospholipids in Rabbit Sarcoplasmic Reticulum. Proc. Natl. Acad. Sci. USA 69:2056-2060.

278. Stier, A. and E. Sackmann. 1973. Spin Labels as Enzyme Substrates: Heterogeneous Lipid Distribution in Liver Microsomal Membranes. Biochim. Biophys. Acta 311:400-408.

279. Kapitza, H.G. and E. Sackmann. 1980. Local Measurement of Lateral Motion in Erythrocyte Membranes by Photobleaching Technique. Biochim. Biophys. Acta 595:56-64.

280. Thompson, N.L. and D. Axelrod. 1980. Reduced Lateral Mobility of a Fluorescent Lipid Probe in Cholesterol-depleted Erythrocyte Membrane. Biochim. Biophys. Acta 597:155-165.

281. Koppel, D.E., M.P. Sheetz, and M. Schindler. 1981. Matrix Control of Protein Diffusion in Biological Membranes. Proc. Natl. Acad. Sci. USA 78:3576-3580.

282. Axelrod, D., P.M. Ravdin, and T.R. Podleski. 1978. Control of Acetylcholine Receptor Mobility and Distribution in Cultured Muscle Membranes. Biochim. Biophys. Acta 511:23-38.

283. Axelrod, D., A. Wight, W. Webb, and A. Horwitz. 1978. Influence of Membrane Lipids on Acetylcholine Receptor and Lipid Probe Diffusion in Cultured Myotube Membrane. Biochem. 17:3604-3609.

284. Elson, H.F. and J. Yguerabide. 1979. Membrane Dynamics of Differentiating Cultured Embryonic Chick Skeletal Muscle Cells by Fluorescence Microscopy Techniques. J. Supramol. Struct. 12:47-61.

285. Searls, D.B. and M. Edidin. 1981. Lipid Composition and Lateral Diffusion in Plasma Membranes of Teratocarcinoma-Derived Cell Lines. Cell 24:511-517.

286. Schindler, M., M.J. Osborn, and D.E. Koppel. 1980. Lateral Diffusion of Lipopolysaccharide in the Outer Membrane of Salmonella typhimurium. Nature 285:261-263.

287. Jacobson, K., Y. Hou, Z. Derzko, J. Wojcieszyn, and D. Organisciak. 1981. Lipid Lateral Diffusion in the Surface Membrane of Cells and in Multibilayers Formed from Plasma Membrane Lipids. Biochem. 20:5268-5275.

288. Smith, L.M., B.A. Smith, and H.M. McConnell. 1979. Lateral Diffusion of M-13 Coat Protein in Model Membranes. Biochem. 18:2256-2259.

289. Derzko, Z. and K. Jacobson. 1980. Comparative Lateral Diffusion of Fluorescent Lipid Analogues in Phospholipid Multibilayers. Biochem. 19:6050-6057.

290. Smith, L.M., J.W. Parce, B.A. Smith, and H.M. McConnell. 1979. Antibodies Bound to Lipid Haptens in Model Membranes Diffuse as Rapidly as the Lipids Themselves. Proc. Natl. Acad. Sci. USA 76:4177-4179.

291. Vaz, W.L.C., H.G. Kaptiza, J. Stumpel, E. Sackmann, and T.M. Jovin. 1981. Translational Mobility of Glycophorin in Bilayer Membranes of Dimyristoylphosphatidylcholine. Biochem. 20: 1392-1396.

292. Smith, L.M., J.L.R. Rubenstein, J.W. Parce, and H.M. McConnell. 1980. Lateral Diffusion of M-13 Coat Protein in Mixtures of Phosphatidylcholine and Cholesterol. Biochem. 19:5907-5911.

293. Vaz, W.L.C., K. Jacobson, E.-S. Wu, and Z. Derzko. 1979. Lateral Mobility of an Amphipathic Apolipoprotein, ApoC-III, Bound to Phosphatidylcholine Bilayers with and without Cholesterol. Proc. Natl. Acad. Sci. USA 76:5645-5649.

294. Kogelnik, H. and T. Li. 1966. Laser Beams and Resonators. Appl. Optics 9:1550-1567.

295. Barisas, B.G. 1980. Criticality of Beam Alignment in Fluorescence Photobleaching Recovery Experiments. Biophys. J. 29:545-548.

296. Barisas, B.G. and M.D. Leuther. 1979. Fluorescence Photobleaching Recovery Measurement of Protein Absolute Diffusion Constants. Biophys. Chem. 10:221-229.

297. Dickson, L.D. 1970. Characteristics of a Propagating Gaussian Beam. Appl. Optics 9:1854-1861.

298. Axelrod, D. 1979. Carbocyanine Dye Orientation in Red Cell Membrane Studied by Microscopic Fluorescence Polarization. Biophys. J. 26:557-573.

299. Cherry, R.J., A. Burkli, M. Busslinger, and G. Schneider. 1976. Rotational Diffusion of Band 3 Proteins in the Human Erythrocyte Membrane. Nature 263:389-393.

300. Cherry, R.J., A. Burkli, M. Busslinger, and G. Schneider. 1977. Rotational Diffusion of Proteins in Membranes. IN: G. Semenza and E. Carafoli (editors), Biochemistry of Membrane Transport, FEBS Symp. 42, pp. 86-95. Berlin: Springer-Verlag.

301. Cherry, R.J. 1978. Measurement of Protein Rotational Diffusion in Membranes by Flash Photolysis. Meth. Enzymol. 54:47-61.

302. Boyam, A. 1968. Isolation of Mononuclear Cells and Granulocytes from Human Blood. Scand. J. Clin. Lab. Invest. 97(Suppl. 21): 77-89.

303. Cherry, R.J., A. Cogoli, M. Opplinger, G. Schneider, and G. Semenza. 1976. A Spectroscopic Technique for Measuring Slow Rotational Diffusion of Macromolecules. I: Preparation and Properties of a Triplet Probe. Biochem. 15:3653-3656.

304. Lowry, O.H., N.J. Rosebrough, A.L. Farr, and R.J. Randall. 1951. Protein Measurement with the Folin Phenol Reagent. J. Biol. Chem. 193:265-275.

305. Laemmli, U.K. 1970. Cleavage of Structural Proteins During the Assembly of the Head of Bacteriophage T4. Nature 227:680-685.

306. Hamaguchi, H. and H. Cleve. 1972. Solubilization and Comparative Analysis of Mammalian Erythrocyte Membrane Glycoproteins. Biochem. Biophys. Res. Commun. 47:459-464.

307. Hammond, K.S. and D.S. Papermaster. 1976. Fluorometric Assay of Sialic Acid in the Picomole Range: A Modification of the Thiobarbituric Acid Assay. Anal. Biochem. 74:292-297.

308. Rando, R.R., F.W. Bangerter, and M.R. Alecio. 1982. The Synthesis and Properties of a Functional Fluorescent Cholesterol Analog. Biochim. Biophys. Acta 684:12-20.

309. Turner, J.D. and G. Rouser. 1974. Removal of Lipid from Intact Erythrocytes and Ghosts by Aqueous Solutions and Its Relevance to Membrane Structure. Lipids 9:49-54.

310. Siakotos, A.N. and G. Rouser. 1965. Analytical Separation of Nonlipid Water Soluble Substances and Gangliosides from Other Lipids by Dextran Gel Column Chromatography. J. Amer. Oil Chemists' Soc. 42:913-919.

311. Ames, B.N. 1966. Assay of Inorganic Phosphate, Total Phosphate and Phosphateses. Meth. Enzymol. 8:115-118.

312. Courchaine, A.J., W.H. Miller, and D.B. Stein. 1959. Rapid Semimicro Procedure for Estimating Free and Total Cholesterol. Clin. Chem. 5:609-614.

313. Zlatkis, A., B. Zak, and A.J. Boyle. 1963. A New Method for the Direct Determination of Serum Cholesterol. J. Lab. Clin. Med. 41:486-492.

314. Lepock, J.R., J.E. Thompson, J. Kruuv, and D.F.H. Wallach. 1978. Photoinduced Crosslinking of Membrane Proteins by Fluorescein Isothiocyanate. Biochem. Biophys. Res. Commun. 85:344-350.

315. Sheetz, M.P. and D.E. Koppel. 1979. Membrane Damage Caused by Irradiation of Fluorescent Concavalin A. Proc. Natl. Acad. Sci. USA 76:3314-3317.

316. Jacobson, K., Y. Hou, and J. Wojcieszyn. 1978. Evidence for a Lack of Damage During Photobleaching Measurements of Lateral Mobility of Cell-Surface Components. Exp. Cell Res. 116:179-189.

317. Wolf, D., M. Edidin, and P. Dragsten. 1980. Effect of Bleaching Light on Measurements of Lateral Diffusion in Cell Membranes by the Fluorescence Photobleaching Recovery Method. Proc. Natl. Acad. Sci. USA 77:2043-2045.

318. Koppel, D.E. and M.P. Sheetz. 1981. Fluorescence Photobleaching Does Not Alter the Lateral Mobility of Erythrocyte Membrane Glycoproteins. Nature 293:159-161.

319. Morrison, W.L. and H. Neurath. 1953. Proteolytic Enzymes of the Formed Elements of Human Blood. I. Erythrocytes. J. Biol. Chem. 200:39-51.

320. Tokes, Z.A. and S.M. Chambers. 1975. Proteolytic Activity Associated with Human Erythrocyte Membranes. Self-Digestion of Isolated Human Erythrocyte Membranes. Biochim. Biophys. Acta 389:325-338.

321. Triplett, R.B., J.M. Wingate, and K.L. Carraway. 1972. Calcium Effects on Erythrocyte Membrane Proteins. Biochem. Biophys. Res. Commun. 49:1014-1020.

322. Carraway, K.L., R.B. Triplett, and D.R. Anderson. 1975. Aggregation of Erythrocyte Membrane Proteins. Biochim. Biophys. Acta 379:571-581.

323. King, L.E., and M. Morrison. 1977. Calcium Effects on Human Erythrocyte Membrane Proteins. Biochim. Biophys. Acta 471:162-168.

324. Quirk, S.J., Q.F. Ahkong, G.M. Bothana, J. Vos, and J. Lucy. 1978. Membrane Proteins in Human Erythrocytes During Cell Fusion Induced by Oleoylglycerol. Biochem. J. 176:159-167.

325. Allen, D.W. and S. Cadman. 1979. Calcium-Induced Erythrocyte Membrane Changes: The Role of Adsorption of Cytosol Proteins and Proteases. Biochim. Biophys. Acta 551:1-9.

326. Siegel, D.L., S.R. Goodman, and D. Branton. 1980. The Effect of Endogenous Proteases on the Spectrin Binding Proteins of Human Erythrocytes. Biochim. Biophys. Acta 598:517-527.

327. Murakami, T., Y. Suzuki, and T. Murachi. 1979. An Acid Protease in Human Erythrocytes and Its Localization in the Inner Membrane. Eur. J. Biochem. 96:221-227.

328. Ballas, S.K. and E.R. Burka. 1979. Protease Activity in the Human Erythrocyte: Localization to the Cell Membrane. Blood 53:875-882.

329. Tarone, G.,N. Hamasaki, M. Fukuda, and V.T. Marchesi. 1979. Proteolytic Degradation of Human Erythrocyte Band 3 by Membrane-Associated Protease Activity. J. Membrane Biol. 48:1-12.

330. Ahkong, Q.F., G.M. Botham, A.W. Woodward, and J.A. Lucy. 1980. Calcium-Activated Thiol-Proteinase Activity in the Fusion of Rat Erythrocytes Induced by Benzyl Alcohol. Biochem. J. 192: 829-836.

331. Lucy, J.A. and A.M. Glauert. 1964. Structure and Assembly of Macromolecular Lipid Complexes Composed of Globular Micelles. J. Mol. Biol. 8:727-748.

332. Shany, S., A.W. Bernheimer, P.S. Grushoff, and K.S. Kim. 1974. Evidence for Membrane Cholesterol as the Common Binding Site for Cereolysin, Streptolysin O and Saponin. Molec. Cellular Biochem. 3:179-186.

333. Seeman, P. 1967. Transient Holes in the Erythrocyte Membrane During Hypotonic Hemolysis and Stable Holes in the Membrane After Lysis by Saponin and Lysolecithin. J. Cell Biology 32:55-70.

334. Seeman, P., D. Cheng, and G.H. Iles. 1973. Structure of Membrane Holes in Osmotic and Saponin Hemolysis. J. Cell Biol. 56:519-527.

335. Seeman, P. 1974. Ultrastructure of Membrane Lesions in Immune Lysis, Osmotic Lysis and Drug-Induced Lysis. Fed. Proc. 33: 2116-2124.

336. Ohtsuki, I., R.M. Manzi, G.E. Palade, and J.D. Jamieson. 1978. Entry of Macromolecular Tracers into Cells Fixed with Low Concentrations of Aldehydes. Biol. Cellulaire 31:119-126.

337. Kliman, H.J. and T.L. Steck. 1980. Association of Glyceraldehyde-3-Phosphate Dehydrogenase with the Human Red Cell Membrane. J. Biol. Chem. 255:6314-6321.

338. Marchesi, V.T. and E. Steers, Jr. 1968. Selective Solubilization of a Protein Component of the Red Cell Membrane. Science 159:203-204.

339. Furthmayr, H. and R. Timpl. 1970. Immunochemical Studies on Structural Proteins of the Red Cell Membrane. Eur. J. Biochem. 15:301-310.

340. Clarke, M. 1971. Isolation and Characterization of a Water-Soluble Protein from Bovine Erythrocyte Membranes. Biochem. Biophys. Res. Commun. 45:1063-1070.

341. Marchesi, S.L., E. Steers, V.T. Marchesi, and T.W. Tillack. 1970. Physical and Chemical Properties of a Protein Isolated from Red Cell Membranes. Biochem. 9:50-57.

342. McCown, J.T., E. Evans, S. Diehl, and H.C. Wiles. 1981. Degree of Hydration and Lateral Diffusion in Phospholipid Multibilayers. Biochemistry 20:3134-3138.

343. Rubenstein, J.L.R., B.A. Smith, and H.M. McConnell. 1979. Lateral Diffusion in Binary Mixtures of Cholesterol and Phosphatidylcholines. Proc. Natl. Acad. Sci. USA 76:15-18.

344. Owicki, J.C. and H.M. McConnell. 1980. Lateral Diffusion in Inhomogeneous Membranes: Model Membranes Containing Cholesterol. Biophys. J. 30:383-398.

345. Snyder, B. and E. Freire. 1980. Compositional Domain Structure in Phosphatidylcholine-Cholesterol and Sphingomyelin-Cholesterol Bilayers. Proc. Natl. Acad. Sci. USA 77:4055-4059.

346. Copeland, B.R. and H.M. McConnell. 1980. The Rippled Structure in Bilayer Membranes of Phosphatidylcholine and Binary Mixtures of Phosphatidylcholine and Cholesterol. Biochim. Biophys. Acta 599:95-109.

347. Recktenwald, D.J. and H.M. McConnell. 1981. Phase Equilibria in Binary Mixtures of Phosphatidylcholine and Cholesterol. Biochemistry 20:4505-4510.

348. Backer, J.M. and E.A. Dawidowicz. 1981. Mechanism of Cholesterol Exchange Between Phospholipid Vesicles. Biochemistry 20:3805-3810.

349. McLean, L.R. and M.C. Phillips. 1981. Mechanism of Cholesterol and Phosphatidylcholine Exchange or Transfer Between Unilamellar Vesicles. Biochemistry 20:2893-2900.

350. Nichols, J.W. and R.E. Pagano. 1981. Kinetics of Soluble Lipid Monomer Diffusion Between Vesicles. Biochemistry 20:2783-2789.

351. Lange, Y., H.B. Cutler, and T.L. Steck. 1980. The Effect of Cholesterol and Other Intercalated Amphipaths on the Contour and Stability of the Isolated Red Cell Membrane. J. Biol. Chem. 255:9331-9337.

352. Rottem, S., W.L. Hubbell, L. Hayflick, and H.M. McConnell. 1970. Motion of Fatty Acid Spin Labels in the Plasma Membrane of Mycoplasma. Biochim. Biophys. Acta 219:104-113.

353. Hong, K. and W.L. Hubbell. 1972. Preparation and Properties of Phospholipid Bilayers Containing Rhodopsin. Proc. Natl. Acad. Sci. USA 69:2617-2621.

354. Sefton, B.M. and B.J. Gaffney. 1974. Effect of the Viral Proteins on the Fluidity of the Membrane Lipids in Sindbis Virus. J. Mol. Biol. 90:343-358.

355. Fraley, R.T., G.S.L. Yen, D.R. Lueking, and S. Kaplan. 1979. The Physical State of the Intracytoplasmic Membrane of Rhodopseudomonas sphaeroides and Its Relationship to the Cell Division Cycle. J. Biol. Chem. 254:1987-1991.

356. Gilmore, R., N. Cohn, and M. Glaser. 1979. Fluidity of LM Cell Membranes with Modified Lipid Compositions as Determined with 1,6-Diphenyl-1,3,5-Hexatriene. Biochemistry 18:1042-1049.

357. Johnson, S.M. and M. Kramers. 1978. Membrane Microviscosity Differences in Normal and Leukaemic Human Lymphocytes. Biochem. Biophys. Res. Commun. 80:451-457.

358. Koppel, D.E. and M.P. Sheetz. 1981. Fluroescence Photobleaching Does Not Alter the Lateral Mobility of Erythrocyte Membrane Glycoproteins. Nature 293:159-161.

359. Sheetz, M.P., P. Febbroriello, and D.E. Koppel. 1982. Triphosphoinositide Increases Glycoprotein Lateral Mobility in Erythrocyte Membranes. Nature 296:91-93.

360. Rudy, B. and C. Gitler. 1972. Microviscosity of the Cell Membrane. Biochim. Biophys. Acta 288:231-236.

361. Radda, G.K. and D.S. Smith. 1970. Retinol: A Fluorescent Probe for Membrane Lipids. FEBS Lett. 9:287-289.

362. Aloni, B., B. Shinitsky, and A. Livne. 1974. Dynamics of Erythrocyte Lipids in Intact Cells, in Ghost Membranes and in Liposomes. Biochim. Biophys. Acta 348:438-441.

363. Kehry, M., J. Yguerabide, and S.J. Singer. 1977. Fluidity in the Membranes of Adult and Neonatal Human Erythrocytes. Science 195:486-487.

364. Shinitzky, M. and M. Inbar. 1976. Microviscosity Parameters and Protein Mobility in Biological Membranes. Biochim. Biophys. Acta 433:133-149.

365. Kinosita, K., R. Kataoka, Y. Kimura, O. Gotoh, and A. Ikegami. 1981. Dynamic Structure of Biological Membranes as Probed by 1,6-Diphenyl-1,3,5-Hexatriene: A Nanosecond Fluorescence Depolarization Study. Biochemistry 20:4270-4277.

366. Solomon, A.K. 1974. Apparent Viscosity of Human Red Cell Membranes. Biochim. Biophys. Acta 373:145-149.

367. Saffman, P.G. and M. Delbruck. 1975. Brownian Motion in Biological Membranes. Proc. Natl. Acad. Sci. USA 72:3111-3113.

368. Cone, R.A. 1972. Rotational Diffusion of Rhodopsin in the Visual Receptor Membrane. Nature (New Biol.) 236:39-43.

369. Nigg, E.A. and R.J. Cherry. 1979. Influence of Temperature and Cholesterol on the Rotational Diffusion of Band 3 in the Human Erythrocyte Membrane. Biochem. 18:3457-3465.

370. Austin, R.H., S.S. Chan, and T.M. Jovin. 1979. Rotational Diffusion of Cell Surface Components by Time-Resolved Phosphorescence Anisotropy. Proc. Natl. Acad. Sci. USA 76:5650-5654.

371. Nigg, E.A. and R.J. Cherry. 1980. Anchorage of a Band 3 Population at the Erythrocyte Cytoplasmic Membrane Surface: Protein Rotational Diffusion Measurements. Proc. Natl. Acad. Sci USA 77:4702-4706.

372. Nigg, E.A., R.J. Cherry, and T. Bachi. 1980. Influence of Influenza and Sendai Virus on the Rotational Mobility of Band 3 Proteins in Human Erythrocyte Membranes. Virology 107:552-556.

373. Nigg, E.A., C.G. Gahmberg, and R.J. Cherry. 1980. Rotational Diffusion of Band 3 Proteins in Membranes from En(a-) and Neuraminidase-treated Normal Human Erythrocytes. Biochim. Biophys. Acta 600:636-642.

374. Gottlieb, M.H. and E.D. Eanes. 1974. On Phase Transitions in Erythrocyte Membranes and Extracted Membrane Lipids. Biochim. Biophys. Acta 373:519-522.

375. Ladbrooke, B.D. and D. Chapman. 1969. Thermal Analysis of Lipids, Proteins, and Biological Membranes. Chem. Phys. Lipids 3:304-367.

376. Bourguignon, L.Y.W. and S.J. Singer. 1977. Transmembrane interactions and the mechanism of capping of surface receptors by their specific ligands. Proc. Natl. Acad. Sci. USA 74: 5031-5035.

377. Ash, J.F., D. Louvard and S.J. Singer. 1977. Antibody-induced linkages of plasma membrane proteins to intracellular actomyosin-containing filaments in cultured fibroblasts. Proc. Natl. Acad. Sci. USA 74:5584-5588.

378. Flanagan, J. and G.L.E. Koch. 1978. Cross-linked surface Ig attaches to actin. Nature 273:278-281.

379. Cherksey, B.D., J.A. Zadunaisky and R.B. Murphy. 1980. Cytoskeletal constraint of the β-adrenergic receptor in frog erythrocyte membranes. Proc. Natl. Acad. Sci. USA 77:6401-6405.

380. Tokuyasu, K.T., R. Schekman and S.J. Singer. 1979. Domains of receptor mobility and endocytosis in the membranes of neonatal human erythrocytes and reticulocytes are deficient in spectrin. J. Cell Biol. 80:481-486.

381. Schindler, M., M.J. Osborn and D.E. Koppel. 1980. Lateral mobility in reconstituted membranes - comparisons with diffusion in polymers. Nature 283:346-350.

382. Jahnig, F. 1981. No need for a new membrane model. Nature 289:694-696.

383. Peters, R. and R.J. Cherry. 1982. Translational diffusion of bacteriorhodopsin and of a lipid analogue in artificial bilayer membranes. Biophys. J. 37:277a.

Appendix A. Machine Language Program for KIM-1 Microprocessor

1. Parameters.

A. Data (0000-001B)

0000	measure on time, sec
0001	measure on time, .01 sec
0005	1st bleach on time, sec
0006	1st bleach on time, .01 sec
000A	2nd bleach on time, sec
000B	2nd bleach on time, .01 sec
0010	1st measure off time, sec
0011	1st measure off time, .01 sec
0012	2nd measure off time, sec
0013	2nd measure off time, .01 sec
0014	3rd measure off time, sec
0015	3rd measure off time, .01 sec
0016	4th measure off time, sec
0017	4th measure off time, .01 sec
0018	5th measure off time, sec
0019	5th measure off time, .01 sec
001A	6th measure off time, sec
001B	6th measure off time, .01 sec

B. Working registers

00A0	working bleach on time, sec
00A1	working bleach on time, .01 sec
00B0	working measure off time, sec
00B1	working measure off time, .01 sec

C. Display

00F9	(INH)	.01 sec elapsed	
00FA	(POINTL)	sec elapsed	
00FB	(POINTH)	shutters open	(04 = S1, 05 = S1 + S3, 06 = S1 + S2)

2. Keyboard Commands.

		jump to
0	Abort, reset parameters	ABORT
3	Start measuring cycle (on first)	START
4	Stop measuring, wait	MEOFF
7	Start bleaching cycle	BLEAON
8	Start measuring cycle (off first)	MEASOFF
1	Transfer 1st bleach on time	BLEACH1
2	Transfer 2nd bleach on time	BLEACH2
A	Transfer 1st measure off time	MEAS1
B	Transfer 2nd measure off time	MEAS2
C	Transfer 3rd measure off time	MEAS3
D	Transfer 4th measure off time	MEAS4
E	Transfer 5th measure off time	MEAS5
F	Transfer 6th measure off time	MEAS6

3. Programs

Main Frame

Address	Code			Label	OP Code	Operand	Comments
0200	A9	00		Main	LDA	#00	
2	85	F1			STA	P	
4	85	F9			STA	INH	
6	85	FA			STA	POINTL	
8	85	FB			STA	POINTH	
A	8D	FA	17		STA	17FA	
D	A9	1C			LDA	#K	
F	8D	FB	17		STA	17FB	
0212	A9	E0			LDA	CLOCKL	
4	8D	FE	17		STA	17FE	
7	A9	03			LDA	CLOCKH	
9	8D	FF	17		STA	17FF	
C	20	82	03		JSR	MEAS1	
F	20	70	03		JSR	BLEACH1	
0222	20	IF	IF	IDLE	JSR	SCAND5	
5	20	00	03		JSR	DIRECT	
8	4C	22	02		JMP	IDLE	
B	A9	00		START	LDA	#00	
D	8D	06	17		STA	1706	
0230	85	F9			STA	INH	
2	85	FA			STA	POINTL	
4	A9	FF			LDA	#FF	
6	8D	01	17		STA	1701	
9	A9	05			LDA	#05	S1 + S3
B	8D	00	17		STA	1700	
E	85	FB			STA	POINTH	
0240	A9	9B			LDA	#9B	
0242	8D	0E	17		STA	170E	
5	20	IF	IF	MONLOOP1	JSR	SCAND5	
8	20	00	03		JSR	DIRECT	
B	A5	F9			LDA	INH	
D	C5	01			CMP	0001	
F	D0	06			BNE	MONLOOP1	
0251	A5	FA			LDA	POINTL	
3	C5	00			CMP	0000	
5	F0	03			BEQ	MEASOFF	
7	4C	45	02		JMP	MONLOOP1	
A	A9	00		MEASOFF	LDA	#00	
C	8D	06	17		STA	1706	
F	8D	00	17		STA	1700	
0262	85	F9			STA	INH	
4	85	FA			STA	POINTL	
6	85	FB			STA	POINTH	
8	A9	9B			LDA	#9B	
A	8D	0E	17		STA	170E	
D	20	IF	IF	MOFLOOP	JSR	SCAND5	

Main Frame (continued)

Address	Code			Label	OP Code	Operand	Comments
0270	20	00	03		JSR	DIRECT	
3	A5	F9			LDA	INH	
5	C5	B1			CMP	00B1	
7	D0	06			BNE	MOFLOOP	
9	A5	FA			LDA	POINTL	
B	C5	B0			CMP	00B0	
D	F0	AC			BEQ	START	-84
F	4C	6D	02		JMP	MOFLOOP	
0282	A9	00		BLEAON	LDA	#00	
4	85	F9			STA	INH	
6	85	FA			STA	POINTL	
8	A9	06			LDA	#06	S1 + S2
A	8D	00	17		STA	1700	
D	85	FB			STA	POINTH	
F	A9	9B			LDA	#9B	
0291	8D	0E	17		STA	170E	
4	20	IF	IF	BONLOOP1	JSR	SCAND5	
7	20	6A	IF		JSR	GETKY	
A	C9	00			CMP	#00	
C	F0	06			BEQ	JDIR	
E	C9	04			CMP	#04	
02A0	F0	02			BEQ	JDIR	
2	D0	03			BNE	CONT	
4	20	00	03	JDIR	JSR	DIRECT	
7	A5	F9		CONT	LDA	INH	
9	C5	A1			CMP	00A1	
B	D0	06			BNE	BONLOOP1	
D	A5	FA			LDA	POINTL	
F	C5	A0			CMP	00A0	
02B1	F0	03			BEQ	BLEAOFF	
3	4C	94	02		JMP	BONLOOP1	
6	A9	04		BLEAOFF	LDA	#04	S1
8	8D	00	17		STA	1700	
B	85	FB			STA	POINTH	
D	A9	00			LDA	#00	
02BF	8D	06	17		STA	1706	
02C2	85	F9			STA	INH	
4	85	FA			STA	POINTL	
6	A9	9B			LDA	#9B	
8	8D	0E	17		STA	170E	
B	20	IF	IF	BOFLOOP	JSR	SCAND5	
E	A5	F9			LDA	INH	
02D0	C5	05			CMP	#05	50 msec
2	D0	F7			BNE	BOFLOOP	
4	A9	00		MEASON2	LDA	#00	
6	8D	06	17		STA	1706	
9	A9	05			LDA	#05	S1 + S3
B	8D	00	17		STA	1700	
E	85	FB			STA	POINTH	

Main Frame (continued)

Address	Code			Label	OP Code	Operand	Comments
02E0	A9	9B			LDA	#9B	
2	8D	0E	17		STA	170E	
5	20	IF	IF	MONLOOP2	JSR	SCAND5	
8	20	6A	IF		JSR	GETKY	
B	C9	00			CMP	#00	
D	F0	0A			BEQ	JDIRECT	
F	C9	04			CMP	#04	
02F1	F0	06			BEQ	JDIRECT	
3	C9	08			CMP	#08	
5	F0	02			BEQ	JDIRECT	
7	D0	03			BNE	CONTIN	
9	20	00	03	JDIRECT	JSR	DIRECT	
C	4C	E5	02	CONTIN	JMP	MONLOOP2	

Directions Ladder

Address	Code			Label	OP Code	Operand	Comments
0300	20	6A	IF	DIRECT	JSR	GETKY	
3	C9	00			CMP	#00	
5	F0	31			BEQ	OJUMP	+49
7	C9	03			CMP	#03	
9	F0	30			BEQ	3J	+48
B	C9	04			CMP	#04	
D	F0	2F			BEQ	4J	+47
F	C9	07			CMP	#07	
0311	F0	2E			BEQ	7J	+46
3	C9	08			CMP	#08	
5	F0	2D			BEQ	8J	+45
7	C9	01			CMP	#01	
9	F0	2C			BEQ	1J	+44
B	C9	02			CMP	#02	
D	F0	2C			BEQ	2J	+44
F	C9	0A			CMP	#0A	
0321	F0	2C			BEQ	AJ	+44
3	C9	0B			CMP	#0B	
5	F0	2C			BEQ	BJ	+44
7	C9	0C			CMP	#0C	
9	F0	2C			BEQ	CJ	+44
B	C9	0D			CMP	#0D	
D	F0	2C			BEQ	DJ	+44
F	C9	0E			CMP	#0E	
0331	F0	2C			BEQ	EJ	+44
3	C9	0F			CMP	#0F	
5	F0	2C			BEQ	FJ	+44
7	60				RTS		
0338	4C	C0	03	OJUMP	JMP	ABORT	
B	4C	2B	02	3J	JMP	START	
E	4C	CB	03	4J	JMP	MEOFF	
0341	4C	82	02	7J	JMP	BLEAON	
4	4C	5A	02	8J	JMP	MEASOFF	
7	20	70	03	1J	JSR	BLEACH1	
A	60				RTS		
B	20	79	03	2J	JSR	BLEACH2	
E	60				RTS		
F	20	82	03	AJ	JAR	MEAS1	
0352	60				RTS		
3	20	8B	03	BJ	JSR	MEAS2	
6	60				RTS		
7	20	94	03	CJ	JSR	MEAS3	
A	60				RTS		
B	20	9D	03	DJ	JSR	MEAS4	
E	60				RTS		
F	20	A6	03	EJ	JSR	MEAS5	
0362	60				RTS		
3	20	AF	03	FJ	JSR	MEAS6	
6	60				RTS		

Transfer Data Subroutines

Address	Code		Label	OP Code	Operand	Comments
0370	A5	05	BLEACH1	LDA	0005	
2	85	A0		STA	00A0	
4	A5	06		LDA	0006	
6	85	A1		STA	00A1	
8	60			RTS		
0379	A5	0A	BLEACH2	LDA	000A	
B	85	A0		STA	00A0	
D	A5	0B		LDA	000B	
F	85	A1		STA	00A1	
0381	60			RTS		
0382	A5	10	MEAS1	LDA	0010	
4	85	B0		STA	00B0	
6	A5	11		LDA	0011	
8	85	B1		STA	00B1	
A	60			RTS		
038B	A5	12	MEAS2	LDA	0012	
D	85	B0		STA	00B0	
F	A5	13		LDA	0013	
0391	85	B1		STA	00B1	
3	60			RTS		
0394	A5	14	MEAS3	LDA	0014	
6	85	B0		STA	00B0	
8	A5	15		LDA	0015	
A	85	B1		STA	00B1	
C	60			RTS		
039D	A5	16	MEAS4	LDA	0016	
F	85	B0		STA	00B0	
03A1	A5	17		LDA	0017	
3	85	B1		STA	00B1	
5	60			RTS		
03A6	A5	18	MEAS5	LDA	0018	
8	85	B0		STA	00B0	
A	A5	19		LDA	0019	
C	85	B1		STA	00B1	
E	60			RTS		
03AF	A5	1A	MEAS6	LDA	001A	
03B1	85	B0		STA	00B0	
3	A5	1B		LDA	001B	
5	85	B1		STA	00B1	
7	60			RTS		

ABORT, MEOFF Subroutines

Address	Code			Label	OP Code	Operand
03C0	A9	00		ABORT	LDA	#00
2	8D	06	17		STA	1706
5	8D	00	17		STA	1700
8	4C	00	02		JMP	MAIN
03CB	A9	00		MEOFF	LDA	#00
D	8D	06	17		STA	1706
03D0	8D	00	17		STA	1700
3	85	F1			STA	P
5	85	F9			STA	INH
7	85	FA			STA	POINTL
9	85	FB			STA	POINTH
B	4C	22	02		JMP	IDLE

Clock IRQ

Address	Code			Label	OP Code	Operand
03E0	48			CLOCK	PHA	
1	A9	9B			LDA	#9B
3	8D	0E	17		STA	170E
6	F8				SED	
7	18				CLC	
8	A5	F9			LDA	INH
A	69	01			ADC	#01
C	85	F9			STA	INH
E	C9	00			CMP	#00
03F0	D0	06			BNE	CONT
2	A5	FA			LDA	POINTL
4	69	00			ADC	#00
6	85	FA			STA	POINTL
8	D8			CONT	CLD	
9	68				PLA	
A	40				RTI	

Appendix B. Schematic of Shutter Interface for KIM-1 Microprocessor

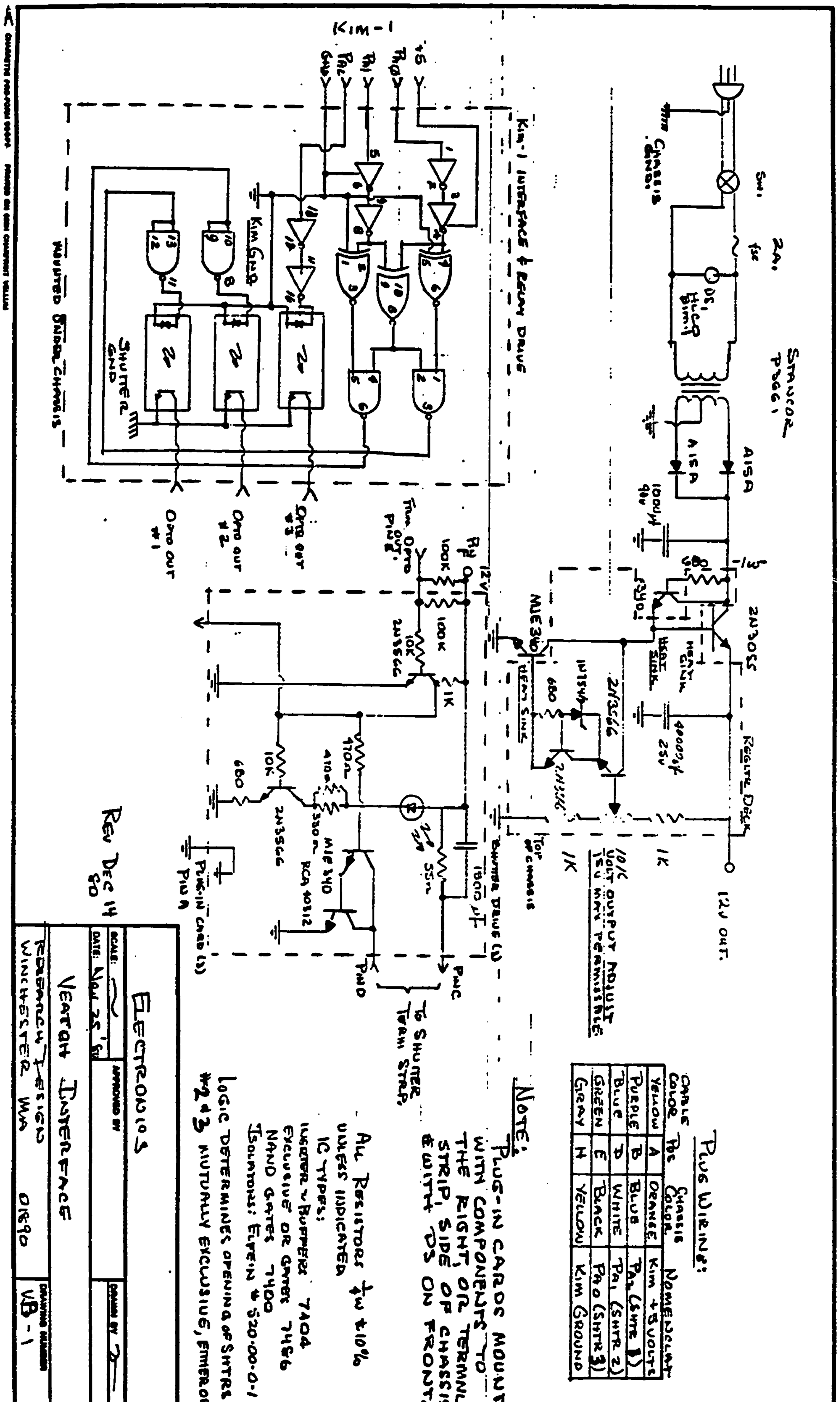
KIM-1
+5
PA0
PA1
PA2
GND
KIM-1 INTERFACE & RELAY DRIVE
KIM GND
MOUNTED UNDER CHASSIS
SHUTTER GND
OPTO OUT #1
OPTO OUT #2
OPTO OUT #3
CHASSIS GND.
SW1
2A. FUSE
DS1 HLCP BIM1
STANCOR P6661
A15A
100µf 40v
12V
2N3055
HEAT SINK
MJE340
2N3566
1N3540
680
4000µf 25v
REGULATE DECK
12V OUT.
1K
10K
VOLT OUTPUT ADJUST 15V MAX PERMISSIBLE
TOP OF CHASSIS
100K
470Ω
410Ω
330Ω
55Ω
150µf
MJE340
RCA 40312
2N3566
PLUG-IN CARD (1)
PLUG-IN CARD (2)
PIN A
PWC
PWD
TO SHUTTER TERM STRIP
PLUG WIRING:
CABLE COLOR	PIN	CHASSIS COLOR	NOMENCLAT
YELLOW	A	ORANGE	KIM +5 VOLTS
PURPLE	B	BLUE	PA0 (SHTR 1)
BLUE	D	WHITE	PA1 (SHTR 2)
GREEN	E	BLACK	PA2 (SHTR 3)
GRAY	H	YELLOW	KIM GROUND
NOTE:
PLUG-IN CARDS MOUNT WITH COMPONENTS TO THE RIGHT, OR TERMNL STRIP SIDE OF CHASSIS & WITH DS ON FRONT!
ALL RESISTORS 1/4W ±10% UNLESS INDICATED
IC TYPES:
INVERTER-BUFFERS 7404
EXCLUSIVE OR GATES 7486
NAND GATES 7400
ISOLATORS: ELFEIN 4 520-00-01
LOGIC DETERMINES OPENING OF SHTRS #2 & 3 MUTUALLY EXCLUSIVE, EITHER OR.
REV DEC 14 80
ELECTRONICS
VEATCH INTERFACE
RESEARCH DESIGN WINCHESTER MA 01890
DATE: NOV 25 '80
VB-1

Appendix B.